

The fat mass and obesity-associated
protein (*Fto*) regulates activity of the
dopaminergic circuitry

In a u g u r a l - D i s s e r t a t i o n

zur Erlangung des Doktorgrades
der Mathematisch-Naturwissenschaftlichen Fakultät
der Universität zu Köln



vorgelegt von
Martin Heß
aus Adenau

Köln 2014

Berichterstatter: **Prof. Dr. Jens C. Brüning**

Prof. Dr. Aleksandra Trifunovic

Tag der mündlichen Prüfung: 27. Januar 2014

*A learning experience is one of those things
that say, "You know that thing you just did?
Don't do that."*

- Douglas Adams -

Contents

Abbreviations	xii
Abstract	xiv
Zusammenfassung	xvi
1 Introduction	1
1.1 Obesity and obesity associated diseases	1
1.1.1 Monogenic obesity	1
1.1.2 Polygenic obesity	2
1.2 Regulation of body weight	4
1.2.1 Energy homeostasis	4
1.2.2 CNS in regulation of energy homeostasis	5
1.3 The dopaminergic system	7
1.3.1 Dopamine and dopaminergic neurons	7
1.3.2 Dopamine receptors and dopamine signaling	8
1.3.3 Dopamine and reward related behaviors	9
1.3.4 Dopamine and obesity	12
1.3.5 DRD2/DRD3 autoreceptor feedback loop	14
1.4 The fat mass and obesity-associated protein (<i>FTO</i>)	15
1.4.1 Genome wide association studies	15
1.4.2 Human <i>FTO</i> phenotypes	21
1.4.3 Murine <i>Fto</i> studies	22
1.4.4 Molecular function of <i>FTO</i>	26
1.5 m ⁶ A RNA modification	29

1.5.1	RNA and RNA modifications	29
1.5.2	N6-methyladenosine (m ⁶ A)	30
1.5.3	The m ⁶ A methylome	33
1.6	Objectives	34
2	Materials and Methods	35
2.1	Animal care	35
2.2	Experimental mouse models	35
2.3	Genotyping	36
2.4	Phenotyping	37
2.4.1	Body weight	37
2.4.2	Insulin tolerance test	37
2.4.3	Glucose tolerance test	37
2.4.4	Indirect calorimetry	37
2.4.5	Food intake and refeeding response	38
2.5	Microarray expression analysis	38
2.6	Quantitative polymerase chain reaction	39
2.6.1	Preparation of RNA	39
2.6.2	Reverse transcription and quantitative PCR	39
2.7	Protein biochemistry	40
2.7.1	Protein preparation	40
2.7.2	Western blot	40
2.8	Behavioural experiments	41
2.8.1	Open Field	41
2.8.2	Conditioned Place Preference	42
2.8.3	Sucrose preference	42
2.9	Electronmicroscopy	43
2.10	Immunohistochemistry	44
2.11	<i>In situ</i> hybridization	45
2.12	Electrophysiology	46

2.13	Microdialysis	47
2.14	MeRIP pulldown	49
2.15	GO analysis	49
2.16	Pathway analysis	50
2.17	Graphical representation of data	50
2.18	Statistics	51
2.19	Chemicals and Materials	51
3	Results	53
3.1	Whole body <i>Fto</i> deficiency alters the function of the dopaminergic circuitry	53
3.1.1	FTO is expressed in midbrain dopaminergic neurons	53
3.1.2	Microarray analysis of <i>Fto</i> -deficient midbrain	54
3.1.3	<i>Fto</i> -deficient mice exhibit attenuated responses to cocaine	60
3.1.4	Attenuation of the DRD2/DRD3 autoreceptor feedback loop in <i>Fto</i> -deficient mice	63
3.2	Dopamine neuron restricted loss of FTO attenuates the function of the DRD2/DRD3 dependent autoreceptor feedback loop	67
3.2.1	Generation of dopamine neuron restricted <i>Fto</i> knock out mice	67
3.2.2	Dopamine restricted <i>Fto</i> knock out does not influence basic metabolic parameters	72
3.2.3	Altered DRD2/DRD3 dependent responses in <i>Fto</i> ^{ΔDAT}	76
3.3	N6-methyladenosine in mRNA depends on FTO demethylase function	81
3.3.1	Methylated RNA immunoprecipitation (MeRIP) sequencing identifies demethylation targets of FTO	81
3.3.2	m ⁶ A in mRNA influences translation of methylated transcripts	83
4	Discussion	92
4.1	<i>Fto</i> deficiency alters D2-like receptor-dependent responses	93
4.1.1	FTO is expressed in midbrain dopaminergic neurons	93

4.1.2	Whole body <i>Fto</i> -deficiency attenuates responses to cocaine	93
4.1.3	Impairment of D2-like autoreceptor signaling	94
4.2	Conditional loss of <i>Fto</i> resembles D2 autoreceptor deficiency	95
4.2.1	Successful generation of dopamine neuron specific knock out mice	95
4.2.2	Cell-autonomous impairment of D2-like autoreceptor signaling	96
4.2.3	Relation of whole body and dopamine restricted FTO deficiency to D2 receptor studies	98
4.3	FTO demethylates m ⁶ A in messenger RNA	100
4.3.1	FTO acts as a m ⁶ A demethylase <i>in vivo</i>	100
4.3.2	Selected candidate transcripts are affected on protein level	101
4.4	Relation to studies of human <i>FTO</i> genomic variation	108
4.5	Conclusions	109
4.6	Perspectives	111
5	Bibliography	113
6	Appendix	139
	Danksagung	169
	Erklärung	170
	Teilpublikationen	171
	Curriculum vitae	174

List of Figures

1.1	Pre- and postsynaptic dopamine receptor signaling	10
1.2	Genome wide association studies link <i>FTO</i> to obesity	16
1.3	Reversible <i>N</i> 6-methyladenosine modification	32
3.1	<i>FTO</i> is expressed in dopaminergic neurons of the midbrain	53
3.2	Loss of <i>FTO</i> does not alter cell number or morphology of dopaminergic midbrain neurons	55
3.3	Microarray analysis of <i>Fto</i> -deficient midbrain tissue	56
3.4	Schematic overlay of the microarray expression data and the dopaminergic signaling pathway	58
3.5	Selected transcripts deregulated in microarray analysis are not altered on protein level	59
3.6	Cocaine fails to increase locomotor activity in <i>Fto</i> -deficient mice	60
3.7	Cocaine fails to increase <i>Fos</i> expression in <i>Fto</i> -deficient mice	61
3.8	Reduction in cocaine-induced extracellular dopamine in the nucleus accumbens of <i>Fto</i> -deficient mice	62
3.9	Altered DRD2/DRD3 receptor dependent responses in <i>Fto</i> -deficient mice	64
3.10	Reduced GIRK dependent current density in <i>Fto</i> -deficient mice	66
3.11	Attenuated quinpirole dependent decrease in locomotor activity in <i>Fto</i> -deficient mice	67
3.12	Schematics of Cre-dependent deletion of <i>Fto</i>	68
3.13	Validation of DA neuron specific <i>Fto</i> deletion	69

3.14	<i>Fto</i> deletion in DA neurons does not affect FTO expression in mid-brain GABAergic neurons	71
3.15	Basic metabolic parameters are unchanged in <i>Fto</i> ^{ΔDAT} mice	73
3.16	Unchanged insulin and glucose tolerance in <i>Fto</i> ^{ΔDAT} mice	74
3.17	Food intake and refeeding response are unaltered in <i>Fto</i> ^{ΔDAT} mice	75
3.18	Sucrose preference is unaltered in <i>Fto</i> ^{ΔDAT} mice	76
3.19	Attenuated responses of midbrain neurons to cocaine and quinpirole in <i>Fto</i> ^{ΔDAT} mice	77
3.20	Reduced GIRK dependent current density in <i>Fto</i> ^{ΔDAT} mice	78
3.21	Altered baseline and cocaine evoked locomotor activity in <i>Fto</i> ^{ΔDAT} mice	79
3.22	Attenuated quinpirole dependent decrease in locomotor activity in <i>Fto</i> ^{ΔDAT} mice	79
3.23	Low dosage of cocaine shifts preference of <i>Fto</i> ^{ΔDAT} mice in conditioned place preference	81
3.24	Gene ontology analysis of transcripts with m ⁶ A hypermethylation in <i>Fto</i> -deficient mice	82
3.25	Gene ontology analysis of transcripts m ⁶ A methylated in control mice	84
3.26	Pathway analysis of m ⁶ A hypermethylated transcripts in <i>Fto</i> -deficient mice	85
3.27	FTO demethylation target <i>Drd3</i>	86
3.28	FTO demethylation target <i>Kcnj6</i>	87
3.29	FTO demethylation target <i>Grin1</i>	88
3.30	FTO demethylation target <i>Gnai1</i>	89
3.31	FTO demethylation target <i>Ikkbb</i>	90
3.32	FTO demethylation targets <i>Gnao1</i> and <i>Gnb5</i>	91
6.1	Reduction in cocaine-induced c-Fos immunoreactivity in <i>Fto</i> -deficient mice	139
6.2	Confirmation of <i>Fto</i> expression by β-galactosidase staining	140

List of Tables

2.1	Genotyping Primer	36
2.2	Realtime PCR probes	39
2.3	Antibodies for Western blot	41
2.4	Chemicals	51
6.1	Electrophysiological properties of <i>Fto</i> -deficient dopamine neurons .	139
6.2	List of transcripts deregulated in <i>Fto</i> -deficient midbrain microarray analysis	141
6.3	Transcripts hypermethylated in <i>Fto</i> -deficient mice	147

Abbreviations

2-OG	2-oxoglutarate
α -MSH	α -melanocyte stimulating hormone
ABH	AlkB homolog
AC	adenylyl cyclase
ADHD	attention-deficit/hyperactivity disorder
AlkB	α -ketoglutarate-dependent dioxygenases
ALKBH	alkB alkylation repair homolog
AgRP	agouti-related peptide
APOE	apolipoprotein
ARC	arcuate nucleus
BDNF	brain-derived neurotrophic factor
BMI	body mass index
BOLD	blood oxygen dependent
BW	body weight
cAMP	cyclic adenosine monophosphate
CART	cocaine and amphetamine regulated transcript
CARTPT	CART prepropeptide
cDNA	complementary DNA
CDS	coding sequence
CPu	caudate putamen
CUTL1	cut-like homeobox 1
DA	dopamine
DAT	dopamine transporter
DAPI	4-,6-Diamidin-2-phenylindol

DNA	deoxyribonucleic acid
DMH	dorsomedial hypothalamus
DRD2	type-2 dopamine receptor
DRD3	type-3 dopamine receptor
ES cells	embryonic stem cells
EUCOMM	European Conditional Mouse Mutagenesis Program
FC	fold change
FDR	false discovery rate
FLP	flippase (recombination enzyme)
Ft	fused toes
FTO	fat mass and obesity associated protein
GABA	γ -aminobutyric acid
GIRK	G protein-coupled inwardly rectifying potassium channel
GO	gene ontology
GRIN1	glutamate receptor, ionotropic, N-methyl-D-aspartate 1
GTT	glucose tolerance test
GWAS	genome wide association studies
ICV	intracerebroventricular
IGF-1	insulin-like growth factor
I.P.	intraperitoneal
IRS	insulin receptor substrate
ITT	insulin tolerance test
kD	kilo Dalton
KO	knock out
LH	lateral hypothalamus
m ³ T	3-methylthymine
m ³ U	3-methyluracil
m ⁵ C	5-methylcytosine
m ⁶ A	N ⁶ -methyladenosine

m ⁶ A _m	<i>N</i> 6 methyl-2'- <i>O</i> -methyladenosine
m ⁷ G	<i>N</i> 7-methylguanosine
MC4R	melanocortin 4 receptor
MCH	melanocyte concentrating hormone
MEF	mouse embryonic fibroblast
meRIP-Seq	methylated RNA immunoprecipitation with next-generation sequencing
mRNA	messenger ribonucleic acid
miRNA	micro RNA
MSC	multi-synthetase complex
mTORC1	mammalian target of rapamycin complex 1
N _m	2'- <i>O</i> -methylnucleotide
NA	noradrenaline
NAc	nucleus accumbens
NMDAR1	<i>N</i> -methyl- <i>D</i> -aspartate receptor subunit 1
NPY	neuropeptide Y
PBS	phosphate buffered saline
PCR	polymerase chain reaction
PFA	paraformaldehyde
PKA	protein kinase A
POMC	pro-opiomelanocortin
PVN	paraventricular nucleus
PYY	peptide YY
qPCR	quantitative polymerase chain reaction
RNA	ribonucleic acid
rRNA	ribosomal RNA
RMA	robust multiarray average
RPKM	reads per kilobase per million reads
RPGRIPL	retinitis pigmentosa GTPase regulator-interacting protein-1 like

RT	room temperature
ssDNA/RNA	single stranded DNA/RNA
SDS	sodium dodecyl sulfate
SEM	standard error of the mean
siRNA	small-interfering RNA
snRNA	small nuclear RNA
SNP	single nucleotide polymorphism
SN	substantia nigra
SNpc	substantia nigra pars compacta
STAT3	signal transducer and activator of transcription 3
TBS	tris buffered saline
TE	Tris/HCl EDTA
TG	transgene
TH	tyrosine hydroxylase
tRNA	transfer RNA
UCP-1	uncoupling protein 1
UPLC	ultra performance liquid chromatography
UTR	untranslated region
UV	ultraviolet
VMH	ventromedial hypothalamus
VTA	ventral tegmental area
WAT	white adipose tissue
WHO	World Health Organization
WT	wildtype

Abstract

In 2007 genome wide sequencing led to the identification of common genetic variations within intronic regions of the human *FTO* gene that are associated with obesity related traits. To date, neither the consequence of these variations for *FTO* expression, nor the exact molecular function of the FTO protein are known.

This study shows that inactivation of the murine *Fto* gene alters the function of the midbrain dopaminergic circuitry. Loss of FTO impairs the dopamine neuron autoreceptor feedback inhibition that depends on dopamine receptors type 2 (DRD2), type 3 (DRD3) and G protein coupled inwardly rectifying potassium channels (GIRKs). This attenuation of the autoinhibitory feedback loop was observed for both whole body *Fto*-deficient and dopamine neuron restricted *Fto* knock out (*Fto*^{ΔDAT}) mice. While *Fto*-deficient mice exhibited deficits in their responses to stimulation with cocaine, *Fto*^{ΔDAT} mice displayed a hypersensitivity to the locomotor and reward stimulating effects of cocaine and resembled DRD2 autoreceptor-deficient mice.

On the molecular level, FTO encodes a nucleic acid demethylase that is able to remove N6-methyladenosine (m⁶A) from messenger RNA. Analysis of m⁶A in mRNA of *Fto*-deficient midbrain and striatum showed that FTO acts as a m⁶A demethylase *in vivo*. Increased methylation, however, was only demonstrated for a subset of all m⁶A methylated transcripts. This subset included many transcripts important for cell-cell and neuronal signaling. Furthermore, many of these hypermethylated transcripts are components of dopaminergic signaling and some of these displayed a deregulation on the protein level in *Fto*-deficient mice, such as DRD3, GIRK2 and NMDAR1.

Taken together, FTO, via acting as a m⁶A demethylase, plays an important role

in regulating the dopamine autoinhibitory feedback loop and hence impinges on dopamine circuit function. Malfunction of dopamine signaling has been implicated in a variety of diseases such as depression, schizophrenia or ADHD and therefore poses the question whether *FTO* genomic variation is associated with diseases other than obesity and whether association with obesity related traits is partly due to alterations in dopamine circuit function.

Zusammenfassung

Genomweite Sequenzierung führte in 2007 zur Entdeckung weit verbreiteter genetischer Variationen in nicht-kodierenden Regionen des humanen *FTO* Gens, welche mit verschiedenen Merkmalen krankhaften Übergewichts assoziiert sind. Bis heute sind sowohl die Auswirkungen dieser Variationen auf die Expression von *FTO*, als auch die exakte molekulare Funktion des FTO Proteins unbekannt.

In dieser Studie konnte gezeigt werden, dass die Inaktivierung von murinem *Fto* die Funktion des dopaminergen Systems des Mittelhirns beeinflusst. Verlust von FTO führte zu einer Beeinträchtigung der autoinhibitorischen Rückkopplungsschleife dopaminergener Neurone, welche von Dopaminrezeptoren des Typs 2 (DRD2), Typs 3 (DRD3) und G Protein gekoppelten einwärts gleichrichtenden Kalium Kanälen (GIRKs) abhängig ist. Diese Fehlfunktion der autoinhibitorischen Rückkopplung konnte sowohl bei ganzkörper-*Fto*-defizienten, als auch bei spezifischem Verlust der *Fto* Expression in dopaminergen Neuronen (*Fto*^{ΔDAT}) beobachtet werden. Während dies in ganzkörper-*Fto*-defizienten Mäusen zu verminderten Antworten auf Kokain Stimulation führte, erfuhren *Fto*^{ΔDAT} Mäuse eine erhöhte Sensitivität für die bewegungs- und belohnungsstimulierende Wirkung von Kokain.

Auf molekularer Ebene kodiert das FTO Protein für eine Nukleinsäure Demethylase, die N6-Methyladenosin (m⁶A) von Boten-RNA (mRNA) entfernen kann. Die Analyse von m⁶A Modifizierungen in mRNA *Fto* defizienter Mäuse zeigte, dass FTO *in vivo* als m⁶A Demethylase agiert. Erhöhte Methylierungsmuster konnten allerdings nur in einem Teil aller prinzipiell m⁶A modifizierten Transkripte nachgewiesen werden. Diese Teilmenge hypermethylierter Transkripte beinhaltet zum großen Teil wichtige Komponenten der Zell-Zell und neuronalen Kommunikation. Darüber hinaus befanden sich unter den hypermethylierten Transkripten wichtige

Bestandteile der dopaminergen Signalweiterleitung. Für einige dieser Komponenten (z.B. DRD₃, GIRK₂ und NMDAR₁) wurde eine verminderte Proteinexpression nachgewiesen.

Zusammengefasst erfüllt FTO als m⁶A Demethylase eine wichtige Rolle in der Kontrolle der autoinhibitorischen Rückkopplungsschleife in dopaminergen Neuronen und beeinflusst die Funktion des dopaminergen Systems sowohl auf Netzwerkebene, als auch auf Einzelzellebene. Fehlfunktionen des dopaminergen Systems treten bei verschiedensten Krankheitsbildern auf, wie z.B. Depression, Schizophrenie oder Aufmerksamkeitsdefizit-/Hyperaktivitätsstörung. Daher stellt sich die Frage, ob genomische Variabilität im *FTO* Locus auch mit anderen Erkrankungen als Übergewicht assoziiert ist, beziehungsweise ob den Assoziationen mit verschiedenen Merkmalen krankhaften Übergewichts zum Teil eine Veränderung des dopaminergen Systems zu Grunde liegt.

1 Introduction

1.1 Obesity and obesity associated diseases

Over the last decades the prevalence of obesity has dramatically increased, prompting the World Health Organisation (WHO) to classify obesity as an epidemic of global proportion. Recent estimations suggest that about 1.4 billion people are overweight of which one third is considered obese (source: WHO). This increase in obesity is not only observed in western society, but is also identified as a threat to developing countries [Malik *et al.*, 2013]. Overweight (body mass index (BMI) ≥ 25 kg/m²) and obesity (BMI ≥ 30 kg/m²) are known risk factors for type 2 diabetes mellitus (T2DM), cardiovascular disease and certain forms of cancer, all of which contribute to the increased mortality that is observed for obese patients [Katzmarzyk *et al.*, 2003]. Moreover, even neurodegenerative diseases such as Alzheimer's disease have been associated with obesity [Hildreth *et al.*, 2012]. These comorbidities render obesity one of the biggest challenges to modern society. Obesity not only decreases the individual quality of life, but is also becoming a far reaching socio-economic problem, placing a massive burden on our health systems [Cawley & Meyerhoefer, 2012; Finkelstein *et al.*, 2009]. Thus, a necessity emerged to understand the genetics and molecular mechanisms of body weight regulation and to develop strategies to tackle the progressing obesity epidemic.

1.1.1 Monogenic obesity

Since obesity has moved into focus, the study of severely obese patients has led to the identification of several loss-of-function mutations within the human genome [Farooqi & O'Rahilly, 2006]. These rare cases of monogenic obesity include e.g.

mutations of leptin [Montague *et al.*, 1997], the leptin receptor [Clément *et al.*, 1998], proopiomelanocortin (POMC)[Krude *et al.*, 1998] and melanocortin 4 receptor (MC4R) [Yeo *et al.*, 1998; Farooqi *et al.*, 2003]. Individuals suffering from one of these mutations inevitably face obesity, regardless of environmental factors. Many of these studies have helped to identify critical components of the mechanisms governing energy homeostasis. Some of these patients have even benefited from treatment made available through their diagnosis. Leptin deficient patients, for example, are treated with recombinant leptin, leading to body weight loss and enabling them to lead a normal life [Farooqi *et al.*, 1999].

Monogenic forms of obesity are rare within the population and the frequency of these genomic variations has not changed since the prevalence of obesity is rising [Caballero, 2007]. Hence, rare loss-of-function mutations are not the underlying reason for the steady increase in overweight people observed since the middle of the 20th century.

1.1.2 Polygenic obesity

Current research on the increasing prevalence of obesity in the general population, hence termed common obesity, investigates the influence of environmental factors on energy homeostasis. Our sedentary lifestyle, lack of physical activity and unlimited access to energy rich, highly palatable nutrition promote a misbalance between energy intake and energy expenditure, ultimately leading to weight gain [Swinburn *et al.*, 2011]. Still, considerable variation of BMI is observed in a given population that in general faces the same environmental changes and temptations. Common variations in the human genome are believed to shape the individual susceptibility to environmental factors, thus leading to the apparent divergence of BMI within a population [Maes *et al.*, 1997]. The sum of the variations carried by an individual may therefore define how environmental factors impact on certain features, such as body weight regulation.

In former years, identification of obesity related traits in the human genome

was a laborious task that had to rely on the candidate approach. Genes that were functionally related to body weight regulation were investigated for variations and subsequently tested for associations with body weight [Loos, 2012]. Due to the hypothesis driven approach, however, this method lacked the power to identify yet unknown players in body weight regulation.

Since whole genome sequencing has become affordable, genome wide association studies (GWAS) represent the means to perform hypothesis generating studies. Increasing sample sizes over the years has increased the discovery rate tremendously. In recent years, GWAS helped to identify several common genetic variations that are associated with obesity related traits, regardless of any known or unknown function for these genes [Loos, 2012; Willer *et al.*, 2009; Speliotes *et al.*, 2010]. To date, 52 loci have been associated with BMI, body fat percentage, waist circumference, waist-to-hip ratio and early onset obesity. Some of those were already known to take part in the regulation of energy homeostasis, such as variants near the insulin receptor substrate (IRS) 1 [Kilpeläinen *et al.*, 2011], near MC4R [Loos *et al.*, 2008] or within the brain-derived neurotrophic factor (BDNF) locus [Thorleifsson *et al.*, 2009]. Many of the identified loci, however, have not been known for any association with obesity related traits before [Loos, 2012].

The effect size of each individual genomic variant is relatively small, increasing the body weight per allele by as little as 200 grams [Loos, 2012]. Rather the effect of all variants present in the genome will define each individual's susceptibility to obesity. Thus, not only identifying predisposing loci and their respective molecular function, but also understanding the network of the entirety of genomic variation is important.

1.2 Regulation of body weight

1.2.1 Energy homeostasis

In order to ensure a steady body weight, a process called energy homeostasis ensures that both energy intake and energy expenditure are balanced. Usually, times of excessive binge eating or undernutrition are compensated over the following course of days or weeks to maintain body weight [Schwartz *et al.*, 2000; Schwartz & Porte, 2005]. Malfunction of these regulatory mechanisms favoring increased energy intake and reduced energy expenditure lead to increased body weight and obesity [Schwartz *et al.*, 2000; Schwartz & Porte, 2005].

Over the past decades, several peripheral hormones have been identified that convey the current energy status of the human organism. The anorectic hormone leptin, produced by white adipocytes relative to their lipid content and released into the blood stream, is a measure for the current energy storage of the body [Friedman, 2011, 2010]. While initially administration of recombinant leptin was thought to be a potential treatment for obesity, studies showed that obese patients have high levels of circulating leptin and the body lost its ability to process the signal [Könner & Brüning, 2012; Myers *et al.*, 2008]. The second hormone insulin is released by pancreatic β -cells in response to increasing blood glucose levels after food intake and ensures the uptake of glucose in peripheral organs such as the liver, muscle and adipose tissue [Kahn, 1994; Könner *et al.*, 2009]. Moreover, insulin, like leptin, was found to signal to specific neuronal populations and regulate food intake [Könner *et al.*, 2009; Könner & Brüning, 2012; Belgardt & Brüning, 2010]. A third hormone, the orexigenic ghrelin, is secreted by the stomach and intestine, with levels decreasing after food intake and increasing with food deprivation [Cummings & Overduin, 2007]. Leptin, insulin and ghrelin, are only three examples of hormones involved in energy homeostasis. Jointly, these hormones are the signal infrastructure conveying information about the peripheral energy status to the central nervous system, the master regulator of energy homeostasis

[Schwartz *et al.*, 2000; Könner *et al.*, 2009]. The evaluation of these hormonal signals within the brain then leads to the behavioral outcome. Further investigations showed, that failure of brain circuits to interpret the circulating signals, e.g. insulin and/or leptin resistance, has major impacts on energy homeostasis [Könner & Brüning, 2012].

1.2.2 CNS in regulation of energy homeostasis

Already more than 70 years ago, lesion experiments in rats demonstrated that the hypothalamic area of the brain plays a critical role in the regulation of body weight [Hetherington & Ranson, 1940]. Since then, further refinement of methodology led to the dissection of different nuclei within the hypothalamus in the control of energy homeostasis [Könner *et al.*, 2009; Belgardt & Brüning, 2010; Kleinridders *et al.*, 2009].

The first order neurons of the homeostatic system reside within the mediobasal hypothalamus [Könner *et al.*, 2009; Belgardt & Brüning, 2010]. The close proximity to the blood-brain barrier render the anorexigenic POMC/CART (pro-opiomelanocortin/cocaine and amphetamine regulated transcript) and the orexigenic AgRP/NPY (agouti-related peptide/neuropeptide Y) neurons of the arcuate nucleus (ARC) sensitive to the hormones circulating in the blood stream. Consistently, activity of these neurons is regulated by insulin, leptin, ghrelin and even circulating levels of glucose [Könner *et al.*, 2009; Belgardt & Brüning, 2010]. POMC/CART neurons release α -MSH (α -melanocyte stimulating hormone), a cleavage product of pro-opiomelanocortin, which in turn activates MC₄ receptors on the second order neurons that reside e.g. within the paraventricular nucleus of the hypothalamus (PVN) [Könner *et al.*, 2009]. Activation of those second order neurons in the PVN leads to a decrease in food intake [Balthasar *et al.*, 2005]. Activation of AgRP/NPY neurons on the other hand silences the POMC/CART neurons through γ -aminobutyric acid (GABA) released from AgRP/NPY neuron synapses [Atasoy *et al.*, 2012; Könner *et al.*, 2009; Belgardt & Brüning, 2010]. Moreover, these neurons

release AgRP, which is an inverse agonist of MC₄ receptors, blocking those receptors and thereby preventing α -MSH mediated activation of second order neurons [Könner *et al.*, 2009; Belgardt & Brüning, 2010]. As a result, food intake is increased, while energy expenditure is reduced [Könner *et al.*, 2009; Belgardt & Brüning, 2010].

Additionally, other hypothalamic nuclei feed into the homeostatic control of body weight, such as the ventromedial (VMH), dorsomedial (DMH) and lateral hypothalamic (LH) areas [Belgardt & Brüning, 2010; Könner *et al.*, 2009]. The LH is of special notion, as it represents one possible link of the homeostatic system to other brain areas, such as the dopaminergic midbrain neurons which control the hedonic and reward related behaviours [Sternson, 2013; Berthoud, 2011; Simerly, 2006; Saper *et al.*, 2002]. Orexin, secreted from orexinergic neurons within the LH, has been demonstrated to be a potent mediator of wakefulness in control of sleep/wake cycles in mammals [Sakurai *et al.*, 1998; Harris & Aston-Jones, 2006; Adamantidis *et al.*, 2007; Tsunematsu *et al.*, 2011]. Consistently, leptin inhibits orexinergic neurons, thus allowing periods of rest and sleep in the satiated state [Yamanaka *et al.*, 2003]. Neurons of the LH project onto midbrain dopaminergic neurons and release orexin, which subsequently alters dopaminergic neuron function via orexin receptors [Sharf *et al.*, 2010; Borgland *et al.*, 2006]. Hence, the LH represents one possible interface of homeostatic and hedonic regulation of food intake. Further evidence points towards projections from the hypothalamus (AgRP/NPY neurons) directly to DA neurons [Palmiter, 2012]. Conceptually, the ventral striatum (nucleus accumbens, NAc), may represent the integrative center, processing information from the energy sensing hypothalamic nuclei, from the midbrain that conveys rewarding aspects of food intake and from higher brain centers that feed experience and decision making into the equation. Consolidation of all inputs will then lead to a subsequent behavioural outcome that may lead to food intake [Simerly, 2006].

1.3 The dopaminergic system

1.3.1 Dopamine and dopaminergic neurons

Dopamine (DA) belongs to the family of catecholamine neurotransmitters and as such is a precursor of norepinephrine and epinephrine [Björklund, 2007]. Initially not regarded as such, dopamine is an independent neurotransmitter involved in important physiological processes [Carlsson *et al.*, 1958]. The total number of dopaminergic neurons (DA neurons) increases in mammals according to the growth of cortical and striatal regions, with mice having approximately 20,000 to 30,000 DA neurons, monkeys 160,000 to 320,000 and humans 400,000 to 600,000 [Björklund, 2007]. About 70 to 75 % of these neurons reside within the midbrain in the ventral tegmental area (VTA), substantia nigra (SN) and retrorubral field, while the remaining dopamine neurons are found, for example, within the hypothalamus and olfactory bulbs [Björklund, 2007; Bentivoglio & Morelli, 2005]. Opposing the relatively low number of dopamine neurons is the fact that each dopaminergic neuron may have synaptic contact to 300-400 neurons, placing the dopaminergic pathways among the most prominent innervating circuits in the brain [Schultz, 1998].

Classically, midbrain dopaminergic neurons have been categorized into three different pathways. First, the nigrostriatal pathway of SN dopamine neurons projecting to the dorsal striatum (caudate putamen, CPu). Second, the mesolimbic pathway of VTA dopamine neurons projecting to the ventral striatum (nucleus accumbens, NAc), the amygdala and olfactory tubercle. Third and finally, the mesocortical pathway of dopamine neurons projecting to cortical areas [Björklund, 2007]. Novel tracing methods, however, question this view of dopaminergic projections and suggest a more complex projection pattern and cross-projections along these classical pathways [Björklund, 2007].

Dopamine has been implicated in a variety of processes including voluntary movement, reward, attention, motivation, sleep, memory and learning [Iversen &

Iversen, 2007; Beaulieu & Gainetdinov, 2011; Björklund, 2007; Di Chiara, 2005; Dunnett, 2005]. Loss of striatal dopamine neuron innervation represents the hallmark of Parkinson's disease, moving dopaminergic function into the focus of Parkinson's treatment [Iversen & Iversen, 2007; Sulzer, 2007].

1.3.2 Dopamine receptors and dopamine signaling

Five different dopamine receptors belonging to two different classes are known. The D₁-like dopamine receptors, including dopamine receptors D₁ (DRD₁) and D₅ (DRD₅), and the D₂-like receptors, including dopamine receptors D₂ (DRD₂), D₃ (DRD₃) and D₄ (DRD₄) [Beaulieu & Gainetdinov, 2011]. Dopamine receptors are widely expressed within the brain, but also in peripheral tissues, such as the adrenal glands and sympathetic ganglia. DRD₁ is mainly expressed within the ventral and dorsal striatum, the substantia nigra, amygdala and olfactory bulb and represents the major receptor of the direct basal ganglia pathway [Beaulieu & Gainetdinov, 2011]. DRD₂s are the main receptors involved in the indirect basal ganglia pathway and are highly expressed in dorsal and ventral striatum, as well as the olfactory tubercle [Beaulieu & Gainetdinov, 2011]. DRD₃s are mainly found within the ventral striatum (NAc) and the olfactory tubercle. DRD₂ and DRD₃, however, are the only receptors that are also expressed presynaptically in the SN and VTA [Beaulieu & Gainetdinov, 2011]. D₄ and D₅ receptors exhibit the lowest expression of all dopamine receptors and are found within a variety of areas, including cortical areas, hippocampus, hypothalamus and midbrain [Beaulieu & Gainetdinov, 2011].

Genes of the DRD₁ and DRD₅ do not have introns and thus these receptors are not expressed in different splice isoforms [Beaulieu & Gainetdinov, 2011]. DRD₂, DRD₃ and DRD₄, however, have intronic regions in their respective genes and several isoforms have been described, the most prominent ones being the DRD₂S (short isoform), that shows preferentially presynaptic expression, and the DRD₂L (long isoform), that is predominantly found postsynaptically [De Mei *et al.*, 2009].

Dopamine receptors belong to the family of G protein-coupled receptors and as such their main target is the regulation of the adenylyl cyclase (AC) and cAMP production [Hyman *et al.*, 2006; Beaulieu & Gainetdinov, 2011]. Whereas D2-like receptors inhibit the AC via $G\alpha_{i/o}$, D1-like receptors increase the activity of AC via $G\alpha_{s/olf}$ and thus increase cAMP levels. As a result of G protein signaling, dopamine receptors modulate activity of important signaling mediators, such as protein kinase A (PKA), phospholipase C (PKC) and protein kinase B (AKT) (see Figure 1.1) [Hyman *et al.*, 2006; Beaulieu & Gainetdinov, 2011].

Despite modulation of AC activity, several other signaling modalities have been reported for dopamine receptors. Both DRD5 and DRD1 have been implicated in regulation of phospholipase C (PLC) via $G\alpha_q$, potentially linking dopamine signaling to intracellular calcium mobilization [Beaulieu & Gainetdinov, 2011]. Whether this connection is mainly through DRD5 or DRD1 (or DRD1:DRD2 heterodimers), however, remains to be elucidated. D2-like receptors, on the other hand, have been demonstrated to activate PLC via $G\beta\gamma$, while inhibiting L- and N-type calcium channels through the same G protein cascade [Beaulieu & Gainetdinov, 2011]. Moreover, D2-like receptors regulate neuronal activity through $G\beta\gamma$ mediated activation of G protein-coupled inwardly rectifying potassium channels (GIRKs), which hyperpolarize and hence inhibit neurons (Figure 1.1) [Lüscher & Slesinger, 2010]. Following activation by dopamine, dopamine receptor signaling may be terminated through phosphorylation by G protein-coupled receptor kinases (GRKs) and subsequent internalization. Phosphorylation, however, may also promote a late signaling event in D2-like receptors that inhibits protein kinase B (AKT/PKB) in a β -arrestin 2 and protein phosphatase 2A (PP2A) dependent manner (Figure 1.1) [Beaulieu & Gainetdinov, 2011].

1.3.3 Dopamine and reward related behaviors

One of the primary functions of the dopaminergic system is the modulation of behavioral responses [Pandit *et al.*, 2011; Volkow *et al.*, 2013; Wise, 2013]. A major

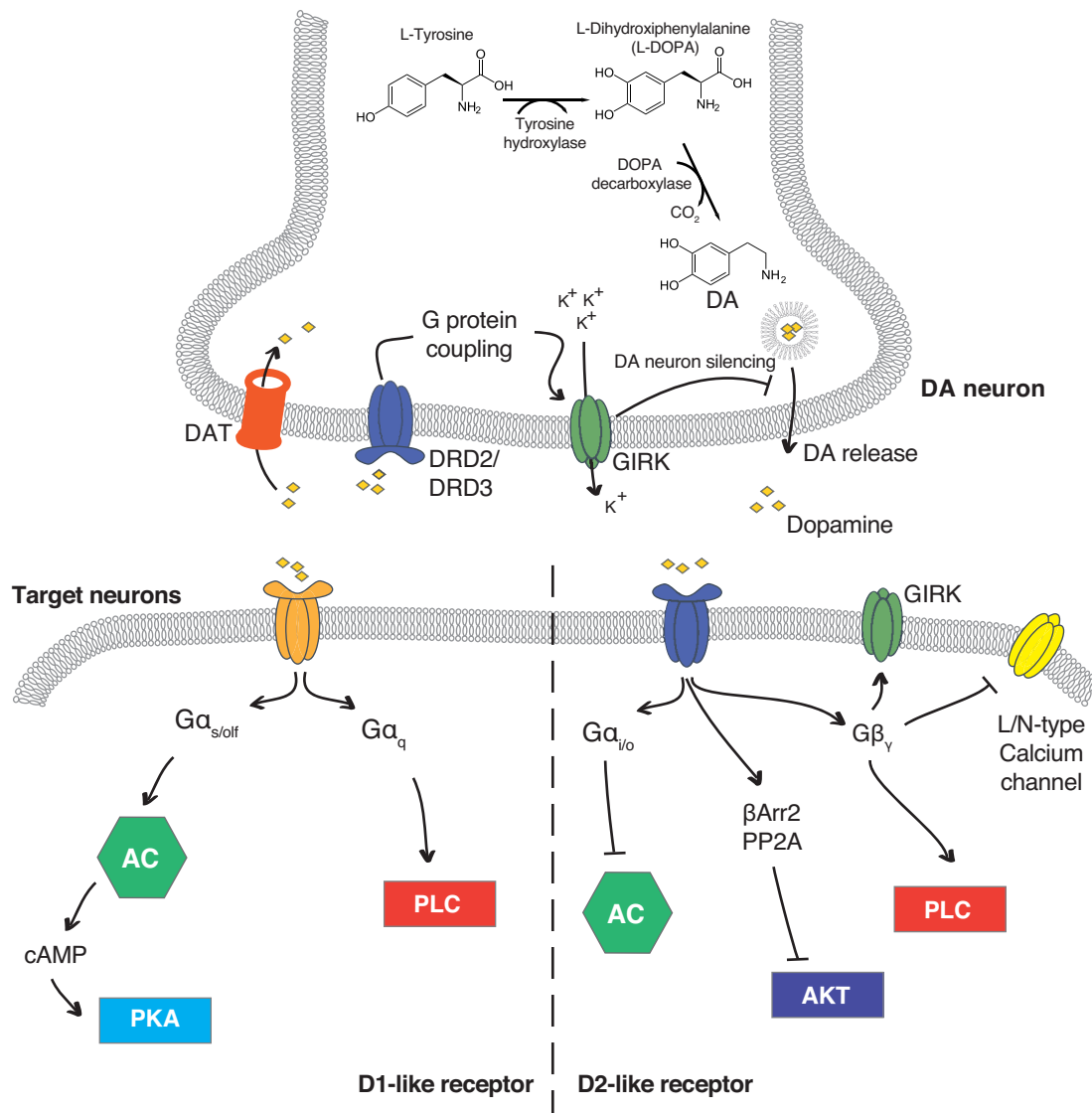


Figure 1.1: **Pre- and postsynaptic dopamine receptor signaling.**

Dopamine is synthesized from tyrosine via the tyrosine hydroxylase and subsequent decarboxylation via the DOPA decarboxylase. Dopamine receptors are divided into two groups, the D₁-like receptors (DRD₁ and DRD₅) and the D₂-like receptors (DRD₂, DRD₃ and DRD₄). While D₁-like receptors are only present postsynaptically on dopamine target neurons, DRD₂ and DRD₃ receptors are also found presynaptically on dopamine neurons. Dopamine receptors are G protein-coupled receptors, that are able to trigger several responses. DRD₁-like receptors positively regulate the adenylyl cyclase (AC) via G $\alpha_{s/olf}$ leading to increasing levels of cAMP and protein kinase A (PKA) activity. Moreover, D₁-like receptors phospholipase C (PLC) activity is increased via G α_q . D₂-like receptors, on the other hand, negatively regulate AC activity (via G $\alpha_{i/o}$) and AKT (in a β -arrestin 2 (β Arr2) and protein phosphatase 2A (PP2A) dependent manner). Furthermore, coupling to G $\beta\gamma$ positively regulates PLC and may lead to opening of G protein-coupled inwardly rectifying potassium channels (GIRK), while inhibiting L- and N-type calcium channels. Presynaptic coupling of D₂-like receptors to GIRKs has been found to play an important role in the dopamine autoreceptor feedback loop. Termination of dopaminergic signaling is finally achieved through reuptake of dopamine via the dopamine transporter expressed on dopamine neurons.

aspect of this function is encoding the motivational value, being rewarding or aversive, of substances, such as drugs and food, or behaviors like sexual reproduction [Kenny, 2011; Kelley & Berridge, 2002]. As a consequence, dopamine signaling adjusts the probability for a repetition of a certain behavior, being it e.g. drug abuse or highly palatable food intake [Schultz, 2010; Volkow *et al.*, 2013; Schultz, 2007]. Hence, underlying these alterations is a learning process that depends on reinforcing experiences that describe the 'liking' of the performed behaviors [Iversen & Iversen, 2007; Schultz, 2007].

First evidence for the involvement of dopaminergic pathways in reward related motivation stem from self stimulation studies. Electrical stimulation of dopaminergic afferents along the medial forebrain bundle, the LH that is connecting to the midbrain dopamine neurons or dopamine neurons themselves (VTA) causes a favorable sensation that subsequently leads to increasing self stimulation in both rodents and humans [Wise, 2013; Volkow *et al.*, 2013]. Subsequent studies established the role of the dopaminergic system in a complex system of neuronal circuits shaping motivation and reinforcement of behaviors [Schultz, 2007; Pandit *et al.*, 2011].

To encode the motivational value, dopamine neurons exhibit episodes of burst firing that subsequently lead to increased dopamine levels in the synaptic cleft [Schultz, 2010; Overton & Clark, 1997]. These burst firing events were observed in response to motivating stimuli, such as ingestion of sweet liquid in monkeys [Schultz, 2010, 1998]. Moreover, these rewarding stimuli have been successfully coupled to visual or auditory stimuli that, when preceding the actual reward, elicit anticipatory dopamine neuron burst firing [Schultz, 1998]. Absence of the rewarding stimuli following the conditioned stimulus, however, leads to a paucity in dopamine neuron firing, hence encoding the prediction error of the missing motivational stimulus and adjusting behavior [Schultz, 1998]. The very same mechanism is furthermore hypothesized to underly the drug taking response and subsequent craving and seeking for drugs, hallmarks of drug addiction [Pandit *et al.*, 2011;

Volkow *et al.*, 2013]. Moreover, many addictive drugs directly influence the dopaminergic system. Cocaine, for example, blocks the dopamine transporter (DAT) expressed on dopaminergic neurons and prevents re-uptake of dopamine from the synaptic cleft and thus attenuates DA signaling shut down [Hyman *et al.*, 2006]. Similarly, amphetamine potentiates dopamine signaling through increasing DA release from dopaminergic synapses [Hyman *et al.*, 2006]. Despite drug abuse and addiction, malfunction of the dopaminergic circuitry has been implicated in conditions such as attention deficit/hyperactivity syndrome (ADHD) [Swanson *et al.*, 2007], Tourette's syndrome [McNaught & Mink, 2011], schizophrenia [Beaulieu & Gainetdinov, 2011; Iversen & Iversen, 2007], bipolar disorder and major depression [Beaulieu & Gainetdinov, 2011].

Dopamine signaling is not causing a fast postsynaptic response, but rather modulates the properties of postsynaptic neurons [Kauer & Malenka, 2007; Hyman *et al.*, 2006]. Thus, dopamine is instrumental in synaptic plasticity and adaptations of synaptic transmission, thought to be the underlying mechanism of learning processes [Kauer & Malenka, 2007].

1.3.4 Dopamine and obesity

The dopaminergic system is "the brain's natural reinforcement system" [Salamone & Correa, 2002]. As such, it is believed that the motivational value of natural rewarding stimuli, such as food and the behavior leading to the consumption of food, are encoded in the dopaminergic system [Pandit *et al.*, 2011; Volkow *et al.*, 2013]. From an evolutionary perspective, reinforcing food intake was ensuring the ability to overeat in times of plenty to prepare for times of need [Pandit *et al.*, 2011; Schwartz *et al.*, 2003]. In fact, food has been demonstrated in some cases to be preferred over drugs [Lenoir *et al.*, 2007]. Several studies suggest common alterations of the dopaminergic circuitry in addiction and obesity [Volkow *et al.*, 2013; Wise, 2013; Bello & Hajnal, 2010; Kenny, 2011].

Drugs of abuse increase extra synaptic levels of dopamine [Kauer & Malenka,

2007; Di Chiara & Imperato, 1988]. In the same manner, eating and drinking cause elevated levels of dopamine in the ventral and dorsal striatum [Yoshida *et al.*, 1992; Small *et al.*, 2003]. Both pharmacological dopamine depletion, as well as genetically engineered DA-deficiency in mice causes hypophagia [Salamone *et al.*, 1993; Zhou & Palmiter, 1995]. Moreover, obesity and chronic drug abuse reduce dopamine type 2 receptor (DRD2) availability in human striatum [Volkow *et al.*, 2002; Wang *et al.*, 2001]. Consistently, DRD2 levels are reduced in obese rats [Hamdi *et al.*, 1992; Johnson & Kenny, 2010]. Knock-down of striatal DRD2s, on the other hand, caused obsessive food seeking in rats [Johnson & Kenny, 2010]. Chronic exposure to a high fat diet in rats increases the threshold for electric self stimulation in the LH [Johnson & Kenny, 2010]. The very same is observed in rats after prolonged cocaine treatment [Ahmed *et al.*, 2002]. Moreover, high fat diet exposure dampens the preference for amphetamine cues and lowers the operant response to sucrose [Davis *et al.*, 2008]. Consistently, human obesity has been shown to decrease the lifetime risk for drug abuse [Simon *et al.*, 2006]. Vice versa, food restriction was demonstrated to increase the sensitivity for drugs and to reduce the threshold for lateral hypothalamic self administration [Carroll *et al.*, 1979; Carroll & Meisch, 1981; Davis *et al.*, 2010; Abrahamsen *et al.*, 1995].

During food restriction, levels of endocrine hormones change. In case of leptin and insulin, food deprivation decreases circulating levels [Könner *et al.*, 2009]. Food restriction has been demonstrated to decrease *Dat* mRNA and activity in the striatum, whereas centrally applied insulin increases *Dat* mRNA levels in the midbrain [Patterson *et al.*, 1998; Figlewicz *et al.*, 1994]. Both leptin and insulin receptors are expressed on dopaminergic neurons and both insulin and leptin potently modulate dopamine neuron activity [Figlewicz *et al.*, 2003; Fulton *et al.*, 2006; Könner *et al.*, 2011]. Intracerebroventricular (ICV) injection of leptin inhibited dopamine neuron firing, reducing food intake and dopamine levels in the ventral striatum. Knock down of midbrain leptin receptors, on the other hand, increases food intake and the sensitivity to sucrose and highly palatable food [Hommel *et al.*, 2006; Krügel

et al., 2003]. Consistently, ICV leptin administration is able to modulate LH self stimulation [Fulton *et al.*, 2000] and both insulin and leptin decrease sucrose self stimulation [Figlewicz *et al.*, 2006].

In humans, obesity causes increased brain activity in response to feeding associated cues [Volkow *et al.*, 2008]. The same is observed in leptin deficient patients, however, leptin treatment is able to reduce the increased brain activity, as well as food liking and caloric intake [Farooqi *et al.*, 2007]. Despite insulin and leptin, several other hormones and neuropeptides have been linked to drug abuse and reward related behavior, including orexin, oxytocin, galanin, melanocortin, neuropeptide Y (NPY) and peptide YY (PYY), further supporting the connections of homeostatic and hedonic feeding control [Volkow *et al.*, 2013].

1.3.5 DRD2/DRD3 autoreceptor feedback loop

To regulate dopaminergic synaptic transmission, DA neurons feature an autoinhibitory feedback loop that terminates dopamine release [Beaulieu & Gainetdinov, 2011; De Mei *et al.*, 2009; Joseph *et al.*, 2002; Sibley, 1999; Missale *et al.*, 1998]. Both DRD2 and DRD3, but not D1-like receptors, are presynaptically expressed and were shown to couple to GIRKs (Figure 1.1) [De Mei *et al.*, 2009; Beaulieu & Gainetdinov, 2011; Sibley, 1999; Mercuri *et al.*, 1997]. Upon dopamine release opening of these channels leads to an inhibition of firing and thus termination of dopamine release from DA neurons [Paladini *et al.*, 2003]. Findings for presynaptic D3 receptors, however, are in part controversial, showing potent inhibition for VTA, but not SN dopamine neurons [Davila *et al.*, 2003; Lejeune & Millan, 1995; Kuzhikandathil *et al.*, 1998; Gainetdinov *et al.*, 1996; Joseph *et al.*, 2002]. In addition to the regulation of dopamine neuron firing, presynaptic dopamine receptors are implicated in the direct regulation of dopamine synthesis [Wolf & Roth, 1990; Anzalone *et al.*, 2012; Joseph *et al.*, 2002].

In mice, loss of DRD2 autoreceptors causes cocaine supersensitivity and increases motivation for reward, while body weight and food intake remain unaltered [Bello

et al., 2011]. In humans, reduced dopamine autoreceptor availability is associated with increased impulsivity [Buckholtz *et al.*, 2010]. Taken together, dopamine autoreceptor function is likely to play a critical role in the proper function of the dopaminergic system and may lead to elevated DA neuron excitability and aberrant DA release. Hence, malfunction of the autoinhibitory feedback loop may impinge on complex human behavior, such as impulsivity, reinforcement or drug abuse [Bello *et al.*, 2011; Buckholtz *et al.*, 2010].

1.4 The fat mass and obesity-associated protein (*FTO*)

1.4.1 Genome wide association studies

Associations with obesity-related traits

First identified as one of the genes deleted in the *fused toes (Ft)* mouse mutant [Peters *et al.*, 1999; van der Hoeven *et al.*, 1994], general interest in *FTO* (fat mass and obesity-associated protein) was triggered through the robust association of a single nucleotide polymorphism (SNP, rs9939609) within the *FTO* gene with obesity-related traits (Figure 1.2 a) [Frayling *et al.*, 2007; Dina *et al.*, 2007; Scuteri *et al.*, 2007]. These findings, to date, have been replicated in both adults and children in independent populations of various, though not all, ethnicities [den Hoed *et al.*, 2009; Cecil *et al.*, 2008; Fang *et al.*, 2010; Grant *et al.*, 2008; Bollepalli *et al.*, 2010; Liu *et al.*, 2010; Adeyemo *et al.*, 2010; Chang *et al.*, 2008; Tan *et al.*, 2008; Croteau-Chonka *et al.*, 2011; Yajnik *et al.*, 2009]. While initially *FTO* was associated with changes in BMI, subsequent studies with increased sample size confirmed the associations not only for BMI, but additionally for e.g. body fat percentage, waist circumference and obesity risk [Loos, 2012].

To date, the majority of *FTO* single nucleotide polymorphisms associated with obesity are situated in the first intron of the human gene, forming a cluster of SNPs that predisposes to obesity (Figure 1.2 a) [Willer *et al.*, 2009; Jacobsson *et al.*, 2012]. The overall effect size for the human *FTO* obesity-associated risk alleles,

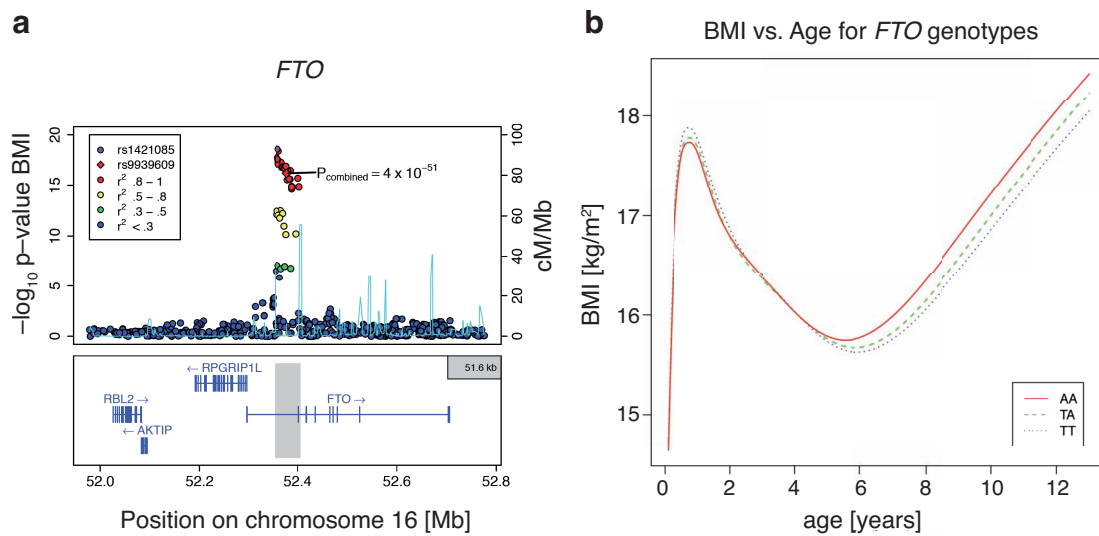


Figure 1.2: **Genome wide association studies link *FTO* to obesity** (a) A cluster of single nucleotide polymorphisms (SNPs) within the first intron of the human *FTO* gene is significantly associated with increased BMI. Upstream and in opposite orientation of the *FTO* gene, the ciliary gene *RPGRIP1L* is situated (Figure adapted from Willer *et al.* [2009]). (b) Before adiposity rebound at the age of 5.5 years in children, an inverse association between *FTO* genetic variation and BMI is detected. After the adiposity rebound, the correlation reverses and *FTO* SNPs are associated with increased BMI (A = obesity risk allele, T = non-obesity risk allele; Figure adapted from Sovio *et al.* [2011]).

however, is relatively small. One copy of the risk allele may account for as much as 1.5 kg increased body mass or approximately 0.4 kg/m² higher body mass index [Frayling *et al.*, 2007]. This, however, renders the *FTO* SNPs not only the genomic variants with the strongest obesity association, but also the variant with the biggest effect size [Loos, 2012].

Interestingly, the positive association of *FTO* genomic variation develops at the age of 5.5 years and is detectable in adults and elderly (Figure 1.2 b) [Sovio *et al.*, 2011; Frayling *et al.*, 2007; Dina *et al.*, 2007; Scuteri *et al.*, 2007]. Before the age of 2.5 years, however, an inverse association of *FTO* genotype and BMI is detected [Sovio *et al.*, 2011]. The reversal of the relationship seems to coincide with the adiposity rebound, the time point at which the BMI of children starts to steadily increase after a period of decline from 2 to 5 years of age. Interestingly, each copy of the rs9939609 risk-allele accelerates development by 2.4 %, resulting in a shift of adiposity rebound in children.

Influence on energy intake

Additional assessment of eating behaviour revealed an increased energy intake for *FTO* risk-allele carriers in comparison to controls [Cecil *et al.*, 2008; Timpson *et al.*, 2008; Speakman *et al.*, 2008; Wardle *et al.*, 2009; Haupt *et al.*, 2009], possibly due to an increase in fat consumption [Timpson *et al.*, 2008; Tanofsky-Kraff *et al.*, 2009]. At the point of adiposity rebound (age 4-5) that coincides with the beginning of the positive correlation of *FTO* variants with BMI, children with the obesity risk-alleles already show increased consumption of highly palatable food [Wardle *et al.*, 2009]. Hence, this shift in food preference may represent, at least partly, the underlying mechanism leading to increased BMIs observed later in life. Further studies assessing the eating behaviour of children support this notion, reporting increased food responsiveness (ages 3-4, questionnaire example: "Even if my child is full, he/she finds room to eat his/her favourite food") [Velders *et al.*, 2012], impaired satiety response (age 8-11 years; questionnaire example: "My child cannot eat a meal if he/she has had a snack just before.") [Wardle *et al.*, 2008], loss of control over eating (ages 6-19) [Tanofsky-Kraff *et al.*, 2009] and lower postprandial responses in hungry or satiated state [den Hoed *et al.*, 2009; Karra *et al.*, 2013].

Further attempts to link *FTO* variants to changes in energy expenditure have been inconclusive so far. Both decreased, as well as increased energy expenditure have been reported [Keller *et al.*, 2011; Jonsson & Franks, 2009]. The majority of studies, however, failed to find any association between *FTO* genotypes and energy expenditure [Speakman *et al.*, 2008; Goossens *et al.*, 2009; Hakanen *et al.*, 2009; Haupt *et al.*, 2009; Berentzen *et al.*, 2008]. On the contrary, physical activity attenuates the impact of *FTO* genotypes on BMI [Vimalaswaran *et al.*, 2009; Kilpelainen *et al.*, 2011].

Non obesity-related associations

Despite the robust association with obesity-related traits, *FTO* SNPs have recently been associated with non obesity-related conditions. Some of these associations, however, may indirectly impinge on energy intake. Decreased total consumption of

alcohol (beer and spirits) independently of BMI is observed for rs9939609 risk-allele carriers, with the consumption of larger amounts distributed over fewer occasions as compared to controls [Sobczyk-Kopciol *et al.*, 2011]. Correspondingly, the obesity risk-allele was inversely correlated with alcohol dependency. Moreover, smokers amongst obesity risk-allele carriers started tobacco consumption later in life and smoke less cigarettes during times of heavy smoking [Sobczyk-Kopciol *et al.*, 2011].

Both rs9930609 and rs8050136 *FTO* SNPs are linked to attention-deficit/ hyperactivity syndrome (ADHD) [Velders *et al.*, 2012; Choudhry *et al.*, 2013]. Despite the fact that unmedicated ADHD is associated with increasing risk of childhood obesity [Waring *et al.*, 2008], these *FTO* variants are inversely correlated with ADHD independent of BMI. Independent of the assessed ADHD symptoms, rs9930609 carriers furthermore exhibited improved emotional control and increased food responsiveness [Velders *et al.*, 2012].

First associations between several *FTO* genomic variations and major depressive disorder described the modifying effects of this psychiatric disease on the *FTO* dependent differences in BMI [Rivera *et al.*, 2012]. Subsequently, the inverse relation between depression and the rs9930609 *FTO* SNP was demonstrated [Samaan *et al.*, 2012]. Since depression is known to correlate positively with obesity [Pine *et al.*, 2001; Dockray *et al.*, 2009], this inverse association is surprising. These findings suggest a protective effect of the *FTO* obesity risk-alleles for major depressive disorder, with each copy of the allele decreasing the risk to develop depression by approximately 8% [Samaan *et al.*, 2012].

Despite psychiatric disorders that manifest early in life, *FTO* genomic variation was furthermore linked to aging-associated cognitive decline. Reduced verbal fluency is observed for obese male homozygous carriers of the obesity associated rs9939609 'A' allele [Benedict *et al.*, 2011]. Normal weight SNP carriers, as well as normal and overweight non-carriers, however, retain their verbal capabilities. Correspondingly, elderly subjects in treatment for cardiovascular disease and positive for the rs8050136 risk-allele perform worse in a memory performance test (Califor-

nia Verbal Learning Test) [Alosco *et al.*, 2013]. Cognitive decline for *FTO* genotypes was further confirmed, independent of age, gender, BMI or diabetes [Bressler *et al.*, 2013].

Dementia and Alzheimer's disease are additional aging-associated diseases that are linked to genotypic variation of the *FTO* gene. Carrying two copies of the rs9930609 obesity risk-allele increases the risk to develop dementia and Alzheimer's, with no influence of physical activity, cardiovascular disease, BMI or diabetes on this association [Keller *et al.*, 2011]. Strikingly, the risk for dementia and Alzheimer's is almost triplicated by an interaction of *FTO* and apolipoprotein E (APOE) ϵ_4 risk alleles. In line with these findings, healthy elderly rs3751812 SNP carriers exhibit structural brain changes with an average reduction in brain volume of 8% (frontal lobes) to 12% (occipital lobes) [Ho *et al.*, 2010].

Finally, the mortality rate was shown to be increased for rs9939609 SNP carriers, independent of obesity [Zimmermann *et al.*, 2009]. Non carriers exhibit a 42% reduced mortality rate, when compared to risk-allele carriers. Of note, diseases of the nervous system were only found in risk-allele carriers as a cause of death. These fatalities are, however, not the underlying reason for the overall elevated mortality rate of risk-allele carriers.

Functional aspects of *FTO* single nucleotide polymorphisms

To date, the functional outcome of the genetic variation found within human *FTO* is unknown. In fact, it still remains elusive, whether *FTO* is affected by these variations at all. So far, only few studies tried to address the outcome of single nucleotide polymorphism in the first intron of the *FTO* gene on its expression and found increased *FTO* expression in peripheral blood cells and fibroblasts of rs9939609 risk allele carriers [Karra *et al.*, 2013; Berulava & Horsthemke, 2010]. Due to the small sample size of these studies and the questionable functional relevance of *FTO* expression in peripheral blood cells and fibroblasts, however, these results are not compelling with respect to the biological function of *FTO*.

Orientated in the opposite direction and close to the first exon of *FTO*, lies

the transcriptional start site of the *RPGRIP1L* gene (retinitis pigmentosa GTPase regulator-interacting protein-1 like), that may as well be affected by the SNPs situated within this chromosomal area [Jacobsson *et al.*, 2012; Stratigopoulos *et al.*, 2008]. Two putative CUX1 (CUTL1; cut-like homeobox 1) binding sites were found within the SNP cluster, potentially leading to a transcriptional co-regulation of *FTO* and *RPGRIP1L* [Frayling *et al.*, 2007; Stratigopoulos *et al.*, 2008, 2011]. Binding of the p110 CUX1 isoform was further demonstrated to increase the activity of human *FTO* and *RPGRIP1L* minimal promoters, whereas the p200 isoform decreased the activity [Stratigopoulos *et al.*, 2011]. Additional evidence gathered in rodent cell culture experiments points to a role of *FTO* and *RPGRIP1L* in leptin receptor clustering at the ciliary pole. Thus, through increasing *Fto* and *Rpgrip1l* expression, *Cux1* may increase leptin receptor trafficking to the ciliary pole and increase leptin sensitivity [Stratigopoulos *et al.*, 2011]. As a result, *FTO* and *RPGRIP1L* may alter food intake by affecting leptin sensitivity. Interestingly, the binding affinity of the promoter activity increasing p110 isoform was found to be decreased in carriers of the obesity-associated rs8050136 SNP. The potential decrease in *FTO* and *RPGRIP1L* expression may in turn lead to a decreased leptin sensitivity, which could be the underlying reason for the increased energy intake observed in obesity risk-allele carriers [Stratigopoulos *et al.*, 2011]. How *FTO* and/or *RPGRIP1L* would affect leptin receptor clustering is not known in detail. *RPGRIP1L*, however, is part of the basal cilium [Vierkotten *et al.*, 2007; Delous *et al.*, 2007] and is thus a potential link to ciliopathies, some of which are known to be related to obesity, such as the Alström and Bardet Biedl syndromes [Berbari *et al.*, 2013; Heydet *et al.*, 2013; Girard & Petrovsky, 2011; Ansley *et al.*, 2003; Davenport *et al.*, 2007]. Conversely, though, *Ftm*-deficient mice (the ortholog of *RPGRIP1L*) have renal, hepatic and brain abnormalities and no body weight phenotype [Delous *et al.*, 2007]. Moreover, patients with the Joubert and Meckel syndromes, both caused by loss-of-function mutations in *RPGRIP1L*, are not obese, but suffer from brain and renal malformations [Devuyst & Arnould, 2008]. Hence, the proposed co-regulatory function of

both FTO and RPGRIP1L in leptin receptor clustering at the ciliary pole demand further investigation, to identify the underlying molecular mechanisms.

1.4.2 Human FTO phenotypes

Loss-of-function mutations

The importance of a functional FTO protein for the human organism was indicated by the analysis of a rare loss-of-function mutation in the genomic sequence of *FTO* in a palestinian arab family [Boissel *et al.*, 2009]. The mutation, leading to an amino acid substitution at position 316 of the FTO protein (arginine to glutamine, R316Q), most likely impairs the interaction of FTO with the cosubstrate 2-oxoglutarate and thus renders the protein non-functional. As a result, all of the eight examined patients born with the autosomal recessive mutation died before the age of 3 while suffering from a severe phenotype, characterized by postnatal growth retardation, microcephaly, brain malformations, severe psychomotor delay, functional brain deficits, facial malformations and cardiac deficits [Boissel *et al.*, 2009]. Both, cognitive defects and changes in brain structure are also observed in carriers of the human obesity risk-alleles, however, they do not reach the severity of the *FTO*-deficient patients [Ho *et al.*, 2010; Benedict *et al.*, 2011].

FTO trisomy

In contrast to the aforementioned loss-of-function mutation, genomic triplications (trisomies) including the *FTO* gene show the other end of altered gene dosage. Only few cases of partial trisomies of the human chromosome 16q are known so far. Interestingly however, these cases share some phenotypic characteristics including obesity, learning difficulties and aggressive behaviour [Barber *et al.*, 2006; van den Berg *et al.*, 2010]. Due to the fact that the triplications of the proximal arm of chromosome 16 include more than just one gene these observations cannot be unambiguously attributed to *FTO*. Moreover, not all of the investigated patients exhibited for example obesity [Barber *et al.*, 2006].

1.4.3 Murine *Fto* studies

Fto deficiency

Triggered by the growing interest in FTO and its function in regulation of body weight, mouse models were employed to investigate the role of murine FTO in energy homeostasis. Germline deletion of FTO through deletion of exons 2 and 3 of the murine *Fto* gene causes severe defects. *Fto*-deficient mice exhibit postnatal growth retardation accompanied by a 50% reduction in survival rate [Fischer *et al.*, 2009]. Furthermore, *Fto*-deficient mice have both reduced lean and fat mass compared to wildtype littermates, caused by increased energy expenditure and increased systemic sympathetic tone and despite reduced home cage activity and relative hyperphagia. These characteristics, are at least partly in line with human FTO-deficiency [Boissel *et al.*, 2009], demonstrating again the importance of functional FTO protein for mammalian organisms. Notably, heterozygous loss of FTO renders mice tolerant to high fat feeding, while severe defects are rescued by one functional *Fto* allele [Fischer *et al.*, 2009]. Recently, these findings were confirmed for the germline deletion of exon 3 in a conditional mouse model [McMurray *et al.*, 2013]. Furthermore, the conditional model enabled the adult onset, global FTO deletion in mice through usage of a tamoxifen inducible Cre-recombinase (Cre-ER). Since FTO expression was only altered after 6 weeks of age, these mice overcame the postnatal growth retardation and premature death of germline FTO deletion. 3 weeks after tamoxifen treatment, adult onset *Fto*-deficient mice start losing weight, mainly due to a loss of lean mass possibly caused by increased protein utilization [McMurray *et al.*, 2013]. During the course of the following weeks, this initial loss of weight was compensated by an increase in fat mass, despite any changes in absolute food intake or energy expenditure.

Fto overexpression

To this end, the exact function of the single nucleotide polymorphisms in the human FTO gene are not known. Two studies, however, showed increased FTO

mRNA expression in peripheral blood cells of homozygous rs9939609 risk-allele carriers suggesting that *FTO* genomic variation may cause increased *FTO* expression [Karra *et al.*, 2013; Berulava & Horsthemke, 2010].

In mice, global overexpression of *FTO* causes obesity in a dose dependent manner [Church *et al.*, 2010]. Both on normal chow as well as on high fat diet, these mice have an increased body weight and fat mass. Since no changes in energy expenditure or locomotor activity are detected, the observed elevated food intake is the most probable cause for the body weight changes [Church *et al.*, 2010]. The increase in food intake in those mice is in line with the reported alterations of energy intake in human *FTO* variants, further supporting the notion that human variation is associated with increased *FTO* expression or activity.

Peripheral tissue function

FTO is expressed in peripheral tissues [Gerken *et al.*, 2007; Frayling *et al.*, 2007; Stratigopoulos *et al.*, 2008]. To date, however, studies on peripheral *FTO* function are scarce. In a mouse model of reduced *FTO* function (point mutation I367F), gene expression analysis of white adipose tissue (WAT) revealed the downregulation of several genes involved in inflammation, while multiple genes clustering with the control of fat metabolism were found to be deregulated [Church *et al.*, 2009]. Several genes with known function in fatty acid metabolism, as well as carbohydrate metabolism were upregulated in muscle of *FTO*^{I367F} animals. The observed gene expression changes may be related to some of the phenotypic observations for this mouse model, such as increased lean mass, reduced fat mass and changes in metabolic rate. Cause and effect, as well as the connection between *FTO* enzymatic function and expression changes, however, remain unanswered [Church *et al.*, 2009].

In human visceral and subcutaneous adipose tissue, *FTO* mRNA levels inversely correlate with body mass index and age [Kloeting *et al.*, 2008]. Moreover, *FTO* mRNA expression is downregulated during human adipocyte differentiation [Tews *et al.*, 2011]. Furthermore, a reduced lipolytic activity was reported for female

rs9939609 risk-allele carriers *in vivo* and *in vitro* [Wåhlén *et al.*, 2008].

Recently, a reduced *de novo* lipogenesis was observed for human adipocytes after lentiviral knock down of *FTO* [Tews *et al.*, 2013]. More strikingly, however, was the browning of white adipocytes, both in *Fto*-deficient mice, as well as in human adipocytes after shRNA mediated *FTO* knock down [Tews *et al.*, 2013]. Concomitantly, significant upregulation of UCP-1 was detected in *Fto*-deficient mouse adipose tissue and *FTO*-deficient human adipocytes. In *FTO*-deficient human adipocytes, this led to increased mitochondrial uncoupling in comparison to control cells. Reminiscent of a UCP-1 upregulation in brown adipocytes, *Fto*-deficient mice have a higher energy expenditure [Fischer *et al.*, 2009]. Therefore, loss of *FTO* and the resulting functional browning of white adipocytes may serve as an explanation for the increased energy expenditure in *Fto*-deficient mice.

Fto in the central nervous system

FTO is ubiquitously expressed, however, by far the highest levels of *FTO* are detected in the central nervous system [Gerken *et al.*, 2007; Frayling *et al.*, 2007; McTaggart *et al.*, 2011; Fredriksson *et al.*, 2008]. Within the brain, *FTO* is found in the majority of neurons [McTaggart *et al.*, 2011]. Due to the high expression in feeding related nuclei of the hypothalamus (paraventricular nucleus PVN; arcuate nucleus ARC; ventromedial nucleus VMH; dorsomedial nucleus DMH), an important role for *FTO* in the regulation of energy homeostasis was proposed [Gerken *et al.*, 2007; Tung *et al.*, 2010].

Brain specific *Fto* deletion in mice recapitulates several phenotypic characteristics of whole body *Fto*-deficiency [Gao *et al.*, 2010; Fischer *et al.*, 2009]. Comparable to *Fto*-deficient mice, brain specific loss of *FTO* leads to postnatal growth retardation, decreased IGF-1 serum concentrations and reduced body weight due to a reduction in lean mass. Since the Nestin-cre line used to generate the brain specific knock out model was reported to suffer from a hypopituitarism phenotype which could potentially cause several of the observed alterations [Galichet *et al.*, 2010], the results of this study have to be viewed cautiously.

Several studies addressed the role of FTO within the feeding related nuclei of the hypothalamus through virus mediated manipulation of FTO expression. Over-expression of FTO in the rat arcuate nucleus resulted in a decreased daily food intake, while a reduction in FTO caused an increase in food intake [Tung *et al.*, 2010]. Virus mediated knock out of *Fto* in the mediobasal hypothalamus of a conditional mouse model, however, led to the opposite result, causing a decrease in food intake [McMurray *et al.*, 2013]. Since the latter study targeted a larger area of the hypothalamus, the behavioural outcome of *Fto* knock down may depend on the affected neuronal population.

Recently, for the first time, *FTO* genomic variation was investigated regarding human brain function. In line with previous findings, carriers of the risk-allele (rs9939609 'A' allele) displayed attenuated suppression of hunger following a standard test meal [den Hoed *et al.*, 2009; Karra *et al.*, 2013]. Moreover, regardless of feeding state, neuronal activity assessed by functional MRI in response to food images was altered in homozygous rs9939609 risk-allele carriers [Karra *et al.*, 2013]. Changes in BOLD signal were detected in homeostatic, as well as hedonic brain areas. Furthermore, while the neuronal response to pictures of highly palatable food in control subjects positively covaried with increasing acyl-ghrelin levels, it negatively covaried in risk-allele carriers [Karra *et al.*, 2013]. Acyl-ghrelin is known to potently stimulate hunger and to increase food intake [Uchida *et al.*, 2013]. Hence, altered responses to acyl-ghrelin, or changes in acyl-ghrelin levels could potentially alter energy intake in *FTO* risk-allele carriers. Postprandially, rs9939609 SNP carriers show an increased acyl-ghrelin to ghrelin ratio, due to a failure in reduction of acyl-ghrelin levels after a meal [Karra *et al.*, 2013]. The same increase in acyl-ghrelin to ghrelin ratio was observed *in vitro*, if FTO was overexpressed. In *Fto*-deficient mice, on the other hand, this ratio is decreased [Karra *et al.*, 2013]. Hence, FTO may play a critical role in regulating ghrelin and acyl-ghrelin levels. Moreover, it may modulate the responses of homeostatic, as well as hedonic brain areas and thus shape hunger and/or satiety responses.

1.4.4 Molecular function of FTO

Cellular localisation

FTO is ubiquitously expressed [Gerken *et al.*, 2007; Frayling *et al.*, 2007; Fredriksson *et al.*, 2008]. The highest levels are, however, reported for the central nervous system and especially for feeding related brain areas [Gerken *et al.*, 2007; Frayling *et al.*, 2007; Tung *et al.*, 2010; McTaggart *et al.*, 2011; Stratigopoulos *et al.*, 2008; Fredriksson *et al.*, 2008]. Hence, it was proposed that FTO plays a critical role in the central nervous system. FTO primarily localizes to the nucleus of a cell [Gerken *et al.*, 2007; McTaggart *et al.*, 2011]. Only limited evidence so far suggests the presence of FTO in the cytoplasm depending on feeding state [Vujovic *et al.*, 2013]. Within the nucleus, it colocalizes in nuclear speckles with splicing factors, such as SART1 (U4/U6.U5 tri-snRNP-associated protein 1), SC35 (serine/arginine-rich-splicing factor 2) and Pol II-S2P (RNA polymerase II phosphorylated at Ser2) [Jia *et al.*, 2011]. Therefore, despite direct evidence for a connection to mRNA processing, FTO was proposed to play a role in splicing processes.

In mice, FTO is reported to be coexpressed with the satiety mediator oxytocin [Olszewski *et al.*, 2009, 2011]. Furthermore, overexpression of FTO *in vitro* leads to increased oxytocin mRNA levels [Olszewski *et al.*, 2011].

Since FTO was associated with the development of obesity and aberrant feeding behaviour [Cecil *et al.*, 2008; Timpson *et al.*, 2008; Speakman *et al.*, 2008; Wardle *et al.*, 2009; Haupt *et al.*, 2009; Tanofsky-Kraff *et al.*, 2009], *FTO* expression may vary with nutritional status. So far, however, findings are contradictory. In rats, fasting (48h) led to increased *Fto* transcript levels [Fredriksson *et al.*, 2008], whereas the same 48h fast in mice and long term food restriction in rats (60% of ad libitum) cause decreases in *Fto* mRNA [Gerken *et al.*, 2007; Wang *et al.*, 2011]. In a different restriction scheme in mice (food only available from 13:00 to 15:00h each day), however, *Fto* transcript levels were significantly increased in the arcuate and ventromedial hypothalamus [Boender *et al.*, 2012]. Other studies failed to detect differences for *Fto* mRNA in mice for both long term (40h) [Stratigopoulos *et al.*,

2008] or overnight fasting [McTaggart *et al.*, 2011]. On the protein level, FTO levels were unchanged in response to a overnight fast [McTaggart *et al.*, 2011], whereas reduced levels were measured after long term food restriction (60% of ad libitum) in rat hypothalamus and brainstem [Wang *et al.*, 2011]. Of note, the reduction of FTO protein caused by food restriction depends on leptin receptors and functional STAT3 signaling. A reduction of FTO levels due to caloric restriction was not observed on a leptin-deficient background [Wang *et al.*, 2011]. Furthermore, centrally administered leptin reduced *Fto* mRNA levels in mouse hypothalamus, a result reproduced by application of leptin on a hypothalamic slice preparation [Wang *et al.*, 2011].

Vice versa, FTO was proposed to influence leptin signaling through alteration of leptin receptor clustering [Stratigopoulos *et al.*, 2011]. Furthermore, overexpression of FTO in rat arcuate nucleus increased STAT3 mRNA levels by 4-fold [Tung *et al.*, 2010]. Moreover, global *Fto* overexpression in mice resulted in reduced fasting plasma levels of leptin at 8 weeks of age, but not at 20 weeks [Church *et al.*, 2010]. Hence, the relationship between leptin and FTO, as well as the regulation of FTO expression itself seems to be complex and demands further investigation.

FTO in amino acid sensing

In addition to the aforementioned observations, FTO has been reported to rely on nutrient availability. Glucose deprivation, as well as total amino acid deprivation cause both a reduction in *Fto* mRNA and protein in a hypothalamic cell culture (N46 cells) [Cheung *et al.*, 2013]. Further experiments have proven that essential amino acid deprivation is sufficient to downregulate FTO, presenting a potential link between energy metabolism and FTO expression [Cheung *et al.*, 2013].

Loss of *Fto* leads to growth defects, both *in vitro* and *in vivo*. Postnatal growth retardation is observed in *Fto*-deficient mice, while *Fto*-deficient MEFs (mouse embryonic fibroblasts) have reduced growth rates and translation levels [Gulati *et al.*, 2013; Fischer *et al.*, 2009]. Further analysis revealed a downregulation of the multi-synthetase complex (MSC) in knock out MEFs and a physical interaction of FTO

with several components of the MSC [Gulati *et al.*, 2013]. Through coordination of aminoacyl-tRNA synthetases, the MSC is taking part in the translational regulation. Hence, failure to assemble the complex would lead to reduced translation. Re-expression of *Fto* on a *Fto*-deficient background, however, restored levels of the MSC complex and rescued translational rate [Gulati *et al.*, 2013].

Moreover, loss of *Fto* affects mTORC₁ (mammalian target of rapamycin complex 1) signaling, a key-regulatory pathway of translation and growth. *Fto* deficiency leads to reduced phosphorylation of the mTOR effector kinase S6K₁ (S6-kinase 1) [Gulati *et al.*, 2013]. Furthermore, the downregulation of mTORC₁ in response to amino acid deprivation, a physiologically relevant process, is prevented by overexpression of exogenous FTO [Gulati *et al.*, 2013]. Expression of a catalytically inactive form of FTO (R₃₁₆Q), however, is not able to block this downregulation of mTORC₁. Hence, mTORC₁ depends on the enzymatic activity of *Fto* [Gulati *et al.*, 2013]. The apparent amino acid dependent regulation of *Fto* expression and further coupling of FTO activity to the MSC and mTORC₁ signaling present a possible model for the integration of FTO in metabolic processes. The exact mechanisms, however, demand further investigation.

2-oxoglutarate dependent nucleic acid demethylase

Interestingly, the *FTO* gene is only present in algae and vertebrates, but is absent in invertebrates, plants, fungi, bacteria or archaea [Fredriksson *et al.*, 2008; Gerken *et al.*, 2007; Sanchez-Pulido & Andrade-Navarro, 2007; Robbins *et al.*, 2008]. Using bioinformatical sequence comparison, FTO was found to be closely related to the bacterial AlkB (alpha-ketoglutarate-dependent dioxygenase) and human AlkB homologs (ABH₁, ABH₂ and ABH₃) [Gerken *et al.*, 2007; Sanchez-Pulido & Andrade-Navarro, 2007; Han *et al.*, 2010]. The FTO protein features the conserved 2-oxoglutarate (2-OG) and Fe(II) binding sites, typical for the 2-OG dependent dioxygenases of the AlkB family of enzymes [Gerken *et al.*, 2007]. Due to its role as an intermediate product of the Krebs-cycle, 2-OG was proposed to link FTO to metabolic processes. Since the 2-OG K_m for FTO (2.88 μ M), however, is 10 fold below physi-

ologically relevant concentrations of 2-OG, FTO is unlikely to convey information of the current metabolic status through sensing 2-OG levels [Ma *et al.*, 2012].

AlkB and human AlkB homologs (ABH2 and 3) have been described as DNA repair enzymes, which demethylate cytotoxic 1 - methyladenine and 3 - methylcytosine [Trewick *et al.*, 2002; Aas *et al.*, 2003]. Correspondingly, FTO was demonstrated to demethylate 3 - methylthymine (m³T) in single stranded DNA (ssDNA) and 3 - methyluracil (m³U), as well as N⁶ - methyladenosine (m⁶A) in ssRNA [Gerken *et al.*, 2007; Jia *et al.*, 2008, 2011; Meyer *et al.*, 2012]. A C-terminal loop, unique to 2-OG dependent oxygenases, was identified through solving the crystal structure of FTO and probably causes its preference for single stranded rather than double stranded DNA/RNA [Han *et al.*, 2010]. Moreover, its demethylase efficiency is slightly higher for RNA than DNA and m⁶A does not occur in DNA, thus suggesting that RNA is the primary target of FTO [Jia *et al.*, 2008; Ratel *et al.*, 2006].

1.5 m⁶A RNA modification

1.5.1 RNA and RNA modifications

RNA (ribonucleic acid) is a central molecule in any organism that may appear in many different forms, serving a plethora of different functions. The relatively short-lived and low-abundant messenger RNA (mRNA) is the carrier molecule for the genetic information encoded in the genome. Approximately 97% of the RNA in a cell, however, belongs to the non protein coding RNA families, including transfer RNA (tRNA), ribosomal RNA (rRNA), small nuclear RNA (snRNA), small-interfering RNA (siRNA), micro RNA (miRNA) and long noncoding RNA (lncRNA) [Sharp, 2009]. The most abundant type of RNA is rRNA, which forms the catalytic domain in ribosomes and hence is a key component of protein synthesis. During protein synthesis, tRNA molecules are the mediators that match the correct amino acid to the corresponding base triplet found within the protein coding mRNA molecule. In both rRNA and tRNA, the secondary and tertiary structure

is of importance for their correct function. Small nuclear RNAs play an important role in pre-mRNA splicing in the nucleus [Sharp, 2009]. Small-interfering and micro RNAs on the other hand, represent the means for silencing gene expression at the RNA level through translational/transcriptional silencing or mRNA decay [Sharp, 2009]. Regulation of gene expression is also regulated by long noncoding RNAs, however, their mode of action most probably involves binding of proteins such as transcription factors or formation of protein complexes [Rinn & Chang, 2012].

Modification of the four nucleotides enhances the diversity of RNA species and is needed for the complex functional purposes of RNA. To date, 109 post-transcriptional modifications have been identified in most of the different types of RNA species [Cantara *et al.* [2011] and 'The RNA Modification Database': <http://mods.rna.albany.edu/>, date: 09/20/2013]. Interestingly, the RNA modifications are dynamic and thus may represent yet another level of epigenetic adjustments to environmental input [Yi & Pan, 2011]. Most of the modifications have been described in tRNA and rRNA. However, 13 modifications are reported for mRNA. These modifications include *N*⁷-methylguanosine (m⁷G), 2'-*O*-methylnucleotide (N_m), 5-methylcytosine (m⁵C), *N*⁶-methyladenosine (m⁶A), *N*⁶-methyl-2'-*O*-methyladenosine (m⁶A_m). m⁷G and 2'-*O*-methylnucleotide are modifications found within and being important for the 5'CAP structure of a mRNA molecule [Jia *et al.*, 2012], thus enabling the recruitment of initiation factors and translation, nuclear export, as well as promoting mRNA stability [Sonenberg & Hinnebusch, 2009]. m⁶A and m⁵C, on the other hand, are internal modifications found within the 5'UTR, coding sequence (CDS) or 3' UTR of mRNAs, whose functions so far are largely unknown [Jia *et al.*, 2012].

1.5.2 *N*⁶-methyladenosine (m⁶A)

Despite the fact that the *N*⁶-methyladenosine (m⁶A) RNA modification has been known since the 1970s, to date the purpose of this most abundant RNA methyl-

tion remains largely unknown [Desrosiers *et al.*, 1974; Harper *et al.*, 1990; Jia *et al.*, 2012]. m^6A is present in a variety of organisms, including plants [Nichols, 1979; Zhong *et al.*, 2008], yeast [Clancy *et al.*, 2002; Bodi *et al.*, 2010], flies [Levis & Penman, 1978] and mammals [Wei *et al.*, 1975; Shatkin, 1976; Desrosiers *et al.*, 1974; Jia *et al.*, 2011]. Moreover, it has been detected in viral RNA [Krug *et al.*, 1976; Kane & Beemon, 1985]. m^6A has been found in rRNA and tRNA [Saneyoshi *et al.*, 1969; Iwanami & Brown, 1968]. Despite the scarce knowledge, m^6A is suggested to be important for mRNA processing, export from the nucleus, stability and translational efficiency [Harper *et al.*, 1990; Pan, 2013; Jia *et al.*, 2012; Niu *et al.*, 2013; Dominissini *et al.*, 2012; Tuck *et al.*, 1999]. The methylation mark is also found in intronic regions of pre-mRNA, showing that it is present before splicing [Carroll *et al.*, 1990]. Moreover, m^6A on RNA may serve as a label for endogenous RNA that helps the innate immune system to identify foreign RNA molecules [Karikó *et al.*, 2005]. To date, several putative m^6A binding proteins have been reported [Dominissini *et al.*, 2012]. Two of those proteins are members of the YTH (YT521 homology) family and have been previously described to be involved in alternative splice site selection and mRNA degradation [Rafalska *et al.*, 2004; Harigaya *et al.*, 2006]. Indeed, most recently, YTHDF2 was shown to bind to a subset of m^6A methylated mRNA transcripts and to subsequently shuttle these transcripts to, for example, processing bodies (p bodies) for RNA degradation [Wang *et al.*, 2013]. Hence, mRNA stability and lifetime depends on m^6A methylation status and thus will limit the pool of templates available for translation [Wang *et al.*, 2013]. Furthermore, m^6A sites are overrepresented in transcripts that harbor putative miRNA binding sites and highly expressed miRNAs in the brain have a greater percentage of target transcripts with m^6A sites, suggesting, that miRNA levels may be involved in the methylation process itself [Meyer *et al.*, 2012]. Despite mRNA, m^6A is also found in long noncoding RNA, whose mode of action is yet to be finally determined [Meyer *et al.*, 2012].

Before the development of deep sequencing techniques, only two mRNAs were identified that harbor m^6A sites. One was found to be in the 3'UTR of bovine

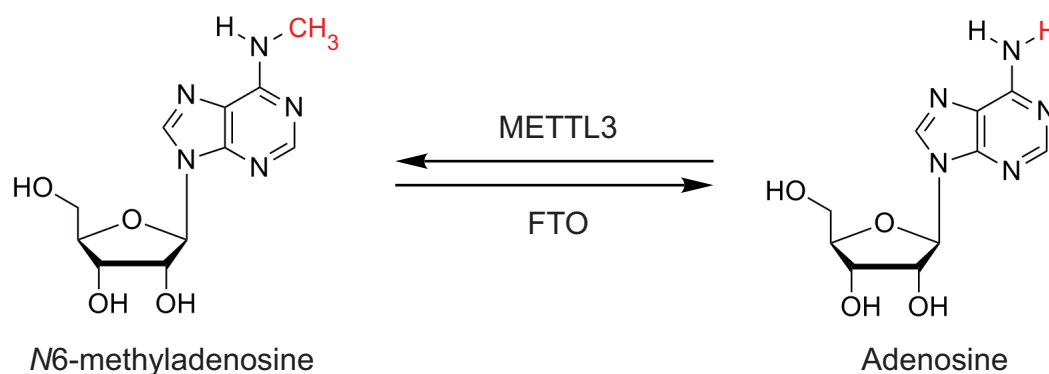


Figure 1.3: **Reversible N6-methyladenosine modification** FTO demethylates N6-methyladenosine (m^6A) in a 2-oxoglutarate and Fe(II) dependent manner. The reverse reaction of m^6A demethylation involves a m^6A -methyltransferase complex that contains several subunits, one of which is METTL3.

prolactin [Horowitz *et al.*, 1984], whereas several sites were identified in the Rous sarcoma virus RNA [Kane & Beemon, 1985]. Further analysis led to the description of the consensus site: RRACH (R = G or A, H = A, C or U) [Horowitz *et al.*, 1984; Harper *et al.*, 1990; Csepany *et al.*, 1990]. Within each mRNA, however, not all m^6A sites are methylated. Prevalence for m^6A in the Rous sarcoma virus RNA is within 20 to 90 % of all sites [Kane & Beemon, 1985] and only about 20 % for bovine prolactin [Horowitz *et al.*, 1984; Narayan *et al.*, 1994].

So far, only one subunit of a nuclear human m^6A -methyltransferase complex was described [Bokar *et al.*, 1994, 1997]. METTL3 (or MTA70) is a homolog of the yeast IME4 (inducer of meiosis), which methylates mRNA in yeast during sporulation (Figure 1.3) [Clancy *et al.*, 2002; Bodi *et al.*, 2010]. Both in plants, as well as in flies, the homologs of METTL3 are important regulators of development [Zhong *et al.*, 2008; Hongay & Orr-Weaver, 2011]. Consistently, knock down of METTL3 affects HepG2 cells, resulting in deregulation of p53 signaling components and apoptosis [Dominissini *et al.*, 2012]. METTL3 colocalizes in the nucleus with nuclear speckles. Hence, the methylation may occur already during transcription [Bokar *et al.*, 1997].

Recently, FTO was shown to demethylate m^6A in single stranded RNA and single stranded DNA *in vitro* (Figure 1.3) [Jia *et al.*, 2011]. Since m^6A is not detected in genomic DNA, RNA represents the physiological substrate of FTO [Ratel *et al.*,

2006]. Further experiments confirmed the demethylation of m⁶A in mRNA by FTO [Jia *et al.*, 2011; Meyer *et al.*, 2012]. Like METTL3, FTO localizes primarily in the nucleus and was furthermore reported to colocalize with splicing factors such as SART1 and SC35 in nuclear speckles [Jia *et al.*, 2011; McTaggart *et al.*, 2011; Gerken *et al.*, 2007]. In addition to FTO, a second m⁶A demethylase, alkB alkylation repair homolog (ALKBH5), has been identified [Zheng *et al.*, 2012]. ALKBH5, like FTO, is ubiquitously expressed, but in contrast to FTO exhibits highest expression levels in peripheral tissues and relatively low levels in the central nervous system [Zheng *et al.*, 2012]. Loss of ALKBH5 in mice affects nuclear mRNA export, RNA metabolism and influences the localization of RNA processing proteins in the nucleus [Zheng *et al.*, 2012]. *Alkbh5*-deficient mice exhibit impaired fertility due to increased apoptosis and abnormal spermatogenesis [Zheng *et al.*, 2012].

Taken together, the identification of the m⁶A methyltransferase METTL3 and the m⁶A demethylases FTO and ALKBH5 demonstrates once more that RNA methylation is probably a dynamic process putatively in control of mRNA processing, nuclear export, turnover, translation and first evidence for a role in mRNA stability [Wang *et al.*, 2013; Pan, 2013; Jia *et al.*, 2012].

1.5.3 The m⁶A methylome

The development of next-generation sequencing enabled the thorough analysis of the whole transcriptome with respect to m⁶A methylation sites, the m⁶A methylome [Dominissini *et al.*, 2012; Meyer *et al.*, 2012]. Approximately 100 nucleotide long RNA fragments were immunoprecipitated with a m⁶A antibody and subsequently subjected to high-throughput sequencing. Both studies identified the m⁶A mark in more than 7000 mRNA transcripts and approximately 300 non coding RNAs in both humans [Dominissini *et al.*, 2012] and mice [Meyer *et al.*, 2012], showing that m⁶A is a common and conserved modification. m⁶A sites were found to be enriched in the 3'UTR near the stop codon, coding sequence and to a lesser extent in the 5'UTR of mRNA transcripts [Dominissini *et al.*, 2012; Meyer *et al.*,

2012]. m⁶A levels are increasing during the course of mouse brain development and show tissue dependent prevalence [Meyer *et al.*, 2012]. Environmental stimuli, such as heat shock, UV irradiation or hepatocyte growth factor did not influence the m⁶A peak positions, however some dynamic modulation was observed upon interferon γ treatment [Dominissini *et al.*, 2012]. Levels of m⁶A-methylation depend on FTO and its enzymatic activity *in vitro* [Dominissini *et al.*, 2012; Meyer *et al.*, 2012]. Hence, FTO most probably plays a critical role in what may represent a novel and dynamic RNA epigenetic process affecting cellular programs important for e.g. energy homeostasis.

1.6 Objectives

The aim of this study was to investigate the potential role of the fat mass and obesity-associated gene (*Fto*) in the dopaminergic system. Since some of the characteristics of *Fto*-deficient mice resemble features of *DRD2*-deficient mice [García-Tornadu *et al.*, 2010; Díaz-Torga *et al.*, 2002; Sibley, 1999; Kelly *et al.*, 1998; Beaulieu & Gainetdinov, 2011] and as both *FTO*, and dopamine have been implicated in the etiology of obesity [Scuteri *et al.*, 2007; Dina *et al.*, 2007; Frayling *et al.*, 2007; Volkow *et al.*, 2013; Wang *et al.*, 2001], *FTO* might play a critical role in dopaminergic signaling. To investigate this hypothesis, both whole body, as well as DA neuron restricted *Fto*-deficient mice were utilized.

2 Materials and Methods

2.1 Animal care

Mice (*Mus musculus*, C57Bl/6) were housed in a virus-free facility at 22-24°C on a 12 h light/ 12 h dark cycle. Animals were either fed standard rodent chow (Teklad Global Rodent 2018; 53.5% carbohydrates, 18.5% protein, 5.5% fat (12% calories from fat); Harlan, IN, USA) or a high fat diet (C1057; 32.7% carbohydrates, 20% protein, 35.5% fat (55.2% calories from fat); Altromin, Lage, Germany). All animals had access to water and food *ad libitum*, except 16h fasting prior to glucose tolerance test and refeeding experiments. Procedures and euthanasias were reviewed by the animal care committee, approved by local government authorities (Tierschutzkommission acc. §15 TSchG of the Landesamt für Natur, Umwelt und Verbraucherschutz North Rhine Westphalia) and were in accordance with NIH guidelines.

2.2 Experimental mouse models

For the investigation of the effect of global deficiency, mice with a germline deletion of exon 2 and 3 of the *Fto* gene were employed [Fischer *et al.*, 2009]. For all experiments, whole body *Fto* deficient mice (homozygous knock outs) and wildtype littermates were used. To investigate the role of FTO specifically in dopaminergic neurons, mice expressing the Cre-recombinase under the control of the endogenous *Dat* promoter [Ekstrand *et al.*, 2007] were crossed to mice with a loxP site flanked third *Fto* exon (provided by EUComm). If not otherwise stated, DAT-Cre^{tg/wt}; *Fto*^{fl/fl} and their respective littermate controls DAT-Cre^{wt/wt}; *Fto*^{fl/fl} were used for experiments.

2.3 Genotyping

Isolation of genomic DNA

Mouse tail biopsies were taken at weaning age and subsequently digested in 500 μ l tail lysis buffer (100 mM Tris-HCl pH 8.5, 5 mM EDTA pH 8.0, 0.2% SDS, 200 mM NaCl) containing proteinase K (1/100) at 55°C. DNA was precipitated using 500 μ l 100% isopropanol and centrifugation at 17.000g. Afterwards, DNA was washed with 750 μ l 70% ethanol, centrifuged at 17.000g and dried. The DNA pellet was resuspended in TE buffer (10 mM Tris-HCl pH 7.5, 1 mM EDTA) containing RNase (1/1000) or ddH₂O.

Polymerase chain reaction

For genotypic analysis, polymerase chain reaction (PCR) was performed on tail DNA using the primers given in table 2.1. For PCR DreamTaq PCR MasterMix and DNA polymerase (Fermentas/Fisher Scientific Germany GmbH, Schwerte, Germany) was used. Standard PCR contained approx. 50 ng DNA, 25 pMol of each primer, 25 μ M dNTP mix and 1 unit DNA polymerase in a 25 μ l reaction mix.

Table 2.1: Genotyping Primer

Mouse Line	Primer	Sequence 5'-3'
DAT-Cre	DAT_F3	CATGGAATTCAGGTGCTTGG
	Cre_R2	CGCGAACATCTTCAGGTTCT
	DAT_R1	ATGAGGGTGGAGTTGGTCAG
Fto flox (FLP deleted)	Fto_5b	TCAATCCTGGGCTAACATTTACCA
	Fto_3b	TTTATGGCCTTCGGCTTCAC
Fto flox (non FLP deleted)	Fto_5b	TCAATCCTGGGCTAACATTTACCA
	Fto_3b_euc	GGGATCCTCTAGAGTCCAGAT
	Fto_3b_wt	CAGCGGCGATCTCAGCCTC
Fto deletion	Fto_5b	TCAATCCTGGGCTAACATTTACCA
	Fto_3a	TGGTGA CTCCAACCATTTCATC
Fto conventional	Fto_5'	ACCCCTCTCCCCATCTAAATCCT
	Fto_3'	AAGCCAAGAACAAGTCCATACCTG
	Neo_5'	CTGTGCTCGACGTTGTCACTG
	Neo_3'	GTCCCGCTCAGAAGA ACTCGT

2.4 Phenotyping

2.4.1 Body weight

Body weight was assessed weekly for each individual mouse for ages 4-16 (18) weeks. After weaning, animals were either fed a normal chow diet or high fat diet.

2.4.2 Insulin tolerance test

For insulin tolerance test, baseline blood glucose levels (time point 0 min) were measured using a glucometer (GlucoMen PC, A.Menarini Diagnostics, Italy). Following intraperitoneal administration of insulin ($0.75 \text{ units ml}^{-1}$; $0.75 \text{ units kg}^{-1}$ body weight), blood glucose levels were measured 15, 30 and 60 minutes after injection. For determination of insulin tolerance, 15, 30 and 60 min values were calculated relative to baseline blood glucose levels for each individual mouse and plotted over time.

2.4.3 Glucose tolerance test

Mice were fasted 16h prior to glucose tolerance test. Fasting state blood glucose levels (time point 0 min) were determined using a glucometer (GlucoMen PC, A.Menarini Diagnostics, Italy). Following intraperitoneal administration of glucose solution (20%, 10 ml kg^{-1} body weight), blood glucose levels were measured at 15, 30, 60 and 120 minutes after injection. For determination of glucose tolerance, blood glucose levels (in mg dl^{-1} blood) were plotted over time.

2.4.4 Indirect calorimetry

Energy expenditure was measured using indirect calorimetric measurements in a PhenoMaster System (TSE systems, Bad Homburg, Germany). Animals were allowed to adapt to the single housing in metabolic chambers (7.1 liter) for a training phase of 5 days. During that time, animals were monitored daily to ensure proper adaptation to the drinking and feeding dispensers. Calorimetric measurement was

conducted at 22-24°C over a period of 48-72 hours, assessing oxygen consumption, carbon dioxide production and locomotor activity (light barrier frame, TSE systems). Moreover, water and food intake was assessed using automated measuring devices (TSE Systems). Indirect calorimetry was performed with great help and advice of Hella Brönneke and Jens Alber.

2.4.5 Food intake and refeeding response

Daily food intake was either measured automatically during calorimetric measurements (figure 3.15 e and f) or manually using a food hopper (figure 3.17). In either case, mice were allowed to adapt to single housing and food hoppers for 4-5 days. Food intake measurements were conducted for at least 3 consecutive days. All food intake measurements were performed for single caged mice. Refeeding response was measured after a 16h over night fast. Consumed food was measured manually 1, 2, 4, 8 and 24h after returning the food hopper to the home cage.

2.5 Microarray expression analysis

RNA was isolated from midbrain tissue (VTA/SN) using peqGOLD TriFast and following the recommended protocols (peqlab, Erlangen, Germany). Quality of RNA (n=3/genotype) was assessed on a Bioanalyzer chip and subsequently hybridized on GeneChip Mouse Gene 1.0 ST Arrays (Affymetrix, Santa Clara CA, USA). RNA quality check and array hybridization was performed by the Cologne Center for Genomics (CCG, Cologne, Germany). Background correction and normalization for the intensity values were performed using the Affymetrix Power-tools (Affymetrix, Santa Clara CA, USA) and robust multi-array average (RMA). Fold change of intensity values, as well as statistics (calculation of p-value and false discovery rate (FDR)) were calculated in R (using the bioconductor software package). Genes were considered significantly dysregulated for p-values ≤ 0.05 and FDR ≤ 0.25 . HeatMap of significantly deregulated genes was generated using R.

2.6 Quantitative polymerase chain reaction

2.6.1 Preparation of RNA

Fresh brain samples of different brain areas were prepared using a brain slicer (Braintree Scientific, Braintree MA, USA) and snap frozen in liquid nitrogen. RNA was isolated from tissues using peqGOLD TriFast (Peqlab, Erlangen, Germany) according to the manufacturer's protocol and RNA pellets were resuspended in DEPC water. RNA concentrations were assessed by measuring absorption at 260 and 280 nm using a NanoDrop ND-1000 UV-Vis Spectrophotometer (Thermo Fisher Scientific Inc., Schwerte, Germany). Afterwards, RNA samples were adjusted to equal concentrations for further processing.

2.6.2 Reverse transcription and quantitative PCR

RNA (100 to 200 ng μl^{-1} per sample) was reversely transcribed with High-Capacity cDNA Reverse Transcription kit (Applied Biosystems, Foster City CA, USA) and amplified using TaqMan Gene Expression Master Mix with TaqMan Assay-on-demand kits (Applied Biosystems) following the manufacturer's protocol. Realtime probes used for gene expression analysis are listed in table 2.2. Relative expression was determined for target mRNA and samples were adjusted for total mRNA content by quantitative PCR for housekeeping genes (*Gusb*, *Hprt*, *Tfrc*). Calculations were performed by comparative method ($2^{-\Delta\Delta C_T}$) [Livak & Schmittgen, 2001].

Table 2.2: Realtime PCR probes

Symbol	Transcript Name	Probe
<i>Fos</i>	FBJ murine osteosarcoma viral oncogene homolog	Mm00487425_m1
<i>Dbh</i>	Dopamine beta hydroxylase	Mm00460472_m1
<i>Drd2</i>	Dopamine receptor D2	Mm00438545_m1
<i>Drd3</i>	Dopamine receptor D3	Mm00432887_m1
<i>Grin1</i>	glutamate receptor, ionotropic, NMDAR1 (zeta 1)	Mm01336437_m1
<i>Gusb</i>	Beta-glucuronidase	Mm00446953_m1
<i>Hprt</i>	Hypoxanthin-phosphoribosyl-transferase	Mm00446968_m1

Continued on next page

Table 2.2 – continued from previous page

Symbol	Transcript Name	Probe
<i>Kcnj6</i>	potassium inwardly-rectifying channel, subfamily J, member 6	Mm00440070_m1
<i>Slc6a3</i>	Dopamine transporter	Mm00438388_m1
<i>Tfrc</i>	Transferrin receptor	Mm00441941_m1
<i>Th</i>	Tyrosine hydroxylase	Mm00447557_m1

2.7 Protein biochemistry

2.7.1 Protein preparation

Tissues, initially frozen in liquid nitrogen, were thawed and homogenized in RIPA buffer (20 mM Tris-HCl pH 8.0, 150 mM NaCl, 1% NP-40, 10 mM NaF, 1 mM sodium vanadate, 1 mM sodium pyrophosphate, 1 protease inhibitor (cOmplete Mini, Roche Diagnostics, Basel, Switzerland) for 10 ml RIPA buffer and, if necessary, 1 PhosSTOP phosphatase inhibitor (Roche Diagnostics, Basel, Switzerland)) using either a Ultra-Turrax homogenizer (IKA Werke, Staufen, Germany) or manually with a pestle. Following homogenization, samples were incubated for 10 min on ice and subsequently centrifuged for 20 min at 4°C. Supernatant was transferred to fresh tubes and kept on -80°C for long term storage.

2.7.2 Western blot

For Western blots, protein samples were boiled for 5 minutes in SDS-PAGE sample buffer (1:3 dilution in 4x SDS loading buffer: 125 mM Tris-HCl pH 6.8, 5% SDS, 43.5% glycerol, 100 mM DTT, and 0.02% bromphenol blue). Proteins were separated by SDS-PAGE and blotted onto PVDF membranes (Bio-Rad, Munich, Germany). Membranes were incubated for at least 1h with 1% blocking reagent in TBS/T at room temperature (Roche, Mannheim, Germany) and subsequently with primary antibody diluted in 0.5% blocking solution for 1 h at room temperature or over night at 4°C. After three washing steps with TBS/T, membranes were incubated for 1 h at RT with the respective secondary antibodies. Antibodies used

for Western blot are listed in table 2.3. The signals were visualized after 3 washing steps with TBS/T using Pierce ECL Western Blotting Substrate (Perbio Science, Bonn, Germany) and exposition to Amersham Hyperfilm chemiluminescent film (GE Healthcare, Little Chalfont, UK).

Table 2.3: Antibodies for Western blot

Antibody	Cat.No.	Supplier
β -ACTIN	A5441	Sigma Aldrich Co. LLC.
CALNEXIN	208880	Calbiochem
DAT	SC-14002	Santa Cruz Biotechnology, Inc.
DRD2	ab21218	Abcam, Inc.
	ab32349	Abcam, Inc.
	sc-5303	Santa Cruz Biotechnology, Inc.
DRD3	ab42114	Abcam, Inc.
FTO	custom antibody produced in guinea-pig	provided by U. R��ther/Pineda antibody services, Berlin, Germany
GIRK2	ab30738	Abcam, Inc.
GNAI1	#5290	Cell Signaling Technology, Inc.
HSC70	sc-7298	Santa Cruz Biotechnology, Inc.
IKK2	#2370	Cell Signaling Technology, Inc.
NMDAR1	#5704	Cell Signaling Technology, Inc.
TH	ab112	Abcam, Inc.

2.8 Behavioural experiments

2.8.1 Open Field

Open field experiments were performed in open field box for mice (TSE Systems, Bad Homburg, Germany). One day before experiments, mice were injected intraperitoneally (i.p.) with saline and allowed to explore the open field box for 5 minutes. For baseline locomotor activity, mice were injected i.p. with vehicle (saline). The following days, mice were administered cocaine hydrochloride (10 or 20 mg kg⁻¹ body weight; C5776, Sigma Aldrich) or (-)-quinpirole (30 or 100 μ g kg⁻¹ body weight; Q102, Sigma Aldrich). The distance for each mouse was measured over a period of 45 minutes using an automated video-based system in an open field (50x50 cm, VideoMot 2, TSE Systems, Bad Homburg, Germany). Data are expressed as relative increase compared to baseline (saline). Absolute values

are given for baseline locomotor activity.

2.8.2 Conditioned Place Preference

Conditioned place preference (CPP) experiments were performed in the conditioned place preference box for mice (TSE Systems, Bad Homburg, Germany). Activity and location in the CPP box were monitored by a video recording system (VideoMot 2, TSE Systems).

Pre-conditioning test (2 days): To determine whether a pre-existing bias exists, two single 30 min test sessions (1 session/day) were performed during which mice were allowed to freely explore the CPP box with doors open. Both sessions were video-taped to determine the preferred side.

Conditioning phase (6 days): During the conditioning phase mice of different genotypes received a positive stimulus of 0.5 mg cocaine kg⁻¹ body weight via i.p. injection prior to placement in the non-preferred side of the box (doors closed) and on the intervening days, all mice received an injection of vehicle (saline) prior to placement in the preferred side of the box. The six conditioning sessions lasted 30 min each, one session per day.

Drug place preference test (1 day): One single 30 min test session has been performed during which mice were allowed to freely explore the CPP box with doors open. The session has been video-taped to determine the location of the mice in the CPP box.

Data analysis: Data are expressed as relative increase compared to baseline (neutral middle part of CPP box excluded). For statistical analysis a paired *t*-test was performed.

2.8.3 Sucrose preference

To assess sucrose preference, mice were housed individually and restricted to 75% of *ad libitum* food intake. Each cage was fitted with 2 drinking bottles and one additional cage without experimental animal was set up as a control for handling

and evaporation water loss. After 2 days of habituation, the following 3 days water consumption and bottle preference was measured for each mouse. Afterwards, mice were presented with a choice of one bottle of water and one bottle of sucrose, with concentrations increasing over the course of the experiment (0.5, 1, 2, 4, 8%). Each concentration was measured for 2 days, changing the location (bottle 1 or bottle 2) of the sucrose solution after the first 24h to adjust for bottle preference. In between different sucrose concentrations, both bottles were changed to water for a period of 24h. Sucrose preference was calculated as sucrose solution intake relative to total liquid intake.

2.9 Electronmicroscopy

A tissue block containing the midbrain was dissected from each brain. 50 μm thick vibratome sections were cut and thoroughly washed in 0.1 M phosphate buffer (PB). To eliminate unbound aldehydes, sections were incubated in 1% sodiumborohydride for 15 min, then rinsed in PB. Next, sections were incubated with primary antibody (α -Tyrosine hydroxylase; dilution 1:1000 in PB) for 24 h at room temperature. Subsequently, sections were incubated in biotinylated goat anti-rabbit immunoglobulin (dilution 1: 250; Vector Laboratories, Burlingame, CA, USA) at room temperature. After a thorough wash in PB, sections were placed in avidin-biotin-complex (ABC Elite Kit, Vector Labs) for 2 hr at room temperature. The tissue-bound peroxidase was visualized by a diaminobenzidine reaction. After the immunostaining, the sections were osmicated (15 min in 1% osmic acid in PB), and dehydrated in increasing ethanol concentrations. During the dehydration, 1% uranyl-acetate was added to the 70% ethanol to enhance ultrastructural membrane contrast. Dehydration was followed by flatembedding in Araldite. Ultrathin sections were cut on a microtome, collected on Formvar-coated single-slot grids and analyzed with a Tecnai 12 Biotwin (FEI Company) electron microscope. The plasma membranes of selected cells were outlined on photomicrographs and their length was measured with the help of a chartographic wheel. Plasma membrane length

values measured in the individual animals were added and the total length was corrected to the magnification applied. Section thickness was determined by using the Small's minimal fold method.

2.10 Immunohistochemistry

For double immunohistochemical stainings, mice were anesthetized and transcardially perfused with saline. The dissected brains were frozen in tissue-freezing medium. 7 μm thick coronal sections were fixed in 4% paraformaldehyde (PFA). Following washing in PBS, slices were incubated in 0.3% glycine (in PBS). Subsequently, samples were washed in PBS and treated with 0.03% SDS (in PBS). Prior to antibody treatment, blocking was performed with donkey serum. Incubation with the primary antibody was conducted overnight (α -Tyrosine hydroxylase, 1:1000, ab112, Abcam); α -FTO, 1:1000; custom antibody produced in guinea-pig, provided by U. R  ther/Pineda antibody services, Berlin, Germany; Fischer *et al.* [2009]). Preceding secondary antibody treatment, samples were washed in PBS. Secondary antibodies used for immunofluorescent stainings were Cy3 α -guinea pig (Jackson Immuno Research, 706-165-148, donkey, 1:500) and Alexa 488 α -rabbit (Invitrogen, A11008, goat, 1:500). Finally, following 3 washing steps for 10 min in PBS, brain slices were embedded in Vectashield (Vector Laboratories, Burlingame, CA, USA) containing DAPI (4-,6-Diamidin-2-phenylindol).

For staining of c-Fos, mice were anesthetized and transcardially perfused with saline followed by 4% PFA. Brains were dissected, postfixed in PFA for 4 h, soaked in 20% sucrose overnight at 4°C, and frozen in tissue-freezing medium. c-Fos immunoreactivity was labeled with α -c-Fos antibody (PC38, Calbiochem, EMD Millipore, Billerica MA, USA) and peroxidase coupled secondary antibody (α -rabbit).

For β -galactosidase stainings, mice were transcardially perfused with saline, and dissected brains were frozen in tissue-freezing medium. X-gal staining was performed using standard protocols. Briefly, coronal sections (8 μm thick) were fixed

in cold 100% EtOH, washed in PBS and subjected to X-gal staining overnight at 37°C (X-gal solution: 5 mM $K_3Fe(CN)_6$, 5 mM $K_4Fe(CN)_6$, 2 mM $MgCl_2$, 1 mg ml⁻¹ X-gal in PBS, pH 7.4). After staining, sections were rinsed in PBS and counter-stained with Nuclear Fast Red.

2.11 *In situ* hybridization

In situ hybridization for GAD67 on fresh frozen sections was performed based on a protocol described previously [Hommel *et al.*, 2006]. Briefly, brains were sliced on a cryostat (16 μ m) and kept at -80°C until usage. Slices from freezer were dried and subsequently fixed in 4% PFA in PBS for 20 min. After a 3 x 3 minute washing step in PBS, slices were acetylated (2.38 ml triethanolamine, 0.32 ml HCL, 0.45 ml acetic anhydride ad 180 ml H₂O) for 10 minutes on a stirrer. Following 3 x 5 minutes wash in PBS, slices were preincubated for 2h at room temperature with hybridization solution (50% deionized formamide, 5x SSC, 5x 50x-Denhardt's solution, 250 μ g ml⁻¹ tRNA bakers yeast, 500 μ g ml⁻¹ sonicated salmon sperm DNA). Afterwards, slices were incubated over night at 72°C in hybridization mixture (150 μ l including 400 ng of dig-labeled RNA probe). The following digoxigenin (DIG)-labeled probe was used: *Gad67* bp 1064-2046 of the mouse coding sequence (PCR amplification primers: 5'GAD67: TGTGCCCAAACCTGGTCCT, 3'GAD67: TGGCCGATGATTCTGGTT). The next day, slices are washed for 2h in 0.2xSSC at 72°C, followed by 5 minutes in 0.2xSSC at room temperature. Fluorescent labeling of the RNA probe was performed using the TSATM Plus Cyanine 3/Fluorescein System kit (Perkin Elmer, Inc., Waltham MA, USA), following the manufacturer's protocols. In situ hybridization was followed by immunostaining for FTO as described in section 2.10. The fluorescence images were captured with a confocal microscope (Leica SP8X, Leica, Wetzlar, Germany).

2.12 Electrophysiology

All electrophysiology experiments were performed by Simon Hess in the lab of Peter Kloppenburg (University of Cologne, Cologne, Germany). Experiments were performed on brain slices containing the substantia nigra from 21- to 28-day old female and male $Fto^{-/-}$ and $Fto^{\Delta DAT/\Delta}$ mice and their respective littermates as controls. The general experimental procedure has recently been described in detail with additional information in the following paragraphs [Klöckener *et al.*, 2011]. Brain slices were transferred into carbogenated artificial cerebrospinal fluid (aCSF). First, they were kept for 20 min in a 35 °C 'recovery bath' and then stored at room temperature (24 °C) for at least 30 min prior to recording. aCSF contained (in mM): 125 NaCl, 2.5 KCl, 2 MgCl₂, 2 CaCl₂, 1.2 NaH₂PO₄, 21 NaHCO₃, 10 HEPES, and 5 Glucose adjusted to pH 7.2 (with NaOH) resulting in an osmolarity of 310 mOsm. For voltage-clamp experiments, the patch pipette was tip filled with internal solution and back filled with gramicidin-containing solution (2.5 – 10 µg ml⁻¹; G5002; Sigma Aldrich) to achieve perforated patch recordings. For stable long-term current-clamp recordings Amphotericin B (200 µg ml⁻¹; A4888; Sigma Aldrich) was used as poreforming agent. Gramicidin and Amphotericin B were dissolved in dimethyl sulfoxide (final concentration: 0.4 - 0.5%; DMSO; D8418, Sigma Aldrich) as described previously [Rae *et al.*, 1991; Kyrozis & Reichling, 1995] and was added to the modified pipette solution shortly before use. Drugs were bath-applied at a flow rate of 2 ml min⁻¹. Cocaine hydrochloride (10 µM; C5776; Sigma Aldrich) and (-)-quinpirole (10 – 1000 nM; Q102; Sigma Aldrich) were added to the normal aCSF shortly before the experiments. In order to quantify DRD₂-dependent GIRK currents, we used BaCl₂ (1 mM) which is known to block GIRK channels [Lacey *et al.*, 1988; Takigawa & Alzheimer, 1999; Cruz *et al.*, 2004]. Dopaminergic (DA) neurons in the substantia nigra pars compacta (SNpc) were identified by their slow and regular firing and the presence of a large I_h-dependent "sag"-potential [Ungless *et al.*, 2001; Lacey *et al.*, 1989; Richards *et al.*, 1997]. In voltage-clamp experiments,

dopaminergic neurons were additionally identified by their immunoreactivity for tyrosine hydroxylase (TH) or the dopamine transporter (DAT). All labelled cells which were identified using the aforementioned electrophysiological criteria exhibited DAT or TH immunoreactivity. Upon completion of the recordings, perforated-patch recordings were converted to the whole cell configuration and biocytin (1%; B4261; Sigma) was allowed to diffuse into the cell for 3 – 5 min. Brain slices were fixed in Roti-Histofix (Po873; Carl Roth, Karlsruhe, Germany) overnight at 4°C and rinsed in TBS. Afterwards, the slices were incubated in TBS-T and 10% normal goat serum (30 min). Brain slices were washed in TBS (3 x 10 min) and subsequently incubated for 2 days at 4°C in rabbit anti-TH (1:1000; ab112; Abcam, Cambridge, UK) or rat anti-DAT (1:500; ab5990; Abcam, Cambridge, UK) that was dissolved in TBS-T and 10% normal goat serum. Afterwards, brain slices were rinsed in TBS (3 x 15 min) and incubated with secondary antibodies: Alexa 633-conjugated streptavidin (1:600; S21375; Invitrogen, Karlsruhe, Germany), dylight 488 anti-rabbit IgG (1:200; ab96883; Abcam) or dylight 488 anti-rat IgG (1:200; ab96887; Abcam) for 2h at RT in TBS-T. Brain slices were rinsed in TBS (5 x 10 min), dehydrated, and then cleared and mounted in Permount. The fluorescence images were captured with a confocal microscope (LSM 510, Carl Zeiss, Göttingen, Germany). Data analysis was performed with Spike2 (Cambridge Electronics, Cambridge, UK), Igor Pro 6 (Wavemetrics) and Graphpad Prism (version 5.0b; Graphpad Software Inc., La Jolla, CA, USA). For each neuron, the firing rate was averaged over a time period of 60s under control conditions and after the drug treatment had reached a steady-state.

2.13 Microdialysis

The intracerebral microdialysis technique enables concentration measurements of neurotransmitters in freely moving animals. In these experiments, the effect of a single cocaine injection on the release of extracellular dopamine levels in the NAc was investigated. Experimental animals were anesthetized by i.p. injection of Ketamin (Albrecht GmbH, Germany) and Rompun (Bayer HealthCare, Germany) and

were stereotactically provided unilateral with a microdialysis guide cannula (CMA Microdialysis AB, Sweden). The tip of the microdialysis guide cannula was positioned just lateral to the NAc (coordinates: 2.0 mm anterior to bregma, 0.9 mm lateral from midline, and 2.9 mm below the surface of the brain; with toothbar set to obtain flat skull position). Dental cement was used to secure the microdialysis guide cannula to two stainless screws inserted in the skull. After surgery, animals were individually housed and allowed to recover for at least two weeks before the microdialysis experiment. The day before the start of intracerebral microdialysis, animals were anesthetized as described above, the dummy of the microdialysis guide cannula was retracted and a microdialysis probe (CMA7 probe (Microdialysis AB, Sweden), 6 kD cut-off membrane, 2 mm length) was inserted. After overnight recovery, the probe was then connected to a microperfusion pump and perfused with Ringer solution at a rate of $1 \mu\text{l min}^{-1}$. After four hours of habituation to the microdialysis perfusion set-up, perfusion samples were collected every 20 minutes. After collecting six baseline samples, cocaine (20 mg kg^{-1}) was administered i.p. and another six perfusion samples were collected after drug treatment. For absolute quantification of dopamine levels, a nano Acquity UPLC (Waters) was connected to a XevoTM TQ (Waters). An Acquity UPLC BEH Phenyl $1.7 \mu\text{m}$, $1 \text{ mm} \times 100 \text{ mm}$ column was used at room temperature. Solvent A was 0.1% formic acid and B acetonitril/0.1% formic acid. A linear gradient from 97% A to 5% in 8 min at a flow rate of $17 \mu\text{l min}^{-1}$ was used. $8 \mu\text{l}$ of sample were injected. The TQ was operated in positive ESI MRM (multi reaction monitoring) mode. The source temperature was set at 120°C , desolvation temperature was 200°C and desolvation gas was set to 400 l h^{-1} . The following MRM transitions were used; m/z 154.1 (M+H⁺) to 91.04 (quantifier) collision energy 22V, m/z 154.1 to 64.94 (qualifier) collision 30V, m/z 154.1 to 109.05 (qualifier) collision 18V, m/z 154.1 to 119.01 m/z (qualifier) collision 18V, 154.1 to 137.02 (qualifier) collision 10V, cone was in all cases 12V. As data management software MassLynx 4.1 (Waters) and for data evaluation and absolute quantification TargetLynx (Waters) were used. As external standard do-

pamine hydrochloride (Sigma-Aldrich, Germany) was dissolved in Ringer solution (DeltaSelect, Dreieich, Germany) containing 0.1% perchloric acid. With dopamine eluting at 6.23 min a standard calibration curve was calculated using concentrations ranging from 2.5 – 100 ng ml⁻¹. Correlation coefficient; $r < 0.995$, $r^2 < 0.992$; response type: external standard, area; curve type linear; weighting $1/x$. The peak integrations were corrected manually, if necessary. Quality control standards were used during sample analysis and showed between 0.5% and 40% deviation respectively. Blanks after the standard, quality control and sample batch proved to be sufficient. No carry over was detected. For the samples a slight shift in the retention time at 6.35 was observed due to the matrix. Microdialysis was performed with help of Linda A.W. Verhagen and Hella S. Brönneke. UPLC measurements of dopamine was performed by Thomas Franz and Yvonne Masekowitz (Max Planck Institute for Ageing, Cologne, Germany).

2.14 MeRIP pulldown

MeRIP pulldown of provided *Fto*-deficient midbrain RNA was performed by Kate D. Meyer in the lab of Samie R. Jaffrey. Immunoprecipitation of methylated RNAs was performed as described previously [Meyer *et al.*, 2012] using a rabbit anti-m6A antibody (Synaptic Systems, Göttingen, Germany). MeRIP-Seq was done using three biological replicates of midbrain RNA isolated from *Fto*-deficient and wild type (WT) littermate mice. Reads were aligned to the genome using the Burrows-Wheeler Aligner (BWA), and m⁶A peaks were called as previously described [Meyer *et al.*, 2012]. Only the peaks which reached significance in all three replicates for each sample were included in the final peak analysis.

2.15 GO analysis

GO analysis was performed by Yogesh Saletore and Olivier Elemento (Dept. of Physiology and Biophysics, Cornell University NY, USA). Peaks were identified

for *Fto*-deficient and WT samples as described above, and the genome coordinates of *Fto*-deficient peaks were intersected with those of WT peaks to determine the peaks that were specific to the *Fto* knockout samples. Pathway analysis was then performed using iPAGE46 and the GO database. Briefly, iPAGE identifies pathways that are informative about the distinction between two or more groups of genes using mutual information. For all highly informative pathways, it calculates hypergeometric enrichment and depletion P values in all gene groups considered and represents these pathways as red-blue heat maps. A similar analysis was performed comparing genes with m⁶A peaks in WT-expressed genes (reads per kilobase per million reads (RPKM) >1) compared to all other expressed genes (RPKM >1).

2.16 Pathway analysis

Pathway analysis was performed for deregulated transcripts in the microarray expression analysis (see section 3.1.2) and hypermethylated transcripts identified in MeRIP pulldown for *Fto*-deficient mice (see section 3.3.1). For pathway analysis, Ingenuity Pathway Analysis software (IPA, Ingenuity Systems, Inc., Redwood City CA, USA) was used.

2.17 Graphical representation of data

If not otherwise mentioned, all graphical representations were created using GraphPad Prism (GraphPad Software, Inc., La Jolla CA, USA) and Adobe Illustrator CS4 (Adobe Systems, San Jose CA, USA). Box plot whiskers indicate the minimum and maximum values, centerlines indicate the median and plus signs indicate the means. Sample sizes are indicated in parentheses.

2.18 Statistics

Statistical calculations were performed using Microsoft Excel (Microsoft Corp., Redmond WA, USA) and GraphPad Prism (GraphPad Software, Inc., La Jolla CA, USA). Details on statistical analysis are given in the respective figure legends.

2.19 Chemicals and Materials

Table 2.4: Chemicals

Chemical	Supplier
β -mercaptoethanol	Applichem, Darmstadt, Germany
0.9% saline (sterile)	AlleMan Pharma GmbH, Pfullingen, Germany
Acrylamide	Roth, Karlsruhe, Germany
Agarose	Peqlab, Erlangen, Germany
Agarose (Ultra Pure)	Invitrogen, Karlsruhe, Germany
Ammoniumpersulfat (APS)	Sigma-Aldrich, Seelze, Germany
Bacillol	Bode Chemie, Hamburg, Germany
Bovine serum albumin (BSA)	Sigma-Aldrich, Seelze, Germany
Bromphenol blue	Merck, Darmstadt, Germany
Chloroform	Merck, Darmstadt, Germany
Cocaine hydrochloride	Sigma-Aldrich, Seelze, Germany
Denhardt's Solution	Applichem, Darmstadt, Germany
Desoxy-ribonucleotid-triphosphates (dNTPs)	Amersham, Freiburg, Germany
Developer G153	AGFA, Mortsel, Belgium
DEPC	Applichem, Darmstadt, Germany
Dimethylsulfoxide (DMSO)	Merck, Darmstadt, Germany
di-Natriumhydrogenphosphat	Merck, Darmstadt, Germany
Enhanced chemiluminescence (ECL) Kit	Perbio Science, Bonn, Germany
Ethanol, absolute	Applichem, Darmstadt, Germany
Ethidium bromide	Sigma-Aldrich, Seelze, Germany
Ethylendiamine tetraacetate (EDTA)	Applichem, Darmstadt, Germany
Fixer G354	AGFA, Mortsel, Belgium
Forene (isoflurane)	Abbot GmbH, Wiesbaden, Germany
Formamide	Applichem, Darmstadt, Germany
Glucose 20%	DeltaSelect, Pfullingen, Germany
Glycerol	Serva, Heidelberg, Germany

Continued on next page

Table 2.4 – continued from previous page

Chemical	Supplier
Glycine	Applichem, Darmstadt, Germany
HEPES	Applichem, Darmstadt, Germany
Hydrochloric acid (37%)	KMF Laborchemie, Lohmar, Germany
Insulin	Novo Nordisk, Bagsvaerd, Denmark
Isopropanol (2-propanol)	Roth, Karlsruhe, Germany
Magnesium chloride	Merck, Darmstadt, Germany
Methanol	Roth, Karlsruhe, Germany
Nitrogen (liquid)	Linde, Pullach, Germany
NP-40	Roche Diagnostics GmbH, Mannheim, Germany
Paraformaldehyde (PFA)	Sigma-Aldrich, Seelze, Germany
Phosphate buffered saline (PBS)	Gibco BRL, Eggenstein, Germany
Potassium chloride	Merck, Darmstadt, Germany
Potassium dihydrogenphosphat	Merck, Darmstadt, Germany
Potassium hydroxide	Merck, Darmstadt, Germany
(-)-Quinpirole	Sigma-Aldrich, Seelze, Germany
Sage tea	Bad Heilbrunner Naturheilmittel GmbH
Sodium acetate	Applichem, Darmstadt, Germany
Sodium chloride	Applichem, Darmstadt, Germany
Sodium citrate	Merck, Darmstadt, Germany
Sodium dodecyl sulfate	Applichem, Darmstadt, Germany
Sodium fluoride	Merck, Darmstadt, Germany
Sodium hydrogen phosphate	Merck, Darmstadt, Germany
Sodium hydroxide	Applichem, Darmstadt, Germany
Sodium orthovanadate	Sigma-Aldrich, Seelze, Germany
Sodium pyrophosphate	Sigma-Aldrich, Seelze, Germany
Tetramethylethylenediamine (TEMED)	Sigma-Aldrich, Seelze, Germany
Tissue Freezing Medium	Jung, Heidelberg, Germany
Tramadolhydrochlorid (Tramal)	Grünenthal, Aachen, Germany
Trishydroxymethylaminomethane (Tris)	Applichem, Darmstadt, Germany
Triton X-100	Applichem, Darmstadt, Germany
Trizol	Applichem, Darmstadt, Germany
Tween 20	Applichem, Darmstadt, Germany
Vectashield Mounting Medium with DAPI	Vector, Burlingame, USA
Western Blocking Reagent	Roche Diagnostics GmbH, Mannheim, Germany

3 Results

3.1 Whole body *Fto* deficiency alters the function of the dopaminergic circuitry

3.1.1 FTO is expressed in midbrain dopaminergic neurons

FTO is ubiquitously expressed with highest levels detected in the brain, especially in feeding related nuclei [Gerken *et al.*, 2007; McTaggart *et al.*, 2011]. To test whether FTO is expressed in dopaminergic neurons, midbrain slices of wildtype C57Bl/6 mice were immunohistochemically stained for FTO and tyrosine hydroxylase, the rate limiting enzyme in dopamine synthesis and hence a suitable marker for dopamine neurons in the midbrain (Figure 3.1).

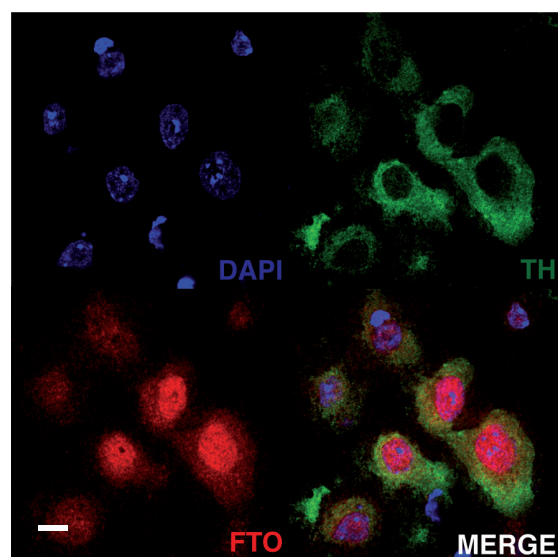


Figure 3.1: **FTO is expressed in dopaminergic neurons of the midbrain**

Double immunofluorescent labeling of tyrosine hydroxylase (TH, green) and FTO (red) in wildtype C57Bl/6 midbrain slices. Nuclear staining with DAPI (blue). Representative picture of $n > 3$, scale bar = 10 μm .

FTO is present in dopaminergic neurons and, consistently with previous reports, immunoreactivity was found to be primarily localized in the nucleus [Gerken *et al.*, 2007; McTaggart *et al.*, 2011]. Moreover, a slight cytosolic immunoreactivity was observed for FTO. Whether this signal is specific to any FTO function remains elusive.

Furthermore, expression of *Fto* was investigated using a mouse model carrying a knock in of the β -galactosidase gene into the endogenous *Fto* locus (*Fto::tm1a*-(EUCOMM)Wtsi, see Section 3.2.1 for further description). X-gal staining of brain sections confirmed the expression of *Fto* throughout the central nervous system, including the hypothalamus (ARC, VMH, DMH, PVN) and midbrain (VTA, SN)(Figure 6.2 in appendix).

***Fto* deficiency does not change the number or morphology of midbrain dopaminergic neurons**

Since *Fto*-deficient mice suffer from a severe phenotype including growth retardation and decreased postnatal survival rate [Fischer *et al.*, 2009], loss of FTO may potentially impact cell viability. Thus, to test whether the health of dopaminergic cells is affected by *Fto* deficiency, cell number and morphology was assessed in whole body *Fto*-deficient (*Fto*^{-/-}) and control (*Fto*^{+/+}) mice (see Figure 3.2).

No significant differences in cell number as well as cell area and perimeter were detected for dopamine neurons. Hence, loss of FTO does not alter the general health of dopaminergic neurons.

3.1.2 Microarray analysis of *Fto*-deficient midbrain

Expression analysis of *Fto*-deficient midbrain tissue

To generate a general hypothesis for possible effects of *Fto* deficiency on dopaminergic neuron function, gene expression was compared between *Fto*-deficient and control midbrain tissue using microarray analysis. For this purpose, RNA was isolated from midbrain tissue (RNA integrity number determined by bioanalyzer chip ≥ 8.9) and subsequently the RNA was hybridized to an Affymetrix GeneChip

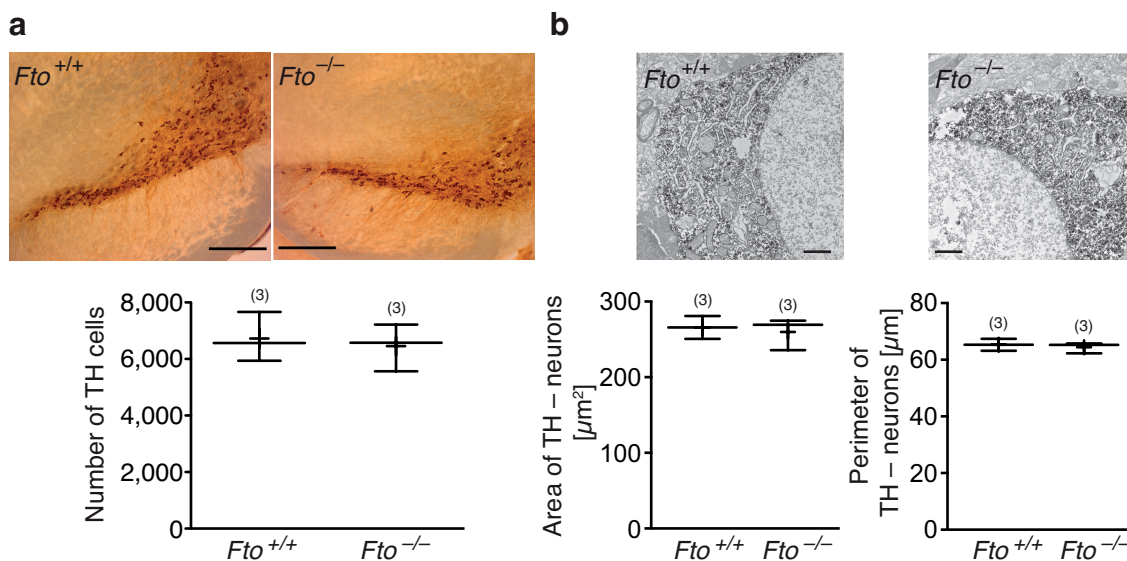


Figure 3.2: **Loss of FTO does not alter cell number or morphology of dopaminergic mid-brain neurons**

(a) Immunohistochemical labeling of FTO and quantification of cells was performed on midbrain sections of control and *Fto*-deficient mice. Experiments performed by Marcelo O. Dietrich and Tamas L. Horvath. Sample sizes are indicated in parentheses, no significant differences were detected. (b) Electron microscopy of wildtype and *Fto*-deficient dopaminergic neurons. *Fto* deficiency does not alter the morphology of dopaminergic neurons as assessed by quantification of cell area and perimeter. Experiments performed by Marcelo O. Dietrich and Tamas L. Horvath. Sample sizes are indicated in parentheses, no significant differences were detected.

Mouse Gene 1.0 ST array. Transcripts were considered significantly deregulated for p-values ≤ 0.05 (*t*-test) and a false discovery rate (q-value) of ≤ 0.25 .

In total, 5785 transcripts were significantly deregulated, of which 2382 were down- and 3403 were up-regulated. The relative changes in transcript expression, however, were relatively low, with the highest downregulation observed for *Cartpt* (-4.807) and the highest up-regulation for *TdGF1* ($+2.774$) (see Figure 3.3 and Table 6.2).

Most of the transcripts exhibited minor expression changes (Figure 3.3 fold change (fc) cut off ± 1.80 ; table 6.2 fc cut off ± 1.50). Among the deregulated mRNAs, several transcripts were identified that are directly or indirectly related to dopaminergic signaling. Significantly downregulated transcripts included the dopamine transporter (*Slc6a3*, fc = -2.558), tyrosine hydroxylase (*Th*, fc = -1.880), dopamine

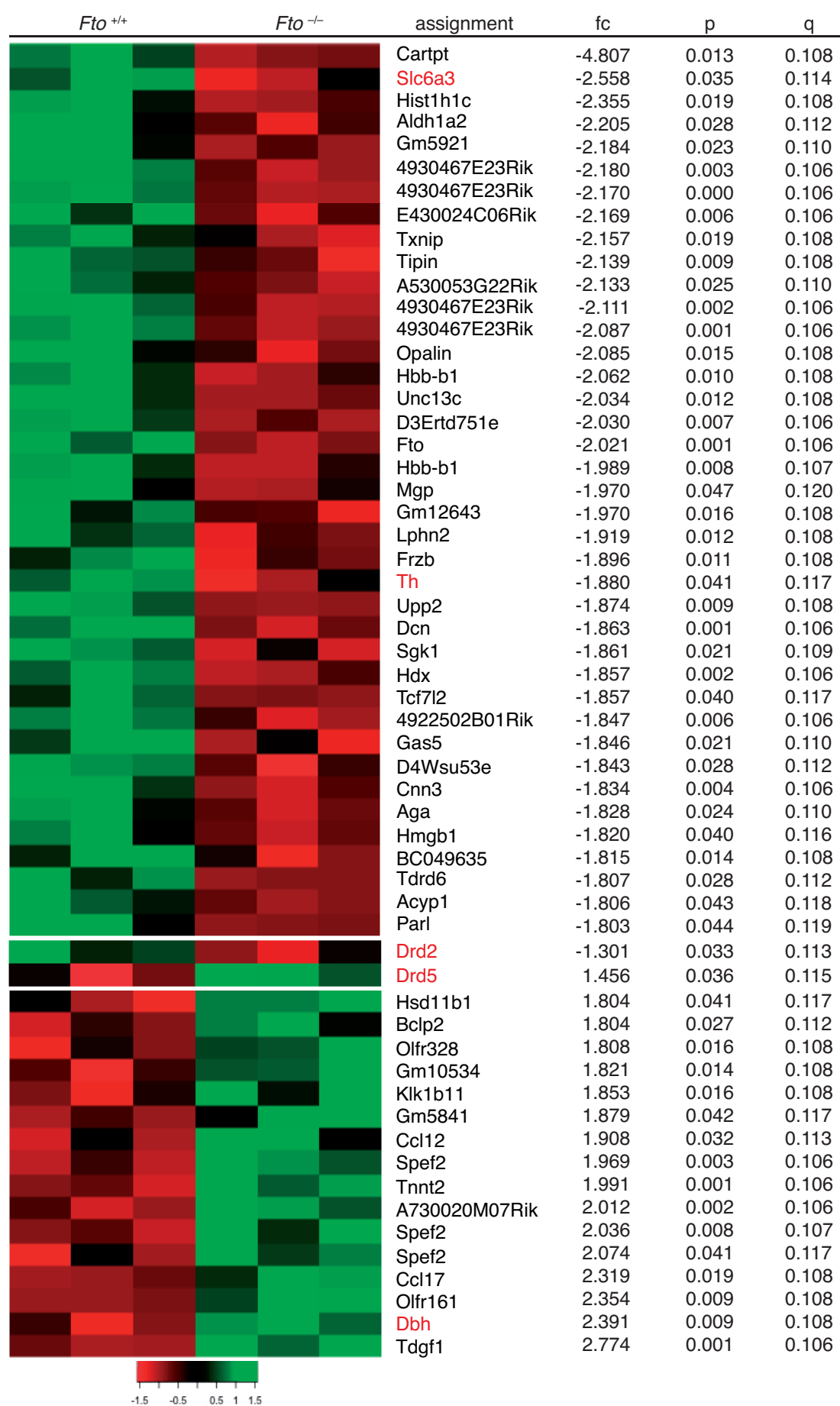
Figure 3.3: Microarray analysis of *Fto*-deficient midbrain tissue

Figure 3.3: Microarray analysis of *Fto*-deficient midbrain tissue

Microarray analysis was performed for control and *Fto*-deficient midbrain tissue. Normalized intensities are presented as a heatmap (each row scaled individually), key indicates Z-Score for color coding. Fold change (fc), p-value (p) and false discovery rate (q-value, q) are shown for a selection of significantly deregulated genes. Highlighted in red are components related to dopaminergic signaling. n = 3 per genotype

type 2 receptor (*Drd2*, fc = -1.301), dopa decarboxylase (*Ddc*, fc = -1.371) and the vesicular monoamine transporter (*Slc18a2*, fc = -1.306). Transcripts of the dopamine type 5 receptor (*Drd5*, fc = $+1.456$) and the dopamine beta hydroxylase (*Dbh*, fc = $+2.391$) were found to be upregulated.

Critical components of dopaminergic signaling are deregulated in *Fto*-deficient mice

The overlay of deregulated transcripts using pathway analysis revealed that several components implicated in dopaminergic function were affected in *Fto*-deficient mice (see Figure 3.4). Transcripts of three enzymes involved in the dopamine synthesis were deregulated. The mRNA levels of both the tyrosine hydroxylase, converts L-tyrosine to L-DOPA, and the dopa decarboxylase, converts L-DOPA to dopamine, were reduced in *Fto*-deficient mice, while the transcript levels of the dopamine beta hydroxylase, catalyzes the reaction from dopamine to norepinephrine, was increased (Figure 3.4). These alterations could potentially affect dopamine availability through a reduction in dopamine synthesis and an increase in conversion of dopamine to norepinephrine.

Additionally, a downregulation of the vesicular monoamine transporter, which transports monoamines such as dopamine into synaptic vesicles, could lead to a reduction in dopamine release. On the other hand the downregulation of the dopamine transporter via a reduction in dopamine reuptake from the synaptic cleft, may prolong dopaminergic signaling and thus counteract the potentially decreased levels of secreted dopamine.

Moreover, dopaminergic neurons express dopamine autoreceptors of the D2-like dopamine receptor family (DRD2 and DRD3). One of these, the type 2 dopamine

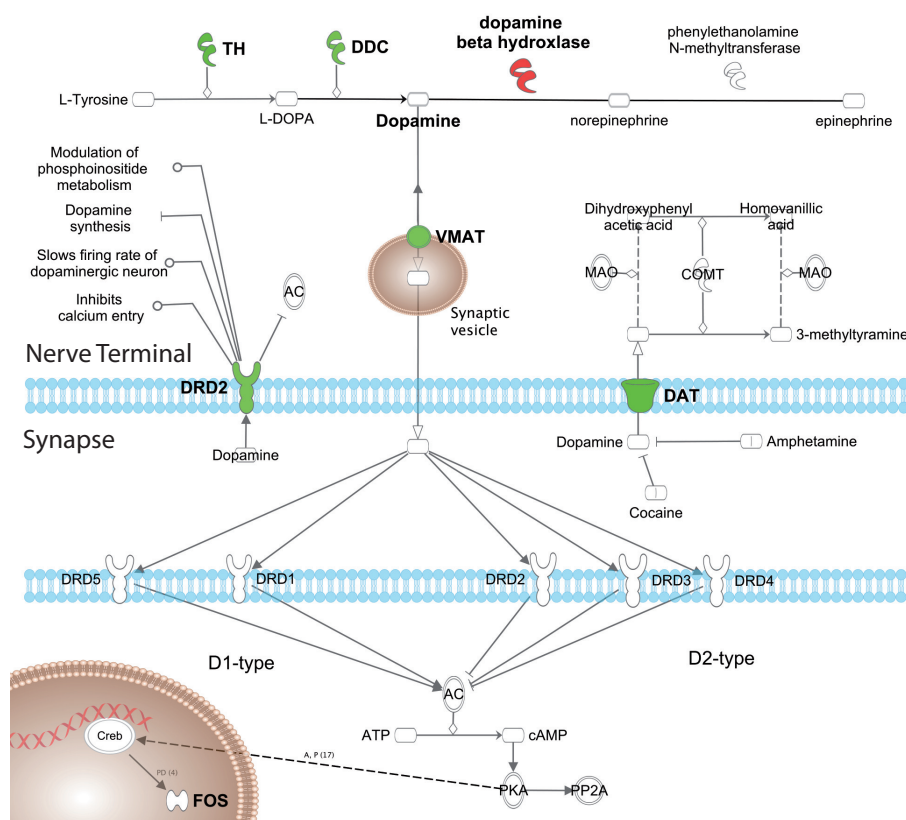


Figure 3.4: **Schematic overlay of the microarray expression data and the dopaminergic signaling pathway**

Key components of dopaminergic signaling and dopamine syntheses exhibit altered expression in midbrain of *Fto*-deficient mice. TH: tyrosine hydroxylase, DDC: dopa decarboxylase, VMAT: vesicular monoamine transporter, DAT: dopamine transporter, AC: adenylyl cyclase, COMT: catechol-O-methyl transferase, MAO: monoamine oxidase. Overlay was created using Ingenuity Pathway Analysis software. Green indicates downregulation and red indicates upregulation of the respective transcripts.

receptor (DRD2), was found to be downregulated on the mRNA level. A reduction in DRD2 autoreceptor signaling could potentially impinge on the regulation of dopamine release through attenuation of the autoreceptor feedback loop [Beaulieu & Gainetdinov, 2011; Bello *et al.*, 2011].

Selected deregulated transcripts are not altered on protein level

To confirm the alterations of transcript levels observed in the microarray analysis, quantitative PCR was conducted on a selected subset of deregulated transcripts. To this end, qPCR analysis of *Drd2*, *Th*, and *Slc6a3* verified the observed downregulations for midbrain tissue of *Fto*-deficient mice (Figure 3.5 a, b, c).

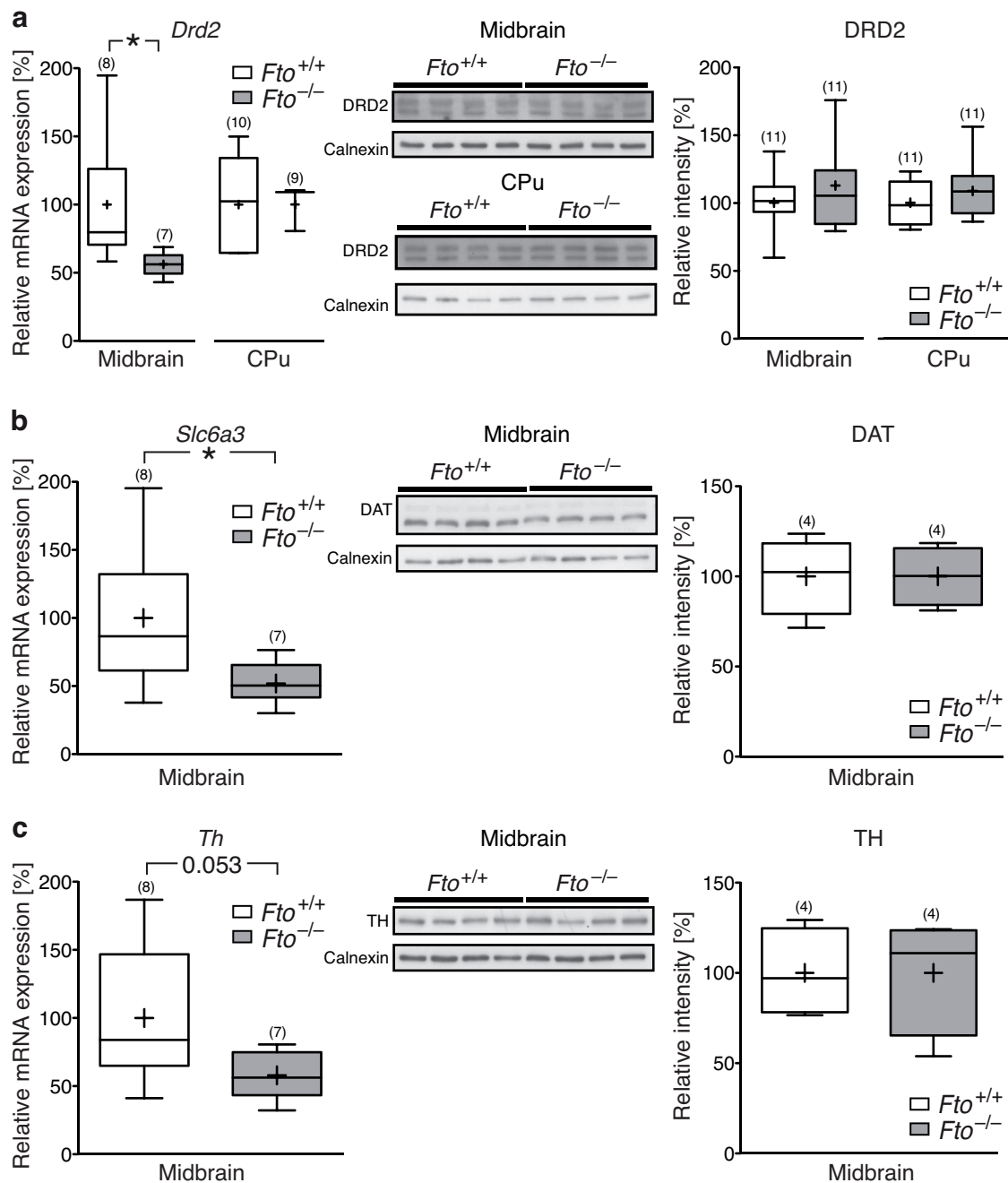


Figure 3.5: **Selected transcripts deregulated in microarray analysis are not altered on protein level**

Quantitative PCR on selected deregulated transcripts confirmed the microarray analysis. mRNA levels for (a) *Drd2* and (b) *Slc6a3* are significantly downregulated, whereas a strong tendency is detected for (c) *Th*. Western blot analysis, however, reveals no changes on protein level for DRD2, DAT and TH. Western blot for DRD2 (a) was performed using three different antibodies. Sample blot shows α -DRD2 ab21218 (Abcam, Inc.) with two bands corresponding to the long (DRD2L, 51 kDa) and short form (DRD2S, 47 kDa) of DRD2. Sample sizes indicated in parentheses, * $P < 0.05$, unpaired two-tailed t -test.

Since mRNA levels may not necessarily reflect protein levels, western blot analysis was performed for DRD2, TH and DAT. In contrast to the changes on the mRNA level, no alterations of protein levels were observed (Figure 3.5 a, b, c).

3.1.3 *Fto*-deficient mice exhibit attenuated responses to cocaine

Cocaine fails to increase locomotor activity in *Fto*-deficient mice

Many addictive substances affect dopaminergic signaling [Beaulieu & Gainetdinov, 2011; Koob & Volkow, 2010]. One of the most prominent drugs of abuse is cocaine, which potently blocks the dopamine transporter [Beaulieu & Gainetdinov, 2011]. Due to the resulting prolonged dopaminergic signaling, the primary effect of cocaine administration is an increase in locomotor activity. For this reason, many studies use cocaine to test the functionality of the dopaminergic system, utilizing locomotor activity as the primary readout [Koob & Volkow, 2010; Seale & Carney, 1991].

To test whether the functionality of the dopaminergic system is altered, locomotor activity after intraperitoneal (i.p.) cocaine administration was assessed in *Fto*-deficient and control mice. After baseline measurement of locomotor activity (saline injection), mice were challenged with two different cocaine concentrations

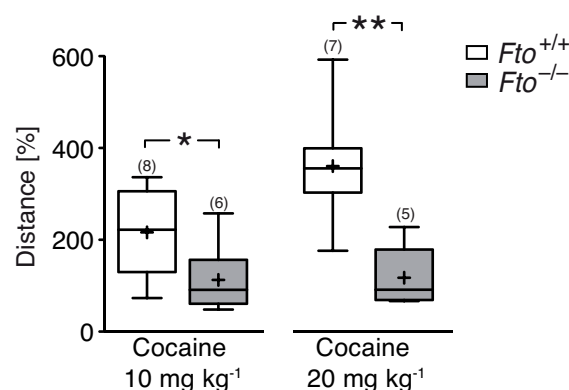


Figure 3.6: Cocaine fails to increase locomotor activity in *Fto*-deficient mice

Control and *Fto*-deficient mice were injected i.p. with 10 mg kg⁻¹ and 20 mg kg⁻¹ cocaine. Data is represented as percent relative to baseline saline injection (sample sizes indicated in parentheses, * $P < 0.05$, ** $P < 0.01$, unpaired two-tailed t -test).

(10 mg kg⁻¹ and 20 mg kg⁻¹ body weight). While wildtype control mice significantly increased their locomotor activity at both 10 mg kg⁻¹ (216±34%) and 20 mg kg⁻¹ (361±47%) cocaine, *Fto*-deficient mice failed to increase their locomotor activity (10 mg kg⁻¹: 113±31%, 20mg kg⁻¹: 117±30%, Figure 3.6). These results indicate that dopaminergic function is severely attenuated, rendering *Fto*-deficient mice insensitive to the locomotor stimulatory effect of cocaine.

Cocaine fails to increase *Fos* expression in *Fto*-deficient mice

To assess the observed insensitivity to cocaine on the network level, *Fto*-deficient mice were treated with 20 mg kg⁻¹ cocaine i.p. and subsequently midbrain, NAc and CPU tissue was analyzed for *Fos* expression. *Fos*, as one of the immediate early genes, is a widely used marker for neuronal activity [Knight *et al.*, 2012; Dragunow & Faull, 1989]. As such, cocaine-induced stimulation of dopamine signaling is able to induce *Fos* expression as a result of the modulation of neuronal activity.

Fos mRNA expression significantly increased 2h after i.p. cocaine treatment in wildtype control mice in all brain areas investigated (Figure 3.7). Conversely, in *Fto*-deficient mice cocaine failed to increase the *Fos* mRNA levels (Figure 3.7, also

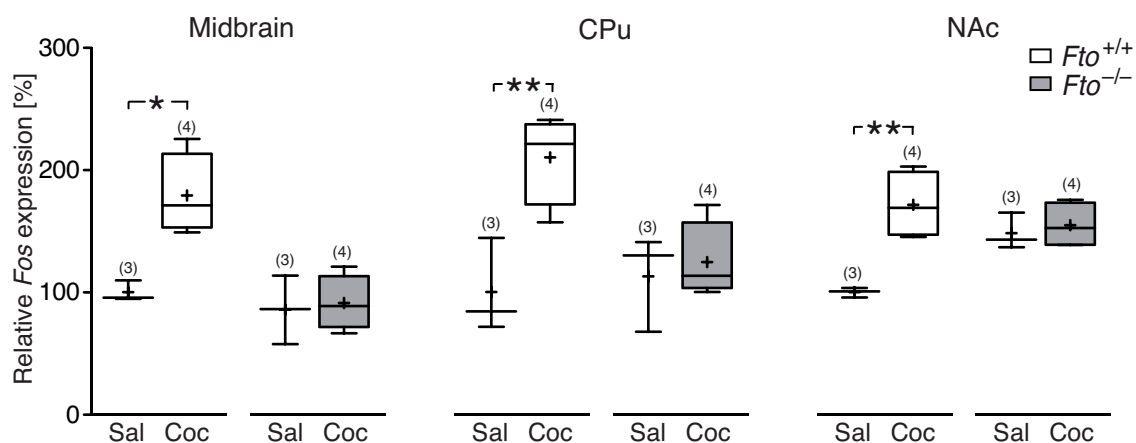


Figure 3.7: **Cocaine fails to increase *Fos* expression in *Fto*-deficient mice**

Midbrain, caudate putamen (CPU) and nucleus accumbens (NAc) of control and *Fto*-deficient mice were dissected 2h after either saline (Sal) or 20 mg kg⁻¹ cocaine (Coc) i.p. injection. *Fos* expression was measured using qPCR and is represented as relative increase compared to saline (Sal) injected control animals. (**P*<0.05, ***P*<0.01, unpaired two-tailed *t*-test, sample sizes are indicated in parentheses).

confirmed on the protein level see Figure 6.1 in appendix). Of note, *Fos* mRNA levels were elevated under baseline conditions (saline) in the NAc of *Fto*-deficient mice. Thus, the *Fos* expression analysis was consistent with the observed failure of *Fto*-deficient mice to increase their locomotor activity in response to cocaine.

Cocaine evoked extracellular levels of dopamine are reduced in *Fto*-deficient mice

In order to test whether the loss of FTO affected dopamine release and/or reuptake, extracellular levels of dopamine were measured in the NAc of *Fto*-deficient and control mice via implantation of a microdialysis probe and subsequent detection of dopamine via ultra performance liquid chromatography (UPLC) coupled to mass spectrometry. During the experiment, mice were challenged with either 10 or 20 mg kg⁻¹ body weight cocaine i.p. injection.

In both *Fto*-deficient and control mice extracellular levels of dopamine increased in response to cocaine administration, due to the blockade of the dopamine transporter preventing dopamine reuptake. Comparing *Fto*-deficient and control mice, no differences in the relative increase in extracellular dopamine levels were de-

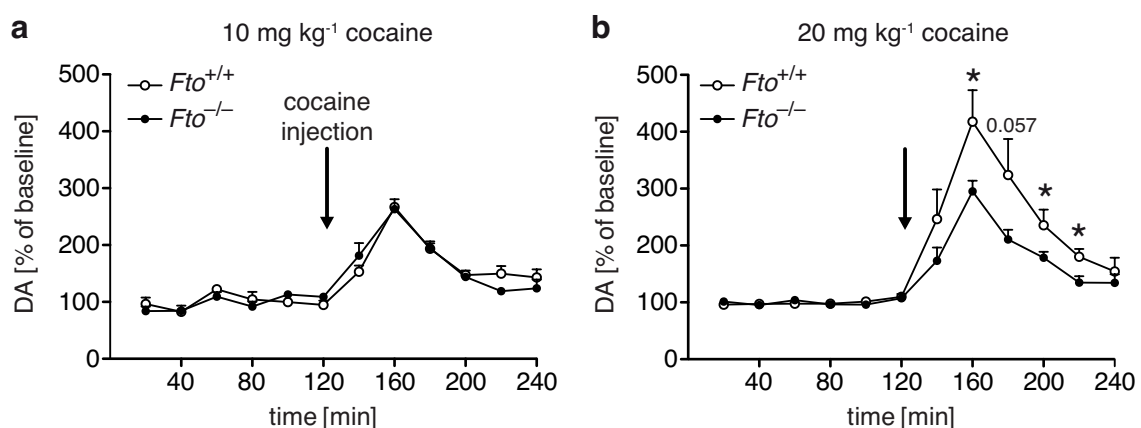


Figure 3.8: **Reduction in cocaine-induced extracellular dopamine in the nucleus accumbens of *Fto*-deficient mice**

Levels of extracellular dopamine in response to 10 mg kg⁻¹ (a) and 20 mg kg⁻¹ (b) i.p. cocaine administration were measured in the NAc of control (n=6) and *Fto*-deficient (n=7) mice using microdialysis. Dopamine was subsequently detected by ultra performance liquid chromatography (UPLC). Graph shows mean \pm s.e.m. for each individual measurement time point (**P*<0.05, unpaired two-tailed *t*-test).

tected for the 10 mg kg⁻¹ cocaine treatment (Figure 3.8 a). At a higher cocaine dosage (20 mg kg⁻¹) however, dopamine levels significantly varied between *Fto*-deficient and control mice (Figure 3.8 b). In comparison to the lower cocaine dosage, control mice had even further elevated dopamine content in the NAc in response to 20 mg kg⁻¹ cocaine injection. *Fto*-deficient mice, on the other hand, displayed similar relative increases at both cocaine concentrations. Hence, dopamine release appears to have reached a maximum at 10 mg kg⁻¹ cocaine in *Fto*-deficient mice. Unfortunately, whether these differences are due to alterations in dopamine synthesis rates, dopamine release or dopamine reuptake cannot be addressed using the microdialysis technique.

3.1.4 Attenuation of the DRD2/DRD3 autoreceptor feedback loop in *Fto*-deficient mice

DRD2/DRD3 receptor dependent responses are altered in *Fto*-deficient mice

To investigate the effects of *Fto* deficiency on the cellular level, neuronal activity of single cells was measured in midbrain slices of *Fto*-deficient and control mice using the patch-clamp technique. No differences in the general properties of dopaminergic neurons were detected, except a slightly reduced conductance density for *Fto*-deficient mice (Table 6.1 in appendix). While under baseline conditions, dopaminergic neurons fired tonically at a rate of approximately 2 Hz, bath application of cocaine (10 μM) potently reduced the firing rate of these neurons in control mice on average by 86% (Figure 3.9 a). In *Fto*-deficient mice, however, cocaine's ability to reduce the firing rate of dopaminergic neurons was significantly attenuated (reduction by 46%, Figure 3.9 a).

Since dopamine neurons express autoreceptors, blocking of the dopamine transporter by cocaine increases the amount of extracellular dopamine, which then binds to these D2-like receptors, leading to the activation of an autoinhibitory feedback loop that silences the neurons in a G protein-coupled inwardly rectifying potassium channel (GIRK) dependent manner [Lüscher & Slesinger, 2010].

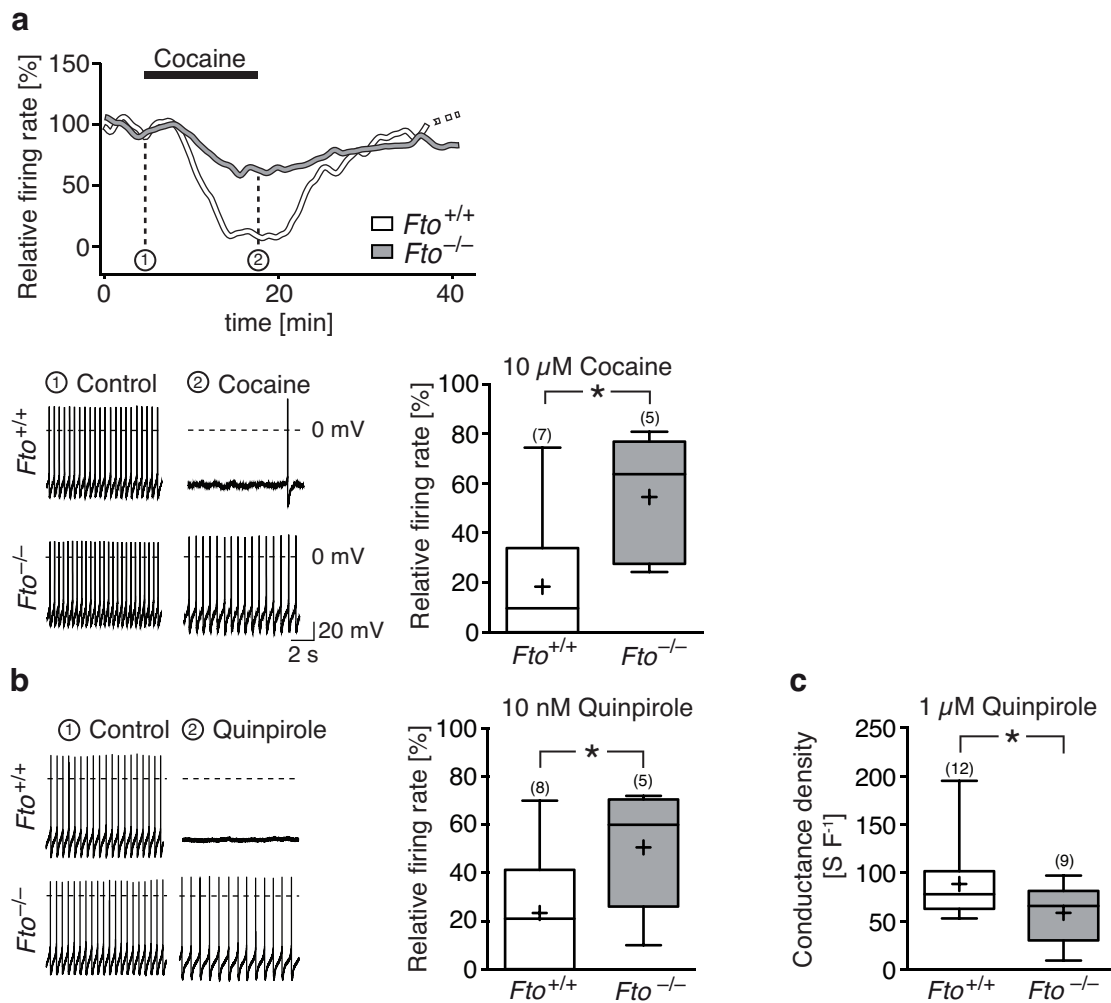


Figure 3.9: **Altered DRD₂/DRD₃ receptor dependent responses in *Fto*-deficient mice**

(a) Relative firing rate of SNpc dopaminergic neurons in patch clamp recordings during bath application of cocaine (10 μ M, 10 min). Sample trace shows recording of firing rate before, during and after bath application of cocaine (sample sizes indicated in parentheses, * $P < 0.05$, unpaired two-tailed t -test). (b) Bath application of the D₂-D₃-receptor agonist quinpirole (10 nM) on control and *Fto*-deficient dopamine neurons (sample sizes indicated in parentheses, * $P < 0.05$, unpaired one-tailed t -test). (c) In line with the attenuated reduction in firing rate, quinpirole (1 μ M) mediated increase in conductance density is significantly reduced in *Fto*-deficient mice (sample sizes indicated in parentheses, * $P < 0.05$, unpaired one-tailed t -test). All electrophysiological experiments were conducted by Simon Hess.

To further assess whether the observed alteration in autoinhibition was directly related to receptor function, the selective DRD₂/DRD₃ agonist quinpirole (10 nM) was applied during patch clamp recordings of midbrain dopaminergic neurons. In line with the previous finding, quinpirole potently inhibited firing in control neurons, while the response in *Fto*-deficient neurons was significantly attenuated (Figure 3.9 b). Consistently, the quinpirole (1 μ M) evoked conductance density, a measure of the membrane's ability to pass current, was significantly reduced in *Fto*-deficient mice (Figure 3.9 c).

Taken together, these results demonstrate that the DRD₂/DRD₃ dependent autoreceptor feedback loop was affected by the loss of FTO. Since the primary function of the autoreceptor feedback loop is the opening of GIRKs, the attenuated ability to reduce the firing rate in *Fto*-deficient mice may be a result of a reduction in DRD₂/DRD₃ or GIRK expression. Moreover, malfunction of the intracellular coupling of the dopamine receptors to GIRKs could potentially represent the underlying cause of the attenuated cocaine and quinpirole-mediated reduction in firing rate.

Reduced GIRK dependent current density in *Fto*-deficient mice

To directly assess the GIRK mediated and dopamine autoreceptor dependent changes in membrane conductance, brain slices were incubated with quinpirole (300 nM) to fully activate the DRD₂/DRD₃ autoreceptor feedback loop. Subsequently, bath application of barium chloride (1 mM), a potent potassium channel blocker, was used to measure the change in current density mediated by GIRKs (Figure 3.10). Confirming the previous results, the increase in quinpirole-dependent current density was attenuated in *Fto*-deficient mice. Furthermore, these quinpirole mediated changes were almost completely reversed by the blockade of GIRK channels, demonstrating that GIRK currents are the main driver of dopamine autoinhibition. The GIRK dependent current density was significantly lower in *Fto*-deficient mice, further supporting the notion that the DRD₂-DRD₃ dependent feedback loop depends on GIRK function and FTO expression (Figure 3.10).

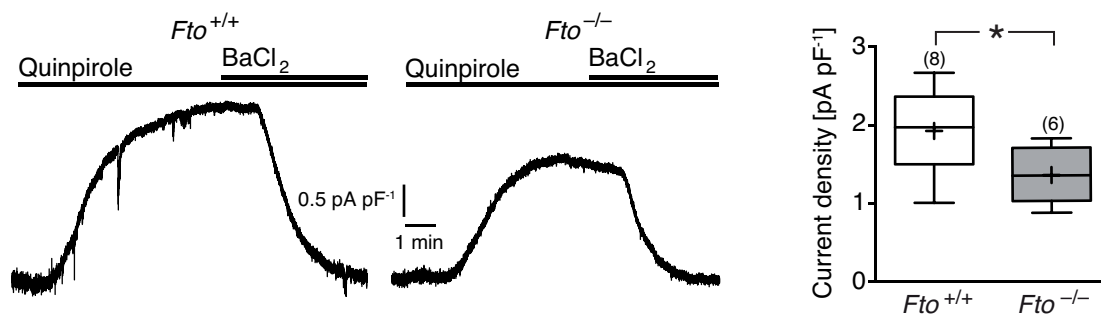


Figure 3.10: **Reduced GIRK dependent current density in *Fto*-deficient mice**

DRD2 mediated activation of GIRK channels is attenuated in *Fto*-deficient dopamine neurons. GIRK currents were measured by activation of D2 receptors by quinpirole (300 nM) and subsequent blocking of GIRKs by BaCl₂ (1 mM) (sample sizes indicated in parentheses, * $P < 0.05$, unpaired two-tailed *t*-test). All electrophysiological experiments were conducted by Simon Hess.

Attenuated quinpirole dependent decrease in locomotor activity in

Fto-deficient mice

As on the cellular level, *Fto*-deficient mice showed an attenuated response to quinpirole, the ability of quinpirole to reduce locomotor activity was tested in freely moving animals [Mattingly *et al.*, 1993; Bello *et al.*, 2011]. Intraperitoneal injection of quinpirole dose dependently decreased locomotor activity in both *Fto*-deficient, as well as control mice (Figure 3.11). *Fto*-deficient mice, however, exhibited an attenuated response to quinpirole, retaining a higher relative locomotor activity than control littermates. Locomotor activity was significantly higher at 100 $\mu\text{g kg}^{-1}$ i.p. quinpirole injection and showed a tendency for 30 $\mu\text{g kg}^{-1}$ as compared to controls (Figure 3.11).

Taken together, *Fto*-deficient mice displayed a significant attenuation of cocaine and quinpirole evoked locomotor responses. Furthermore, cocaine's ability to induce *Fos* expression was blunted and *Fto*-deficient mice exhibited a reduction in cocaine evoked extracellular levels of dopamine in the NAc (20 mg kg^{-1} cocaine i.p.). On the cellular level, *Fto*-deficiency altered the ability of the DRD2/DRD3-GIRK dependent autoreceptor feedback loop to inhibit dopamine neuron firing.

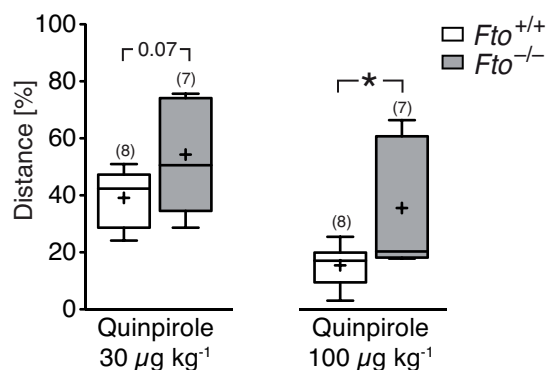


Figure 3.11: **Attenuated quinpirole dependent decrease in locomotor activity in *Fto*-deficient mice**

Control and *Fto*-deficient mice were injected i.p. with 30 $\mu\text{g kg}^{-1}$ and 100 $\mu\text{g kg}^{-1}$ quinpirole. Data is represented as percent relative to baseline saline injection. (* $P < 0.05$, unpaired two-tailed *t*-test, sample sizes are indicated in parentheses).

3.2 Dopamine neuron restricted loss of FTO attenuates the function of the DRD2/DRD3 dependent autoreceptor feedback loop

3.2.1 Generation of dopamine neuron restricted *Fto* knock out mice

Conventional whole body deletion of *Fto* causes a severe phenotype that, with respect to dopaminergic function, affects dopamine neurons as well as target neurons of the midbrain dopamine system. Hence, the loss of *Fto* most probably alters pre- as well as postsynaptic signaling events. Therefore, mice with a dopamine neuron restricted *Fto* deletion ($Fto^{\Delta\text{DAT}}$) were generated using the Cre-loxP system, to investigate the role of FTO specifically in dopaminergic neurons.

Mouse models for dopamine neuron restricted *Fto* deletion

To generate a dopamine neuron restricted FTO knock out, mice with a loxP site flanked exon 3 of the *Fto* gene (knock out first allele EUCOMM, $Fto::tm1a$ - (EUCOMM)Wtsi; Figure 3.12 a) were crossed to FLP-deleter mice and subsequently to transgenic mice expressing the Cre recombinase under the control of the endogenous dopamine transporter (*Dat*) promoter (Figure 3.12 b; Ekstrand *et al.* [2007]).

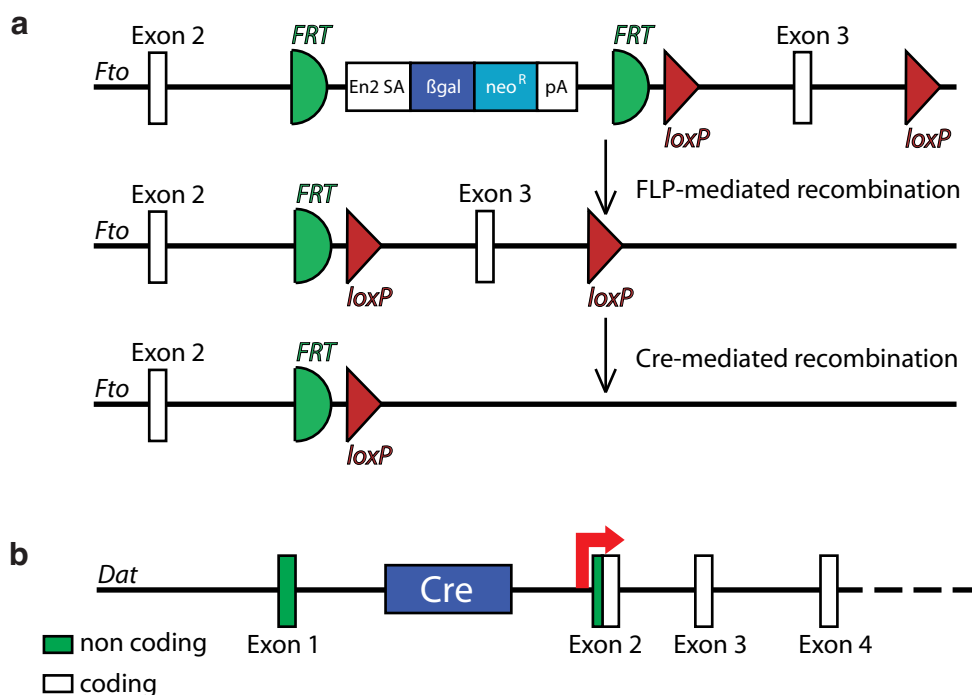


Figure 3.12: **Schematics of Cre-dependent deletion of *Fto***

(a) *Fto::tm1a*(EUCOMM)Wtsi mice provided by the European Conditional Mouse Mutagenesis program carry a flippase recognition target (FRT) site flanked knock in of the β -galactosidase gene in conjunction with a neomycin resistance cassette (knock out first allele). Furthermore, loxP sites were introduced flanking the third exon of the *Fto* gene. Prior to FLP deletion, the knock out first construct was used for β -galactosidase stainings. The conditional allele was generated through crossing of mice with FLP-recombinase, deleting the β -galactosidase and neomycin cassette and restoring endogenous *Fto* expression levels. (b) Subsequent crossing of mice carrying the conditional allele with mice expressing the Cre recombinase under the control of the endogenous *Dat* promoter Ekstrand *et al.* [2007] led to the generation of dopamine neuron restricted *Fto* knock outs (*Fto* ^{Δ DAT}) and controls (*Fto*^{fl/fl}).

The dopamine transporter is regarded as a selective marker for dopaminergic neurons [Ciliax *et al.*, 1995; Freed *et al.*, 1995]. Therefore, directing the expression of Cre to DAT expressing neurons caused a dopamine neuron restricted recombination of loxP sites. Deletion of the loxP site flanked third exon of *Fto* leads to a frame shift, causing a premature translational stop signal. Moreover, exon 3 encodes for approximately 40% of the FTO protein. The remaining truncated *Fto* mRNA is likely to undergo degradation via nonsense-mediated decay mechanisms. Hence, excision of the third *Fto* exon was expected to efficiently delete FTO.

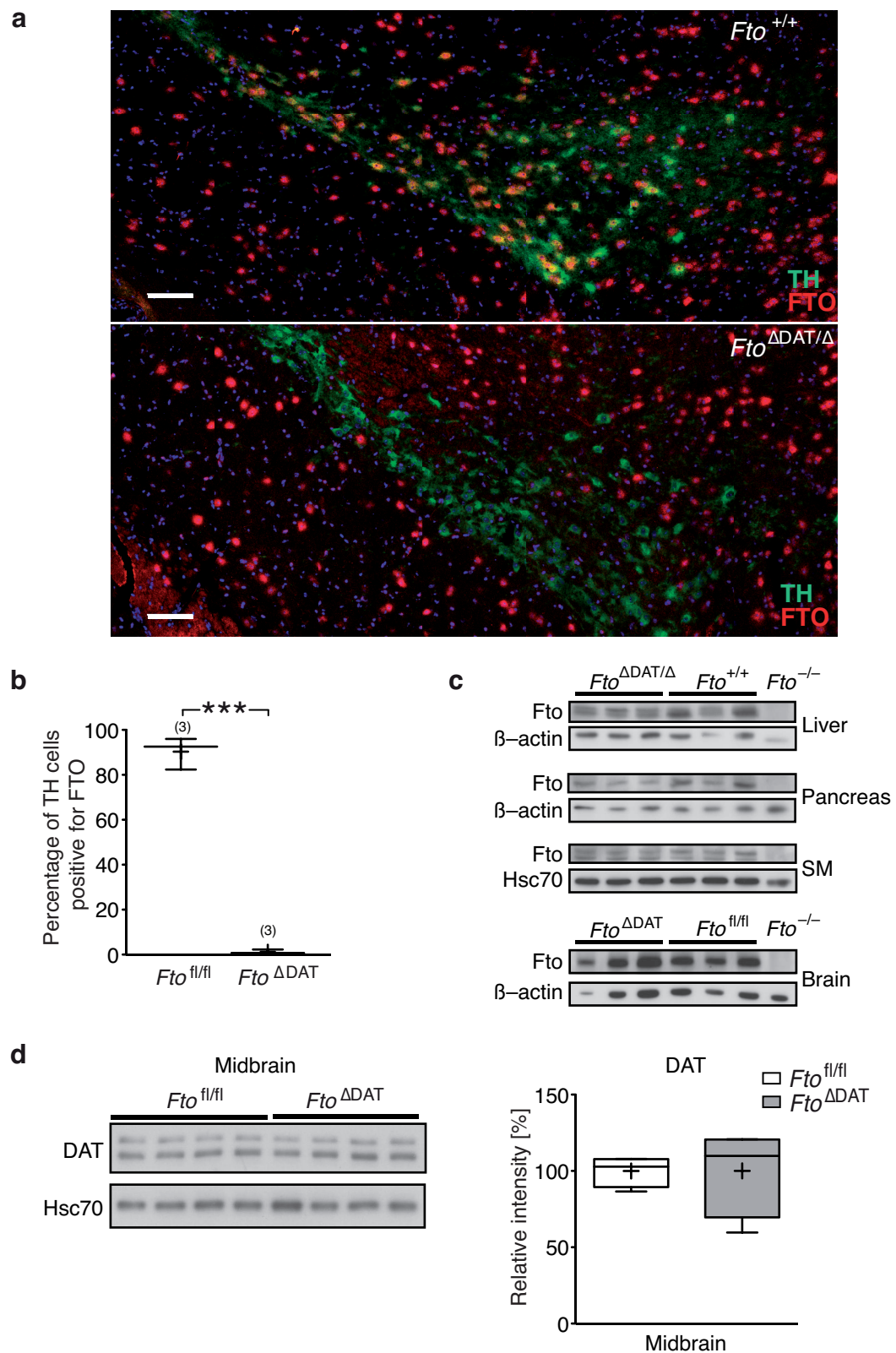


Figure 3.13: Validation of DA neuron specific *Fto* deletion

Figure 3.13: Validation of DA neuron specific *Fto* deletion

(a) Midbrain dopaminergic neurons were stained in *Fto*^{ΔDAT/Δ} and *Fto*^{+/+} mice using an antibody directed against the tyrosine hydroxylase (TH), a marker for dopaminergic neurons in the midbrain. Further labeling of FTO revealed the absence of FTO in dopamine neuron restricted *Fto* knock out mice. (b) Quantification of FTO immunofluorescence in TH positive neurons in the midbrain (n = 3 for each *Fto*^{ΔDAT} and *Fto*^{fl/fl}, ****P* < 0.001, unpaired two-tailed *t*-test). (c) Western blot analysis of liver, pancreas, skeletal muscle and rest brain (non-midbrain). (d) Western blot analysis of DAT expression between *Fto*^{ΔDAT} mice carrying a copy of the Cre recombinase in the endogenous *Dat* locus and controls.

Validation of DA neuron specific *Fto* deletion

To verify the efficient and selective loss of FTO in *Fto*^{ΔDAT} mice, immunohistochemical stainings of midbrain sections were performed. To identify the genetically targeted neurons, tyrosine hydroxylase (TH, Figure 3.13 a, green) was used as a marker for dopamine neurons in the midbrain. Immunolabeling of FTO confirmed the presence of FTO in approximately 90% of midbrain TH expressing neurons of control mice (Figure 3.13 a, b; FTO labeled in red, representative staining shows midbrain sections of *Fto*^{ΔDAT/Δ} and *Fto*^{+/+} mice). In *Fto*^{ΔDAT} mice, FTO immunoreactivity was only observed in 1.14% of TH neurons (Figure 3.13 a, b; quantification was performed for *Fto*^{ΔDAT} and *Fto*^{fl/fl} controls).

To exclude unspecific deletion of the loxP-flanked third exon in untargeted peripheral or remaining brain tissue, Western blot analysis was performed. For analysis of liver, pancreas and skeletal muscle (SM), tissue derived from *Fto*^{ΔDAT/Δ} was used, while Western blot of rest brain (non-midbrain) tissue was conducted for *Fto*^{ΔDAT} mice. No aberrant loss of FTO was observed for all non-targeted tissues tested. Hence, the targeted deletion of FTO in dopaminergic neurons was considered efficient and specific (Figure 3.13 c).

In DAT-cre mice the cre-recombinase cDNA was cloned into the endogenous *Dat* locus between exon 1 and 2 [Ekstrand *et al.*, 2007]. Using this strategy, the endogenous transcription site was used for cre expression, while not affecting the *Dat* coding region with its translational start codon in exon 2. To ensure that this strategy was not affecting the endogenous DAT expression, western blot on mid-

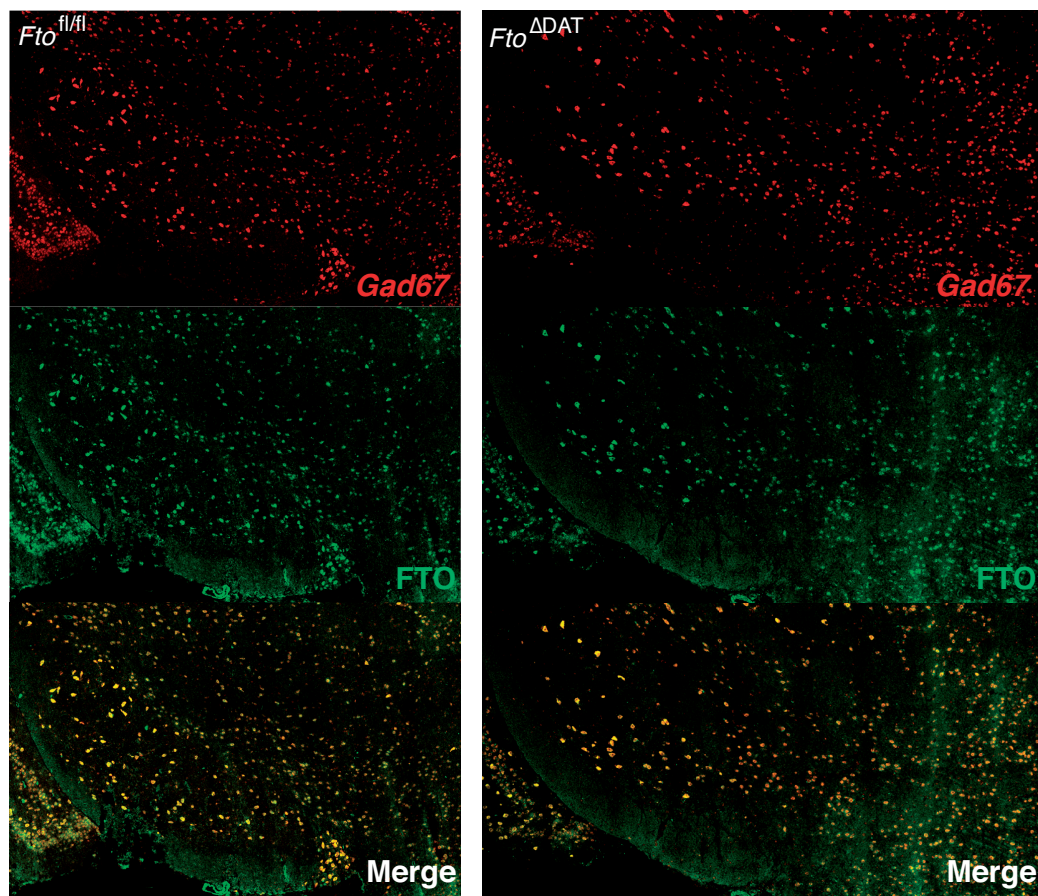


Figure 3.14: *Fto* deletion in DA neurons does not affect FTO expression in midbrain GABAergic neurons

Combined *in situ* hybridization for *Gad67* (red), a marker for GABAergic neurons, and immunofluorescent staining of FTO (green) revealed no loss of FTO in GABAergic neurons of *Fto*^{ΔDAT} mice.

brain lysates of *Fto*^{ΔDAT} and *Fto*^{fl/fl} was performed. This analysis confirmed no differences in DAT expression between genotypes (Figure 3.13 d).

Fto deletion in DA neurons does not affect FTO expression in midbrain GABAergic neurons

To further exclude unspecific deletion of *Fto* within the midbrain, FTO expression was assessed in GABAergic neurons of midbrain slices. For this purpose, combined *in situ* hybridization for *Gad67* (glutamate decarboxylase; marker for GABAergic neurons) and FTO immunohistochemistry was performed. No loss of FTO in GABAergic neurons of the midbrain was observed (Figure 3.14).

Taken together, FTO was shown to be efficiently and specifically deleted in mid-

brain dopaminergic neurons of *Fto*^{ΔDAT} mice. Neither FTO expression in peripheral or remaining brain tissue was affected nor was FTO unspecifically deleted in non-dopaminergic neurons.

3.2.2 Dopamine restricted *Fto* knock out does not influence basic metabolic parameters

Dopamine neuron restricted loss of FTO does not affect body weight

Whole body *Fto*-deficient mice have a lower body weight, due to a reduced lean and fat mass [Fischer *et al.*, 2009]. Since dopamine signaling is implicated in the etiology of obesity, alteration of dopaminergic function through loss of FTO may impact body weight regulation [Volkow *et al.*, 2013]. Therefore, the body weight of *Fto*^{ΔDAT} and control mice was monitored over the course of 16-18 weeks (Figure 3.15 a, b). No significant differences were detected for both males and females on either a normal chow diet (NCD) or a high fat diet (HFD).

Consistently, no differences in metabolic rate (depicted as O₂-consumption, 12-13 weeks of age) were found for males on either NCD or HFD (Figure 3.15 c, d). Moreover, food intake was unchanged for male *Fto*^{ΔDAT} mice as compared to controls on both NCD and HFD (Figure 3.15 e, f).

Dopamine neuron restricted loss of FTO does not affect insulin and glucose tolerance

To investigate glucose metabolism in *Fto*^{ΔDAT} mice, insulin and glucose tolerance tests were performed at 12 weeks (ITT) and 13 weeks (GTT) of age. No differences in either insulin sensitivity or glucose tolerance were observed between male *Fto*^{ΔDAT} and control mice on either high fat (Figure 3.16 a, c) or normal chow diet (Figure 3.16 b, d).

Hence, insulin's ability to reduce blood glucose levels, as well as the insulin mediated counter response to elevated glucose levels are not altered in *Fto*^{ΔDAT} mice. These results are consistent with the paucity of body weight differences for *Fto*^{ΔDAT} mice.

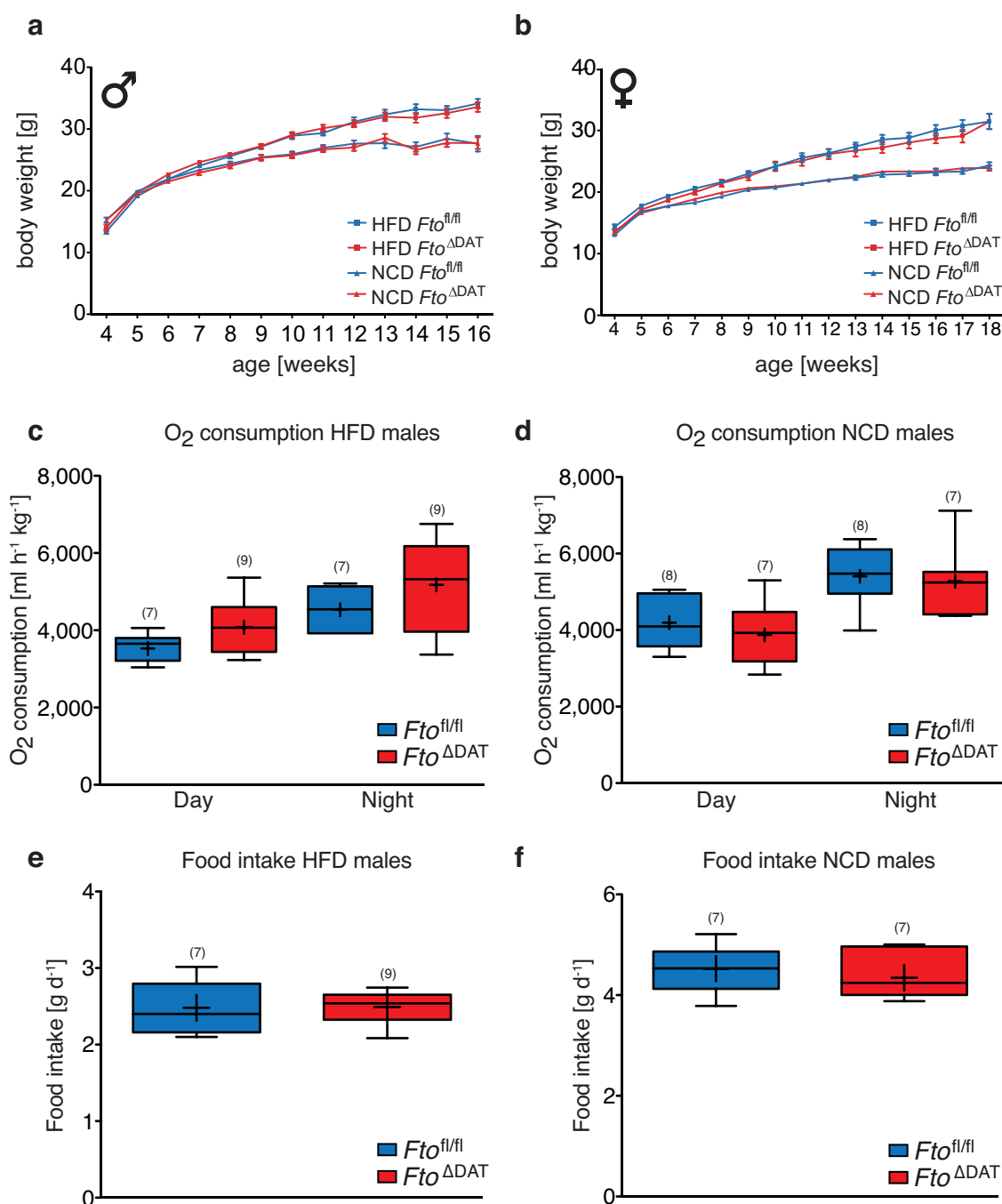


Figure 3.15: **Basic metabolic parameters are unchanged in $Fto^{\Delta DAT}$ mice**

(a) Body weight of male $Fto^{\Delta DAT}$ and control mice was monitored until 16 weeks of age on both normal (NCD) and high fat diet (HFD). (b) Body weight of female $Fto^{\Delta DAT}$ and control mice was monitored until 18 weeks of age on both normal (NCD) and high fat diet (HFD). (c) O₂ consumption of male $Fto^{\Delta DAT}$ and control mice on a HFD. (d) O₂ consumption of male $Fto^{\Delta DAT}$ and control mice on a NCD. (e) Food intake of male $Fto^{\Delta DAT}$ and control mice on a HFD. (f) Food intake of male $Fto^{\Delta DAT}$ and control mice on a NCD (sample sizes are indicated in parentheses).

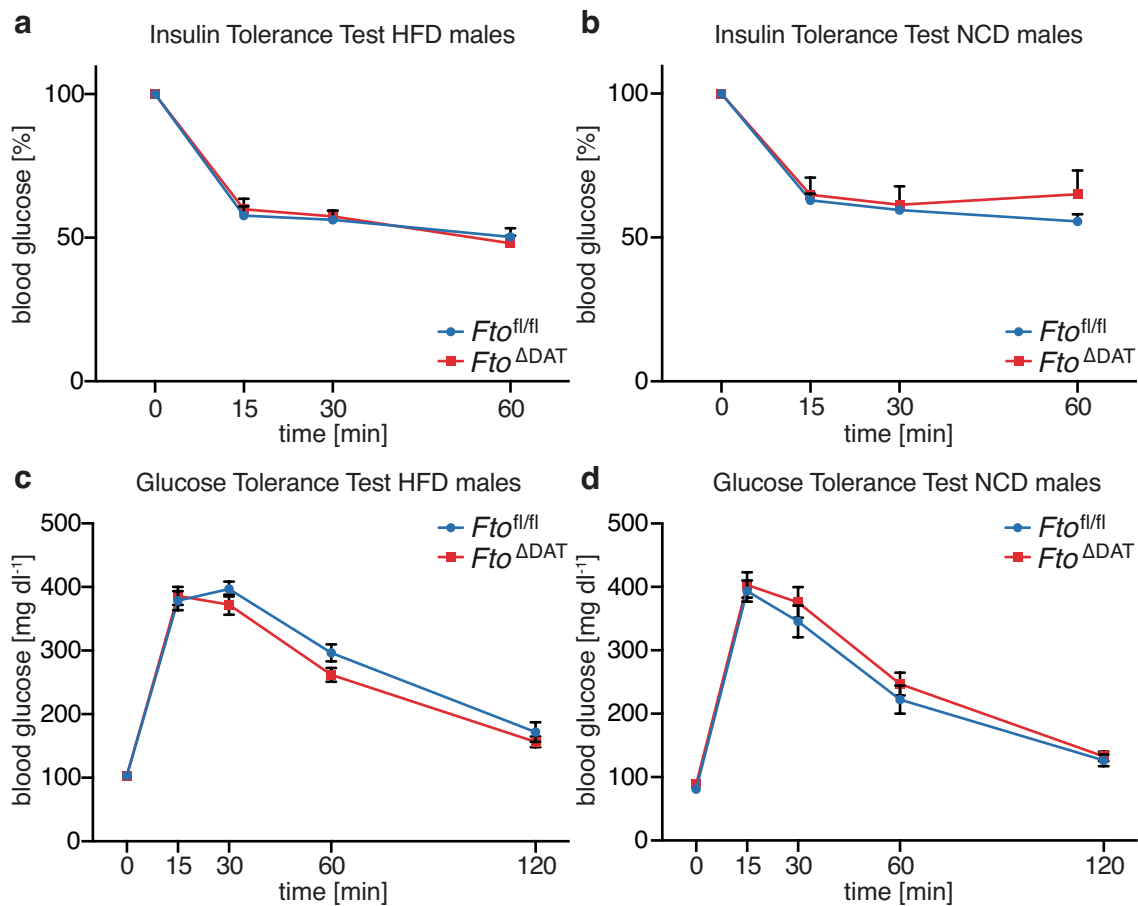


Figure 3.16: **Unchanged insulin and glucose tolerance in $Fto^{\Delta DAT}$ mice**

(a) Insulin tolerance test was performed on male $Fto^{\Delta DAT}$ (n=24) and control (n=22) mice fed a HFD. (b) Insulin tolerance test was performed on male $Fto^{\Delta DAT}$ (n=18) and control (n=14) mice fed a NCD. (c) Glucose tolerance test was performed on male $Fto^{\Delta DAT}$ (n=23) and control (n=24) mice fed a HFD. (d) Glucose tolerance test was performed on male $Fto^{\Delta DAT}$ (n=16) and control (n=12) mice fed a NCD.

Dopamine neuron restricted loss of FTO does not affect food intake and refeeding responses

In order to further investigate feeding behavior in $Fto^{\Delta DAT}$ mice, the refeeding response to a 16h over night fast was assessed. In line with the previous results (Figure 3.15 e, f), baseline food intake was unaltered between $Fto^{\Delta DAT}$ and control mice (Figure 3.17 a).

Following the 16h over night fasting period, the cumulative food intake was measured 1h, 2h, 4h, 8h and 24h after refeeding. During early hours of refeeding, $Fto^{\Delta DAT}$ mice showed a slightly increased food intake as compared to their control

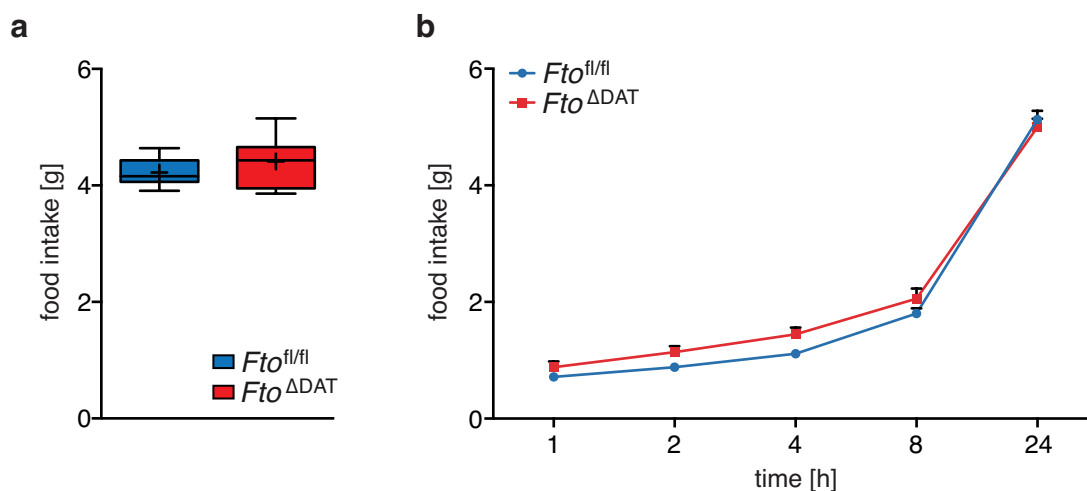


Figure 3.17: **Food intake and refeeding response are unaltered in *Fto^{ΔDAT}* mice**
(a) Baseline food intake was unaltered in male *Fto^{ΔDAT}* mice on NCD. **(b)** Refeeding behavior was assessed in response to a 16h over night fast. Food intake was measured 1, 2, 4, 6, and 24h after refeeding in male *Fto^{ΔDAT}* and control mice fed a NCD (RM two-way ANOVA, $F_{1,14} = 1.06$, $P = 0.3196$).

littermates, however, no significant changes were observed ($F_{1,14} = 1.06$, $P = 0.3196$; Figure 3.17).

Dopamine neuron restricted loss of FTO does not affect sucrose preference

Both anhedonia and depression are closely related to dopaminergic function [Nestler & Carlezon, 2006; Krishnan & Nestler, 2008]. To test, whether dopamine neuron restricted deletion of *Fto* affected anhedonia in mice, *Fto^{ΔDAT}* and control mice were subjected to a sucrose preference test, a measure for anhedonia in animals [Strekalova *et al.*, 2004]. With increasing concentrations, both *Fto^{ΔDAT}* and control mice significantly increased their preference for sucrose (0.5 - 8% sucrose solution, RM two-way ANOVA, $F_{4,60} = 42.68$, $P < 0.0001$, Figure 3.18). Between genotypes, *Fto^{ΔDAT}* mice exhibited slightly higher sucrose preference values. However, these differences were not significant (RM two-way ANOVA, $F_{1,15} = 0.4338$, $P = 0.5201$), showing that anhedonia is not affected in *Fto^{ΔDAT}* mice (Figure 3.18).

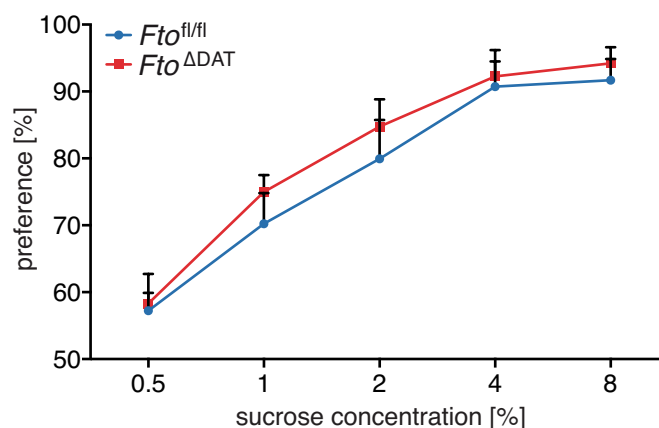


Figure 3.18: **Sucrose preference is unaltered in $Fto^{\Delta DAT}$ mice**

Sucrose preference was assessed for $Fto^{\Delta DAT}$ and control mice. Sucrose consumption was monitored for each sucrose concentration (0.5, 1, 2, 4 and 8% sucrose solution) for 2 consecutive days and calculated relative to total liquid consumption. $Fto^{fl/fl}$ (n = 10); $Fto^{\Delta DAT}$ (n = 7).

3.2.3 Altered DRD2/DRD3 dependent responses in $Fto^{\Delta DAT}$

Attenuated DRD2/DRD3 autoreceptor feedback loop in $Fto^{\Delta DAT}$ mice

To investigate whether $Fto^{\Delta DAT}$ mice exhibited comparable alterations on the cellular level as Fto -deficient mice, patch-clamp recordings were performed and firing rate was measured for dopaminergic midbrain neurons challenged with 10 μ M cocaine or 10 nM quinpirole. In line with the results obtained for Fto -deficient mice (see Figure 3.9 a, b), $Fto^{\Delta DAT}$ mice exhibited attenuated cocaine and quinpirole dependent reductions in firing rate compared to control mice, demonstrating that the DRD2/DRD3 mediated autoinhibition was malfunctional (Figure 3.19 a, b). Furthermore, the quinpirole (10 nM) dependent conductance density was reduced, demonstrating that activation of presynaptic DRD2/DRD3 receptors in $Fto^{\Delta DAT}$ mice is not able to elicit the same relative current flow (Figure 3.19 c). Hence, the loss of FTO in dopaminergic neurons cell autonomously affects the DRD2/DRD3 autoreceptor feedback loop.

Reduced GIRK dependent current density in $Fto^{\Delta DAT}$ mice

To further assess whether the change in feedback inhibition could be attributed to GIRK currents, GIRK-dependent current density was measured as described

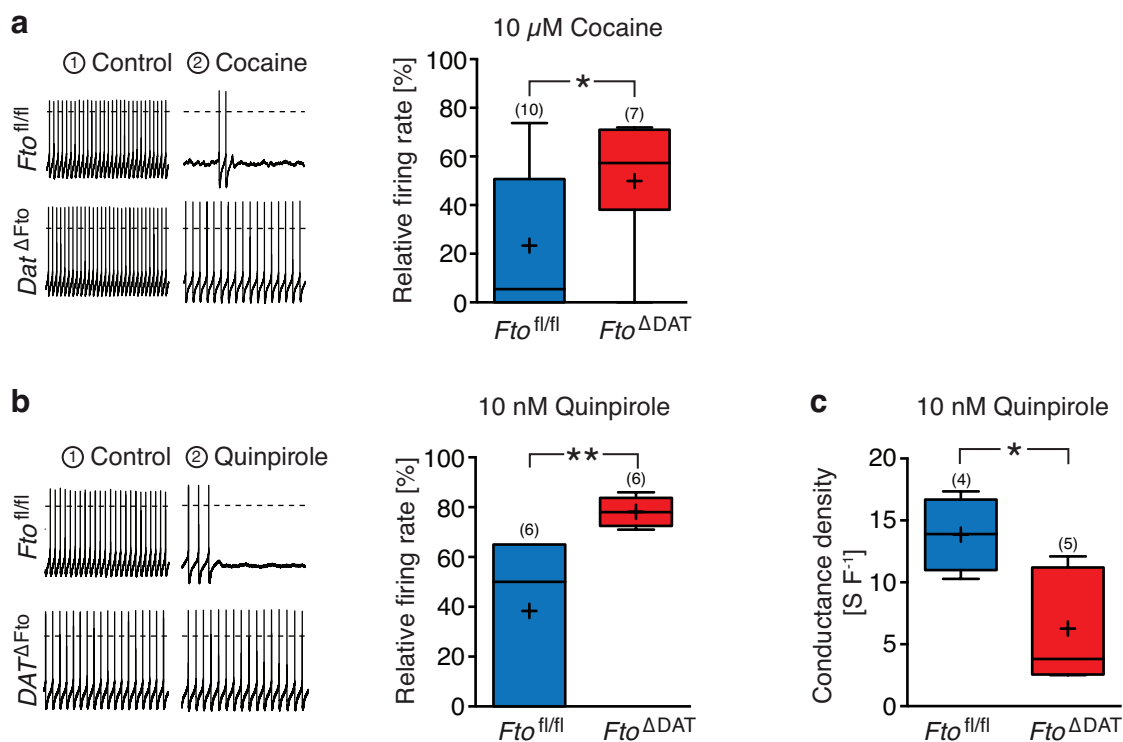


Figure 3.19: **Attenuated responses of midbrain neurons to cocaine and quinpirole in $Fto^{\Delta DAT}$ mice**

(a) Relative firing rate of SNpc dopaminergic neurons in patch clamp recordings during bath application of cocaine ($10 \mu\text{M}$, 10 min, sample sizes indicated in parentheses, $*P < 0.05$, unpaired one-tailed t -test). (b) Bath application of the D2-D3-receptor agonist quinpirole (10 nM) on control and $Fto^{\Delta DAT}$ dopamine neurons. (sample sizes indicated in parentheses, $**P < 0.01$, unpaired two-tailed t -test). (c) In line with the attenuated reduction in firing rate, quinpirole (10 nM) mediated increase in conductance density is significantly reduced in $Fto^{\Delta DAT}$ mice (sample sizes indicated in parentheses, $*P < 0.05$, unpaired two-tailed t -test). All electrophysiological experiments were conducted by Simon Hess.

in section 3.1.4. Consistent with the attenuated responses to bath application of cocaine and quinpirole on firing rate and mirroring the results obtained for Fto -deficient mice (Figure 3.10), the GIRK dependent current density was significantly reduced in $Fto^{\Delta DAT}$ mice (Figure 3.20).

Hence, the autoreceptor feedback loop is malfunctioning through the attenuation of DRD2-DRD3-GIRK dependent changes in conductance. Whether a reduction in GIRK channel availability or whether attenuated activation of these channels due to changes further upstream in the signaling pathway are responsible for these observations remains unclear.

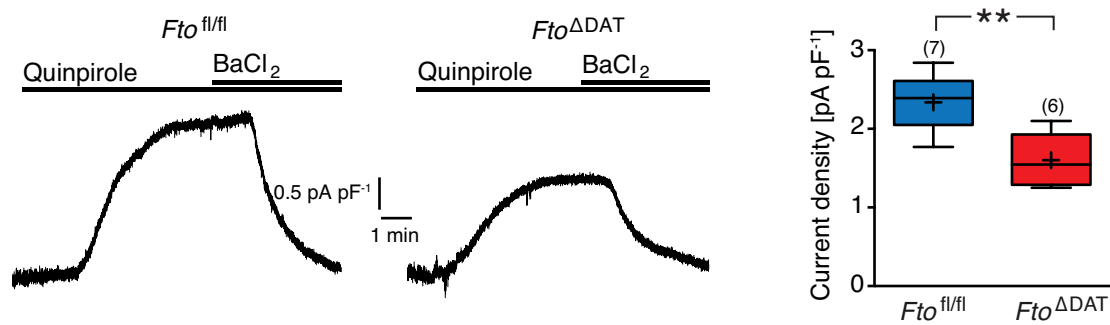


Figure 3.20: **Reduced GIRK dependent current density in *Fto^{ΔDAT}* mice**

DRD2 mediated activation of GIRK channels is attenuated in *Fto^{ΔDAT}* dopamine neurons. GIRK currents were measured by activation of D₂/D₃ receptors by quinpirole (300 nM) and subsequent blocking of GIRKs by BaCl₂ (1 mM) (sample sizes indicated in parentheses, ** $P < 0.01$, unpaired two-tailed t -test). All electrophysiological experiments were conducted by Simon Hess.

Altered baseline and cocaine evoked locomotor activity in *Fto^{ΔDAT}* mice

Since dopamine is involved in motor control, malfunction of the dopaminergic autoinhibitory feedback loop may alter locomotor activity. To probe motor function, baseline and cocaine-induced locomotor activity was assessed for *Fto^{ΔDAT}* mice in the open field paradigm. For baseline locomotor activity, the distance travelled over the course of 45 minutes was assessed in saline injected mice. These measurements revealed baseline hyperlocomotion for *Fto^{ΔDAT}* mice as compared to controls (Figure 3.21 a).

When challenged with cocaine, *Fto^{ΔDAT}* mice exhibited a hypersensitivity towards lower cocaine concentration (10 mg kg⁻¹), while no differences at the higher concentration (20 mg kg⁻¹) were observed (Figure 3.21 b).

Attenuated quinpirole dependent decrease in locomotor activity in *Fto^{ΔDAT}* mice

To directly address the impact of the activation of the DRD₂/DRD₃ autoreceptors on locomotor activity, *Fto^{ΔDAT}* mice and control mice were challenged with i.p. injections of 30 and 100 μg kg⁻¹ quinpirole. In line with the previous results obtained for *Fto*-deficient mice, *Fto^{ΔDAT}* mice exhibited an attenuated response in the quinpirole-dependent decrease of locomotor activity (Figure 3.22).

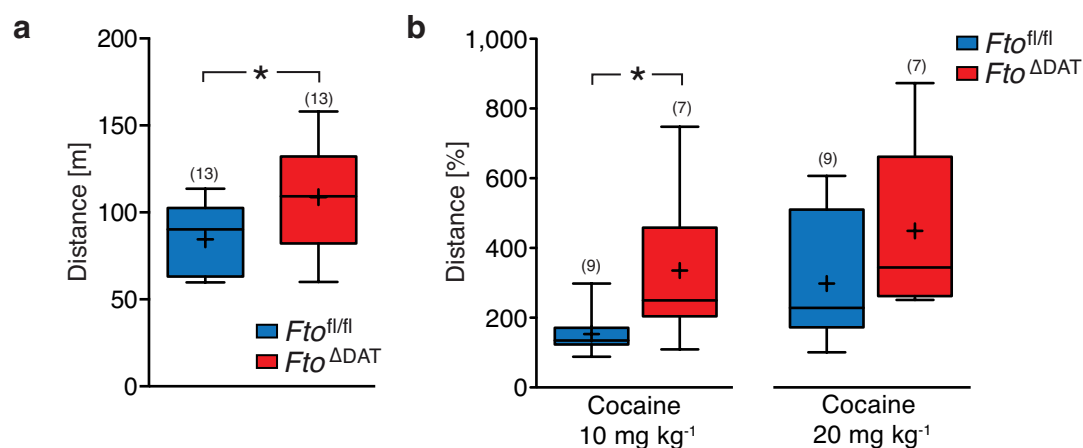


Figure 3.21: **Altered baseline and cocaine evoked locomotor activity in *Fto*^{ΔDAT} mice**
 (a) Baseline locomotor activity during open field experiments in *Fto*^{ΔDAT} mice (sample sizes indicated in parentheses, * $P < 0.05$, unpaired two-tailed t -test) (b) Cocaine induced locomotor activity in the open field paradigm after 10 mg kg⁻¹ BW and 20 mg kg⁻¹ cocaine i.p. injection in *Fto*^{ΔDAT} compared to control mice. Cocaine evoked locomotor activity is expressed as percent increase compared to baseline activity following saline injection (sample sizes indicated in parentheses, * $P < 0.05$, unpaired two-tailed t -test).

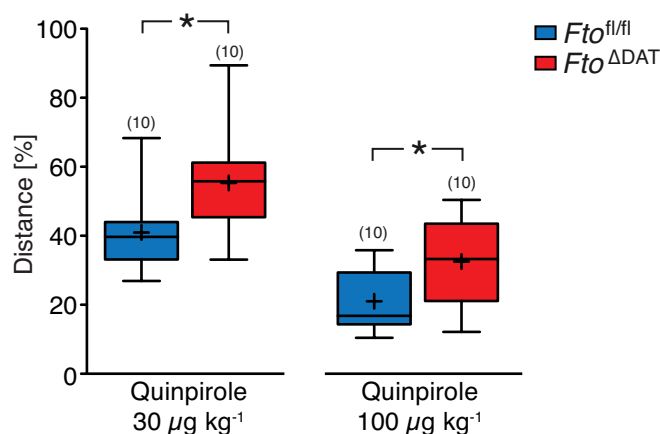


Figure 3.22: **Attenuated quinpirole dependent decrease in locomotor activity in *Fto*^{ΔDAT} mice**
 Control and *Fto*^{ΔDAT} mice were injected i.p. with 30 μg kg⁻¹ and 100 μg kg⁻¹ quinpirole. Data is represented as percent relative to baseline saline injection (* $P < 0.05$, unpaired two-tailed t -test, sample sizes are indicated in parentheses).

After both 30 and 100 $\mu\text{g kg}^{-1}$ quinpirole administration $Fto^{\Delta\text{DAT}}$ mice retained significantly more of their locomotor activity. Hence, the ability of the DRD2/DRD3 agonist quinpirole to reduce activity of the dopaminergic neurons and thereby reducing the dopaminergic network tone was significantly attenuated. These results are consistent with the proposed cell autonomous reduction in DRD2/DRD3-GIRK dependent autoinhibition in $Fto^{\Delta\text{DAT}}$ mice and are in line with the results obtained for Fto -deficient mice.

Hypersensitivity of $Fto^{\Delta\text{DAT}}$ mice to cocaine in the conditioned place preference

Finally, to assess the function of the dopaminergic system with respect to processing reward-related behavior, $Fto^{\Delta\text{DAT}}$ mice were tested in the conditioned place preference paradigm. $Fto^{\Delta\text{DAT}}$ mice featured several aspects of the previously reported DRD2 autoreceptor knock out mouse, including increased baseline and cocaine-induced locomotor activity and the attenuated responses to quinpirole both on the cellular as well as the behavioral level [Bello *et al.*, 2011]. Therefore, the conditioned place preference was performed with a very low dose cocaine bait (0.5 mg kg^{-1}), a concentration that was able to affect place preference in DRD2 autoreceptor knock out mice [Bello *et al.*, 2011]. While this concentration failed to show any effect in control mice, place preference in $Fto^{\Delta\text{DAT}}$ mice was significantly enhanced (Figure 3.23).

This result is in line with the concept that decreased inhibitory tone in dopaminergic neurons would result in enhanced responses to conditioned stimuli and again supports the notion that loss of FTO cell autonomously attenuates the DRD2/DRD3-GIRK-dependent autoinhibitory feedback loop.

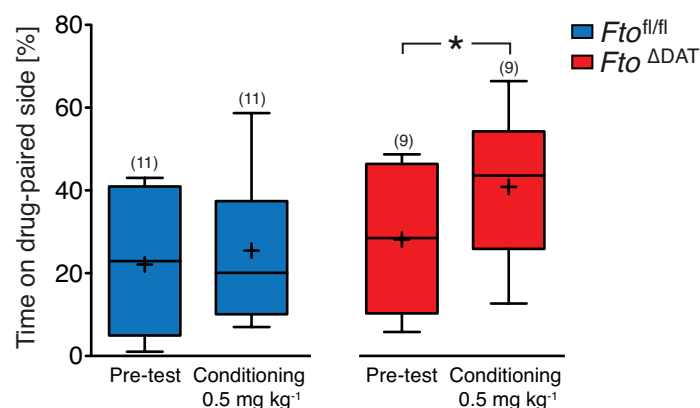


Figure 3.23: Low dosage of cocaine shifts preference of *Fto*^{ΔDAT} mice in conditioned place preference

Reward processing was assessed in the conditioned place preference paradigm for *Fto*^{ΔDAT} and control mice using a low dose cocaine bait (0.5 mg kg⁻¹, sample size indicated in parenthesis, **P*<0.05, paired two-tailed *t*-test).

3.3 N6-methyladenosine in mRNA depends on FTO demethylase function

3.3.1 Methylated RNA immunoprecipitation (MeRIP) sequencing identifies demethylation targets of FTO

On the molecular level, FTO was identified as a Fe(II) and 2-oxoglutarate dependent demethylase that is able to demethylate 3 - methyluracil and N6 - methyladenosine (m⁶A) *in vitro* [Jia *et al.*, 2011; Gerken *et al.*, 2007]. Recently, the m⁶A mark was identified in over 7600 mRNA transcripts *in vivo* [Meyer *et al.*, 2012; Dominissini *et al.*, 2012]. To investigate the potential role of this enzymatic capability of FTO with respect to dopaminergic function, the m⁶A methylation profile was assessed in *Fto*-deficient mice. To this end, mRNA of midbrain and striatal (CPu and NAc) tissue was isolated and subsequently processed using established methylated RNA immunoprecipitation (MeRIP) protocols, followed by next generation sequencing [Meyer *et al.*, 2012]. In total, 42.000 m⁶A peaks were found, and 5000 peaks in over 1500 transcripts were unique to *Fto*-deficient mice (Table 6.3). In line with previously published results, one or more m⁶A marks were found in the 5' UTR, CDS or 3'UTR of individual transcripts (Table 6.3, Meyer *et al.* [2012]).

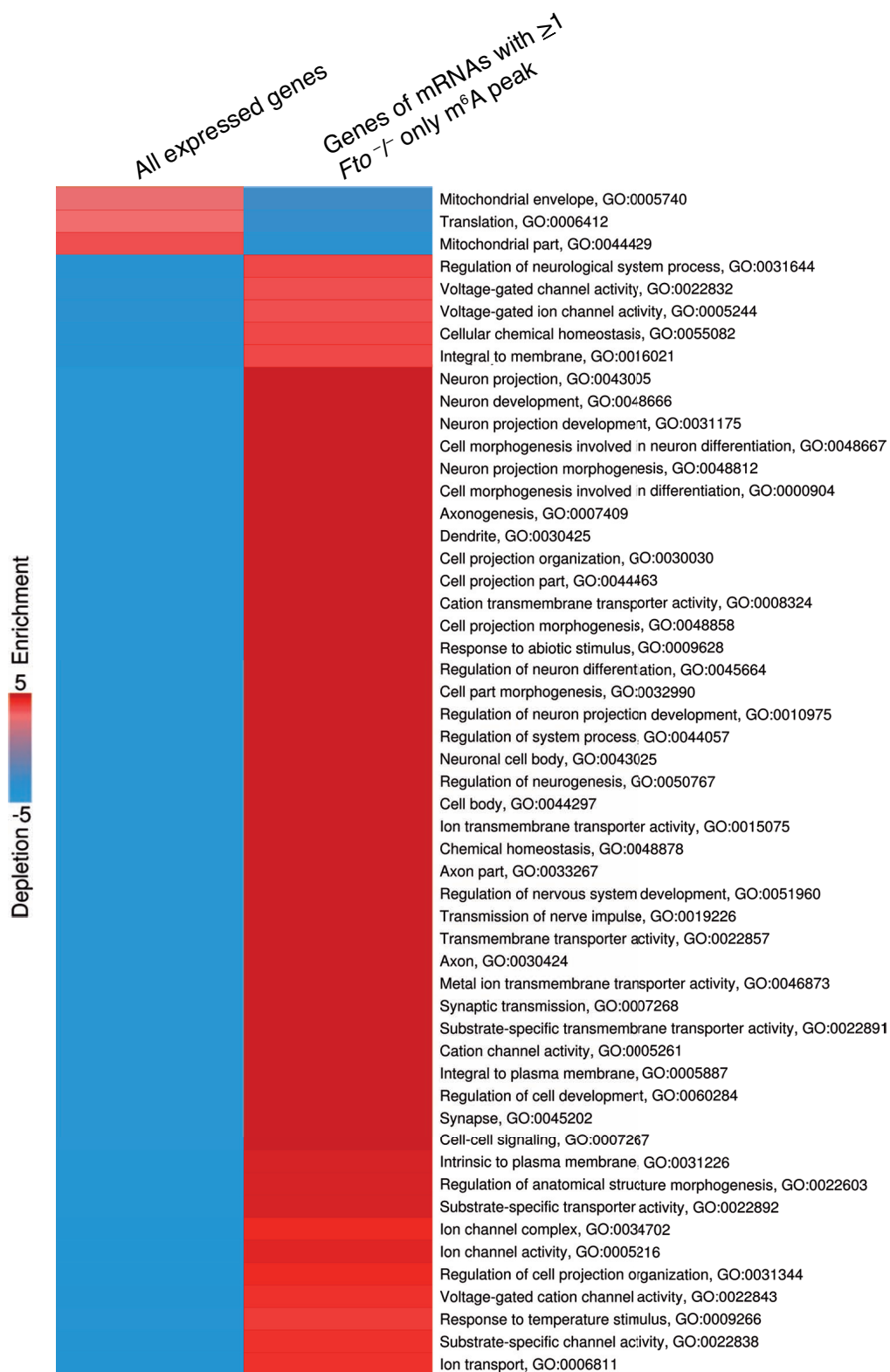


Figure 3.24: Gene ontology analysis of transcripts with m⁶A hypermethylation in *Fto*-deficient mice

Gene ontologies of m⁶A hypermethylated midbrain and striatal mRNA transcripts cluster in categories of synaptic transmission and cell-cell signaling in *Fto*-deficient mice. Gene ontology analysis was performed by Yogesh Saletore and Olivier Elemento

Gene ontology analysis of transcripts hypermethylated in *Fto*-deficient mice

Since the loss of FTO leads to a hypermethylation of a subset of m⁶A modified mRNAs, gene ontology analysis was performed to investigate the potential connection between the observed phenotype of *Fto*-deficient mice and the hypermethylated transcripts. This analysis showed that in comparison to the whole transcriptome, gene ontologies related to synaptic transmission and cell-cell signaling were overrepresented in *Fto*-deficient mice (Figure 3.24).

In wildtype control mice, however, enrichment of these categories identified in *Fto*-deficient mice were not found, suggesting that FTO targets a functionally distinct subset of transcripts (Figure 3.25).

3.3.2 m⁶A in mRNA influences translation of methylated transcripts

To identify putative candidate transcripts, whose m⁶A methylation in *Fto*-deficient mice might be functionally implicated in dopamine signaling, pathway analysis was performed to generate an overlay of dopaminergic signaling and hypermethylated mRNAs (Table 6.3, Figure 3.26). A number of hypermethylated transcripts in *Fto*-deficient mice encode for proteins that are components of dopaminergic signaling, including DRD₃, GIRK₂, NMDAR₁, GNAO₁ and SYN₁ (Figure 3.26). Several of these components were selected for further analysis.

The type 3 dopamine receptor (DRD₃) is expressed both pre- and postsynaptically [Beaulieu & Gainetdinov, 2011]. MeRIP-seq identified a m⁶A methylation site within the coding sequence of the *Drd3* transcript (Figure 3.27 a, Table 6.3). Using quantitative PCR, significant upregulation of *Drd3* mRNA levels were detected in *Fto*-deficient midbrain and CPu (Figure 3.27 b). On the protein level, however, a significant downregulation was observed for DRD₃ in *Fto*-deficient mice (Figure 3.27 c, d).

Comparable results were obtained for the G protein coupled inwardly rectifying potassium channel 2, whose transcript was m⁶A methylated within the 5'UTR (Figure 3.28 a). This 5' UTR, however, is only present in the *Girk2A* and *Girk2B*,

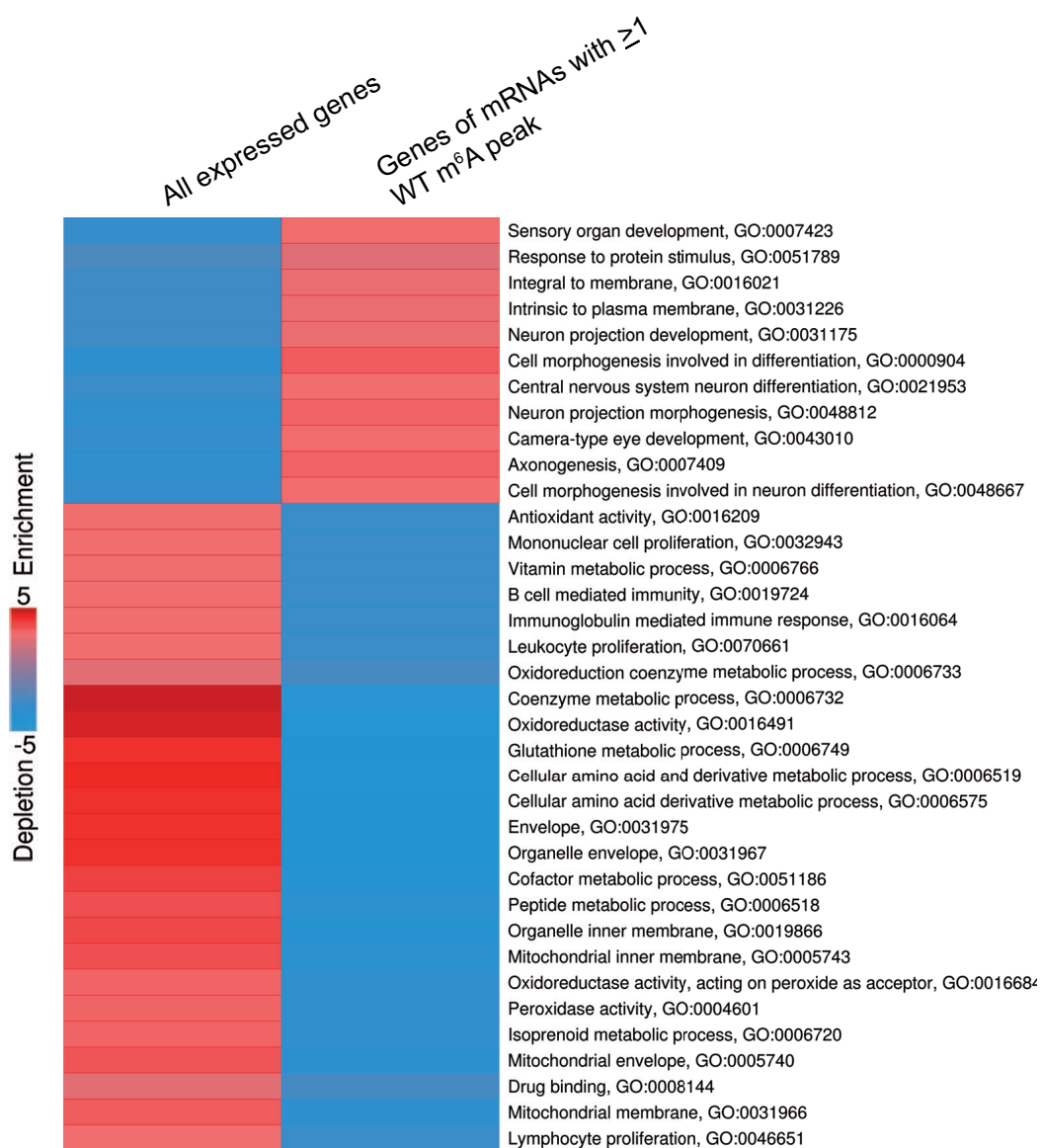


Figure 3.25: **Gene ontology analysis of transcripts m⁶A methylated in control mice**
 m⁶A methylated mRNA transcripts, isolated from wildtype midbrain and striatum, do not cluster in gene ontologies of synaptic transmission or cell-cell signaling. Gene ontology analysis was performed by Yogesh Saletore and Olivier Elemento

but not *Girk2C* transcripts. qPCR analysis of total *Kcnj6* revealed a significant up-regulation of mRNA levels in *Fto*-deficient midbrain tissue (Figure 3.28 b; isoform unspecific *Kcnj6* qPCR probe). Consistent with the previous results for DRD₃, GIRK₂ protein levels were significantly downregulated in both midbrain and CPU of *Fto*-deficient mice (Figure 3.28 c, d).

For the N-methyl-D-aspartate (NMDA) receptor subunit 1, hypermethylated m⁶A

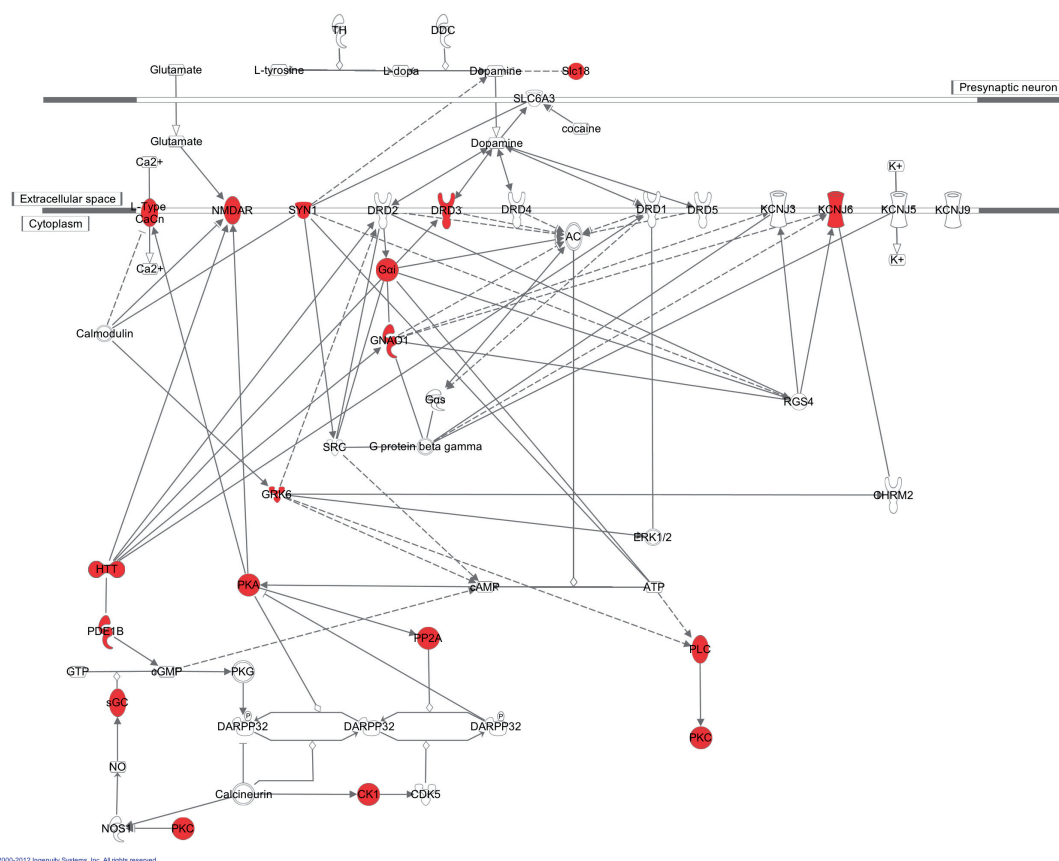


Figure 3.26: **Pathway analysis of m⁶A hypermethylated transcripts in *Fto*-deficient mice**
 Overlay of dopaminergic signaling and m⁶A hypermethylated transcripts identified via MeRIP-Seq in *Fto*-deficient midbrain and striatal tissue was performed to identify putative candidates functionally related to the phenotype observed in *Fto*-deficient mice

sites were detected in both the 5' and 3' UTR of *Fto*-deficient mice (Figure 3.29 a, only 3' UTR shown). *Grin1* transcripts showed significant upregulation in *Fto*-deficient midbrain but not CPu (Figure 3.29 b), while protein levels were significantly downregulated in both midbrain and CPu (Figure 3.29 c, d).

Whilst the upregulation of m⁶A hypermethylated on mRNA level was detected for additional transcripts (*Gnai1*, *Ikbkb*, *Gnao1*, *Gnb5*; Figure 3.30 a, 3.31 a, 3.32), downregulation of the protein level was not confirmed for GNAI1 nor IKK2 (Figure 3.30 b, c, 3.31 b, c), suggesting a more complicated mechanism through which m⁶A methylation functionally impacts specific transcripts.

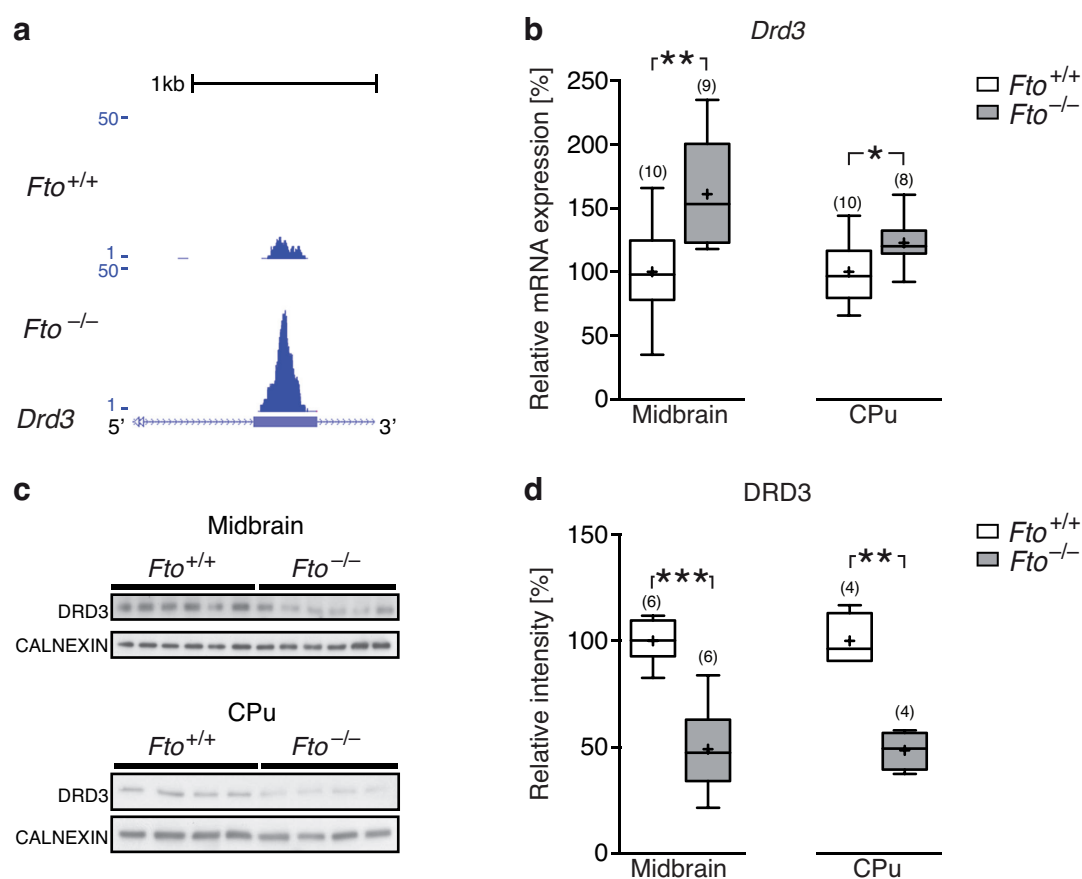


Figure 3.27: **FTO demethylation target *Drd3***

(a) MeRIP-Seq identified a hypermethylated m⁶A site in the coding sequence of the *Drd3* mRNA transcript of *Fto*-deficient mice. MeRIP pulldown was performed by Kate Meyer. (b) Quantitative PCR of *Drd3* mRNA isolated from *Fto*-deficient and control midbrain and dorsal striatum (CPu). (c) Western blot analysis of DRD3 protein in *Fto*-deficient and control midbrain and CPu lysates. (d) Quantification of DRD3 western blot analysis. (* $P < 0.05$, ** $P < 0.01$, *** $P < 0.001$; unpaired two-tailed t -test, sample sizes are indicated in parenthesis).

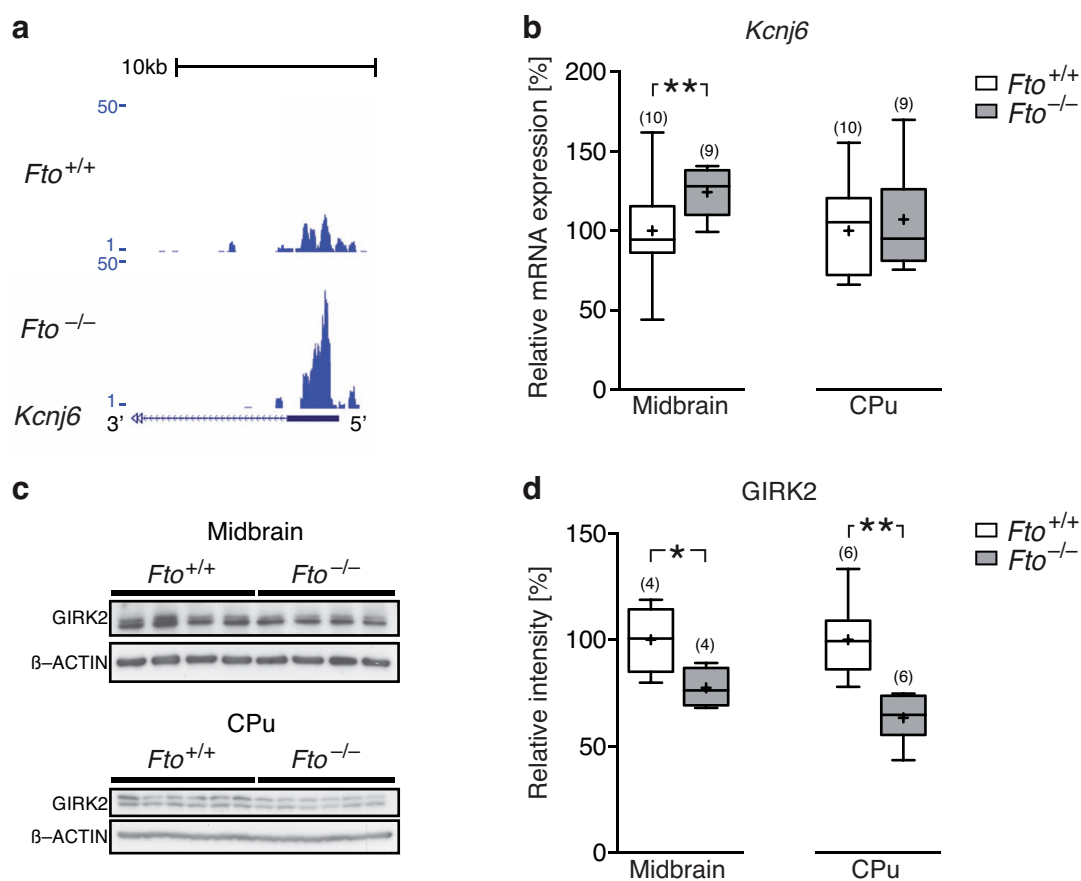


Figure 3.28: **FTO demethylation target *Kcnj6***

(a) MeRIP-Seq identified a hypermethylated m⁶A site in the 5' UTR of *Kcnj6* mRNA transcripts of *Fto*-deficient mice. MeRIP pulldown was performed by Kate Meyer. (b) Quantitative PCR of *Kcnj6* mRNA isolated from *Fto*-deficient and control midbrain and dorsal striatum (CPu). (c) Western blot analysis of GIRK2 protein in *Fto*-deficient and control midbrain and CPu lysates (bands in blot correspond to GIRK2A and GIRK2B isoforms). (d) Quantification of GIRK2 western blot analysis. (* $P < 0.05$, ** $P < 0.01$; unpaired two-tailed *t*-test, sample sizes are indicated in parenthesis).

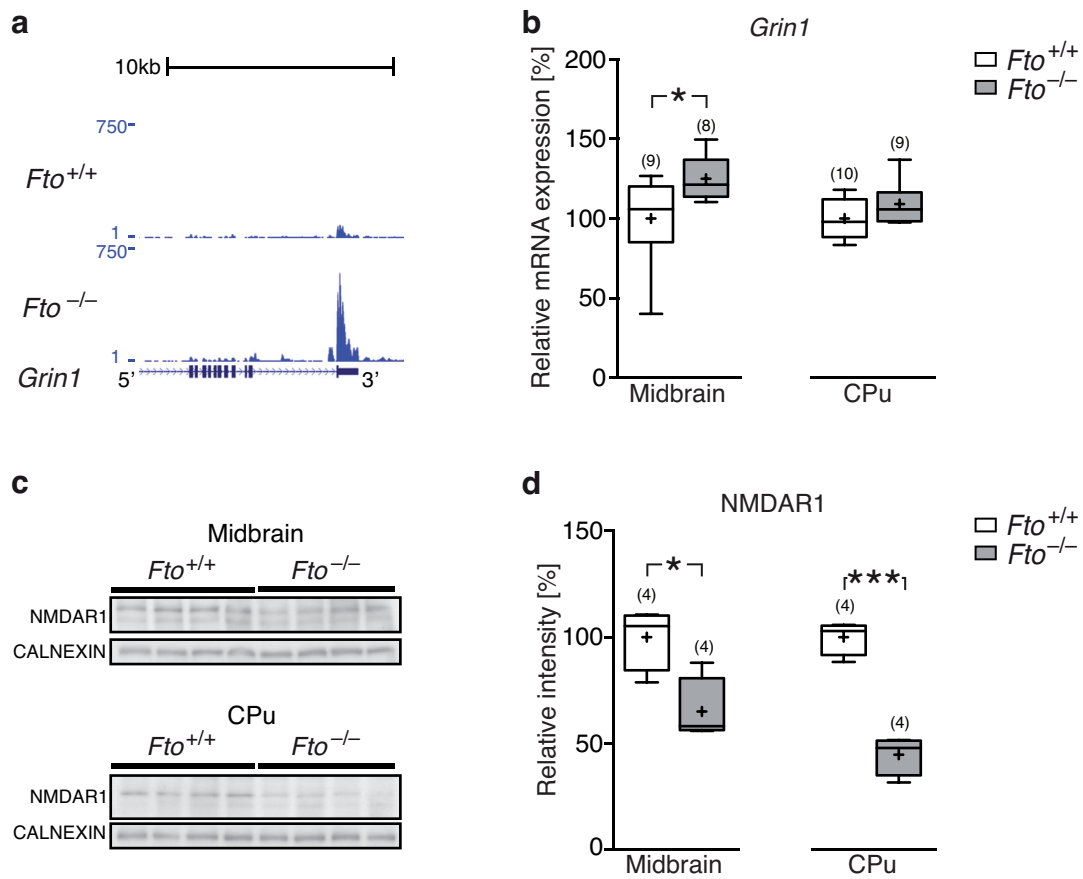


Figure 3.29: **FTO demethylation target *Grin1***

(a) MeRIP-Seq identified hypermethylated m⁶A sites in the 5' and 3' UTR of *Grin1* (glutamate receptor, ionotropic, N-methyl-D-aspartate 1) mRNA transcripts of *Fto*-deficient mice (5' UTR not depicted). MeRIP pulldown was performed by Kate Meyer. (b) Quantitative PCR of *Grin1* mRNA isolated from *Fto*-deficient and control midbrain and dorsal striatum (CPu). (c) Western blot analysis of NMDAR1 (N-methyl-D-aspartate receptor subunit 1) protein in *Fto*-deficient and control midbrain and CPu lysates. (d) Quantification of NMDAR1 western blot analysis. (* $P < 0.05$, *** $P < 0.001$; unpaired two-tailed t -test, sample sizes are indicated in parenthesis).

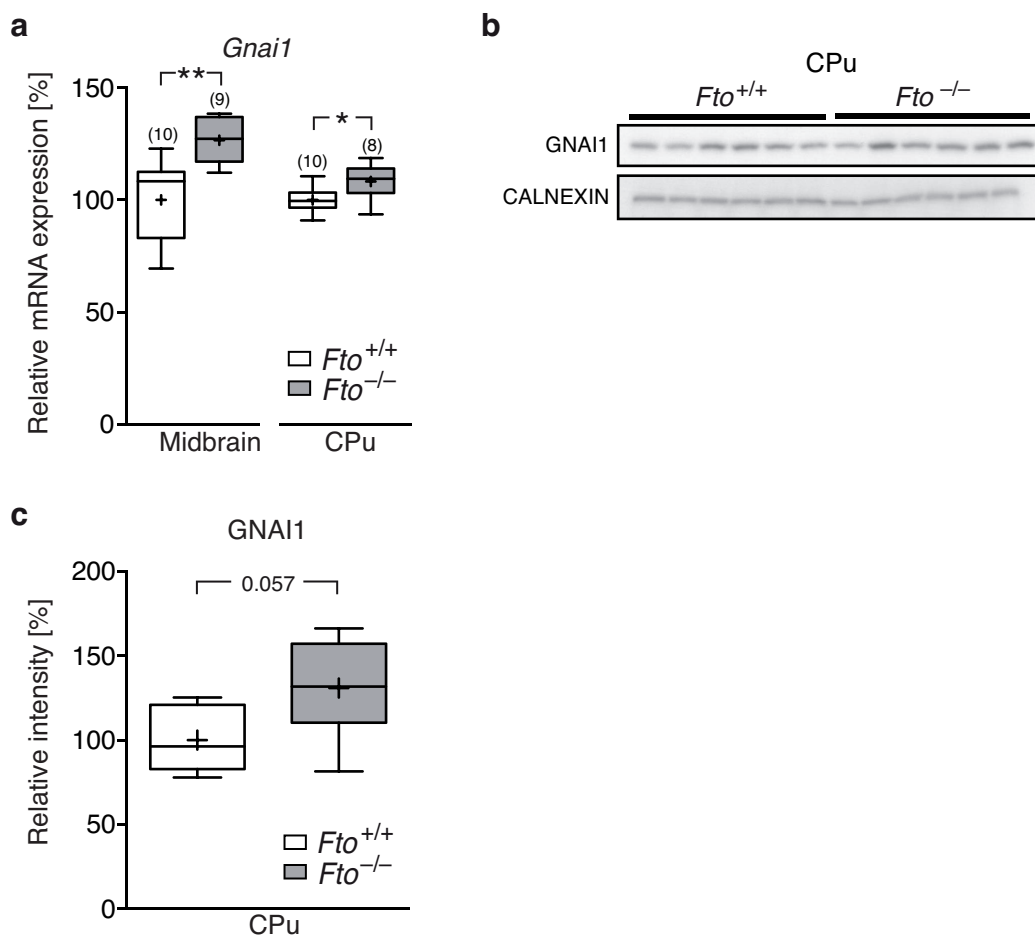


Figure 3.30: **FTO demethylation target *Gnai1***

MeRIP-Seq identified a hypermethylated m⁶A site in the 5' UTR of *Gnai1* mRNA transcripts of *Fto*-deficient mice. **(a)** Quantitative PCR of *Gnai1* mRNA isolated from *Fto*-deficient and control midbrain and dorsal striatum (CPu). **(b)** Western blot analysis of GNAI1 protein in *Fto*-deficient and control CPu lysates. **(c)** Quantification of GNAI1 western blot analysis. (* $P < 0.05$, ** $P < 0.01$; unpaired two-tailed *t*-test, sample sizes are indicated in parenthesis).

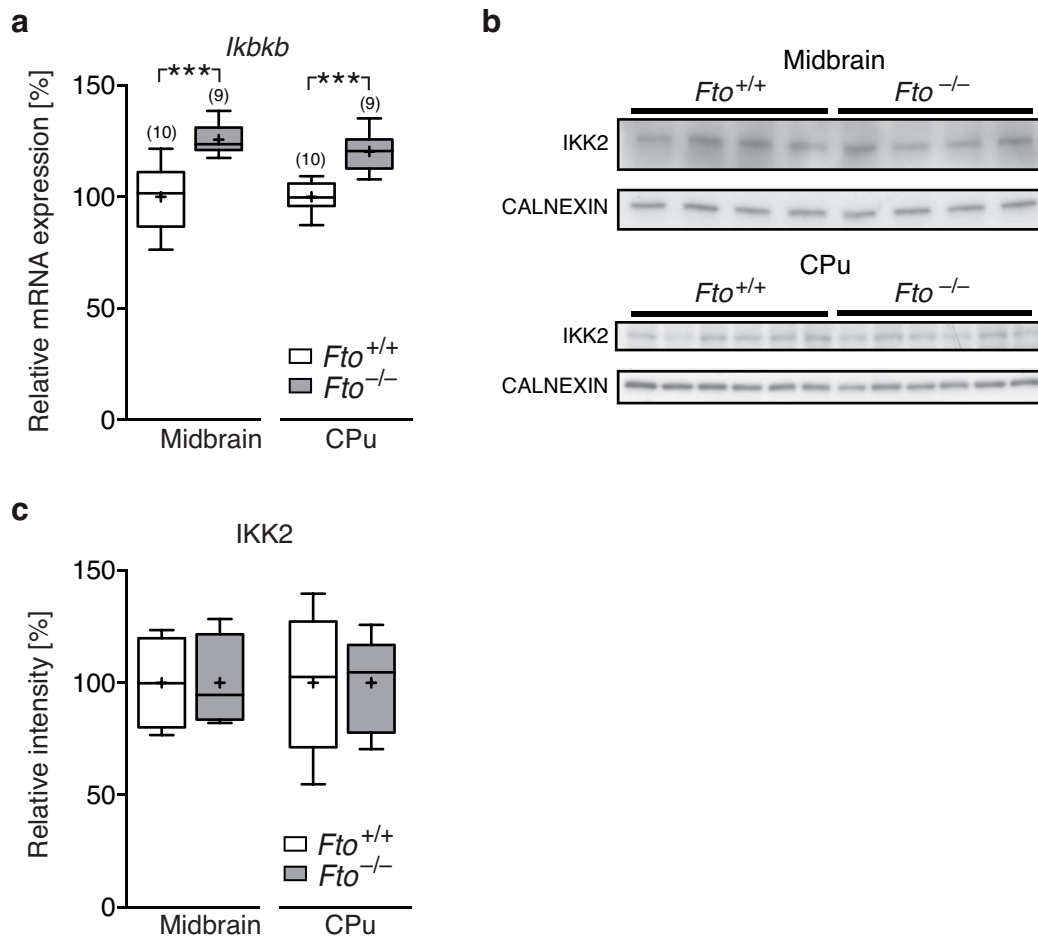


Figure 3.31: **FTO demethylation target *Ikbkb***

MeRIP-Seq identified hypermethylated m⁶A sites in the coding sequence and 3' UTR of *Ikbkb* mRNA transcripts of *Fto*-deficient mice. **(a)** Quantitative PCR of *Ikbkb* mRNA isolated from *Fto*-deficient and control midbrain and CPu. **(b)** Western blot analysis of IKK2 protein in *Fto*-deficient and control CPu lysates. **(c)** Quantification of IKK2 western blot analysis. (***) $P < 0.001$; unpaired two-tailed *t*-test, sample sizes are indicated in parenthesis).

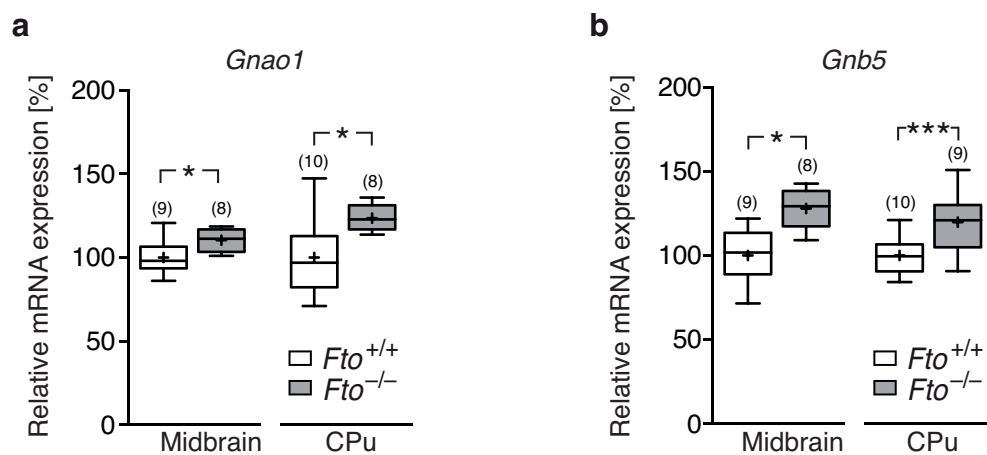


Figure 3.32: **FTO demethylation targets *Gnao1* and *Gnb5***

MeRIP-Seq identified hypermethylated m⁶A sites in the coding sequence and 5' UTR of *Gnao1* and the 5' UTR of *Gnb5* mRNA transcripts of *Fto*-deficient mice. **(a)** Quantitative PCR of *Gnao1* mRNA isolated from *Fto*-deficient and control midbrain and dorsal striatum (CPu). **(b)** Quantitative PCR of *Gnb5* mRNA isolated from *Fto*-deficient and control midbrain and CPu. (* $P < 0.05$, *** $P < 0.001$; unpaired two-tailed *t*-test) Sample sizes are indicated in parenthesis.

4 Discussion

The worldwide increase in prevalence of obesity is going to be one of the major challenges of modern society, causing a plethora of health problems and placing a burden on health care systems [Cawley & Meyerhoefer, 2012; Finkelstein *et al.*, 2009; Caballero, 2007]. The reason for the increase in obesity which started in the middle of the 20th century, is unlikely to be caused by rare mutations. It is rather a cause of environmental changes including sedentary life style and the constant availability of highly palatable food in conjunction with a genetic susceptibility to gain weight in such conditions [Swinburn *et al.*, 2011; Caballero, 2007].

This susceptibility is believed to be shaped by common genetic variations and the sum of their individual effects on body weight [Loos, 2012]. Hence, identification of these single nucleotide polymorphisms (SNPs) underlying common obesity has become a primary goal. Some of the SNPs can directly impact the function of genes through changes in the coding sequence, while others are situated in intronic regions and may indirectly affect gene function.

In 2007, a cluster of SNPs was identified within the first intron of the human *FTO* gene and these SNPs were subsequently the targets of extensive studies, due to their robust association with obesity related traits [Frayling *et al.*, 2007; Dina *et al.*, 2007; Scuteri *et al.*, 2007]. To date, the exact function of these SNPs within the first intron as well as the exact function of the *FTO* gene product are not known. Hence, the aim of this thesis was the investigation of *FTO* by means of genetic manipulations in mice to identify *FTO*'s function and depending pathways, to ultimately shed light on the connection between *FTO* genomic variation and common obesity.

Whole body *FTO* deletion in mice causes a severe phenotype that partly resembles the phenotype of *Drd2*-deficient mice, including growth retardation, reduced

IGF-1 levels, lean phenotype, increased energy expenditure and reduced voluntary locomotor activity [Fischer *et al.*, 2009; Klinker *et al.*, 2013; Kim *et al.*, 2010; García-Tornadu *et al.*, 2010; Díaz-Torga *et al.*, 2002; Sibley, 1999; Kelly *et al.*, 1998; Beaulieu & Gainetdinov, 2011]. Moreover, both FTO and DRD2 are linked to the etiology of obesity [Scuteri *et al.*, 2007; Dina *et al.*, 2007; Frayling *et al.*, 2007; Volkow *et al.*, 2013; Wang *et al.*, 2001]. For this reason, the potential role of FTO in dopaminergic signaling was investigated.

4.1 *Fto* deficiency alters D2-like receptor–dependent responses

4.1.1 FTO is expressed in midbrain dopaminergic neurons

Although *Fto* is ubiquitously expressed, its highest levels are detected within the central nervous system [Gerken *et al.*, 2007; McTaggart *et al.*, 2011]. In line with these results, endogenous *Fto* expression in midbrain dopaminergic neurons was confirmed using a mouse model with a knock in of the β -galactosidase gene into the endogenous *Fto* locus (Section 3.1.1). Moreover, FTO immunoreactivity was demonstrated for midbrain dopaminergic neurons (Section 3.1.1). Hence, FTO potentially plays a role in dopaminergic neurons and dopaminergic signaling.

Since the loss of FTO leads to increased mortality in both men and mice, *Fto* deficiency may affect cell viability [Fischer *et al.*, 2009; Boissel *et al.*, 2009]. In *Fto*-deficient mice, however, no changes in number or morphology of dopaminergic neurons were observed, showing that viability of dopamine neurons is not affected by the loss of FTO (Section 3.1.1).

4.1.2 Whole body *Fto*-deficiency attenuates responses to cocaine

To investigate the function of the dopaminergic circuitry, *Fto*-deficient mice were challenged with cocaine injections. Cocaine is a potent psychostimulatory substance, whose primary effect is the blockade of the dopamine transporter and hence many of its effects impinge on dopaminergic signaling [Beaulieu & Gainetdinov,

2011; Hyman *et al.*, 2006; Nestler, 2001]. Loss of FTO had severe impacts on the cocaine evoked responses in mice. Firstly, the cocaine mediated increase in locomotor activity was blunted (Section 3.1.3). Secondly, cocaine-induced *Fos* expression in midbrain and striatal tissue was attenuated (Section 3.1.3). And thirdly, although cocaine was able to stimulate increases in extracellular dopamine in the NAc, significant differences were detected between control and *Fto*-deficient mice at higher cocaine dosages (Section 3.1.3). Since all neurons are affected in *Fto*-deficient mice, the individual contributions of pre- and postsynaptic loss of FTO in these experiments are not known. Failure to increase locomotor activity and *Fos* expression may stem from a failure of cocaine to block the dopamine transporter and would resemble aspects of a dopamine transporter mutant mouse insensitive to cocaine [Chen *et al.*, 2006]. The fact that dopamine levels increased in response to cocaine in *Fto*-deficient mice, however, suggests that other factors may contribute to the observed cocaine insensitivity, though not ruling out an alteration of dopamine transporter function. As DAT protein levels were demonstrated to be unchanged in *Fto*-deficient mice, loss of FTO might indirectly affect DAT function.

4.1.3 Impairment of D2-like autoreceptor signaling

Dopaminergic neurons express D2 and D3 autoreceptors that are activated by dopamine and trigger a feedback loop that subsequently terminates dopamine signaling through the activation of GIRK channels and hyperpolarization of dopamine neurons [Beaulieu & Gainetdinov, 2011; Lüscher & Slesinger, 2010]. While dopamine neurons fire tonically in a slice preparation, cocaine administration leads to a decrease in firing by increasing extracellular dopamine levels and activating the autoinhibitory feedback loop. Consistently, cocaine decreased the firing rate of dopamine neurons in the midbrain of control mice (see Section 3.1.4). In *Fto*-deficient mice, however, the ability of cocaine to reduce firing of dopamine neurons was significantly attenuated (Section 3.1.4).

Since cocaine acts indirectly via increasing extracellular levels of dopamine, the

DRD2/DRD3 selective agonist quinpirole was used to directly address the function of the autoinhibitory feedback loop. In line with the previous experiments, activation of the feedback loop by quinpirole potently reduced the firing rate of dopamine neurons in control mice, while this response was significantly attenuated in *Fto*-deficient mice (Section 3.1.4). Consistently, the quinpirole and GIRK dependent conductance density was decreased in *Fto*-deficient mice. On the behavioral level, injection of quinpirole in control mice caused a reduction in locomotor activity via inhibiting dopamine neuron activity. Consistently with the impairment observed on the cellular level, quinpirole's ability to reduce locomotor activity was significantly attenuated in *Fto*-deficient mice, demonstrating that the impaired autoinhibitory feedback directly translates into a behavioral phenotype.

Taken together, *Fto* deficiency led to a malfunction of the DRD2-DRD3-GIRK-dependent autoinhibitory feedback loop of dopaminergic neurons and impaired, in conjunction with postsynaptic alterations, responses of the dopaminergic circuitry to cocaine and quinpirole.

4.2 Conditional loss of *Fto* resembles D2 autoreceptor deficiency

4.2.1 Successful generation of dopamine neuron specific knock out mice

To investigate the role of FTO in altering the dopaminergic circuitry, dopamine neuron restricted knock out mice were utilized in addition to whole body *Fto*-deficient mice. To generate a specific deletion of FTO in dopaminergic cells, mice carrying the Cre recombinase under the control of the endogenous *Dat* promoter were crossed to mice with a loxP site flanked third exon of *Fto* (Section 3.2.1). Successful generation of *Fto*^{ΔDAT} mice was confirmed using immunohistochemical investigation of midbrain slices. Here, tyrosine hydroxylase (TH) immunolabeling was used to identify dopaminergic neurons. These experiments showed that the majority of dopamine cells in the VTA/SN of mice expressed FTO (approximately 90%). After

Cre-mediated recombination in $Fto^{\Delta DAT}$ mice, however, only 1.14% of TH positive neurons were found to express FTO, demonstrating the efficient deletion of FTO in dopaminergic neurons. Using Western blot analysis on peripheral tissues, the specificity of FTO deletion was further confirmed (Section 3.2.1).

4.2.2 Cell-autonomous impairment of D2-like autoreceptor signaling

On the cellular level, the responses of $Fto^{\Delta DAT}$ to cocaine and quinpirole mirrored those obtained in Fto -deficient mice. The ability of both cocaine and quinpirole to inhibit the firing of midbrain dopamine neurons was significantly attenuated (Section 3.2.3). Moreover, the GIRK channel-dependent conductance density was reduced in $Fto^{\Delta DAT}$ as compared to control mice. These results show that the dopamine neuron restricted knock out resembled whole body FTO deletion on the cellular level and that the autoinhibitory feedback loop was cell-autonomously affected by loss of FTO.

The duration of dopamine signaling is limited by the presynaptic autoinhibition. Hence, attenuation of the feedback loop that terminates dopamine signaling, prolongs synaptic dopamine transmission [Bello *et al.*, 2011]. Targeted disruption of D2 autoreceptors in mice demonstrated that blunted autoreceptor function results on the single cell level in comparable loss of inhibitory currents in response to quinpirole bath application as observed for Fto -deficient and $Fto^{\Delta DAT}$ mice [Bello *et al.*, 2011]. In addition, D2 autoreceptor knock out mice displayed increased baseline and cocaine-induced locomotor activity, whereas quinpirole failed to reduce locomotor activity. Moreover, increased conditioned place preference in response to very low dose cocaine injections was observed in D2 autoreceptor knock out mice, showing that these mice are hypersensitive to the locomotor and rewarding effects of cocaine [Bello *et al.*, 2011].

In comparison, $Fto^{\Delta DAT}$ mice displayed increased baseline as well as cocaine induced locomotor activity at low concentrations, while no significant difference were detected at higher concentrations. Hypersensitivity to cocaine in $Fto^{\Delta DAT}$ mice was

further assessed in the conditioned place preference paradigm, challenging the mice with a very low dose of cocaine (0.5 mg kg^{-1} , Section 3.2.3). While control mice were indifferent to the treatment, $Fto^{\Delta DAT}$ mice responded to the subthreshold dosage by increasing their preference for the baited side. Hence, in line with the assumption that dopamine neuron restricted loss of FTO resembles the hypersensitivity observed in D2 autoreceptor knock out mice, very low dosages of cocaine were able to elicit a response in the conditioned place preference paradigm. Furthermore, dopamine neuron restricted knock out of FTO significantly attenuated quinpirole's ability to inhibit locomotor activity (Section 3.2.3). In contrast to D2 autoreceptor knock out mice, quinpirole still retained a portion of its agonist potential and markedly decreased locomotor activity in $Fto^{\Delta DAT}$ mice as compared to baseline levels [Bello *et al.*, 2011]. Therefore, $Fto^{\Delta DAT}$ mice share several features of D2 autoreceptor deficiency, but are not a phenocopy of the D2 autoreceptor-deficient mice. Dopamine neuron restricted loss of FTO rather leads to a loss of autoinhibition through more complex mechanisms as compared to loss of D2 autoreceptors. In line with this notion, no differences in DRD2 expression were detected in Fto -deficient mice, showing that attenuation of autoinhibition would involve other components of the feedback loop or may indirectly affect DRD2 autoreceptor function.

Dopamine signaling has been implicated in the etiology of obesity [Volkow *et al.*, 2013; Wang *et al.*, 2001], hence, attenuation of dopamine autoinhibitory feedback may impact body weight regulation. Since Fto -deficient mice suffer from a complex phenotype, alterations of body weight regulation in these mice may stem from multiple sources, thereby making it impossible to draw unambiguous conclusions [Fischer *et al.*, 2009]. Therefore, basic metabolic parameters were assessed in $Fto^{\Delta DAT}$ mice. To this end, no alterations in body weight, food intake, insulin sensitivity, glucose tolerance, re-feeding response or sucrose preference were detected, demonstrating that loss of FTO specifically in dopaminergic neurons, while affecting dopamine autoinhibition, does not impact energy homeostasis. These results

are consistent with the findings obtained for D2 autoreceptor-deficient mice, that do not exhibit changes in body weight [Bello *et al.*, 2011]. Both of these findings suggest that D2 autoreceptor function is not critical for body weight regulation. Possibly, postsynaptic adaptations at the network level compensate in every day life for the aberrant autoreceptor function, thereby preventing malfunctional body weight regulation. Only as the dopaminergic circuitry is pushed by non-natural stimuli, such as cocaine, the attenuated autoinhibitory feedback leads to behavioral alteration. In contrast, in whole body *Fto*-deficient mice loss of FTO affects postsynaptic sites of dopamine action as well. Hence, these mice share several phenotypic characteristics of whole body *Drd2*-deficient mice, such as growth retardation, reduced IGF-1 levels, lean phenotype, increased energy expenditure and reduced voluntary locomotor activity [Fischer *et al.*, 2009; Klinker *et al.*, 2013; Kim *et al.*, 2010; García-Tornadu *et al.*, 2010; Díaz-Torga *et al.*, 2002; Sibley, 1999; Kelly *et al.*, 1998; Beaulieu & Gainetdinov, 2011].

Taken together, loss of FTO in dopaminergic neurons attenuates function of the DRD2-DRD3-GIRK-dependent autoinhibitory feedback loop that ensures termination of dopamine synaptic transmission. While this led to a hypersensitivity to locomotor and reward stimulating effects of cocaine in *Fto*^{ΔDAT} mice, *Fto*-deficient mice were insensitive to cocaine. Therefore, in addition to control of presynaptic dopamine signaling, FTO is likely to affect postsynaptic signaling events in target neurons of the dopaminergic system as well.

4.2.3 Relation of whole body and dopamine restricted FTO deficiency to D2 receptor studies

Although DRD2 was not downregulated on the protein level in *Fto*-deficient mice (Section 3.1.2), FTO deficiency resembles several aspects of DRD2 deficiency. In addition to the previously described similarities, both *Fto*- and *Drd2*-deficient mice exhibit comparable loss of cocaine-induced locomotor activity and *Fos* induction [Welter *et al.*, 2007]. Likewise, *Fto*^{ΔDAT} mice resemble characteristics of DRD2

autoreceptor-deficient mice [Bello *et al.*, 2011]. Hence, the phenotypic differences between *Fto*-deficient and *Fto*^{ADAT} mice mirrors the differences between DRD2 whole body knock out and DRD2 autoreceptor-deficient mice [Bello *et al.*, 2011; Welter *et al.*, 2007; Chausmer *et al.*, 2002; Kelly *et al.*, 1998].

Despite the paucity of DRD2 protein downregulation in *Fto*-deficient mice, the striking similarities to loss of DRD2s suggests to view loss of FTO in the context of D2 receptor studies. Postsynaptic DRD2 receptor availability influences drug abuse, with increased levels of DRD2 corresponding with lower self administration in monkeys and rodents and decreased levels of DRD2 observed in human drug abusers [Volkow *et al.*, 2009; Morgan *et al.*, 2002; Thanos *et al.*, 2001]. Decreased postsynaptic DRD2 availability was suggested to cause repetitive drug abuse to compensate for the decreased postsynaptic dopamine signaling [Volkow *et al.*, 1999]. Similarly, obese subjects exhibit decreased DRD2 levels in the striatum and are believed to compensate for the decreased receptor availability and decreased downstream activation of striatal DRD2 signaling via compulsive increase in intake of highly palatable food that stimulates dopamine release [Volkow *et al.*, 2013; Stice *et al.*, 2008; Wang *et al.*, 2001]. Consistently, rapid development of compulsive overeating in rats has been observed after virus-mediated knock down of striatal DRD2 [Johnson & Kenny, 2010]. A different theory suggests downregulation of postsynaptic DRD2s as a compensatory response to increased dopaminergic transmission [Bello *et al.*, 2011; Stice *et al.*, 2008]. In line with this notion, reduced levels of DRD2/DRD3 in human midbrain are associated with higher impulsivity and increased stimulant craving due to increased substance-mediated DA release [Buckholtz *et al.*, 2010]. Moreover, DRD2 autoreceptor-deficient mice exhibit increased responses to the rewarding properties of cocaine [Bello *et al.*, 2011]. Although, cause and consequence of the changes in D2 receptor expression are still a matter of debate, both obesity and addiction share deregulations of DRD2 availability [Volkow *et al.*, 2013]. Therefore, FTO, via regulating presynaptic dopamine autoreceptor feedback and/or postsynaptic dopamine signaling, may impinge on obesity

or addictive behavior. Consistently, *Fto*^{ΔDAT} mice exhibited cocaine supersensitivity in the conditioned place preference paradigm. Dopamine neuron restricted loss of FTO, however, had no influence on body weight or food intake, which is consistent with the paucity of body weight differences for DRD2 autoreceptor-deficient mice. Hence, in detail investigation of postsynaptic loss of FTO is warranted, that ultimately may affect food intake via attenuation of dopamine signaling in striatal dopamine target neurons, thereby resembling downregulation of DRD2 in human drug abusers and obese subjects [Volkow *et al.*, 2009; Wang *et al.*, 2001].

4.3 FTO demethylates m⁶A in messenger RNA

To date, the exact molecular function of FTO is not known. Growing evidence suggests that FTO demethylates N⁶-methyladenosine in messenger RNA [Meyer *et al.*, 2012; Dominissini *et al.*, 2012; Jia *et al.*, 2011]. First evidence demonstrated a role for m⁶A in mRNA stability [Wang *et al.*, 2013]. Whether this modification serves additional functions in mRNA processing, splicing, translation and/or other cellular functions remains elusive. Moreover, additional enzymatic functions of FTO, other than m⁶A demethylation, cannot be excluded at this point.

4.3.1 FTO acts as a m⁶A demethylase *in vivo*

To investigate whether FTO demethylates m⁶A in mRNA *in vivo* and thereby potentially impacts dopaminergic signaling, the m⁶A methylation pattern was assessed for *Fto*-deficient and control mice. In line with previous studies, a total of 42,000 m⁶A peaks were identified in mRNA isolated from midbrain and striatal tissue [Meyer *et al.*, 2012; Dominissini *et al.*, 2012]. This widespread occurrence of m⁶A in brain tissue is in line with previously reported results [Meyer *et al.*, 2012]. In comparison to control tissue over 5000 additional m⁶A peaks in over 1500 transcripts were identified in *Fto*-deficient mice, demonstrating that FTO demethylates m⁶A in mRNA *in vivo*. Moreover, loss of FTO only affected a subset of m⁶A sites and consequently only a subset of all methylated transcripts. For this reason, it

seems that FTO is acting only on specific transcripts and potentially affects specific pathways or cellular functions. Indeed, gene ontology analysis of those transcripts hypermethylated in *Fto*-deficient mice (FTO demethylation targets) revealed an enrichment of categories related to synaptic transmission and cell-cell signaling, while methylated transcripts in control mice did not cluster within these categories. This supports the notion that FTO plays a critical role in the central nervous system and is in line with the severe brain malformations observed for loss of FTO in humans [Gao *et al.*, 2010; Boissel *et al.*, 2009; Gerken *et al.*, 2007]. FTO demethylase activity was directed against a specific subset of transcripts, however, this analysis only included specific parts of the brain. Hence, different transcripts may be affected in other brain areas. Moreover, other demethylases may act in parallel on yet different subsets of mRNA in a tissue specific manner. Supporting this concept is the recent identification of AlkBH5, a second m⁶A demethylase, that is highly expressed in peripheral tissues rather than the central nervous system [Zheng *et al.*, 2012]. Hence, FTO, AlkBH5 and yet unidentified demethylases may alter methylation status and as a consequence mRNA function in a tissue specific manner.

Albeit the yet unknown function of the m⁶A mark, hypermethylated transcripts in *Fto*-deficient midbrain and striatal tissue were further investigated for a potential involvement in the dopamine signaling related phenotype observed in *Fto*-deficient and *Fto*^{ADAT} mice. Overlay of hypermethylated transcripts with dopaminergic signaling using pathway analysis revealed several transcripts encoding proteins important for neuronal signaling in general, such as GNAO1 and NMDAR1(zeta-1), and dopaminergic signaling specifically, such as DRD3, GIRK2, GNAO1, PDE1b, CACNA1A -1C -1D and SYN1 (Section 3.3.2).

4.3.2 Selected candidate transcripts are affected on protein level

Following the identification of hypermethylated transcripts that putatively impact dopaminergic signaling, several candidates were selected for further investigation. All investigated candidates showed no differences or minor increases on the tran-

script level. Several candidates, however, were downregulated on the protein level (DRD3, GIRK2, NMDAR1), suggesting a role for the m⁶A mark in regulating translation. These observations are in line with a reduced global translation reported for *Fto*-deficient cells and the loss of lean mass in adult onset *Fto*-deficient mice [Gulati *et al.*, 2013; McMurray *et al.*, 2013]. Furthermore, downregulated protein levels are in agreement with the recent finding that m⁶A affects mRNA stability via binding of YTHDF2 to methylated transcripts and subsequent recruitment to RNA decay sites [Wang *et al.*, 2013]. Thereby, the pool of available mRNA templates is limited and would subsequently lead to a reduction in translation and protein levels. Hypermethylation as caused by loss of FTO would thus lead to decreased mRNA stability and lifetime and as a consequence reduced protein levels as observed for DRD3, GIRK2 and NMDAR1 in *Fto*-deficient mice.

Since not all investigated hypermethylated transcripts exhibited downregulation on protein level, the m⁶A modification does not necessarily influence translation, suggesting complex mechanisms underlying the role of m⁶A in mRNA. Binding of YTHDF2 was reported to only occur for a subset of m⁶A methylated transcripts and therefore the YTHDF2-dependent regulation of mRNA stability does not affect all m⁶A modified mRNAs [Wang *et al.*, 2013]. Both GNAI1 and IKK2 transcripts were hypermethylated in *Fto*-deficient mice, but showed normal protein expression. Hence, these candidates may represent transcripts that, although they exhibit m⁶A hypermethylation, are not bound by YTHDF2 and are not removed from the mRNA translation pool. Moreover, it cannot be ruled out that the observed downregulations merely present indirect effects through downregulation of proteins involved in RNA processing, metabolism or translation. Furthermore, m⁶A may influence splicing patterns, thus affecting expression and protein levels of certain isoforms.

Since only midbrain and striatal tissue were analyzed in these experiments, it remains to be determined whether the hypermethylated transcripts identified in this study reflect a general population that is demethylated by FTO or whether different

subsets of transcripts are affected in different brain areas. Furthermore, detailed investigation of the role of m⁶A in regulating mRNA stability and translation is warranted in order to define the exact context of FTO action.

With respect to dopaminergic signaling, the downregulation of DRD₃, GIRK₂ and NMDAR₁ protein levels may, at least partly, explain the mechanism underlying the attenuation of the DRD₂-DRD₃-GIRK dependent autoinhibitory feedback loop in *Fto*-deficient and *Fto*^{ΔDAT} mice.

The dopamine D3 receptor

The DRD₃, like the DRD₂, is found presynaptically on dopamine neurons [Diaz *et al.*, 2000]. While the D₂ receptor is known to reduce firing rate of dopaminergic neurons through coupling to potassium channels of the GIRK family and subsequent membrane hyperpolarization [Bello *et al.*, 2011; Lacey *et al.*, 1987], evidence on D₃ receptors with regards to this function are so far contradictory. Both the coupling and the paucity of coupling to GIRKs has been reported for DRD₃ autoreceptors [Kuzhikandathil *et al.*, 1998; Davila *et al.*, 2003]. Nevertheless, both DRD₃ and DRD₂ may share the ability to reduce dopamine neuron firing as a mean of feedback inhibition.

Furthermore, the whole body deletion of DRD₃ in mice led to increased locomotor activity, increased grooming and enhanced reactivity to drug-paired cues [Accili *et al.*, 1996; Xu *et al.*, 1997; Le Foll *et al.*, 2005; Narita *et al.*, 2003; Francès *et al.*, 2004]. All of these behaviors are related to dopamine levels and consistently, DRD₃-deficient mice have higher levels of extracellular dopamine [Koeltzow *et al.*, 1998; Joseph *et al.*, 2002]. In contrast, DRD₂-deficient mice have unaltered dopamine levels, suggesting that control of basal dopamine levels depends on DRD₃ rather than DRD₂ function [Dickinson *et al.*, 1999]. *Fto*-deficient mice are hypoactive, whereas *Fto*^{ΔDAT} mice were relatively hyperactive [Fischer *et al.*, 2009]. As baseline locomotor activity would partially depend on baseline dopamine levels, detailed investigation of absolute dopamine values may aid in further outlining the exact outcome of conditional and whole body loss of FTO [Giros *et al.*, 1996;

Zhou & Palmiter, 1995]. Taken together, decreased availability of DRD₃ autoreceptors due to FTO deficiency may directly affect the feedback loop, leading to the attenuation of dopamine neuron autoinhibition in *Fto*-deficient and *Fto*^{ΔDAT} mice.

In humans variation within the *DRD3* gene affecting dopamine binding affinity has been linked to impulsivity and substance abuse [Agrawal *et al.*, 2013; Huang *et al.*, 2008; Limosin *et al.*, 2005; Retz *et al.*, 2003; Krebs *et al.*, 1998; Duaux *et al.*, 1998]. Moreover, *DRD3* variation was linked to some aspects of ADHD related to violent behavior [Retz *et al.*, 2003]. Therefore, FTO may likewise impinge on behaviors such as impulsivity through affecting *DRD3* transcript methylation. In line with this notion, first associations of genomic variation in *FTO* with ADHD have been reported [Choudhry *et al.*, 2013; Velders *et al.*, 2012]. Thus, investigation of *Fto*-deficient mice led to the identification of a putative candidate transcript, *Drd3*, linking human *FTO* genotypes to psychiatric diseases such as ADHD. Consequently, investigation of human *FTO* and *DRD3* genotypes may hold the potential to identify synergistic or antagonistic actions with respect to psychiatric and obesity related traits.

G protein-coupled inwardly rectifying potassium channel 2

G protein-coupled inwardly rectifying potassium channels (GIRK) are mediating slow inhibitory currents, both pre- and postsynaptically [Lüscher & Slesinger, 2010]. Furthermore, they shape the resting membrane potential and thus influence the excitability of neurons [Mark & Herlitze, 2000]. The four known GIRK subunits (GIRK₁₋₄) form homo- or heterotetrameric channels [Lüscher & Slesinger, 2010]. Within the brain, the dominant form of this channel is compromised by GIRK₁ and GIRK₂. Knock out studies in mice have demonstrated that GIRK₂ (*Kcnj6*) is the primary channel subunit mediating inhibitory currents [Lüscher & Slesinger, 2010]. Hence, one of the consequences of the downregulation of GIRK₂ in *Fto*-deficient mice is the reduction of dopamine autoreceptor-mediated inhibitory currents. Furthermore, *Girk2*-deficient mice exhibited reduced anxiety, increased activity, reduced cocaine self-administration and reduced conditioned taste aversion [Arora *et al.*, 2010; Pravetoni & Wickman, 2008; Hill *et al.*, 2003; Morgan *et al.*, 2003].

While a reduction in cocaine self-administration is reminiscent of the cocaine insensitivity in *Fto*-deficient mice, increased activity of *Girk2*-deficient mice is opposing the hypoactivity of whole body FTO knock out mice [Fischer *et al.*, 2009]. Therefore, *Fto*-deficient mice do not resemble all aspects of GIRK2 deficiency, but are rather subject to a number of alterations (including DRD₃, NMDAR₁ and GIRK₂) shaping their phenotype. GIRKs are not only coupling to autoreceptors, but also to other non-dopaminergic receptors in dopamine neurons, thereby representing one of the major factors controlling dopamine neuron function [Lüscher & Slesinger, 2010]. Widely expressed, both pre- and postsynaptic, GIRKs are important mediators of long term depression (LTD) and long term potentiation (LTP), synaptic mechanisms underlying various forms of learning behaviors [Lüscher & Slesinger, 2010]. Hence, the reduced GIRK availability in midbrain dopaminergic neurons of *Fto*-deficient and *Fto*^{ΔDAT} mice would not only affect autoreceptor inhibition of dopamine neurons, but also impact the responsiveness of dopaminergic neurons to various other synaptic inputs (e.g. GABAergic). Additionally, postsynaptic loss of GIRKs in target neurons of the dopamine circuitry in *Fto*-deficient mice would attenuate LTD and/or LTP and thus prevent the encoding of motivational value by dopaminergic signaling [Volkow *et al.*, 2013; Kauer & Malenka, 2007; Hyman *et al.*, 2006].

In humans, GIRK channels are implicated in diseases such as epilepsy, Down's syndrome, Parkinson's disease and addiction, demonstrating their importance for neuronal function [Lüscher & Slesinger, 2010].

Taken together, FTO dependent regulation of GIRK₂ availability would not only affect dopamine neuron function via coupling of GIRKs to both DRD₂ and DRD₃ autoreceptors, but may also represent a possible reason for the strong contrast between whole body and dopamine neuron restricted FTO deficiency, via postsynaptic alterations of GIRK expression.

N-methyl-D-aspartate receptor subunit 1

The NMDAR₁ (*Grin1*) subunit is a critical component of N-methyl-D-aspartate receptors, which belong to the family of voltage-gated ionotropic receptors [Paoletti *et al.*, 2013; Kauer & Malenka, 2007]. NMDARs are activated by membrane depolarization in conjunction with co-binding of the excitatory neurotransmitters glutamate and either glycine or D-serine [Paoletti *et al.*, 2013]. Within the brain, NMDARs are important mediators of LTD and LTP. Opening of NMDARs leads to an influx of sodium and importantly calcium, which triggers intracellular signaling molecules, such as the CamKII protein kinase (in LTP) or phosphatases (in LTD) [Paoletti *et al.*, 2013; Kauer & Malenka, 2007]. Both LTP and LTD depend on changes in α -amino-3-hydroxy-5-methyl-4-isoxazole propionic acid receptor (AMPA) availability, which is regulated by NMDAR signaling [Kauer & Malenka, 2007]. Deletion of the critical NMDAR₁ subunit caused a complete loss of NMDA receptor function [Forrest *et al.*, 1994; Tsien *et al.*, 1996]. Hence, reduced availability of NMDAR₁ in *Fto*-deficient mice would lead to an attenuation of the synaptic alterations in LTP and LTD underlying dopaminergic signaling, thereby impairing fundamental mechanisms of synaptic plasticity [Kauer & Malenka, 2007; Hyman *et al.*, 2006]. Once again, loss of these mechanisms may represent one possible cause for the insensitivity of *Fto*-deficient mice to cocaine-induced increases in synaptic dopamine levels. Since NMDARs are also expressed on dopaminergic neurons [Wang *et al.*, 2010; Paquet *et al.*, 1997], dopamine neuron restricted FTO knock out mice may also exhibit a deregulation of NMDAR₁ signaling in DA neurons, implicated in synaptic plasticity and addiction [Zweifel *et al.*, 2008].

In humans, malfunctional NMDAR dependent synaptic plasticity has been linked to various psychiatric diseases, including schizophrenia, mood disorders, Huntington's and Alzheimer's disease [Lakhan *et al.*, 2013]. Therefore, malfunctional FTO-dependent regulation of NMDA receptor availability may play a role in these neuropsychiatric diseases and could possibly represent a link to the observed associations of human *FTO* variants with major depressive disorder or ADHD [Samaan

et al., 2012; Rivera *et al.*, 2012; Velders *et al.*, 2012; Choudhry *et al.*, 2013]. Furthermore, the importance of NMDA receptors for synaptic plasticity, poses the question, whether human *FTO* variation affects learning and memory. Limited evidence suggests that *FTO* risk alleles worsen memory performance and negatively impact cognitive decline [Alosco *et al.*, 2013; Bressler *et al.*, 2013].

Taken together, via its proposed function as a m⁶A demethylase, *FTO* may regulate *Grin1* transcript methylation, reducing NMDAR₁ availability and thus would downregulate a major component of the mechanistic machinery needed for synaptic plasticity in learning, memory and addiction [Zweifel *et al.*, 2008; Kauer & Malenka, 2007].

Most probably, additional hypermethylated transcripts not covered by the current study are affected on protein level in *Fto*-deficient mice. Therefore, it is likely that, in addition to DRD₃, GIRK₂ and NMDAR₁, other components involved in the function of dopaminergic signaling participate in the attenuation of the DRD₂-DRD₃-GIRK-dependent autoreceptor function observed for *Fto*-deficient and *Fto*^{ΔDAT} mice. Moreover, it cannot be ruled out at this point that loss of *FTO* affects processes involved in the development of the central nervous system in general and formation of synapses in particular. Adult onset loss of *FTO* in mice overcomes many of the aspects of the germline *Fto* knock out phenotype, including postnatal growth retardation [McMurray *et al.*, 2013; Fischer *et al.*, 2009]. The first three postnatal weeks of life in mice (third trimester of pregnancy in humans) are known as the critical time frame for central nervous system development, during which circuits are wired and/or rewired [Bouret, 2010]. Hence, developmental defects observed for growth may also affect the development of the neuronal circuitry and hypermethylation of transcripts leading to deregulation on the protein level may underly these developmental alterations.

So far, all of the above described observations on *FTO*-dependent m⁶A hypermethylation and subsequent alterations of protein levels have been conducted in

Fto-deficient mice. Further experiments will need to address whether comparable results are observed for dopamine neuron restricted loss of FTO and hence dissect pre- and postsynaptic effects of FTO demethylase activity.

4.4 Relation to studies of human *FTO* genomic variation

Genomic variation of *FTO* in humans is associated with obesity related traits. To date the mechanisms causing this relation remain elusive. Although the exact function of the *N*6-methyladenosine modification in mRNA is largely unknown, a putative regulation of expression through demethylation by FTO may represent a mechanism by which physiological networks such as the homeostatic and hedonic circuitry are controlled. FTO expression has been demonstrated to depend on amino acid availability [Cheung *et al.*, 2013]. Hence, environmental changes e.g. leading to starvation could affect FTO expression and subsequently change the methylation pattern in a given tissue or neuronal circuitry affecting a whole set of genes simultaneously. These changes in methylation and subsequent expression changes may alter network properties, setting a new baseline for the responsiveness of for example the hedonic circuitry, potentially rendering an organism more susceptible to e.g. rewarding stimuli. *Fto*-deficient as well as dopamine neuron restricted FTO knock out mice exhibited alterations of the dopaminergic circuitry. FTO expression decreases with a reduction of amino acid availability [Cheung *et al.*, 2013; Gulati *et al.*, 2013]. Hence, starvation may reflect a knock down of FTO that would potentially lead to an attenuation of the dopamine autoinhibitory feedback loop, subsequently hypersensitizing dopaminergic pathways and setting a new baseline that could increase the responsiveness to rewarding stimuli. Further supporting this hypothesis are studies of human FTO 'risk-allele' carriers demonstrating altered responsiveness of different brain areas, including nuclei of the reward circuitry, to food representations [Karra *et al.*, 2013]. Hence, FTO may be an important relay enzyme, conveying environmental changes to hedonic and energy homeostasis centers in the brain, finally leading to an adaptation of behavior.

The human *FTO* phenotype is predominately related to energy intake, with *FTO* 'risk-allele' carriers showing elevated consumption of highly palatable food [Haupt *et al.*, 2009; Speakman *et al.*, 2008; Cecil *et al.*, 2008; Timpson *et al.*, 2008]. Moreover, 'risk-allele' carriers display deviant food responsiveness and satiety [Wardle *et al.*, 2009, 2008; Velders *et al.*, 2012]. Despite the robust associations with obesity related traits, *FTO* variants were furthermore associated with addictive behavior, ADHD and depression [Sobczyk-Kopciol *et al.*, 2011; Velders *et al.*, 2012; Choudhry *et al.*, 2013; Rivera *et al.*, 2012; Samaan *et al.*, 2012]. These, however, are inverse associations rendering the obesity 'risk-allele' protective against depression, certain addictive behavior and ADHD. Earlier studies established that ADHD and depression are associated with increased body weight [Luppino *et al.*, 2010; Cortese & Vincenzi, 2012]. Therefore, the inverse associations of *FTO* variants with these conditions are surprising. Malfunction of the dopaminergic circuitry has been previously linked to psychiatric disorders such as addictive behavior, ADHD and depression [Swanson *et al.*, 2007; Beaulieu & Gainetdinov, 2011; Koob & Volkow, 2010]. Intake of highly palatable food and the concomitant pleasure felt by its consumption affect the dopaminergic circuitry as well. Hence, Velders and colleagues proposed a mechanism through which overeating and enjoyment of food represent self-medication that ameliorates the symptoms of ADHD, addiction and depression [Velders *et al.*, 2012]. As a result, carriers of the obesity risk allele for *FTO* would benefit from protective aspects of the increased intake of highly palatable food via rewarding stimulation of the dopaminergic circuitry and attenuation of psychiatric symptoms such as depression.

4.5 Conclusions

In summary, loss of *FTO* leads to the attenuation of the DRD2-DRD3-GIRK-dependent autoreceptor feedback loop in both *Fto*-deficient and *Fto*^{ΔDAT} mice. While this leads to a cocaine hypersensitivity in *Fto*^{ΔDAT} mice, *Fto*-deficient mice are insensitive to the stimulatory effects of cocaine. On the molecular level, *FTO* was

demonstrated to act as a m⁶A demethylase in midbrain and striatal tissue, acting only on a subset of all m⁶A methylated transcripts and thus suggesting that FTO acts on specific pathways implicated in neuronal signaling. As a consequence of loss of FTO and m⁶A hypermethylation, protein levels of DRD₃, GIRK₂ and NMDAR₁ were found to be downregulated and would, at least partly, explain malfunction of the autoreceptor feedback loop in dopaminergic neurons. Moreover, this finding is in perfect agreement with the recent demonstration that m⁶A mRNA methylation leads to shuttling of transcripts to mRNA degradation sites in a YTHDF2-dependent manner and hence limiting the template pool of mRNA transcripts [Wang *et al.*, 2013].

Despite the yet unknown consequence of human *FTO* genomic variation on FTO function and/or expression, the malfunction of the dopaminergic circuitry in *Fto*-deficient and *Fto*^{ADAT} mice warrants the detailed investigation of dopaminergic function in human *Fto* SNP carriers. Aberrant function of the dopaminergic circuitry may underly the associations of human *FTO* variation with addictive behavior, ADHD and depression [Sobczyk-Kopciol *et al.*, 2011; Velders *et al.*, 2012; Choudhry *et al.*, 2013; Rivera *et al.*, 2012; Samaan *et al.*, 2012]. Moreover, malfunction of dopaminergic signaling could represent a major component causing changes in food responsiveness and preference, thereby influencing eating behavior and, at least partly, causing the increase in energy intake described for human *FTO* risk allele carriers [Karra *et al.*, 2013; Velders *et al.*, 2012; Wardle *et al.*, 2009; Haupt *et al.*, 2009; Cecil *et al.*, 2008; Timpson *et al.*, 2008; Speakman *et al.*, 2008].

Importantly, this study defined molecular targets (DRD₃, GIRK₂ and NMDAR₁) and a pathway (dopamine signaling and dopamine autoreceptor function) for FTO demethylase activity in mice, indicating potential targets for human *FTO* studies. This warrants the broadening of the scientific scope for FTO investigation beyond obesity and towards reward processing, reward based decision making and psychiatric diseases such as depression, ADHD and addiction.

4.6 Perspectives

The investigation of both whole body *Fto*-deficient and dopamine neuron restricted knock out mice revealed a FTO-dependent alteration of the DRD2-DRD3-GIRK-dependent autoinhibitory feedback loop of midbrain dopaminergic neurons. Comparison of both mouse models suggests that in addition to the changes in dopamine neuron function, loss of FTO may attenuate postsynaptic signaling events as well. Hence, conditional deletion of FTO in both pre- and postsynaptic sites of dopaminergic signaling through usage of Cre lines expressing the recombinase under the control of the *Drd1*, *Drd2* or *Adora2a* (targeting DRD2 expressing neurons in striatum and not dopaminergic neurons, [Durieux *et al.*, 2009]) promoters may aid in further delineating the effect of FTO on the dopaminergic circuitry. Furthermore, a double knock out of FTO in both DRD1 and DRD2 expressing neurons, leading to a loss of FTO in almost every pre- and postsynaptic dopamine signaling site, would be best suited to investigate FTO's function in the reward circuitry and may restore features of *Fto*-deficient mice with respect to dopamine network function. Since human *FTO* phenotypes are associated with increased energy intake, additional studies could address FTO function in other feeding related nuclei, such as the PVN and LH. Especially the LH, as it represents an integrative center for homeostatic and hedonic pathways, may prove a viable target for specific FTO manipulations [Berthoud, 2011; Simerly, 2006; Saper *et al.*, 2002]. In addition, these investigations should be used to assess the putative tissue specificity of FTO by comparison of methylation patterns identified in different brain areas.

To date, human studies addressing *FTO* phenotypes have focused primarily on its associations with obesity related traits. However, it becomes more and more evident that FTO may play a role in more than just homeostatic, feeding related nuclei. Therefore, the notion that the loss of FTO in mice alters dopamine neuron function cell autonomously as well as on the network level should aid in generating hypotheses for the study of human *FTO* phenotypes. Based on this notion,

investigation of human *FTO* 'risk-allele' carriers should be expanded to reward processing and reward based decision making, developing the appropriate behavioral tests and functional MRI paradigms. Moreover, identification of pathways altered by the loss of *FTO* in rodents may aid in selecting additional risk factors for polygenic obesity for a combined investigation with *FTO* variants. Thus, the combined effects, being synergistic or opposing, could be investigated to better understand the complex interplay of risk factors for polygenic obesity shaping each individual's susceptibility to gain weight.

5 Bibliography

- AAS, P. A, OTTERLEI, M, FALNES, P. O, VÅGBØ, C. B, SKORPEN, F, AKBARI, M, SUNDHEIM, O, BJØRÅS, M, SLUPPHAUG, G, SEEBERG, E, & KROKAN, H. E. 2003. Human and bacterial oxidative demethylases repair alkylation damage in both RNA and DNA. *Nature*, **421**(6925), 859–863. [29]
- ABRAHAMSEN, G. C, BERMAN, Y, & CARR, K. D. 1995. Curve-shift analysis of self-stimulation in food-restricted rats: relationship between daily meal, plasma corticosterone and reward sensitization. *Brain research*, **695**(2), 186–194. [13]
- ACCILI, D, FISHBURN, C. S, DRAGO, J, STEINER, H, LACHOWICZ, J. E, PARK, B. H, GAUDA, E. B, LEE, E. J, COOL, M. H, SIBLEY, D. R, GERFEN, C. R, WESTPHAL, H, & FUCHS, S. 1996. A targeted mutation of the D3 dopamine receptor gene is associated with hyperactivity in mice. *Proceedings of the national academy of sciences of the united states of america*, **93**(5), 1945–1949. [103]
- ADAMANTIDIS, A. R, ZHANG, F, ARAVANIS, A. M, DEISSEROTH, K, & DE LECEA, L. 2007. Neural substrates of awakening probed with optogenetic control of hypocretin neurons. *Nature*, **450**(7168), 420–424. [6]
- ADEYEMO, A, CHEN, G, ZHOU, J, SHRINER, D, DOUMATEY, A, HUANG, H, & ROTIMI, C. 2010. FTO genetic variation and association with obesity in West Africans and African Americans. *Diabetes*, **59**(6), 1549–1554. [15]
- AGRAWAL, A, WETHERILL, L, BUCHOLZ, K. K, KRAMER, J, KUPERMAN, S, LYNKEY, M. T, NURNBERGER, J. I, SCHUCKIT, M, TISCHFIELD, J. A, EDENBERG, H. J, FOROUD, T, & BIERUT, L. J. 2013. Genetic influences on craving for alcohol. *Addictive behaviors*, **38**(2), 1501–1508. [104]
- AHMED, S. H, KENNY, P. J, KOOB, G. F, & MARKOU, A. 2002. Neurobiological evidence for hedonic allostasis associated with escalating cocaine use. *Nature neuroscience*, **5**(7), 625–626. [13]
- ALOSCO, M. L, BENITEZ, A, GUNSTAD, J, SPITZNAGEL, M. B, MCCAFFERY, J. M, MCGEARY, J. E, POPPAS, A, PAUL, R. H, SWEET, L. H, & COHEN, R. A. 2013. Reduced memory in fat mass and obesity-associated allele carriers among older adults with cardiovascular disease. *Psychogeriatrics : the official journal of the japanese psychogeriatric society*, **13**(1), 35–40. [19, 107]
- ANSLEY, S. J, BADANO, J. L, BLACQUE, O. E, HILL, J, HOSKINS, B. E, LEITCH, C. C, KIM, J. C, ROSS, A. J, EICHERS, E. R, TESLOVICH, T. M, MAH, A. K, JOHNSEN, R. C, CAVENDER, J. C, LEWIS, R. A, LEROUX, M. R, BEALES, P. L, & KATSANIS, N. 2003. Basal body dysfunction is a likely cause of pleiotropic Bardet-Biedl syndrome. *Nature*, **425**(6958), 628–633. [20]
- ANZALONE, A, LIZARDI-ORTIZ, J. E, RAMOS, M, DE MEI, C, HOPE, F. W, IACCARINO, C, HALBOUT, B, JACOBSEN, J, KINOSHITA, C, WELTER, M, CARON, M. G, BONCI, A, SULZER, D, & BORRELLI, E. 2012. Dual control of dopamine synthesis and release by presynaptic and postsynaptic dopamine D2 receptors. *Journal of neuroscience*, **32**(26), 9023–9034. [14]

- ARORA, D, HALUK, D. M, KOURRICH, S, PRAVETONI, M, FERNÁNDEZ-ALACID, L, NICOLAU, J. C, LUJÁN, R, & WICKMAN, K. 2010. Altered neurotransmission in the mesolimbic reward system of Girk mice. *Journal of neurochemistry*, **114**(5), 1487–1497. [104]
- ATASOY, D, BETLEY, J. N, SU, H. H, & STERNSON, S. M. 2012. Deconstruction of a neural circuit for hunger. *Nature*, **488**(7410), 172–177. [5]
- BALTHASAR, N, DALGAARD, L. T, LEE, C. E, YU, J, FUNAHASHI, H, WILLIAMS, T, FERREIRA, M, TANG, V, MCGOVERN, R. A, KENNY, C. D, CHRISTIANSEN, L. M, EDELSTEIN, E, CHOI, B, BOSS, O, ASCHKENASI, C, ZHANG, C.-Y, MOUNTJOY, K, KISHI, T, ELMQUIST, J. K, & LOWELL, B. B. 2005. Divergence of melanocortin pathways in the control of food intake and energy expenditure. *Cell*, **123**(3), 493–505. [5]
- BARBER, J. C. K, ZHANG, S, FRIEND, N, COLLINS, A. L, MALONEY, V. K, HASTINGS, R, FARREN, B, BARNICOAT, A, POLITYKO, A. D, RUMYANTSEVA, N. V, STARKE, H, & YE, S. 2006. Duplications of proximal 16q flanked by heterochromatin are not euchromatic variants and show no evidence of heterochromatic position effect. *Cytogenetic and genome research*, **114**(3-4), 351–358. [21]
- BEAULIEU, J.-M, & GAINETDINOV, R. R. 2011. The physiology, signaling, and pharmacology of dopamine receptors. *Pharmacological reviews*, **63**(1), 182–217. [7, 8, 9, 12, 14, 34, 58, 60, 83, 93, 94, 98, 109]
- BELGARDT, B. F, & BRÜNING, J. C. 2010. CNS leptin and insulin action in the control of energy homeostasis. *Annals of the new york academy of sciences*, **1212**(Nov.), 97–113. [4, 5, 6]
- BELLO, E. P, MATEO, Y, GELMAN, D. M, NOAÍN, D, SHIN, J. H, LOW, M. J, ALVAREZ, V. A, LOVINGER, D. M, & RUBINSTEIN, M. 2011. Cocaine supersensitivity and enhanced motivation for reward in mice lacking dopamine D2 autoreceptors. *Nature neuroscience*, **14**(8), 1033–1038. [14, 15, 58, 66, 80, 96, 97, 98, 99, 103]
- BELLO, N. T, & HAJNAL, A. 2010. Dopamine and binge eating behaviors. *Pharmacology, biochemistry, and behavior*, **97**(1), 25–33. [12]
- BENEDICT, C, JACOBSSON, J. A, RÖNNEMAA, E, SALLMAN ALMEN, M, BROOKS, S, SCHULTES, B, FREDRIKSSON, R, LANNFELT, L, KILANDER, L, & SCHIÖTH, H. B. 2011. The fat mass and obesity gene is linked to reduced verbal fluency in overweight and obese elderly men. *Neurobiology of aging*, **32**(6), 1159.e1–5. [18, 21]
- BENTIVOGLIO, M, & MORELLI, M. 2005. Chapter I The organization and circuits of mesencephalic dopaminergic neurons and the distribution of dopamine receptors in the brain. *Pages 1–107 of: S B DUNNETT, M. B. A. B, & HÖKFELT, T (eds), Handbook of chemical neuroanatomy*. Elsevier. [7]
- BERBARI, N. F, PASEK, R. C, MALARKEY, E. B, YAZDI, S. M. Z, MCNAIR, A. D, LEWIS, W. R, NAGY, T. R, KESTERSON, R. A, & YODER, B. K. 2013. Leptin resistance is a secondary consequence of the obesity in ciliopathy mutant mice. *Proceedings of the national academy of sciences*, **110**(19), 7796–7801. [20]
- BERENTZEN, T, KRING, S. I. I, HOLST, C, ZIMMERMANN, E, JESS, T, HANSEN, T, PEDERSEN, O, TOUBRO, S, ASTRUP, A, & SØRENSEN, T. I. A. 2008. Lack of association of fatness-related FTO gene variants with energy expenditure or physical activity. *The journal of clinical endocrinology and metabolism*, **93**(7), 2904–2908. [17]

- BERTHOUD, H.-R. 2011. Metabolic and hedonic drives in the neural control of appetite: who is the boss? *Current opinion in neurobiology*, **21**(6), 888–896. [6, 111]
- BERULAVA, T, & HORSTHEMKE, B. 2010. The obesity-associated SNPs in intron 1 of the FTO gene affect primary transcript levels. *European journal of human genetics : Ejhg*, **18**(9), 1054–1056. [19, 23]
- BJÖRKLUND, A. 2007. Dopamine neuron systems in the brain: an update. *Trends in neurosciences*, **30**(5), 194–202. [7]
- BODI, Z, BUTTON, J. D, GRIERSON, D, & FRAY, R. G. 2010. Yeast targets for mRNA methylation. *Nucleic acids research*, **38**(16), 5327–5335. [31, 32]
- BOENDER, A. J, VAN ROZEN, A. J, & ADAN, R. A. H. 2012. Nutritional state affects the expression of the obesity-associated genes *Etv5*, *Faim2*, *Fto*, and *Negr1*. *Obesity*, **20**(12), 2420–2425. [26]
- BOISSEL, S, REISH, O, PROULX, K, KAWAGOE-TAKAKI, H, SEDGWICK, B, YEO, G. S. H, MEYRE, D, GOLZIO, C, MOLINARI, F, KADHOM, N, ETCHEVERS, H. C, SAUDEK, V, FAROOQI, I. S, FROGUEL, P, LINDAHL, T, O'RAHILLY, S, MUNNICH, A, & COLLEAUX, L. 2009. Loss-of-function mutation in the dioxygenase-encoding FTO gene causes severe growth retardation and multiple malformations. *American journal of human genetics*, **85**(1), 106–111. [21, 22, 93, 101]
- BOKAR, J. A, RATH-SHAMBAUGH, M. E, LUDWICZAK, R, NARAYAN, P, & ROTTMAN, F. 1994. Characterization and partial purification of mRNA N6-adenosine methyltransferase from HeLa cell nuclei. Internal mRNA methylation requires a multisubunit complex. *Journal of biological chemistry*, **269**(26), 17697–17704. [32]
- BOKAR, J. A, SHAMBAUGH, M. E, POLAYES, D, MATERA, A. G, & ROTTMAN, F. M. 1997. Purification and cDNA cloning of the AdoMet-binding subunit of the human mRNA (N6-adenosine)-methyltransferase. *Rna (new york, n.y.)*, **3**(11), 1233–1247. [32]
- BOLLEPALLI, S, DOLAN, L. M, DEKA, R, & MARTIN, L. J. 2010. Association of FTO gene variants with adiposity in African-American adolescents. *Obesity*, **18**(10), 1959–1963. [15]
- BORGLAND, S. L, TAHA, S. A, SARTI, F, FIELDS, H. L, & BONCI, A. 2006. Orexin A in the VTA is critical for the induction of synaptic plasticity and behavioral sensitization to cocaine. *Neuron*, **49**(4), 589–601. [6]
- BOURET, S. G. 2010. Development of hypothalamic neural networks controlling appetite. *Forum of nutrition*, **63**, 84–93. [107]
- BRESSLER, J, FORNAGE, M, DEMERATH, E. W, KNOPMAN, D. S, MONDA, K. L, NORTH, K. E, PENMAN, A, MOSLEY, T. H, & BOERWINKLE, E. 2013. Fat mass and obesity gene and cognitive decline: The Atherosclerosis Risk in Communities Study. *Neurology*, **80**(1), 92–99. [19, 107]
- BUCKHOLTZ, J. W, TREADWAY, M. T, COWAN, R. L, WOODWARD, N. D, LI, R, ANSARI, M. S, BALDWIN, R. M, SCHWARTZMAN, A. N, SHELBY, E. S, SMITH, C. E, KESSLER, R. M, & ZALD, D. H. 2010. Dopaminergic network differences in human impulsivity. *Science (new york, ny)*, **329**(5991), 532. [15, 99]
- CABALLERO, B. 2007. The global epidemic of obesity: an overview. *Epidemiologic reviews*, **29**, 1–5. [2, 92]

- CANTARA, W. A, CRAIN, P. F, ROZENSKI, J, McCLOSKEY, J. A, HARRIS, K. A, ZHANG, X, VENDEIX, F. A. P, FABRIS, D, & AGRIS, P. F. 2011. The RNA Modification Database, RNAMDB: 2011 update. *Nucleic acids research*, **39**(Database issue), D195–201. [30]
- CARLSSON, A, LINDQVIST, M, MAGNUSSON, T, & WALDECK, B. 1958. On the presence of 3-hydroxytyramine in brain. *Science (new york, ny)*, **127**(3296), 471. [7]
- CARROLL, M. E, & MEISCH, R. A. 1981. Determinants of increased drug self-administration due to food deprivation. *Psychopharmacology*, **74**(3), 197–200. [13]
- CARROLL, M. E, FRANCE, C. P, & MEISCH, R. A. 1979. Food deprivation increases oral and intravenous drug intake in rats. *Science (new york, ny)*, **205**(4403), 319–321. [13]
- CARROLL, S. M, NARAYAN, P, & ROTTMAN, F. M. 1990. N6-methyladenosine residues in an intron-specific region of prolactin pre-mRNA. *Molecular and cellular biology*, **10**(9), 4456–4465. [31]
- CAWLEY, J, & MEYERHOEFER, C. 2012. The medical care costs of obesity: an instrumental variables approach. *Journal of health economics*, **31**(1), 219–230. [1, 92]
- CECIL, J. E, TAVENDALE, R, WATT, P, HETHERINGTON, M. M, & PALMER, C. N. A. 2008. An obesity-associated FTO gene variant and increased energy intake in children. *The new england journal of medicine*, **359**(24), 2558–2566. [15, 17, 26, 109, 110]
- CHANG, Y.-C, LIU, P.-H, LEE, W.-J, CHANG, T.-J, JIANG, Y.-D, LI, H.-Y, KUO, S.-S, LEE, K.-C, & CHUANG, L.-M. 2008. Common variation in the fat mass and obesity-associated (FTO) gene confers risk of obesity and modulates BMI in the Chinese population. *Diabetes*, **57**(8), 2245–2252. [15]
- CHAUSMER, A. L, ELMER, G. I, RUBINSTEIN, M, LOW, M. J, GRANDY, D. K, & KATZ, J. L. 2002. Cocaine-induced locomotor activity and cocaine discrimination in dopamine D2 receptor mutant mice. *Psychopharmacology*, **163**(1), 54–61. [99]
- CHEN, R, TILLEY, M. R, WEI, H, ZHOU, F, ZHOU, F.-M, CHING, S, QUAN, N, STEPHENS, R. L, HILL, E. R, NOTTOLI, T, HAN, D. D, & GU, H. H. 2006. Abolished cocaine reward in mice with a cocaine-insensitive dopamine transporter. *Proceedings of the national academy of sciences of the united states of america*, **103**(24), 9333–9338. [94]
- CHEUNG, M. K, GULATI, P, O'RAHILLY, S, & YEO, G. S. H. 2013. FTO expression is regulated by availability of essential amino acids. *International journal of obesity (2005)*, **37**(5), 744–747. [27, 108]
- CHOUDHRY, Z, SENGUPTA, S. M, GRIZENKO, N, THAKUR, G. A, FORTIER, M.-E, SCHMITZ, N, & JOOBER, R. 2013. Association between obesity-related gene FTO and ADHD. *Obesity*, Mar. [18, 104, 106, 109, 110]
- CHURCH, C, LEE, S, BAGG, E. A. L, McTAGGART, J. S, DEACON, R, GERKEN, T, LEE, A, MOIR, L, MECINOVIĆ, J, QUWAILID, M. M, SCHOFIELD, C. J, ASHCROFT, F. M, & COX, R. D. 2009. A mouse model for the metabolic effects of the human fat mass and obesity associated FTO gene. *Plos genetics*, **5**(8), e1000599. [23]
- CHURCH, C, MOIR, L, McMURRAY, F, GIRARD, C, BANKS, G. T, TBOUL, L, WELLS, S, BRÜNING, J. C, NOLAN, P. M, ASHCROFT, F. M, & COX, R. D. 2010. Overexpression of Fto leads to increased food intake and results in obesity. *Nature genetics*, **42**(12), 1086–1092. [23, 27]

- CILIAUX, B. J, HEILMAN, C, DEMCHYSHYN, L. L, PRISTUPA, Z. B, INCE, E, HERSCH, S. M, NIZNIK, H. B, & LEVEY, A. I. 1995. The dopamine transporter: immunochemical characterization and localization in brain. *The journal of neuroscience : the official journal of the society for neuroscience*, **15**(3 Pt 1), 1714–1723. [68]
- CLANCY, M. J, SHAMBAUGH, M. E, TIMPTE, C. S, & BOKAR, J. A. 2002. Induction of sporulation in *Saccharomyces cerevisiae* leads to the formation of N6-methyladenosine in mRNA: a potential mechanism for the activity of the IME4 gene. *Nucleic acids research*, **30**(20), 4509–4518. [31, 32]
- CLÉMENT, K, VAISSE, C, LAHLOU, N, CABROL, S, PELLOUX, V, CASSUTO, D, GOURMELEN, M, DINA, C, CHAMBAZ, J, LACORTE, J. M, BASDEVANT, A, BOUGNÈRES, P, LEBOU, Y, FROGUEL, P, & GUY-GRAND, B. 1998. A mutation in the human leptin receptor gene causes obesity and pituitary dysfunction. *Nature*, **392**(6674), 398–401. [2]
- CORTESE, S, & VINCENZI, B. 2012. Obesity and ADHD: Clinical and Neurobiological Implications. *Current topics in behavioral neurosciences*, **9**, 199–218. [109]
- CROTEAU-CHONKA, D. C, MARVELLE, A. F, LANGE, E. M, LEE, N. R, ADAIR, L. S, LANGE, L. A, & MOHLKE, K. L. 2011. Genome-wide association study of anthropometric traits and evidence of interactions with age and study year in Filipino women. *Obesity*, **19**(5), 1019–1027. [15]
- CRUZ, H. G, IVANOVA, T, LUNN, M.-L, STOFFEL, M, SLESINGER, P. A, & LÜSCHER, C. 2004. Bi-directional effects of GABA(B) receptor agonists on the mesolimbic dopamine system. *Nature neuroscience*, **7**(2), 153–159. [46]
- CSEpany, T, LIN, A, BALDICK, C. J, & BEEMON, K. 1990. Sequence specificity of mRNA N6-adenosine methyltransferase. *Journal of biological chemistry*, **265**(33), 20117–20122. [32]
- CUMMINGS, D. E, & OVERDUIN, J. 2007. Gastrointestinal regulation of food intake. *The journal of clinical investigation*, **117**(1), 13–23. [4]
- DAVENPORT, J. R, WATTS, A. J, ROPER, V. C, CROYLE, M. J, VAN GROEN, T, WYSS, J. M, NAGY, T. R, KESTERSON, R. A, & YODER, B. K. 2007. Disruption of intraflagellar transport in adult mice leads to obesity and slow-onset cystic kidney disease. *Current biology : Cb*, **17**(18), 1586–1594. [20]
- DAVILA, V, YAN, Z, CRACIUN, L. C, LOGOTHETIS, D, & SULZER, D. 2003. D3 dopamine autoreceptors do not activate G-protein-gated inwardly rectifying potassium channel currents in substantia nigra dopamine neurons. *Journal of neuroscience*, **23**(13), 5693–5697. [14, 103]
- DAVIS, J. F, TRACY, A. L, SCHURDAK, J. D, TSCHÖP, M. H, LIPTON, J. W, CLEGG, D. J, & BENOIT, S. C. 2008. Exposure to elevated levels of dietary fat attenuates psychostimulant reward and mesolimbic dopamine turnover in the rat. *Behavioral neuroscience*, **122**(6), 1257–1263. [13]
- DAVIS, J. F, CHOI, D. L, & BENOIT, S. C. 2010. Insulin, leptin and reward. *Trends in endocrinology and metabolism: Tem*, **21**(2), 68–74. [13]
- DE MEI, C, RAMOS, M, IITAKA, C, & BORRELLI, E. 2009. Getting specialized: presynaptic and post-synaptic dopamine D2 receptors. *Current opinion in pharmacology*, **9**(1), 53–58. [8, 14]
- DELOUS, M, BAALA, L, SALOMON, R, LACLEF, C, VIERKOTTEN, J, TORY, K, GOLZIO, C, LACOSTE, T, BESSE, L, OZILOU, C, MOUTKINE, I, HELLMAN, N. E, ANSELME, I, SILBERMANN, F, VESQUE, C,

- GERHARDT, C, RATTENBERRY, E, WOLF, M. T. F, GUBLER, M. C, MARTINOVIC, J, ENCHA-RAZAVI, F, BODDAERT, N, GONZALES, M, MACHER, M. A, NIVET, H, CHAMPION, G, BERTHÉLÉMÉ, J. P, NIAUDET, P, McDONALD, F, HILDEBRANDT, F, JOHNSON, C. A, VEKEMANS, M, ANTIGNAC, C, RÜTHER, U, SCHNEIDER-MAUNOURY, S, ATTIE-BITACH, T, & SAUNIER, S. 2007. The ciliary gene RPGRIP1L is mutated in cerebello-oculo-renal syndrome (Joubert syndrome type B) and Meckel syndrome. *Nature genetics*, **39**(7), 875–881. [20]
- DEN HOED, M, WESTERTERP-PLANTENGA, M. S, BOUWMAN, F. G, MARIMAN, E. C. M, & WESTERTERP, K. R. 2009. Postprandial responses in hunger and satiety are associated with the rs9939609 single nucleotide polymorphism in FTO. *The american journal of clinical nutrition*, **90**(5), 1426–1432. [15, 17, 25]
- DESROSIERS, R, FRIDERICI, K, & ROTTMAN, F. 1974. Identification of methylated nucleosides in messenger RNA from Novikoff hepatoma cells. *Proceedings of the national academy of sciences of the united states of america*, **71**(10), 3971–3975. [31]
- DEVUYST, O, & ARNOULD, V. J. 2008. Mutations in RPGRIP1L: extending the clinical spectrum of ciliopathies. *Nephrology, dialysis, transplantation : official publication of the european dialysis and transplant association - european renal association*, **23**(5), 1500–1503. [20]
- DI CHIARA, G, & IMPERATO, A. 1988. Drugs abused by humans preferentially increase synaptic dopamine concentrations in the mesolimbic system of freely moving rats. *Proceedings of the national academy of sciences of the united states of america*, **85**(14), 5274–5278. [12]
- DI CHIARA, G. 2005. Chapter VI Dopamine, motivation and reward. *Pages 303–394 of: S B DUNNETT, M. B. A. B, & HÖKFELT, T (eds), Handbook of chemical neuroanatomy*. Elsevier. [7]
- DIAZ, J, PILON, C, LE FOLL, B, GROS, C, TRILLER, A, SCHWARTZ, J. C, & SOKOLOFF, P. 2000. Dopamine D3 receptors expressed by all mesencephalic dopamine neurons. *Journal of neuroscience*, **20**(23), 8677–8684. [103]
- DÍAZ-TORGA, G, FEIERSTEIN, C, LIBERTUN, C, GELMAN, D, KELLY, M. A, LOW, M. J, RUBINSTEIN, M, & BECÚ-VILLALOBOS, D. 2002. Disruption of the D2 dopamine receptor alters GH and IGF-I secretion and causes dwarfism in male mice. *Endocrinology*, **143**(4), 1270–1279. [34, 93, 98]
- DICKINSON, S. D, SABETI, J, LARSON, G. A, GIARDINA, K, RUBINSTEIN, M, KELLY, M. A, GRANDY, D. K, LOW, M. J, GERHARDT, G. A, & ZAHNISER, N. R. 1999. Dopamine D2 receptor-deficient mice exhibit decreased dopamine transporter function but no changes in dopamine release in dorsal striatum. *Journal of neurochemistry*, **72**(1), 148–156. [103]
- DINA, C, MEYRE, D, GALLINA, S, DURAND, E, KÖRNER, A, JACOBSON, P, CARLSSON, L. M. S, KIESS, W, VATIN, V, LECOEUR, C, DELPLANQUE, J, VAILLANT, E, PATTOU, F, RUIZ, J, WEILL, J, LEVY-MARCHAL, C, HORBER, F, POTOCZNA, N, HERCBERG, S, LE STUNFF, C, BOUGNÈRES, P, KOVACS, P, MARRE, M, BALKAU, B, CAUCHI, S, CHÈVRE, J.-C, & FROGUEL, P. 2007. Variation in FTO contributes to childhood obesity and severe adult obesity. *Nature genetics*, **39**(6), 724–726. [15, 16, 34, 92, 93]
- DOCKRAY, S, SUSMAN, E. J, & DORN, L. D. 2009. Depression, cortisol reactivity, and obesity in childhood and adolescence. *The journal of adolescent health : official publication of the society for adolescent medicine*, **45**(4), 344–350. [18]

- DOMINISSINI, D, MOSHITCH-MOSHKOVITZ, S, SCHWARTZ, S, SALMON-DIVON, M, UNGAR, L, OSENBURG, S, CESARKAS, K, JACOB-HIRSCH, J, AMARIGLIO, N, KUPIEC, M, SOREK, R, & REHAVI, G. 2012. Topology of the human and mouse m6A RNA methylomes revealed by m6A-seq. *Nature*, **485**(7397), 201–206. [31, 32, 33, 34, 81, 100]
- DRAGUNOW, M, & FAULL, R. 1989. The use of c-fos as a metabolic marker in neuronal pathway tracing. *Journal of neuroscience methods*, **29**(3), 261–265. [61]
- DUAUX, E, GORWOOD, P, GRIFFON, N, BOURDEL, M. C, SAUTEL, F, SOKOLOFF, P, SCHWARTZ, J. C, ADES, J, LÔO, H, & POIRIER, M. F. 1998. Homozygosity at the dopamine D3 receptor gene is associated with opiate dependence. *Molecular psychiatry*, **3**(4), 333–336. [104]
- DUNNETT, S. B. 2005. Chapter V Motor function(s) of the nigrostriatal dopamine system: Studies of lesions and behavior. *Pages 237–301 of: S B DUNNETT, M. B. A. B, & HÖKFELT, T (eds), Handbook of chemical neuroanatomy*. Elsevier. [7]
- DURIEUX, P. F, BEARZATTO, B, GUIDUCCI, S, BUCH, T, WAISMAN, A, ZOLI, M, SCHIFFMANN, S. N, & DE KERCHOVE D'EXAERDE, A. 2009. D2R striatopallidal neurons inhibit both locomotor and drug reward processes. *Nature neuroscience*, **12**(4), 393–395. [111]
- EKSTRAND, M. I, TERZIOGLU, M, GALTER, D, ZHU, S, HOFSTETTER, C, LINDQVIST, E, THAMS, S, BERGSTRAND, A, HANSSON, F. S, TRIFUNOVIC, A, HOFFER, B, CULLHEIM, S, MOHAMMED, A. H, OLSON, L, & LARSSON, N.-G. 2007. Progressive parkinsonism in mice with respiratory-chain-deficient dopamine neurons. *Proceedings of the national academy of sciences of the united states of america*, **104**(4), 1325–1330. [35, 67, 68, 70]
- FANG, H, LI, Y, DU, S, HU, X, ZHANG, Q, LIU, A, & MA, G. 2010. Variant rs9939609 in the FTO gene is associated with body mass index among Chinese children. *Bmc medical genetics*, **11**, 136. [15]
- FAROOQI, I. S, & O'RAHILLY, S. 2006. Genetics of Obesity in Humans. *Endocrine reviews*, **27**(7), 710–718. [1]
- FAROOQI, I. S, JEBB, S. A, LANGMACK, G, LAWRENCE, E, CHEETHAM, C. H, PRENTICE, A. M, HUGHES, I. A, MCCAMISH, M. A, & O'RAHILLY, S. 1999. Effects of recombinant leptin therapy in a child with congenital leptin deficiency. *The new england journal of medicine*, **341**(12), 879–884. [2]
- FAROOQI, I. S, KEOGH, J. M, YEO, G. S. H, LANK, E. J, CHEETHAM, T, & O'RAHILLY, S. 2003. Clinical spectrum of obesity and mutations in the melanocortin 4 receptor gene. *The new england journal of medicine*, **348**(12), 1085–1095. [2]
- FAROOQI, I, BULLMORE, E, KEOGH, J, GILLARD, J, O'RAHILLY, S, & FLETCHER, P. 2007. Leptin regulates striatal regions and human eating behavior. *Science (new york, ny)*, **317**(5843), 1355. [14]
- FIGLEWICZ, D. P, SZOT, P, CHAVEZ, M, WOODS, S. C, & VEITH, R. C. 1994. Intraventricular insulin increases dopamine transporter mRNA in rat VTA/substantia nigra. *Brain research*, **644**(2), 331–334. [13]
- FIGLEWICZ, D. P, EVANS, S. B, MURPHY, J, HOEN, M, & BASKIN, D. G. 2003. Expression of receptors for insulin and leptin in the ventral tegmental area/substantia nigra (VTA/SN) of the rat. *Brain research*, **964**(1), 107–115. [13]

- FIGLEWICZ, D. P, BENNETT, J. L, NALEID, A. M, DAVIS, C, & GRIMM, J. W. 2006. Intraventricular insulin and leptin decrease sucrose self-administration in rats. *Physiology & behavior*, **89**(4), 611–616. [14]
- FINKELSTEIN, E. A, TROGDON, J. G, COHEN, J. W, & DIETZ, W. 2009. Annual medical spending attributable to obesity: payer-and service-specific estimates. *Health affairs (project hope)*, **28**(5), w822–31. [1, 92]
- FISCHER, J, KOCH, L, EMMERLING, C, VIERKOTTEN, J, PETERS, T, BRÜNING, J. C, & RÜTHER, U. 2009. Inactivation of the Fto gene protects from obesity. *Nature*, **458**(7240), 894–898. [22, 24, 27, 35, 44, 54, 72, 93, 97, 98, 103, 105, 107]
- FORREST, D, YUZAKI, M, SOARES, H. D, NG, L, LUK, D. C, SHENG, M, STEWART, C. L, MORGAN, J. I, CONNOR, J. A, & CURRAN, T. 1994. Targeted disruption of NMDA receptor 1 gene abolishes NMDA response and results in neonatal death. *Neuron*, **13**(2), 325–338. [106]
- FRANCÈS, H, LE FOLL, B, DIAZ, J, SMIRNOVA, M, & SOKOLOFF, P. 2004. Role of DRD3 in morphine-induced conditioned place preference using drd3-knockout mice. *Neuroreport*, **15**(14), 2245–2249. [103]
- FRAYLING, T. M, TIMPSON, N. J, WEEDON, M. N, ZEGGINI, E, FREATHY, R. M, LINDGREN, C. M, PERRY, J. R. B, ELLIOTT, K. S, LANGO, H, RAYNER, N. W, SHIELDS, B, HARRIES, L. W, BARRETT, J. C, ELLARD, S, GROVES, C. J, KNIGHT, B, PATCH, A.-M, NESS, A. R, EBRAHIM, S, LAWLOR, D. A, RING, S. M, BEN-SHLOMO, Y, JARVELIN, M.-R, SOVIO, U, BENNETT, A. J, MELZER, D, FERRUCCI, L, LOOS, R. J. F, BARROSO, I, WAREHAM, N. J, KARPE, F, OWEN, K. R, CARDON, L. R, WALKER, M, HITMAN, G. A, PALMER, C. N. A, DONEY, A. S. F, MORRIS, A. D, SMITH, G. D, HATTERSLEY, A. T, MCCARTHY, M. I, & CONTROL, W. T. C. 2007. A common variant in the FTO gene is associated with body mass index and predisposes to childhood and adult obesity. *Science (new york, ny)*, **316**(5826), 889–894. [15, 16, 20, 23, 24, 26, 34, 92, 93]
- FREDRIKSSON, R, HÄGGLUND, M, OLSZEWSKI, P. K, STEPHANSSON, O, JACOBSSON, J. A, OLSZEWSKA, A. M, LEVINE, A. S, LINDBLOM, J, & SCHIÖTH, H. B. 2008. The obesity gene, FTO, is of ancient origin, up-regulated during food deprivation and expressed in neurons of feeding-related nuclei of the brain. *Endocrinology*, **149**(5), 2062–2071. [24, 26, 28]
- FREED, C, REVAY, R, VAUGHAN, R. A, KRIEK, E, GRANT, S, UHL, G. R, & KUCHAR, M. J. 1995. Dopamine transporter immunoreactivity in rat brain. *The journal of comparative neurology*, **359**(2), 340–349. [68]
- FRIEDMAN, J. M. 2010. *A tale of two hormones*. Vol. 16. The Rockefeller University, New York, New York, USA. friedj@mail.rockefeller.edu: Nat Med. [4]
- FRIEDMAN, J. M. 2011. Leptin and the regulation of body weight. *Pages 1–9 of: The keio journal of medicine*. Rockefeller University, 1230 York avenue, New York, NY 10065, USA. friedj@mail.rockefeller.edu. [4]
- FULTON, S, WOODSIDE, B, & SHIZGAL, P. 2000. Modulation of brain reward circuitry by leptin. *Science (new york, ny)*, **287**(5450), 125–128. [14]
- FULTON, S, PISSIOS, P, MANCHON, R. P, STILES, L, FRANK, L, POTHOS, E. N, MARATOS-FLIER, E, & FLIER, J. S. 2006. Leptin regulation of the mesoaccumbens dopamine pathway. *Neuron*, **51**(6), 811–822. [13]

- GAINETDINOV, R. R, SOTNIKOVA, T. D, GREKHOVA, T. V, & RAYEVSKY, K. S. 1996. In vivo evidence for preferential role of dopamine D₃ receptor in the presynaptic regulation of dopamine release but not synthesis. *European journal of pharmacology*, **308**(3), 261–269. [14]
- GALICHET, C, LOVELL-BADGE, R, & RIZZOTI, K. 2010. Nestin-Cre mice are affected by hypopituitarism, which is not due to significant activity of the transgene in the pituitary gland. *Plos one*, **5**(7), e11443. [24]
- GAO, X, SHIN, Y, LI, M, WANG, F, TONG, Q, & ZHANG, P. 2010. The Fat Mass and Obesity Associated Gene FTO Functions in the Brain to Regulate Postnatal Growth in Mice. *Plos one*. [24, 101]
- GARCÍA-TORNADU, I, RISSO, G, PEREZ-MILLAN, M. I, NOAÍN, D, DIAZ-TORGA, G, LOW, M. J, RUBINSTEIN, M, & BECU-VILLALOBOS, D. 2010. Neurotransmitter modulation of the GHRH-GH axis. *Frontiers of hormone research*, **38**, 59–69. [34, 93, 98]
- GERKEN, T, GIRARD, C. A, TUNG, Y.-C. L, WEBBY, C. J, SAUDEK, V, HEWITSON, K. S, YEO, G. S. H, McDONOUGH, M. A, CUNLIFFE, S, McNEILL, L. A, GALVANOVSKIS, J, RORSMAN, P, ROBINS, P, PRIEUR, X, COLL, A. P, MA, M, JOVANOVIĆ, Z, FAROOQI, I. S, SEDGWICK, B, BARROSO, I, LINDAHL, T, PONTING, C. P, ASHCROFT, F. M, O'RAHILLY, S, & SCHOFIELD, C. J. 2007. The obesity-associated FTO gene encodes a 2-oxoglutarate-dependent nucleic acid demethylase. *Science (new york, ny)*, **318**(5855), 1469–1472. [23, 24, 26, 28, 29, 33, 53, 54, 81, 93, 101]
- GIRARD, D, & PETROVSKY, N. 2011. Alström syndrome: insights into the pathogenesis of metabolic disorders. *Nature reviews. endocrinology*, **7**(2), 77–88. [20]
- GIROS, B, JABER, M, JONES, S. R, WIGHTMAN, R. M, & CARON, M. G. 1996. Hyperlocomotion and indifference to cocaine and amphetamine in mice lacking the dopamine transporter. *Nature*, **379**(6566), 606–612. [103]
- GOOSSENS, G. H, PETERSEN, L, BLAAK, E. E, HUL, G, ARNER, P, ASTRUP, A, FROGUEL, P, PATEL, K, PEDERSEN, O, POLAK, J, OPPERT, J.-M, MARTINEZ, J. A, SØRENSEN, T. I. A, SARIS, W. H. M, & NUGENOB CONSORTIUM. 2009. Several obesity- and nutrient-related gene polymorphisms but not FTO and UCP variants modulate postabsorptive resting energy expenditure and fat-induced thermogenesis in obese individuals: the NUGENOB study. *International journal of obesity (2005)*, **33**(6), 669–679. [17]
- GRANT, S. F. A, LI, M, BRADFIELD, J. P, KIM, C. E, ANNAIAH, K, SANTA, E, GLESSNER, J. T, CASALUNOVO, T, FRACKELTON, E. C, OTIENO, F. G, SHANER, J. L, SMITH, R. M, IMIELINSKI, M, ECKERT, A. W, CHIAVACCI, R. M, BERKOWITZ, R. I, & HAKONARSON, H. 2008. Association analysis of the FTO gene with obesity in children of Caucasian and African ancestry reveals a common tagging SNP. *Plos one*, **3**(3), e1746. [15]
- GULATI, P, CHEUNG, M. K, ANTROBUS, R, CHURCH, C. D, HARDING, H. P, TUNG, Y.-C. L, RIMMINGTON, D, MA, M, RON, D, LEHNER, P. J, ASHCROFT, F. M, COX, R. D, COLL, A. P, O'RAHILLY, S, & YEO, G. S. H. 2013. Role for the obesity-related FTO gene in the cellular sensing of amino acids. *Proceedings of the national academy of sciences*, Jan. [27, 28, 102, 108]
- HAKANEN, M, RAITAKARI, O. T, LEHTIMÄKI, T, PELTONEN, N, PAHKALA, K, SILLANMÄKI, L, LAGSTRÖM, H, VIKARI, J, SIMELL, O, & RÖNNEMAA, T. 2009. FTO genotype is associated with body mass index after the age of seven years but not with energy intake or leisure-time physical activity. *The journal of clinical endocrinology and metabolism*, **94**(4), 1281–1287. [17]

- HAMDI, A, PORTER, J, & PRASAD, C. 1992. Decreased striatal D2 dopamine receptors in obese Zucker rats: changes during aging. *Brain research*, **589**(2), 338–340. [13]
- HAN, Z, NIU, T, CHANG, J, LEI, X, ZHAO, M, WANG, Q, CHENG, W, WANG, J, FENG, Y, & CHAI, J. 2010. Crystal structure of the FTO protein reveals basis for its substrate specificity. *Nature*, **464**(7292), 1205–1209. [28, 29]
- HARIGAYA, Y, TANAKA, H, YAMANAKA, S, TANAKA, K, WATANABE, Y, TSUTSUMI, C, CHIKASHIGE, Y, HIRAOKA, Y, YAMASHITA, A, & YAMAMOTO, M. 2006. Selective elimination of messenger RNA prevents an incidence of untimely meiosis. *Nature*, **442**(7098), 45–50. [31]
- HARPER, J. E, MICELI, S. M, ROBERTS, R. J, & MANLEY, J. L. 1990. Sequence specificity of the human mRNA N6-adenosine methylase in vitro. *Nucleic acids research*, **18**(19), 5735–5741. [31, 32]
- HARRIS, G. C, & ASTON-JONES, G. 2006. Arousal and reward: a dichotomy in orexin function. *Trends in neurosciences*, **29**(10), 571–577. [6]
- HAUPT, A, THAMER, C, STAIGER, H, TSCHRITTER, O, KIRCHHOFF, K, MACHICAO, F, HÄRING, H.-U, STEFAN, N, & FRITSCH, A. 2009. Variation in the FTO gene influences food intake but not energy expenditure. *Experimental and clinical endocrinology & diabetes : official journal, german society of endocrinology [and] german diabetes association*, **117**(4), 194–197. [17, 26, 109, 110]
- HETHERINGTON, A. W, & RANSON, S. W. 1940. Hypothalamic lesions and adiposity in the rat. *The anatomical record*, **78**(2), 149–172. [5]
- HEYDET, D, CHEN, L. X, LARTER, C. Z, INGLIS, C, SILVERMAN, M. A, FARRELL, G. C, & LEROUX, M. R. 2013. A truncating mutation of *Alms1* reduces the number of hypothalamic neuronal cilia in obese mice. *Developmental neurobiology*, **73**(1), 1–13. [20]
- HILDRETH, K. L, VAN PELT, R. E, & SCHWARTZ, R. S. 2012. Obesity, insulin resistance, and Alzheimer's disease. *Obesity*, **20**(8), 1549–1557. [1]
- HILL, K. G, ALVA, H, BLEDNOV, Y. A, & CUNNINGHAM, C. L. 2003. Reduced ethanol-induced conditioned taste aversion and conditioned place preference in *GIRK2* null mutant mice. *Psychopharmacology*, **169**(1), 108–114. [104]
- HO, A. J, STEIN, J. L, HUA, X, LEE, S, HIBAR, D. P, LEOW, A. D, DINOV, I. D, TOGA, A. W, SAYKIN, A. J, SHEN, L, FOROUD, T, PANKRATZ, N, HUENTELMAN, M. J, CRAIG, D. W, GERBER, J. D, ALLEN, A. N, CORNEVEAUX, J. J, STEPHAN, D. A, DECARLI, C. S, DECHAIRO, B. M, POTKIN, S. G, JACK, C. R, WEINER, M. W, RAJI, C. A, LOPEZ, O. L, BECKER, J. T, CARMICHAEL, O. T, THOMPSON, P. M, & THE ALZHEIMER'S DISEASE NEUROIMAGING INITIATIVE. 2010. A commonly carried allele of the obesity-related FTO gene is associated with reduced brain volume in the healthy elderly. *Proceedings of the national academy of sciences of the united states of america*, Apr. [19, 21]
- HOMMEL, J. D, TRINKO, R, SEARS, R. M, GEORGESCU, D, LIU, Z.-W, GAO, X.-B, THURMON, J. J, MARINELLI, M, & DiLEONE, R. J. 2006. Leptin receptor signaling in midbrain dopamine neurons regulates feeding. *Neuron*, **51**(6), 801–810. [13, 45]
- HONGAY, C. F, & ORR-WEAVER, T. L. 2011. *Drosophila* Inducer of MEiosis 4 (IME4) is required for Notch signaling during oogenesis. *Proceedings of the national academy of sciences*, **108**(36), 14855–14860. [32]

- HOROWITZ, S, HOROWITZ, A, NILSEN, T. W, MUNNS, T. W, & ROTTMAN, F. M. 1984. Mapping of N6-methyladenosine residues in bovine prolactin mRNA. *Proceedings of the national academy of sciences of the united states of america*, **81**(18), 5667–5671. [32]
- HUANG, W, PAYNE, T. J, MA, J. Z, & LI, M. D. 2008. A functional polymorphism, rs6280, in DRD₃ is significantly associated with nicotine dependence in European-American smokers. *American journal of medical genetics. part b, neuropsychiatric genetics : the official publication of the international society of psychiatric genetics*, **147B**(7), 1109–1115. [104]
- HYMAN, S. E, MALENKA, R. C, & NESTLER, E. J. 2006. Neural mechanisms of addiction: the role of reward-related learning and memory. *Annual review of neuroscience*, **29**(Jan.), 565–598. [9, 12, 93, 105, 106]
- IVERSEN, S. D, & IVERSEN, L. L. 2007. Dopamine: 50 years in perspective. *Trends in neurosciences*, **30**(5), 188–193. [7, 8, 11, 12]
- IWANAMI, Y, & BROWN, G. M. 1968. Methylated bases of ribosomal ribonucleic acid from HeLa cells. *Archives of biochemistry and biophysics*, **126**(1), 8–15. [31]
- JACOBSSON, J. A, SCHIÖTH, H. B, & FREDRIKSSON, R. 2012. The impact of intronic single nucleotide polymorphisms and ethnic diversity for studies on the obesity gene FTO. *Obesity reviews : an official journal of the international association for the study of obesity*, **13**(12), 1096–1109. [15, 20]
- JIA, G, YANG, C.-G, YANG, S, JIAN, X, YI, C, ZHOU, Z, & HE, C. 2008. Oxidative demethylation of 3-methylthymine and 3-methyluracil in single-stranded DNA and RNA by mouse and human FTO. *Febs letters*, **582**(23-24), 3313–3319. [29]
- JIA, G, FU, Y, ZHAO, X, DAI, Q, ZHENG, G, YANG, Y, YI, C, LINDAHL, T, PAN, T, YANG, Y.-G, & HE, C. 2011. N6-methyladenosine in nuclear RNA is a major substrate of the obesity-associated FTO. *Nature chemical biology*, **7**(12), 885–887. [26, 29, 31, 32, 33, 81, 100]
- JIA, G, FU, Y, & HE, C. 2012. Reversible RNA adenosine methylation in biological regulation. *Trends in genetics : Tig*, **29**(2), 108–115. [30, 31, 33]
- JOHNSON, P. M, & KENNY, P. J. 2010. Dopamine D₂ receptors in addiction-like reward dysfunction and compulsive eating in obese rats. *Nature neuroscience*, **13**(5), 635–641. [13, 99]
- JONSSON, A, & FRANKS, P. W. 2009. Obesity, FTO gene variant, and energy intake in children. *The new england journal of medicine*, **360**(15), 1571–2; author reply 1572. [17]
- JOSEPH, J. D, WANG, Y.-M, MILES, P. R, BUDYGIN, E. A, PICETTI, R, GAINETDINOV, R. R, CARON, M. G, & WIGHTMAN, R. M. 2002. Dopamine autoreceptor regulation of release and uptake in mouse brain slices in the absence of D(3) receptors. *Neuroscience*, **112**(1), 39–49. [14, 103]
- KAHN, C. R. 1994. Banting Lecture. Insulin action, diabetogenes, and the cause of type II diabetes. *Diabetes*, **43**(8), 1066–1084. [4]
- KANE, S. E, & BEEMON, K. 1985. Precise localization of m6A in Rous sarcoma virus RNA reveals clustering of methylation sites: implications for RNA processing. *Molecular and cellular biology*, **5**(9), 2298–2306. [31, 32]

- KARIKÓ, K, BUCKSTEIN, M, NI, H, & WEISSMAN, D. 2005. Suppression of RNA recognition by Toll-like receptors: the impact of nucleoside modification and the evolutionary origin of RNA. *Immunity*, **23**(2), 165–175. [31]
- KARRA, E, O'DALY, O. G, CHOUDHURY, A. I, YOUSSEIF, A, MILLERSHIP, S, NEARY, M. T, SCOTT, W. R, CHANDARANA, K, MANNING, S, HESS, M. E, IWAKURA, H, AKAMIZU, T, MILLET, Q, GELEGEN, C, DREW, M. E, RAHMAN, S, EMMANUEL, J. J, WILLIAMS, S. C. R, RÜTHER, U. U, BRÜNING, J. C, WITHERS, D. J, ZELAYA, F. O, & BATTERHAM, R. L. 2013. A link between FTO, ghrelin, and impaired brain food-cue responsivity. *The journal of clinical investigation*, **123**(8), 3539–3551. [17, 19, 23, 25, 108, 110]
- KATZMARZYK, P. T, JANSSEN, I, & ARDERN, C. I. 2003. Physical inactivity, excess adiposity and premature mortality. *Obesity reviews : an official journal of the international association for the study of obesity*, **4**(4), 257–290. [1]
- KAUER, J. A, & MALENKA, R. C. 2007. Synaptic plasticity and addiction. *Nature reviews neuroscience*, **8**(11), 844–858. [12, 105, 106, 107]
- KELLER, L, XU, W, WANG, H.-X, WINBLAD, B, FRATIGLIONI, L, & GRAFF, C. 2011. The obesity related gene, FTO, interacts with APOE, and is associated with Alzheimer's disease risk: a prospective cohort study. *Journal of alzheimer's disease : Jad*, **23**(3), 461–469. [17, 19]
- KELLEY, A. E, & BERRIDGE, K. C. 2002. The neuroscience of natural rewards: relevance to addictive drugs. *The journal of neuroscience : the official journal of the society for neuroscience*, **22**(9), 3306–3311. [11]
- KELLY, M. A, RUBINSTEIN, M, PHILLIPS, T. J, LESSOV, C. N, BURKHART-KASCH, S, ZHANG, G, BUNZOW, J. R, FANG, Y, GERHARDT, G. A, GRANDY, D. K, & LOW, M. J. 1998. Locomotor activity in D2 dopamine receptor-deficient mice is determined by gene dosage, genetic background, and developmental adaptations. *The journal of neuroscience : the official journal of the society for neuroscience*, **18**(9), 3470–3479. [34, 93, 98, 99]
- KENNY, P. J. 2011. Reward mechanisms in obesity: new insights and future directions. *Neuron*, **69**(4), 664–679. [11, 12]
- KILPELAEINEN, T. O, QI, L, BRAGE, S, SHARP, S. J, SONESTEDT, E, DEMERATH, E, AHMAD, T, MORA, S, KAAKINEN, M, SANDHOLT, C. H, HOLZAPFEL, C, AUTENRIETH, C. S, HYPPOENEN, E, CAUCHI, S, HE, M, KUTALIK, Z, KUMARI, M, STANCAKOVA, A, MEIDTNER, K, BALKAU, B, TAN, J. T, MANGINO, M, TIMPSON, N. J, SONG, Y, ZILLIKENS, M. C, JABLONSKI, K. A, GARCIA, M. E, JOHANSSON, S, BRAGG-GRESHAM, J. L, WU, Y, VAN VLIET-OSTAPTCHOUK, J. V, ONLAND-MORET, N. C, ZIMMERMANN, E, RIVERA, N. V, TANAKA, T, STRINGHAM, H. M, SILBERNAGEL, G, KANONI, S, FEITOSA, M. F, SNITKER, S, RUIZ, J. R, METTER, J, MARTINEZ LARRAD, M. T, ATALAY, M, HAKANEN, M, AMIN, N, CAVALCANTI-PROENCA, C, GRONTVED, A, HALLMANS, G, JANSSEN, J.-O, KUUSISTO, J, KAHONEN, M, LUTSEY, P. L, NOLAN, J. J, PALLA, L, PEDERSEN, O, PERUSSE, L, RENSTROM, F, SCOTT, R. A, SHUNGIN, D, SOVIO, U, TAMMELIN, T. H, RÖNNEMAA, T, LAKKA, T. A, UUSITUPA, M, SERRANO RIOS, M, FERRUCCI, L, BOUCHARD, C, MEIRHAEGHE, A, FU, M, WALKER, M, BORECKI, I. B, DEDOUSSIS, G. V, FRITSCHÉ, A, OHLSSON, C, BOEHNKE, M, BANDINELLI, S, VAN DUIJN, C. M, EBRAHIM, S, LAWLOR, D. A, GUDNASON, V, HARRIS, T. B, SORENSEN, T. I. A, MOHLKE, K. L, HOFMAN, A, UITTERLINDEN, A. G, TUOMILEHTO, J, LEHTIMÄKI, T, RAITAKARI, O, ISOMAA, B, NJOLSTAD, P. R, FLOREZ, J. C, LIU, S, NESS, A, SPECTOR, T. D, TAI, E. S, FROGUEL, P, BOEING, H, LAAKSO, M, MARMOT, M, BERGMANN,

- S, POWER, C, KHAW, K.-T, CHASMAN, D, RIDKER, P, HANSEN, T, MONDA, K. L, ILLIG, T, JARVELIN, M.-R, WAREHAM, N. J, HU, F. B, GROOP, L. C, ORHO-MELANDER, M, EKELUND, U, FRANKS, P. W, & LOOS, R. J. F. 2011. Physical Activity Attenuates the Influence of FTO Variants on Obesity Risk: A Meta-Analysis of 218,166 Adults and 19,268 Children. *Plos medicine*, **8**(11). [17]
- KILPELÄINEN, T. O, ZILLIKENS, M. C, STANCAKOVA, A, FINUCANE, F. M, RIED, J. S, LANGENBERG, C, ZHANG, W, BECKMANN, J. S, LUAN, J, VANDENPUT, L, STYRKARSDOTTIR, U, ZHOU, Y, SMITH, A. V, ZHAO, J. H, AMIN, N, VEDANTAM, S, SHIN, S.-Y, HARITUNIAN, T, FU, M, FEITOSA, M. F, KUMARI, M, HALLDORSSON, B. V, TIKKANEN, E, MANGINO, M, HAYWARD, C, SONG, C, ARNOLD, A. M, AULCHENKO, Y. S, OOSTRA, B. A, CAMPBELL, H, CUPPLES, L. A, DAVIS, K. E, DÖRING, A, EIRIKSDOTTIR, G, ESTRADA, K, FERNÁNDEZ-REAL, J. M, GARCIA, M, GIEGER, C, GLAZER, N. L, GUIDUCCI, C, HOFMAN, A, HUMPHRIES, S. E, ISOMAA, B, JACOBS, L. C, JULA, A, KARASIK, D, KARLSSON, M. K, KHAW, K.-T, KIM, L. J, KIVIMÄKI, M, KLOPP, N, KÜHNEL, B, KUUSISTO, J, LIU, Y, LJUNGGREN, O, LORENTZON, M, LUBEN, R. N, MCKNIGHT, B, MELLSTRÖM, D, MITCHELL, B. D, MOOSER, V, MORENO, J. M, MÄNNISTÖ, S, O'CONNELL, J. R, PASCOE, L, PELTONEN, L, PERAL, B, PEROLA, M, PSATY, B. M, SALOMAA, V, SAVAGE, D. B, SEMPLE, R. K, SKARIC-JURIC, T, SIGURDSSON, G, SONG, K. S, SPECTOR, T. D, SYVÄNEN, A.-C, TALMUD, P. J, THORLEIFSSON, G, THORSTEINSDOTTIR, U, UITTERLINDEN, A. G, VAN DUIJN, C. M, VIDAL-PUIG, A, WILD, S. H, WRIGHT, A. F, CLEGG, D. J, SCHADT, E, WILSON, J. F, RUDAN, I, RIPATTI, S, BORECKI, I. B, SHULDINER, A. R, INGELSSON, E, JANSSON, J.-O, KAPLAN, R. C, GUDNASON, V, HARRIS, T. B, GROOP, L, KIEL, D. P, RIVADENEIRA, F, WALKER, M, BARROSO, I, VOLLENWEIDER, P, WAEBER, G, CHAMBERS, J. C, KOONER, J. S, SORANZO, N, HIRSCHHORN, J. N, STEFANSSON, K, WICHMANN, H.-E, OHLSSON, C, O'RAHILLY, S, WAREHAM, N. J, SPELIOTES, E. K, FOX, C. S, LAAKSO, M, & LOOS, R. J. F. 2011. Genetic variation near IRS1 associates with reduced adiposity and an impaired metabolic profile. *Nature genetics*, **43**(8), 753–760. [3]
- KIM, K. S, YOON, Y. R, LEE, H. J, YOON, S, KIM, S.-Y, SHIN, S. W, AN, J. J, KIM, M.-S, CHOI, S.-Y, SUN, W, & BAIK, J.-H. 2010. Enhanced hypothalamic leptin signaling in mice lacking dopamine D2 receptors. *The journal of biological chemistry*, **285**(12), 8905–8917. [93, 98]
- KLEINRIDERS, A, KÖNNER, A. C, & BRÜNING, J. C. 2009. CNS-targets in control of energy and glucose homeostasis. *Current opinion in pharmacology*, **9**(6), 794–804. [5]
- KLINKER, F, HASAN, K, PAULUS, W, NITSCHKE, M. A, & LIEBETANZ, D. 2013. Pharmacological blockade and genetic absence of the dopamine D2 receptor specifically modulate voluntary locomotor activity in mice. *Behavioural brain research*, **242**(Apr.), 117–124. [93, 98]
- KLÖCKENER, T, HESS, S, BELGARDT, B. F, PAEGER, L, VERHAGEN, L. A. W, HUSCH, A, SOHN, J.-W, HAMPEL, B, DHILLON, H, ZIGMAN, J. M, LOWELL, B. B, WILLIAMS, K. W, ELMQUIST, J. K, HORVATH, T. L, KLOPPENBURG, P, & BRÜNING, J. C. 2011. High-fat feeding promotes obesity via insulin receptor/PI3K-dependent inhibition of SF-1 VMH neurons. *Nature neuroscience*, **14**(7), 911–918. [46]
- KLOETING, N, SCHLEINIZ, D, RUSCHKE, K, BERNDT, J, FASSHAUER, M, TOENJES, A, SCHOEN, M. R, KOVACS, P, STUMVOLL, M, & BLUEHER, M. 2008. Inverse relationship between obesity and FTO gene expression in visceral adipose tissue in humans. *Diabetologia*, **51**(4), 641–647. [23]
- KNIGHT, Z. A, TAN, K, BIRSOY, K, SCHMIDT, S, GARRISON, J. L, WYSOCKI, R. W, EMILIANO, A, EKSTRAND, M. I, & FRIEDMAN, J. M. 2012. Molecular profiling of activated neurons by phosphorylated ribosome capture. *Cell*, **151**(5), 1126–1137. [61]

- KOELTZOW, T. E, XU, M, COOPER, D. C, HU, X. T, TONEGAWA, S, WOLF, M. E, & WHITE, F. J. 1998. Alterations in dopamine release but not dopamine autoreceptor function in dopamine D₃ receptor mutant mice. *The journal of neuroscience : the official journal of the society for neuroscience*, **18**(6), 2231–2238. [103]
- KÖNNER, A. C, & BRÜNING, J. C. 2012. Selective insulin and leptin resistance in metabolic disorders. *Cell metabolism*, **16**(2), 144–152. [4, 5]
- KÖNNER, A. C, KLÖCKENER, T, & BRÜNING, J. C. 2009. Control of energy homeostasis by insulin and leptin: targeting the arcuate nucleus and beyond. *Physiology & behavior*, **97**(5), 632–638. [4, 5, 6, 13]
- KÖNNER, A. C, HESS, S, TOVAR, S, MESAROS, A, SÁNCHEZ-LASHERAS, C, EVERS, N, VERHAGEN, L. A. W, BRÖNNEKE, H. S, KLEINRIDDER, A, HAMPEL, B, KLOPPENBURG, P, & BRÜNING, J. C. 2011. Role for insulin signaling in catecholaminergic neurons in control of energy homeostasis. *Cell metabolism*, **13**(6), 720–728. [13]
- KOOB, G. F, & VOLKOW, N. D. 2010. Neurocircuitry of addiction. *Neuropsychopharmacology : official publication of the american college of neuropsychopharmacology*, **35**(1), 217–238. [60, 109]
- KREBS, M. O, SAUTEL, F, BOURDEL, M. C, SOKOLOFF, P, SCHWARTZ, J. C, OLIÉ, J. P, LÔO, H, & POIRIER, M. F. 1998. Dopamine D₃ receptor gene variants and substance abuse in schizophrenia. *Molecular psychiatry*, **3**(4), 337–341. [104]
- KRISHNAN, V, & NESTLER, E. J. 2008. The molecular neurobiology of depression. *Nature*, **455**(7215), 894–902. [75]
- KRUDE, H, BIEBERMANN, H, LUCK, W, HORN, R, BRABANT, G, & GRÜTERS, A. 1998. Severe early-onset obesity, adrenal insufficiency and red hair pigmentation caused by POMC mutations in humans. *Nature genetics*, **19**(2), 155–157. [2]
- KRUG, R. M, MORGAN, M. A, & SHATKIN, A. J. 1976. Influenza viral mRNA contains internal N⁶-methyladenosine and 5'-terminal 7-methylguanosine in cap structures. *Journal of virology*, **20**(1), 45–53. [31]
- KRÜGEL, U, SCHRAFT, T, KITNER, H, KIESS, W, & ILLES, P. 2003. Basal and feeding-evoked dopamine release in the rat nucleus accumbens is depressed by leptin. *European journal of pharmacology*, **482**(1-3), 185–187. [13]
- KUZHUKANDATHIL, E. V, YU, W, & OXFORD, G. S. 1998. Human dopamine D₃ and D_{2L} receptors couple to inward rectifier potassium channels in mammalian cell lines. *Molecular and cellular neurosciences*, **12**(6), 390–402. [14, 103]
- KYROZIS, A, & REICHLING, D. B. 1995. Perforated-patch recording with gramicidin avoids artifactual changes in intracellular chloride concentration. *Journal of neuroscience methods*, **57**(1), 27–35. [46]
- LACEY, M. G, MERCURI, N. B, & NORTH, R. A. 1987. Dopamine acts on D₂ receptors to increase potassium conductance in neurones of the rat substantia nigra zona compacta. *The journal of physiology*, **392**(Nov.), 397–416. [103]

- LACEY, M. G, MERCURI, N. B, & NORTH, R. A. 1988. On the potassium conductance increase activated by GABAB and dopamine D2 receptors in rat substantia nigra neurones. *The journal of physiology*, **401**(July), 437–453. [46]
- LACEY, M. G, MERCURI, N. B, & NORTH, R. A. 1989. Two cell types in rat substantia nigra zona compacta distinguished by membrane properties and the actions of dopamine and opioids. *The journal of neuroscience : the official journal of the society for neuroscience*, **9**(4), 1233–1241. [46]
- LAKHAN, S. E, CARO, M, & HADZIMICHALIS, N. 2013. NMDA Receptor Activity in Neuropsychiatric Disorders. *Frontiers in psychiatry*, **4**, 52. [106]
- LE FOLL, B, DIAZ, J, & SOKOLOFF, P. 2005. Neuroadaptations to hyperdopaminergia in dopamine D3 receptor-deficient mice. *Life sciences*, **76**(11), 1281–1296. [103]
- LEJEUNE, F, & MILLAN, M. J. 1995. Activation of dopamine D3 autoreceptors inhibits firing of ventral tegmental dopaminergic neurones in vivo. *European journal of pharmacology*, **275**(3), R7–9. [14]
- LENOIR, M, SERRE, F, CANTIN, L, & AHMED, S. H. 2007. Intense sweetness surpasses cocaine reward. *Plos one*, **2**(8), e698. [12]
- LEVIS, R, & PENMAN, S. 1978. 5'-terminal structures of poly(A)+ cytoplasmic messenger RNA and of poly(A)+ and poly(A)- heterogeneous nuclear RNA of cells of the dipteran *Drosophila melanogaster*. *Journal of molecular biology*, **120**(4), 487–515. [31]
- LIMOSIN, F, ROMO, L, BATEL, P, ADES, J, BONI, C, & GORWOOD, P. 2005. Association between dopamine receptor D3 gene Ball polymorphism and cognitive impulsiveness in alcohol-dependent men. *European psychiatry : the journal of the association of european psychiatrists*, **20**(3), 304–306. [104]
- LIU, G, ZHU, H, LAGOU, V, GUTIN, B, STALLMANN-JORGENSEN, I. S, TREIBER, F. A, DONG, Y, & SNIEDER, H. 2010. FTO variant rs9939609 is associated with body mass index and waist circumference, but not with energy intake or physical activity in European- and African-American youth. *Bmc medical genetics*, **11**, 57. [15]
- LIVAK, K. J, & SCHMITTGEN, T. D. 2001. Analysis of relative gene expression data using real-time quantitative PCR and the 2(-Delta Delta C(T)) Method. *Methods (san diego, calif.)*, **25**(4), 402–408. [39]
- LOOS, R. J. F. 2012. Genetic determinants of common obesity and their value in prediction. *Best practice & research. clinical endocrinology & metabolism*, **26**(2), 211–226. [3, 15, 16, 92]
- LOOS, R. J. F, LINDGREN, C. M, LI, S, WHEELER, E, ZHAO, J. H, PROKOPENKO, I, INOUE, M, FREATHY, R. M, ATTWOOD, A. P, BECKMANN, J. S, BERNDT, S. I, BERGMANN, S, BENNETT, A. J, BINGHAM, S. A, BOCHUD, M, BROWN, M, CAUCHI, S, CONNELL, J. M, COOPER, C, SMITH, G. D, DAY, I, DINA, C, DE, S, DERMITZAKIS, E. T, DONEY, A. S. F, ELLIOTT, K. S, ELLIOTT, P, EVANS, D. M, FAROOQI, I. S, FROGUEL, P, GHORI, J, GROVES, C. J, GWILLIAM, R, HADLEY, D, HALL, A. S, HATTERSLEY, A. T, HEBEBRAND, J, HEID, I. M, HERRERA, B, HINNEY, A, HUNT, S. E, JARVELIN, M.-R, JOHNSON, T, JOLLEY, J. D. M, KARPE, F, KENIRY, A, KHAW, K.-T, LUBEN, R. N, MANGINO, M, MARCHINI, J, McARDLE, W. L, MCGINNIS, R, MEYRE, D, MUNROE, P. B, MORRIS, A. D, NESS, A. R, NEVILLE, M. J, NICA, A. C, ONG, K. K, O'RAHILLY, S, OWEN, K. R, PALMER, C. N. A, PAPADAKIS, K, POTTER, S, POUTA, A, QI, L, RANDALL, J. C, RAYNER, N. W, RING, S. M, SANDHU, M. S, SCHERAG, A, SIMS, M. A, SONG, K, SORANZO, N, SPELIOTES, E. K, SYDDALL, H. E, TEICHMANN, S. A, TIMPSON, N. J, TOBIAS, J. H, UDA,

- M, VOGEL, C. I. G, WALLACE, C, WATERWORTH, D. M, WEEDON, M. N, WILLER, C. J, WRAIGHT, V. L, YUAN, X, ZEGGINI, E, HIRSCHHORN, J. N, STRACHAN, D. P, OUWEHAND, W. H, CAULFIELD, M. J, SAMANI, N. J, FRAYLING, T. M, VOLLENWEIDER, P, WAEBER, G, MOOSER, V, DELOUKAS, P, MCCARTHY, M. I, WAREHAM, N. J, BARROSO, I, OVARIAN, P. L. C, KORA, STUDY, N. H, INITIATIVE, D. G, STUDY, S, CONSOR, W. T. C. C, & FUSION. 2008. Common variants near MC4R are associated with fat mass, weight and risk of obesity. *Nature genetics*, **40**(6), 768–775. [3]
- LUPPINO, F. S, DE WIT, L. M, BOUVY, P. F, STIJNEN, T, CUIJPERS, P, PENNINX, B. W. J. H, & ZITMAN, F. G. 2010. Overweight, obesity, and depression: a systematic review and meta-analysis of longitudinal studies. *Archives of general psychiatry*, **67**(3), 220–229. [109]
- LÜSCHER, C, & SLESINGER, P. A. 2010. Emerging roles for G protein-gated inwardly rectifying potassium (GIRK) channels in health and disease. *Nature reviews neuroscience*, **11**(5), 301–315. [9, 63, 94, 104, 105]
- MA, M, HARDING, H. P, O'RAHILLY, S, RON, D, & YEO, G. S. H. 2012. Kinetic analysis of FTO (fat mass and obesity-associated) reveals that it is unlikely to function as a sensor for 2-oxoglutarate. *The biochemical journal*, **444**(2), 183–187. [29]
- MAES, H. H, NEALE, M. C, & EAVES, L. J. 1997. Genetic and environmental factors in relative body weight and human adiposity. *Behavior genetics*, **27**(4), 325–351. [2]
- MALIK, V. S, WILLETT, W. C, & HU, F. B. 2013. Global obesity: trends, risk factors and policy implications. *Nature reviews. endocrinology*, **9**(1), 13–27. [1]
- MARK, M. D, & HERLITZE, S. 2000. G-protein mediated gating of inward-rectifier K⁺ channels. *European journal of biochemistry / febs*, **267**(19), 5830–5836. [104]
- MATTINGLY, B. A, ROWLETT, J. K, & LOVELL, G. 1993. Effects of daily SKF 38393, quinpirole, and SCH 23390 treatments on locomotor activity and subsequent sensitivity to apomorphine. *Psychopharmacology*, **110**(3), 320–326. [66]
- McMURRAY, F, CHURCH, C. D, LARDER, R, NICHOLSON, G, WELLS, S, TEBOUL, L, TUNG, Y. C. L, RIMMINGTON, D, BOSCH, F, JIMENEZ, V, YEO, G. S. H, O'RAHILLY, S, ASHCROFT, F. M, COLL, A. P, & COX, R. D. 2013. Adult onset global loss of the fto gene alters body composition and metabolism in the mouse. *Plos genetics*, **9**(1), e1003166. [22, 25, 102, 107]
- McNAUGHT, K. S. P, & MINK, J. W. 2011. Advances in understanding and treatment of Tourette syndrome. *Nature reviews. neurology*, **7**(12), 667–676. [12]
- McTAGGART, J. S, LEE, S, IBERL, M, CHURCH, C, COX, R. D, & ASHCROFT, F. M. 2011. FTO Is Expressed in Neurons throughout the Brain and Its Expression Is Unaltered by Fasting. *Plos one*, **6**(11). [24, 26, 27, 33, 53, 54, 93]
- MERCURI, N. B, SAIARDI, A, BONCI, A, PICETTI, R, CALABRESI, P, BERNARDI, G, & BORRELLI, E. 1997. Loss of autoreceptor function in dopaminergic neurons from dopamine D2 receptor deficient mice. *Neuroscience*, **79**(2), 323–327. [14]
- MEYER, K. D, SALETORE, Y, ZUMBO, P, ELEMENTO, O, MASON, C. E, & JAFFREY, S. R. 2012. Comprehensive analysis of mRNA methylation reveals enrichment in 3' UTRs and near stop codons. *Cell*, **149**(7), 1635–1646. [29, 31, 33, 34, 49, 81, 100]

- MISSALE, C, NASH, S. R, ROBINSON, S. W, JABER, M, & CARON, M. G. 1998. Dopamine receptors: from structure to function. *Physiological reviews*, **78**(1), 189–225. [14]
- MONTAGUE, C. T, FAROOQI, I. S, WHITEHEAD, J. P, SOOS, M. A, RAU, H, WAREHAM, N. J, SEWTER, C. P, DIGBY, J. E, MOHAMMED, S. N, HURST, J. A, CHEETHAM, C. H, EARLEY, A. R, BARNETT, A. H, PRINS, J. B, & O'RAHILLY, S. 1997. Congenital leptin deficiency is associated with severe early-onset obesity in humans. *Nature*, **387**(6636), 903–908. [2]
- MORGAN, A. D, CARROLL, M. E, LOTH, A. K, STOFFEL, M, & WICKMAN, K. 2003. Decreased cocaine self-administration in Kir3 potassium channel subunit knockout mice. *Neuropsychopharmacology : official publication of the american college of neuropsychopharmacology*, **28**(5), 932–938. [104]
- MORGAN, D, GRANT, K. A, GAGE, H. D, MACH, R. H, KAPLAN, J. R, PRIOLEAU, O, NADER, S. H, BUCHHEIMER, N, EHRENKAUFER, R. L, & NADER, M. A. 2002. Social dominance in monkeys: dopamine D2 receptors and cocaine self-administration. *Nature neuroscience*, **5**(2), 169–174. [99]
- MYERS, M. G, COWLEY, M. A, & MÜNZBERG, H. 2008. Mechanisms of leptin action and leptin resistance. *Annual review of physiology*, **70**, 537–556. [4]
- NARAYAN, P, LUDWICZAK, R. L, GOODWIN, E. C, & ROTTMAN, F. M. 1994. Context effects on N6-adenosine methylation sites in prolactin mRNA. *Nucleic acids research*, **22**(3), 419–426. [32]
- NARITA, M, MIZUO, K, MIZOGUCHI, H, SAKATA, M, NARITA, M, TSENG, L. F, & SUZUKI, T. 2003. Molecular evidence for the functional role of dopamine D3 receptor in the morphine-induced rewarding effect and hyperlocomotion. *Journal of neuroscience*, **23**(3), 1006–1012. [103]
- NESTLER, E. 2001. Molecular basis of long-term plasticity underlying addiction. *Nature reviews neuroscience*, **2**(2), 119–128. [93]
- NESTLER, E. J, & CARLEZON, W. A. 2006. The mesolimbic dopamine reward circuit in depression. *Biological psychiatry*, **59**(12), 1151–1159. [75]
- NICHOLS, J. L. 1979. 'Cap' structures in maize poly(A)-containing RNA. *Biochimica et biophysica acta*, **563**(2), 490–495. [31]
- NIU, Y, ZHAO, X, WU, Y.-S, LI, M.-M, WANG, X.-J, & YANG, Y.-G. 2013. N6-methyl-adenosine (m6A) in RNA: an old modification with a novel epigenetic function. *Genomics, proteomics & bioinformatics*, **11**(1), 8–17. [31]
- OLSZEWSKI, P. K, FREDRIKSSON, R, OLSZEWSKA, A. M, STEPHANSSON, O, ALSIÖ, J, RADOMSKA, K. J, LEVINE, A. S, & SCHIÖTH, H. B. 2009. Hypothalamic FTO is associated with the regulation of energy intake not feeding reward. *Bmc neuroscience*, **10**, 129. [26]
- OLSZEWSKI, P. K, FREDRIKSSON, R, ERIKSSON, J. D, MITRA, A, RADOMSKA, K. J, GOSNELL, B. A, SOLVANG, M. N, LEVINE, A. S, & SCHIÖTH, H. B. 2011. FTO colocalizes with a satiety mediator oxytocin in the brain and upregulates oxytocin gene expression. *Biochemical and biophysical research communications*, Apr. [26]
- OVERTON, P. G, & CLARK, D. 1997. Burst firing in midbrain dopaminergic neurons. *Brain research brain research reviews*, **25**(3), 312–334. [11]

- PALADINI, C. A, ROBINSON, S, MORIKAWA, H, WILLIAMS, J. T, & PALMITER, R. D. 2003. Dopamine controls the firing pattern of dopamine neurons via a network feedback mechanism. *Proceedings of the national academy of sciences of the united states of america*, **100**(5), 2866–2871. [14]
- PALMITER, R. D. 2012. New game for hunger neurons. *Nature neuroscience*, **15**(8), 1060–1061. [6]
- PAN, T. 2013. N6-methyl-adenosine modification in messenger and long non-coding RNA. *Trends in biochemical sciences*, **38**(4), 204–209. [31, 33]
- PANDIT, R, DE JONG, J. W, VANDERSCHUREN, L. J. M. J, & ADAN, R. A. H. 2011. Neurobiology of overeating and obesity: the role of melanocortins and beyond. *European journal of pharmacology*, **660**(1), 28–42. [9, 11, 12]
- PAOLETTI, P, BELLONE, C, & ZHOU, Q. 2013. NMDA receptor subunit diversity: impact on receptor properties, synaptic plasticity and disease. *Nature reviews neuroscience*, **14**(6), 383–400. [106]
- PAQUET, M, TREMBLAY, M, SOGHOMONIAN, J. J, & SMITH, Y. 1997. AMPA and NMDA glutamate receptor subunits in midbrain dopaminergic neurons in the squirrel monkey: an immunohistochemical and in situ hybridization study. *The journal of neuroscience : the official journal of the society for neuroscience*, **17**(4), 1377–1396. [106]
- PATTERSON, T. A, BROTH, M. D, ZAVOSH, A, SCHENK, J. O, SZOT, P, & FIGLEWICZ, D. P. 1998. Food deprivation decreases mRNA and activity of the rat dopamine transporter. *Neuroendocrinology*, **68**(1), 11–20. [13]
- PETERS, T, AUSMEIER, K, & RÜTHER, U. 1999. Cloning of Fatso (Fto), a novel gene deleted by the Fused toes (Ft) mouse mutation. *Mammalian genome : official journal of the international mammalian genome society*, **10**(10), 983–986. [15]
- PINE, D. S, GOLDSTEIN, R. B, WOLK, S, & WEISSMAN, M. M. 2001. The association between childhood depression and adulthood body mass index. *Pediatrics*, **107**(5), 1049–1056. [18]
- PRAVETONI, M, & WICKMAN, K. 2008. Behavioral characterization of mice lacking GIRK/Kir3 channel subunits. *Genes, brain, and behavior*, **7**(5), 523–531. [104]
- RAE, J, COOPER, K, GATES, P, & WATSKY, M. 1991. Low access resistance perforated patch recordings using amphotericin B. *Journal of neuroscience methods*, **37**(1), 15–26. [46]
- RAFALSKA, I, ZHANG, Z, BENDERSKA, N, WOLFF, H, HARTMANN, A. M, BRACK-WERNER, R, & STAMM, S. 2004. The intranuclear localization and function of YT521-B is regulated by tyrosine phosphorylation. *Human molecular genetics*, **13**(15), 1535–1549. [31]
- RATEL, D, RAVANAT, J.-L, CHARLES, M.-P, PLATET, N, BREUILLAUD, L, LUNARDI, J, BERGER, F, & WION, D. 2006. Undetectable levels of N6-methyl adenine in mouse DNA: Cloning and analysis of PRED28, a gene coding for a putative mammalian DNA adenine methyltransferase. *Febs letters*, **580**(13), 3179–3184. [29, 32]
- RETZ, W, RÖSLER, M, SUPPRIAN, T, RETZ-JUNGINGER, P, & THOME, J. 2003. Dopamine D₃ receptor gene polymorphism and violent behavior: relation to impulsiveness and ADHD-related psychopathology. *Journal of neural transmission (vienna, austria : 1996)*, **110**(5), 561–572. [104]

- RICHARDS, C. D., SHIROYAMA, T., & KITAI, S. T. 1997. Electrophysiological and immunocytochemical characterization of GABA and dopamine neurons in the substantia nigra of the rat. *Neuroscience*, **80**(2), 545–557. [46]
- RINN, J. L., & CHANG, H. Y. 2012. Genome regulation by long noncoding RNAs. *Annual review of biochemistry*, **81**, 145–166. [30]
- RIVERA, M., COHEN-WOODS, S., KAPUR, K., BREEN, G., NG, M. Y., BUTLER, A. W., CRADDOCK, N., GILL, M., KORSZUN, A., MAIER, W., MORS, O., OWEN, M. J., PREISIG, M., BERGMANN, S., TOZZI, F., RICE, J., RIETSCHEL, M., RUCKER, J., SCHOSSER, A., AITCHISON, K. J., UHER, R., CRAIG, I. W., LEWIS, C. M., FARMER, A. E., & MCGUFFIN, P. 2012. Depressive disorder moderates the effect of the FTO gene on body mass index. *Molecular psychiatry*, **17**(6), 604–611. [18, 106, 109, 110]
- ROBBENS, S., ROUZÉ, P., COCK, J. M., SPRING, J., WORDEN, A. Z., & VAN DE PEER, Y. 2008. The FTO gene, implicated in human obesity, is found only in vertebrates and marine algae. *Journal of molecular evolution*, **66**(1), 80–84. [28]
- SAKURAI, T., AMEMIYA, A., ISHII, M., MATSUZAKI, I., CHEMELLI, R. M., TANAKA, H., WILLIAMS, S. C., RICHARDSON, J. A., KOZLOWSKI, G. P., WILSON, S., ARCH, J. R., BUCKINGHAM, R. E., HAYNES, A. C., CARR, S. A., ANNAN, R. S., McNULTY, D. E., LIU, W. S., TERRETT, J. A., ELSHOURBAGY, N. A., BERGSMA, D. J., & YANAGISAWA, M. 1998. Orexins and orexin receptors: a family of hypothalamic neuropeptides and G protein-coupled receptors that regulate feeding behavior. *Cell*, **92**(4), 573–585. [6]
- SALAMONE, J. D., MAHAN, K., & ROGERS, S. 1993. Ventrolateral striatal dopamine depletions impair feeding and food handling in rats. *Pharmacology, biochemistry, and behavior*, **44**(3), 605–610. [13]
- SALAMONE, J. D., & CORREA, M. 2002. Motivational views of reinforcement: implications for understanding the behavioral functions of nucleus accumbens dopamine. *Behavioural brain research*, **137**(1-2), 3–25. [12]
- SAMAAN, Z., ANAND, S., ZHANG, X., DESAI, D., RIVERA, M., PARE, G., THABANE, L., XIE, C., GERSTEIN, H., ENGERT, J. C., CRAIG, I., COHEN-WOODS, S., MOHAN, V., DIAZ, R., WANG, X., LIU, L., CORRE, T., PREISIG, M., KUTALIK, Z., BERGMANN, S., VOLLENWEIDER, P., WAEBER, G., YUSUF, S., & MEYRE, D. 2012. The protective effect of the obesity-associated rs9939609 A variant in fat mass- and obesity-associated gene on depression. *Molecular psychiatry*, Nov. [18, 106, 109, 110]
- SANCHEZ-PULIDO, L., & ANDRADE-NAVARRO, M. A. 2007. The FTO (fat mass and obesity associated) gene codes for a novel member of the non-heme dioxygenase superfamily. *Bmc biochemistry*, **8**, 23. [28]
- SANEYOSHI, M., HARADA, F., & NISHIMURA, S. 1969. Isolation and characterization of N⁶-methyladenosine from Escherichia coli valine transfer RNA. *Biochimica et biophysica acta*, **190**(2), 264–273. [31]
- SAPER, C. B., CHOU, T. C., & ELMQUIST, J. K. 2002. The need to feed: homeostatic and hedonic control of eating. *Neuron*, **36**(2), 199–211. [6, 111]
- SCHULTZ, W. 1998. Predictive reward signal of dopamine neurons. *Journal of neurophysiology*, **80**(1), 1–27. [7, 11]

- SCHULTZ, W. 2007. Behavioral dopamine signals. *Trends in neurosciences*, **30**(5), 203–210. [11]
- SCHULTZ, W. 2010. Dopamine signals for reward value and risk: basic and recent data. *Behavioral and brain functions : Bbf*, **6**(1), 24. [11]
- SCHWARTZ, M. W, WOODS, S. C, PORTE, D, SEELEY, R. J, & BASKIN, D. G. 2000. Central nervous system control of food intake. *Nature*, **404**(6778), 661–671. [4, 5]
- SCHWARTZ, M. W, & PORTE, D. 2005. Diabetes, obesity, and the brain. *Science (new york, ny)*, **307**(5708), 375–379. [4]
- SCHWARTZ, M. W, WOODS, S. C, SEELEY, R. J, BARSH, G. S, BASKIN, D. G, & LEIBEL, R. L. 2003. Is the energy homeostasis system inherently biased toward weight gain? *Diabetes*, **52**(2), 232–238. [12]
- SCUTERI, A, SANNA, S, CHEN, W.-M, UDA, M, ALBAI, G, STRAIT, J, NAJJAR, S, NAGARAJA, R, ORRÚ, M, USALA, G, DEI, M, LAI, S, MASCHIO, A, BUSONERO, F, MULAS, A, EHRET, G. B, FINK, A. A, WEDER, A. B, COOPER, R. S, GALAN, P, CHAKRAVARTI, A, SCHLESSINGER, D, CAO, A, LAKATTA, E, & ABECASIS, G. R. 2007. Genome-wide association scan shows genetic variants in the FTO gene are associated with obesity-related traits. *Plos genetics*, **3**(7), e115. [15, 16, 34, 92, 93]
- SEALE, T. W, & CARNEY, J. M. 1991. Genetic determinants of susceptibility to the rewarding and other behavioral actions of cocaine. *Journal of addictive diseases*, **10**(1-2), 141–162. [60]
- SHARE, R, SARHAN, M, & DILEONE, R. J. 2010. Role of orexin/hypocretin in dependence and addiction. *Brain research*, **1314**(Feb.), 130–138. [6]
- SHARP, P. A. 2009. The centrality of RNA. *Cell*, **136**(4), 577–580. [29, 30]
- SHATKIN, A. J. 1976. Capping of eucaryotic mRNAs. *Cell*, **9**(4 PT 2), 645–653. [31]
- SIBLEY, D. R. 1999. New insights into dopaminergic receptor function using antisense and genetically altered animals. *Annual review of pharmacology and toxicology*, **39**, 313–341. [14, 34, 93, 98]
- SIMERLY, R. 2006. Feeding signals and drugs meet in the midbrain. *Nature medicine*, **12**(11), 1244–1246. [6, 111]
- SIMON, G. E, VON KORFF, M, SAUNDERS, K, MIGLIORETTI, D. L, CRANE, P. K, VAN BELLE, G, & KESSLER, R. C. 2006. Association between obesity and psychiatric disorders in the US adult population. *Archives of general psychiatry*, **63**(7), 824–830. [13]
- SMALL, D. M, JONES-GOTMAN, M, & DAGHER, A. 2003. Feeding-induced dopamine release in dorsal striatum correlates with meal pleasantness ratings in healthy human volunteers. *Neuroimage*, **19**(4), 1709–1715. [13]
- SOBCZYK-KOPCIOL, A, BRODA, G, WOJNAR, M, KURJATA, P, JAKUBCZYK, A, KLIMKIEWICZ, A, & PŁOSKI, R. 2011. Inverse association of the obesity predisposing FTO rs9939609 genotype with alcohol consumption and risk for alcohol dependence. *Addiction (abingdon, england)*, **106**(4), 739–748. [18, 109, 110]
- SONENBERG, N, & HINNEBUSCH, A. G. 2009. Regulation of translation initiation in eukaryotes: mechanisms and biological targets. *Cell*, **136**(4), 731–745. [30]

- SOVIO, U, MOOK-KANAMORI, D. O, WARRINGTON, N. M, LAWRENCE, R, BRIOLLAIS, L, PALMER, C. N. A, CECIL, J, SANDLING, J. K, SYVÄNEN, A.-C, KAAKINEN, M, BEILIN, L. J, MILLWOOD, I. Y, BENNETT, A. J, LAITINEN, J, POUTA, A, MOLITOR, J, DAVEY SMITH, G, BEN-SHLOMO, Y, JADDOE, V. W. V, PALMER, L. J, PENNELL, C. E, COLE, T. J, MCCARTHY, M. I, JARVELIN, M.-R, TIMPSON, N. J, & EARLY GROWTH GENETICS CONSORTIUM. 2011. Association between common variation at the FTO locus and changes in body mass index from infancy to late childhood: the complex nature of genetic association through growth and development. *Plos genetics*, 7(2), e1001307. [16]
- SPEAKMAN, J. R, RANCE, K. A, & JOHNSTONE, A. M. 2008. Polymorphisms of the FTO Gene Are Associated With Variation in Energy Intake, but not Energy Expenditure. *Obesity*, 16(8), 1961–1965. [17, 26, 109, 110]
- SPELIOTES, E. K, WILLER, C. J, BERNDT, S. I, MONDA, K. L, THORLEIFSSON, G, JACKSON, A. U, LANGO ALLEN, H, LINDGREN, C. M, LUAN, J, MÄGLI, R, RANDALL, J. C, VEDANTAM, S, WINKLER, T. W, QI, L, WORKALEMAHU, T, HEID, I. M, STEINTHORSDDOTTIR, V, STRINGHAM, H. M, WEEDON, M. N, WHEELER, E, WOOD, A. R, FERREIRA, T, WEYANT, R. J, SEGRÈ, A. V, ESTRADA, K, LIANG, L, NEMESH, J, PARK, J.-H, GUSTAFSSON, S, KILPELÄINEN, T. O, YANG, J, BOUATIA-NAJI, N, ESKO, T, FEITOSA, M. F, KUTALIK, Z, MANGINO, M, RAYCHAUDHURI, S, SCHERAG, A, SMITH, A. V, WELCH, R, ZHAO, J. H, ABEN, K. K, ABSHER, D. M, AMIN, N, DIXON, A. L, FISHER, E, GLAZER, N. L, GODDARD, M. E, HEARD-COSTA, N. L, HOESEL, V, HOTTENGA, J.-J, JOHANSSON, A, JOHNSON, T, KETKAR, S, LAMINA, C, LI, S, MOFFATT, M. F, MYERS, R. H, NARISU, N, PERRY, J. R. B, PETERS, M. J, PREUSS, M, RIPATTI, S, RIVADENEIRA, F, SANDHOLT, C, SCOTT, L. J, TIMPSON, N. J, TYRER, J. P, VAN WINGERDEN, S, WATANABE, R. M, WHITE, C. C, WIKLUND, F, BARLASSINA, C, CHASMAN, D. I, COOPER, M. N, JANSSON, J.-O, LAWRENCE, R. W, PELLIKKA, N, PROKOPENKO, I, SHI, J, THIERING, E, ALAVERE, H, ALIBRANDI, M. T. S, ALMGREN, P, ARNOLD, A. M, ASPELUND, T, ATWOOD, L. D, BALKAU, B, BALMFORTH, A. J, BENNETT, A. J, BEN-SHLOMO, Y, BERGMAN, R. N, BERGMANN, S, BIEBERMANN, H, BLAKEMORE, A. I. F, BOES, T, BONNYCASTLE, L. L, BORNSTEIN, S. R, BROWN, M. J, BUCHANAN, T. A, BUSONERO, F, CAMPBELL, H, CAPPUCIO, F. P, CAVALCANTI-PROENCA, C, CHEN, Y.-D. I, CHEN, C.-M, CHINES, P. S, CLARKE, R, COIN, L, CONNELL, J, DAY, I. N. M, DEN HEIJER, M, DUAN, J, EBRAHIM, S, ELLIOTT, P, ELOSUA, R, EIRIKSDOTTIR, G, ERDOS, M. R, ERIKSSON, J. G, FACHERIS, M. F, FELIX, S. B, FISCHER-POSOVSZKY, P, FOLSOM, A. R, FRIEDRICH, N, FREIMER, N. B, FU, M, GAGET, S, GEJMAN, P. V, GEUS, E. J. C, GIEGER, C, GJESING, A. P, GOEL, A, GOYETTE, P, GRALLERT, H, GRÄSSLER, J, GREENAWALT, D. M, GROVES, C. J, GUDNASON, V, GUIDUCCI, C, HARTIKAINEN, A.-L, HASSANALI, N, HALL, A. S, HAVULINNA, A. S, HAYWARD, C, HEATH, A. C, HENGSTENBERG, C, HICKS, A. A, HINNEY, A, HOFMAN, A, HOMUTH, G, HUI, J, IGL, W, IRIBARREN, C, ISOMAA, B, JACOBS, K. B, JARICK, I, JEWELL, E, JOHN, U, JØRGENSEN, T, JOUSILAHTI, P, JULA, A, KAAKINEN, M, KAJANTIE, E, KAPLAN, L. M, KATHIRESAN, S, KETTUNEN, J, KINNUNEN, L, KNOWLES, J. W, KOLCIC, I, KÖNIG, I. R, KOSKINEN, S, KOVACS, P, KUUSISTO, J, KRAFT, P, KVALØY, K, LAITINEN, J, LANTIERI, O, LANZANI, C, LAUNER, L. J, LECOEUR, C, LEHTIMÄKI, T, LETTRE, G, LIU, J, LOKKI, M.-L, LORENTZON, M, LUBEN, R. N, LUDWIG, B, MAGIC, MANUNTA, P, MAREK, D, MARRE, M, MARTIN, N. G, MCARDLE, W. L, MCCARTHY, A, MCKNIGHT, B, MEITINGER, T, MELANDER, O, MEYRE, D, MIDTHJELL, K, MONTGOMERY, G. W, MORKEN, M. A, MORRIS, A. P, MULIC, R, NGWA, J. S, NELIS, M, NEVILLE, M. J, NYHOLT, D. R, O'DONNELL, C. J, O'RAHILLY, S, ONG, K. K, OOSTRA, B, PARÉ, G, PARKER, A. N, PEROLA, M, PICHLER, I, PIETILÄINEN, K. H, PLATOU, C. G. P, POLASEK, O, POUTA, A, RAFELT, S, RAITAKARI, O, RAYNER, N. W, RIDDERSTRÅLE, M, RIEF, W, RUOKONEN, A, ROBERTSON, N. R, & RZEHA, . 2010. Association analyses of 249,796 individuals reveal 18 new loci associated with body mass index. *Nature genetics*, 42(11), 937–948. [3]

- STERNSON, S. M. 2013. Hypothalamic survival circuits: blueprints for purposive behaviors. *Neuron*, **77**(5), 810–824. [6]
- STICE, E, SPOOR, S, BOHON, C, & SMALL, D. M. 2008. Relation between obesity and blunted striatal response to food is moderated by TaqIA A1 allele. *Science (new york, ny)*, **322**(5900), 449–452. [99]
- STRATIGOPOULOS, G, PADILLA, S. L, LEDUC, C. A, WATSON, E, HATTERSLEY, A. T, MCCARTHY, M. I, ZELTSER, L. M, CHUNG, W. K, & LEIBEL, R. L. 2008. Regulation of Fto/Ftm gene expression in mice and humans. *American journal of physiology. regulatory, integrative and comparative physiology*, **294**(4), R1185–96. [20, 23, 26]
- STRATIGOPOULOS, G, LEDUC, C. A, CREMONA, M. L, CHUNG, W. K, & LEIBEL, R. L. 2011. Cut-like homeobox 1 (CUX1) regulates expression of the fat mass and obesity-associated and retinitis pigmentosa GTPase regulator-interacting protein-1-like (RPGRI1L) genes and coordinates leptin receptor signaling. *The journal of biological chemistry*, **286**(3), 2155–2170. [20, 27]
- STREKALOVA, T, SPANAGEL, R, BARTSCH, D, HENN, F. A, & GASS, P. 2004. Stress-induced anhedonia in mice is associated with deficits in forced swimming and exploration. *Neuropsychopharmacology : official publication of the american college of neuropsychopharmacology*, **29**(11), 2007–2017. [75]
- SULZER, D. 2007. Multiple hit hypotheses for dopamine neuron loss in Parkinson's disease. *Trends in neurosciences*, **30**(5), 7–7. [8]
- SWANSON, J. M, KINSBOURNE, M, NIGG, J, LANPHEAR, B, STEFANATOS, G. A, VOLKOW, N, TAYLOR, E, CASEY, B. J, CASTELLANOS, F. X, & WADHWA, P. D. 2007. Etiologic subtypes of attention-deficit/hyperactivity disorder: brain imaging, molecular genetic and environmental factors and the dopamine hypothesis. *Neuropsychology review*, **17**(1), 39–59. [12, 109]
- SWINBURN, B. A, SACKS, G, HALL, K. D, MCPHERSON, K, FINEGOOD, D. T, MOODIE, M. L, & GORTMAKER, S. L. 2011. The global obesity pandemic: shaped by global drivers and local environments. *Lancet*, **378**(9793), 804–814. [2, 92]
- TAKIGAWA, T, & ALZHEIMER, C. 1999. G protein-activated inwardly rectifying K⁺ (GIRK) currents in dendrites of rat neocortical pyramidal cells. *The journal of physiology*, **517** (Pt 2)(June), 385–390. [46]
- TAN, J. T, DORAJOO, R, SEIELSTAD, M, SIM, X. L, ONG, R. T-H, CHIA, K. S, WONG, T. Y, SAW, S. M, CHEW, S. K, AUNG, T, & TAI, E. S. 2008. FTO variants are associated with obesity in the Chinese and Malay populations in Singapore. *Diabetes*, **57**(10), 2851–2857. [15]
- TANOFKY-KRAFF, M, HAN, J. C, ANANDALINGAM, K, SHOMAKER, L. B, COLUMBO, K. M, WOLKOFF, L. E, KOZLOSKY, M, ELLIOTT, C, RANZENHOFER, L. M, ROZA, C. A, YANOVSKI, S. Z, & YANOVSKI, J. A. 2009. The FTO gene rs9939609 obesity-risk allele and loss of control over eating. *The american journal of clinical nutrition*, **90**(6), 1483–1488. [17, 26]
- TEWS, D, FISCHER-POSOVSZKY, P, & WABITSCH, M. 2011. Regulation of FTO and FTM expression during human preadipocyte differentiation. *Hormone and metabolic research = hormon- und stoffwechselforschung = hormones et métabolisme*, **43**(1), 17–21. [23]
- TEWS, D, FISCHER-POSOVSZKY, P, & FROMME, T. 2013. FTO deficiency induces UCP-1 expression and mitochondrial uncoupling in adipocytes. *Endocrinology*. [24]

- THANOS, P. K, VOLKOW, N. D, FREIMUTH, P, UMEGAKI, H, IKARI, H, ROTH, G, INGRAM, D. K, & HITZEMANN, R. 2001. Overexpression of dopamine D2 receptors reduces alcohol self-administration. *Journal of neurochemistry*, **78**(5), 1094–1103. [99]
- THORLEIFSSON, G, WALTERS, G. B, GUDBJARTSSON, D. F, STEINTHORSDOTTIR, V, SULEM, P, HELGADOTTIR, A, STYRKARSDOTTIR, U, GRETARSDOTTIR, S, THORLACIUS, S, JONSDOTTIR, I, JONSDOTTIR, T, OLAFSDOTTIR, E. J, OLAFSDOTTIR, G. H, JONSSON, T, JONSSON, F, BORCH-JOHNSEN, K, HANSEN, T, ANDERSEN, G, JØRGENSEN, T, LAURITZEN, T, ABEN, K. K, VERBEEK, A. L. M, ROELEVELD, N, KAMPMAN, E, YANEK, L. R, BECKER, L. C, TRYGGVADOTTIR, L, RAFNAR, T, BECKER, D. M, GULCHER, J, KIEMENEY, L. A, PEDERSEN, O, KONG, A, THORSTEINSDOTTIR, U, & STEFANSSON, K. 2009. Genome-wide association yields new sequence variants at seven loci that associate with measures of obesity. *Nature genetics*, **41**(1), 18–24. [3]
- TIMPSON, N. J, EMMETT, P. M, FRAYLING, T. M, ROGERS, I, HATTERSLEY, A. T, MCCARTHY, M. I, & SMITH, G. D. 2008. The fat mass- and obesity-associated locus and dietary intake in children. *The american journal of clinical nutrition*, **88**(4), 971–978. [17, 26, 109, 110]
- TREWICK, S. C, HENSHAW, T. F, HAUSINGER, R. P, LINDAHL, T, & SEDGWICK, B. 2002. Oxidative demethylation by *Escherichia coli* AlkB directly reverts DNA base damage. *Nature*, **419**(6903), 174–178. [29]
- TSIEN, J. Z, HUERTA, P. T, & TONEGAWA, S. 1996. The essential role of hippocampal CA1 NMDA receptor-dependent synaptic plasticity in spatial memory. *Cell*, **87**(7), 1327–1338. [106]
- TSUNEMATSU, T, KILDUFF, T. S, BOYDEN, E. S, TAKAHASHI, S, TOMINAGA, M, & YAMANAKA, A. 2011. Acute Optogenetic Silencing of Orexin/Hypocretin Neurons Induces Slow-Wave Sleep in Mice. *The journal of neuroscience : the official journal of the society for neuroscience*, **31**(29), 10529–10539. [6]
- TUCK, M. T, WIEHL, P. E, & PAN, T. 1999. Inhibition of 6-methyladenine formation decreases the translation efficiency of dihydrofolate reductase transcripts. *The international journal of biochemistry & cell biology*, **31**(8), 837–851. [31]
- TUNG, Y.-C. L, AYUSO, E, SHAN, X, BOSCH, F, O'RAHILLY, S, COLL, A. P, & YEO, G. S. H. 2010. Hypothalamic-Specific Manipulation of Fto, the Ortholog of the Human Obesity Gene FTO, Affects Food Intake in Rats. *Plos one*, **5**(1), e8771. [24, 25, 26, 27]
- UCHIDA, A, ZIGMAN, J. M, & PERELLÓ, M. 2013. Ghrelin and eating behavior: evidence and insights from genetically-modified mouse models. *Frontiers in neuroscience*, **7**, 121. [25]
- UNGLESS, M. A, WHISTLER, J. L, MALENKA, R. C, & BONCI, A. 2001. Single cocaine exposure in vivo induces long-term potentiation in dopamine neurons. *Nature*, **411**(6837), 583–587. [46]
- VAN DEN BERG, L, DE WAAL, H. D.-v, HAN, J. C, YLSTRA, B, EIJK, P, NESTEROVA, M, HEUTINK, P, & STRATAKIS, C. A. 2010. Investigation of a patient with a partial trisomy 16q including the fat mass and obesity associated gene (FTO): fine mapping and FTO gene expression study. *American journal of medical genetics. part a*, **152A**(3), 630–637. [21]
- VAN DER HOEVEN, F, SCHIMMANG, T, VOLKMANN, A, MATTEI, M. G, KYEWSKI, B, & RÜTHER, U. 1994. Programmed cell death is affected in the novel mouse mutant Fused toes (Ft). *Development (cambridge, england)*, **120**(9), 2601–2607. [15]

- VELDERS, F. P, DE WIT, J. E, JANSEN, P. W, JADDOE, V. W. V, HOFMAN, A, VERHULST, F. C, & TIEMEIER, H. 2012. FTO at rs9939609, food responsiveness, emotional control and symptoms of ADHD in preschool children. *Plos one*, **7**(11), e49131. [17, 18, 104, 106, 109, 110]
- VIERKOTTEN, J, DILDROP, R, PETERS, T, WANG, B, & RÜTHER, U. 2007. Ftm is a novel basal body protein of cilia involved in Shh signalling. *Development (cambridge, england)*, **134**(14), 2569–2577. [20]
- VIMALESWARAN, K. S, LI, S, ZHAO, J. H, LUAN, J, BINGHAM, S. A, KHAW, K.-T, EKELUND, U, WAREHAM, N. J, & LOOS, R. J. F. 2009. Physical activity attenuates the body mass index-increasing influence of genetic variation in the FTO gene. *The american journal of clinical nutrition*, **90**(2), 425–428. [17]
- VOLKOW, N. D, WANG, G. J, FOWLER, J. S, LOGAN, J, GATLEY, S. J, GIFFORD, A, HITZEMANN, R, DING, Y. S, & PAPPAS, N. 1999. Prediction of reinforcing responses to psychostimulants in humans by brain dopamine D2 receptor levels. *The american journal of psychiatry*, **156**(9), 1440–1443. [99]
- VOLKOW, N. D, FOWLER, J. S, & WANG, G. J. 2002. Role of dopamine in drug reinforcement and addiction in humans: results from imaging studies. *Behavioural pharmacology*, **13**(5-6), 355–366. [13]
- VOLKOW, N. D, FOWLER, J. S, WANG, G. J, BALER, R, & TELANG, F. 2009. Imaging dopamine's role in drug abuse and addiction. *Neuropharmacology*, **56 Suppl 1**, 3–8. [99, 100]
- VOLKOW, N. D, WANG, G. J, TOMASI, D, & BALER, R. D. 2013. Obesity and addiction: neurobiological overlaps. *Obesity reviews : an official journal of the international association for the study of obesity*, **14**(1), 2–18. [9, 11, 12, 14, 34, 72, 93, 97, 99, 105]
- VOLKOW, N. D, WANG, G.-J, FOWLER, J. S, & TELANG, F. 2008. Overlapping neuronal circuits in addiction and obesity: evidence of systems pathology. *Philosophical transactions of the royal society of london series b, biological sciences*, **363**(1507), 3191–3200. [14]
- VUJOVIC, P, STAMENKOVIC, S, JASNIC, N, LAKIC, I, DJURASEVIC, S. F, CVIJIC, G, & DJORDJEVIC, J. 2013. Fasting induced cytoplasmic Fto expression in some neurons of rat hypothalamus. *Plos one*, **8**(5), e63694. [26]
- WÅHLÉN, K, SJÖLIN, E, & HOFFSTEDT, J. 2008. The common rs9939609 gene variant of the fat mass- and obesity-associated gene FTO is related to fat cell lipolysis. *Journal of lipid research*, **49**(3), 607–611. [24]
- WANG, G. J, VOLKOW, N. D, LOGAN, J, PAPPAS, N. R, WONG, C. T, ZHU, W, NETUSIL, N, & FOWLER, J. S. 2001. Brain dopamine and obesity. *Lancet*, **357**(9253), 354–357. [13, 34, 93, 97, 99, 100]
- WANG, L. P, LI, F, SHEN, X, & TSIEN, J. Z. 2010. Conditional knockout of NMDA receptors in dopamine neurons prevents nicotine-conditioned place preference. *Plos one*, **5**(1), e8616. [106]
- WANG, P, YANG, F.-J, DU, H, GUAN, Y.-F, XU, T.-Y, XU, X.-W, SU, D.-F, & MIAO, C.-Y. 2011. Involvement of leptin receptor long isoform (LepRb)-STAT3 signaling pathway in brain fat mass- and obesity-associated (FTO) downregulation during energy restriction. *Molecular medicine (cambridge, mass.)*, **17**(5-6), 523–532. [26, 27]

- WANG, X, LU, Z, GOMEZ, A, HON, G. C, YUE, Y, HAN, D, FU, Y, PARISIEN, M, DAI, Q, JIA, G, REN, B, PAN, T, & HE, C. 2013. N(6)-methyladenosine-dependent regulation of messenger RNA stability. *Nature*, Nov. [31, 33, 100, 102, 110]
- WARDLE, J, LLEWELLYN, C, SANDERSON, S, & PLOMIN, R. 2009. The FTO gene and measured food intake in children. *International journal of obesity (2005)*, **33**(1), 42–45. [17, 26, 109, 110]
- WARDLE, J, CARNELL, S, HAWORTH, C. M. A, FAROOQI, I. S, O'RAHILLY, S, & PLOMIN, R. 2008. Obesity associated genetic variation in FTO is associated with diminished satiety. *The journal of clinical endocrinology and metabolism*, **93**(9), 3640–3643. [17, 109]
- WARING, M. E, WARING, M. E, LAPANE, K. L, & LAPANE, K. L. 2008. Overweight in children and adolescents in relation to attention-deficit/hyperactivity disorder: results from a national sample. *Pediatrics*, **122**(1), e1–6. [18]
- WEI, C. M, GERSHOWITZ, A, & MOSS, B. 1975. Methylated nucleotides block 5' terminus of HeLa cell messenger RNA. *Cell*, **4**(4), 379–386. [31]
- WELTER, M, VALLONE, D, SAMAD, T. A, MEZIANE, H, USIELLO, A, & BORRELLI, E. 2007. Absence of dopamine D2 receptors unmasks an inhibitory control over the brain circuitries activated by cocaine. *Proceedings of the national academy of sciences of the united states of america*, **104**(16), 6840–6845. [98, 99]
- WILLER, C. J, SPELIOTES, E. K, LOOS, R. J. F, LI, S, LINDGREN, C. M, HEID, I. M, BERNDT, S. I, ELLIOTT, A. L, JACKSON, A. U, LAMINA, C, LETTRE, G, LIM, N, LYON, H. N, MCCARROLL, S. A, PAPADAKIS, K, QI, L, RANDALL, J. C, ROCCASECCA, R. M, SANNA, S, SCHEET, P, WEEDON, M. N, WHEELER, E, ZHAO, J. H, JACOBS, L. C, PROKOPENKO, I, SORANZO, N, TANAKA, T, TIMPSON, N. J, ALMGREN, P, BENNETT, A, BERGMAN, R. N, BINGHAM, S. A, BONNYCASTLE, L. L, BROWN, M, BURTT, NOEL L. P, CHINES, P, COIN, L, COLLINS, F. S, CONNELL, J. M, COOPER, C, SMITH, G. D, DENNISON, E. M, DEODHAR, P, ELLIOTT, P, ERDOS, M. R, ESTRADA, K, EVANS, D. M, GIANNINY, L, GIEGER, C, GILLSON, C. J, GUIDUCCI, C, HACKETT, R, HADLEY, D, HALL, A. S, HAVULINNA, A. S, HEBEBRAND, J, HOFMAN, A, ISOMAA, B, JACOBS, K. B, JOHNSON, T, JOUSILAHTI, P, JOVANOVIC, Z, KHAW, K.-T, KRAFT, P, KUOKKANEN, M, KUUSISTO, J, LAITINEN, J, LAKATTA, E. G, LUAN, J, LUBEN, R. N, MANGINO, M, MCARDLE, W. L, MEITINGER, T, MULAS, A, MUNROE, P. B, NARISU, N, NESS, A. R, NORTHSTONE, K, O'RAHILLY, S, PURMANN, C, REES, M. G, RIDDERSTRÅLE, M, RING, S. M, RIVADENEIRA, F, RUOKONEN, A, SANDHU, M. S, SARAMIES, J, SCOTT, L. J, SCUTERI, A, SILANDER, K, SIMS, M. A, SONG, K, STEPHENS, J, STEVENS, S, STRINGHAM, H. M, TUNG, Y. C. L, VALLE, T. T, VAN DUJN, C. M, VI-MALESWARAN, K. S, VOLLENWEIDER, P, WAEBER, G, WALLACE, C, WATANABE, R. M, WATERWORTH, D. M, WATKINS, N, WITTEMAN, J. C. M, ZEGGINI, E, ZHAI, G, ZILLIKENS, M. C, ALTSHULER, D, CAULFIELD, M. J, CHANOCK, S. J, FAROOQI, I. S, FERRUCCI, L, GURALNIK, J. M, HATTERSLEY, A. T, HU, F. B, JARVELIN, M.-R, LAAKSO, M, MOOSER, V, ONG, K. K, OUWEHAND, W. H, SALOMAA, V, SAMANI, N. J, SPECTOR, T. D, TUOMI, T, TUOMILEHTO, J, UDA, M, UITTERLINDEN, A. G, WAREHAM, N. J, DELOUKAS, P, FRAYLING, T. M, GROOP, L. C, HAYES, R. B, HUNTER, D. J, MOHLKE, K. L, PELTONEN, L, SCHLESSINGER, D, STRACHAN, D. P, WICHMANN, H.-E, MCCARTHY, M. I, BOEHNKE, M, BARROSO, I, ABECASIS, G. R, HIRSCHHORN, J. N, CONTROL, W. T. C, & CONSORTIUM, G. 2009. Six new loci associated with body mass index highlight a neuronal influence on body weight regulation. *Nature genetics*, **41**(1), 25–34. [3, 15, 16]
- WISE, R. A. 2013. Dual roles of dopamine in food and drug seeking: the drive-reward paradox. *Biological psychiatry*, **73**(9), 819–826. [9, 11, 12]

- WOLF, M. E, & ROTH, R. H. 1990. Autoreceptor regulation of dopamine synthesis. *Annals of the new york academy of sciences*, **604**, 323–343. [14]
- XU, M, KOELTZOW, T. E, SANTIAGO, G. T, MORATALLA, R, COOPER, D. C, HU, X. T, WHITE, N. M, GRAYBIEL, A. M, WHITE, F. J, & TONEGAWA, S. 1997. Dopamine D₃ receptor mutant mice exhibit increased behavioral sensitivity to concurrent stimulation of D₁ and D₂ receptors. *Neuron*, **19**(4), 837–848. [103]
- YAJNIK, C. S, JANIPALLI, C. S, BHASKAR, S, KULKARNI, S. R, FREATHY, R. M, PRAKASH, S, MANI, K. R, WEEDON, M. N, KALE, S. D, DESHPANDE, J, KRISHNAVENI, G. V, VEENA, S. R, FALL, C. H. D, MCCARTHY, M. I, FRAYLING, T. M, HATTERSLEY, A. T, & CHANDAK, G. R. 2009. FTO gene variants are strongly associated with type 2 diabetes in South Asian Indians. *Diabetologia*, **52**(2), 247–252. [15]
- YAMANAKA, A, BEUCKMANN, C. T, WILLIE, J. T, HARA, J, TSUJINO, N, MIEDA, M, TOMINAGA, M, YAGAMI, K. I, SUGIYAMA, F, GOTO, K, YANAGISAWA, M, & SAKURAI, T. 2003. Hypothalamic orexin neurons regulate arousal according to energy balance in mice. *Neuron*, **38**(5), 701–713. [6]
- YEO, G. S, FAROOQI, I. S, AMINIAN, S, HALSALL, D. J, STANHOPE, R. G, & O'RAHILLY, S. 1998. A frameshift mutation in MC₄R associated with dominantly inherited human obesity. *Nature genetics*, **20**(2), 111–112. [2]
- YI, C, & PAN, T. 2011. Cellular dynamics of RNA modification. *Accounts of chemical research*, **44**(12), 1380–1388. [30]
- YOSHIDA, M, YOKOO, H, MIZOGUCHI, K, KAWAHARA, H, TSUDA, A, NISHIKAWA, T, & TANAKA, M. 1992. Eating and drinking cause increased dopamine release in the nucleus accumbens and ventral tegmental area in the rat: measurement by in vivo microdialysis. *Neuroscience letters*, **139**(1), 73–76. [13]
- ZHENG, G, DAHL, J. A, NIU, Y, FEDORCSAK, P, HUANG, C.-M, LI, C. J, VÅGBØ, C. B, SHI, Y, WANG, W.-L, SONG, S.-H, LU, Z, BOSMANS, R. P. G, DAI, Q, HAO, Y.-J, YANG, X, ZHAO, W.-M, TONG, W.-M, WANG, X.-J, BOGDAN, F, FURU, K, FU, Y, JIA, G, ZHAO, X, LIU, J, KROKAN, H. E, KLUNGLAND, A, YANG, Y.-G, & HE, C. 2012. ALKBH₅ Is a Mammalian RNA Demethylase that Impacts RNA Metabolism and Mouse Fertility. *Molecular cell*, Nov. [33, 101]
- ZHONG, S, LI, H, BODI, Z, BUTTON, J, VESPA, L, HERZOG, M, & FRAY, R. G. 2008. MTA is an Arabidopsis messenger RNA adenosine methylase and interacts with a homolog of a sex-specific splicing factor. *The plant cell*, **20**(5), 1278–1288. [31, 32]
- ZHOU, Q. Y, & PALMITER, R. D. 1995. Dopamine-deficient mice are severely hypoactive, adipsic, and aphagic. *Cell*, **83**(7), 1197–1209. [13, 103]
- ZIMMERMANN, E, KRING, S. I. I, BERENTZEN, T. L, HOLST, C, PERS, T. H, HANSEN, T, PEDERSEN, O, SORENSEN, T. I. A, & JESS, T. 2009. Fatness-associated FTO gene variant increases mortality independent of fatness—in cohorts of Danish men. *Plos one*, **4**(2), e4428. [19]
- ZWEIFEL, L. S, ARGILLI, E, BONCI, A, & PALMITER, R. D. 2008. Role of NMDA receptors in dopamine neurons for plasticity and addictive behaviors. *Neuron*, **59**(3), 486–496. [106, 107]

6 Appendix

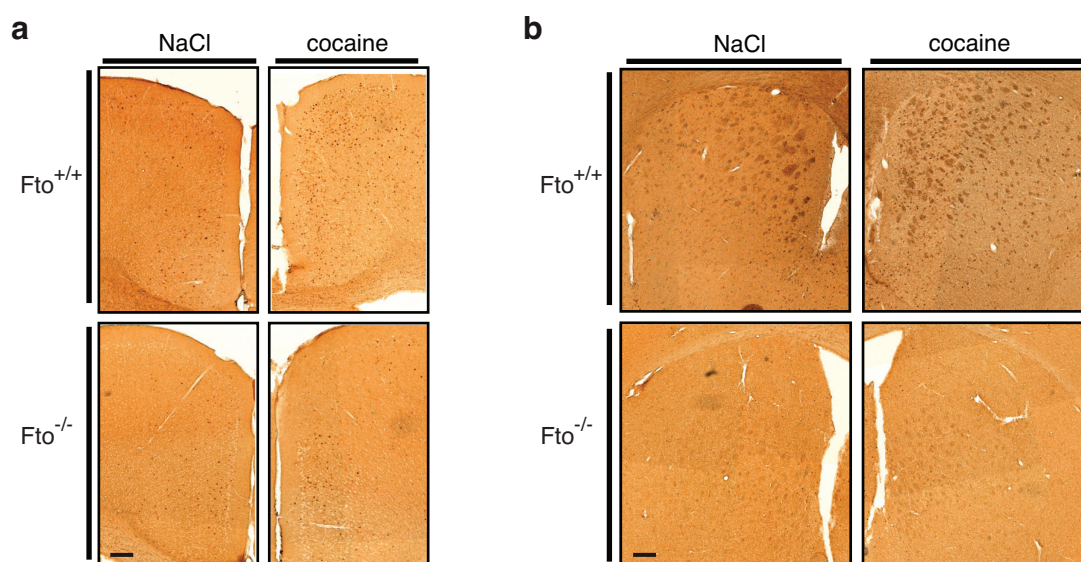


Figure 6.1: Reduction in cocaine-induced c-Fos immunoreactivity in *Fto*-deficient mice
 Immunohistochemistry of cortical areas (**a**, cingulate and sec. motor cortex) and the CPU (**b**) revealed blunted cocaine induced c-Fos expression in *Fto*-deficient mice (20 mg kg⁻¹ cocaine). No increase in c-Fos immunoreactivity is observed in *Fto*-deficient mice following cocaine injection, whereas the number of c-Fos positive cells markedly increased in control mice when challenged with cocaine. Scale bar = 200 μ m.

Table 6.1: Electrophysiological properties of *Fto*-deficient dopamine neurons

	Whole-cell capacitance [pF]	Firing rate [Hz]	Conductance density [$S F^{-1}$]
<i>Fto</i> ^{+/+}	49.5 \pm 1.0 (n=37)	2.1 \pm 0.1 (n=41)	55.3 \pm 2.6 (n=34)
<i>Fto</i> ^{-/-}	49.7 \pm 1.4 (n=34)	1.8 \pm 0.2 (n=31)	48.1 \pm 2.4* (n=31)

Asterisk indicates significant difference (* P <0.05)

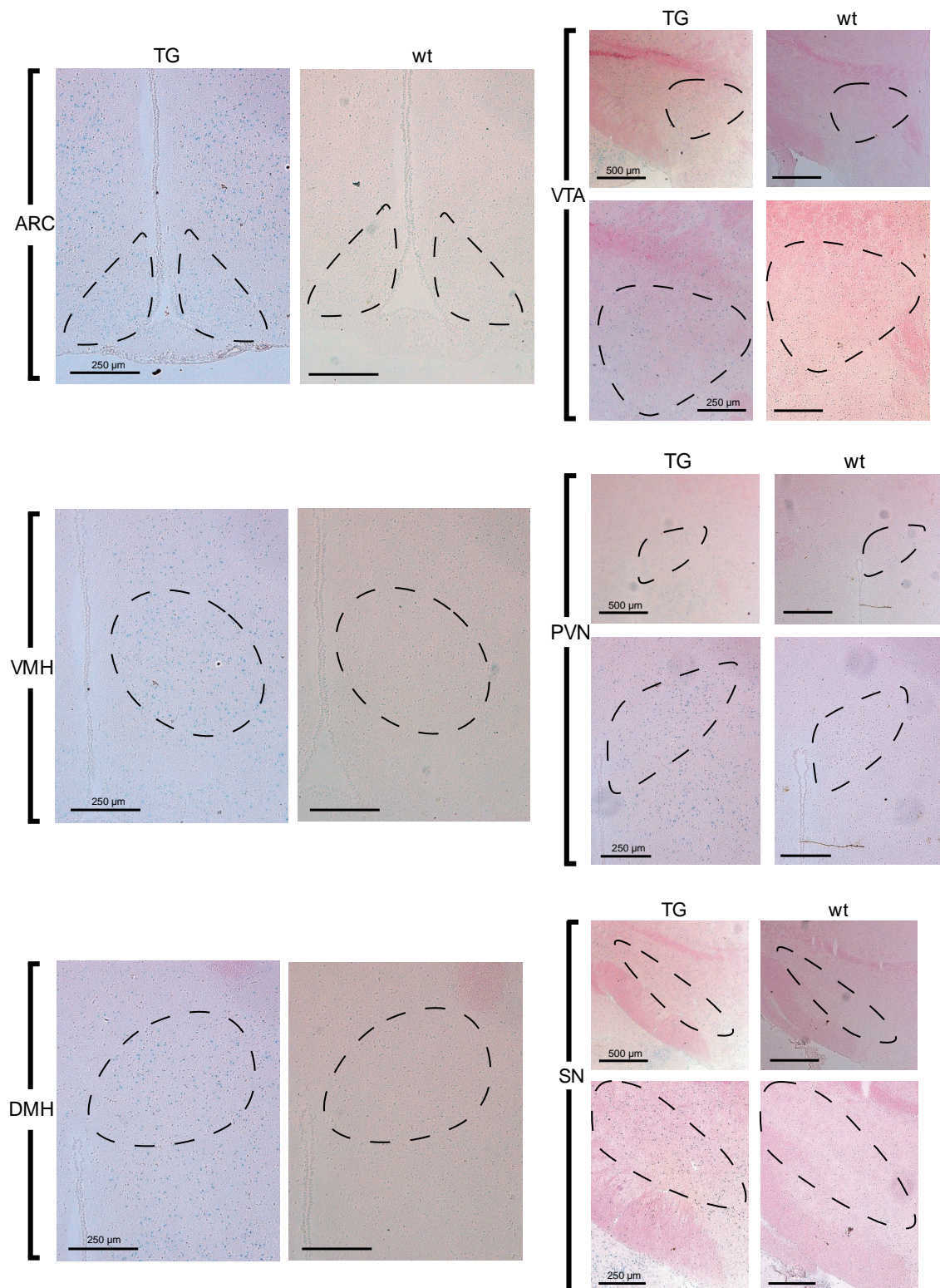


Figure 6.2: **Confirmation of *Fto* expression by β -galactosidase staining**

β -galactosidase staining of animals with a knock-in of the β -galactosidase cDNA into the endogenous *Fto* locus (EUCOMM, *Fto*^{tm1a(EUCOMM)Wtsi}) confirmed *Fto* expression in murine midbrain. In addition, expression was detected in numerous other brain regions including the paraventricular nucleus (PVN), arcuate nucleus (ARC), ventromedial hypothalamus (VMH) and dorsomedial hypothalamus (DMH).

Table 6.2: List of transcripts deregulated in *Fto*-deficient midbrain microarray analysis

Assignment	fc	pv	qv
Cartpt	-4.806744101	0.012692641	0.107723281
Slc6a3	-2.557829322	0.035206712	0.11387349
Hist1h1c	-2.354640266	0.019199099	0.107876683
Aldh1a2	-2.205333231	0.02848494	0.111774003
Gm5921	-2.184485203	0.023360363	0.110058377
4930467E23Rik	-2.179599905	0.002514206	0.105745966
4930467E23Rik	-2.169801901	0.000476167	0.105745966
E430024C06Rik	-2.169055047	0.005632106	0.105745966
E430024C06Rik	-2.169055047	0.005632106	0.105745966
Txnip	-2.157234981	0.018610818	0.107723281
Tipin	-2.138669175	0.009482251	0.107723281
A530053G22Rik	-2.133077919	0.025041702	0.110291413
4930467E23Rik	-2.110614846	0.00183584	0.105745966
4930467E23Rik	-2.087399395	0.000895549	0.105745966
Opalin	-2.08488335	0.015322035	0.107723281
Hbb-b1	-2.06195093	0.010209248	0.107723281
Unc13c	-2.034451658	0.012459516	0.107723281
D3Erttd751e	-2.02987844	0.006774102	0.105745966
Fto	-2.020632093	0.000627479	0.105745966
Hbb-b1	-1.988793289	0.007844134	0.107008823
Mgp	-1.970365583	0.046597259	0.119725282
Gm12643	-1.970128867	0.016207701	0.107723281
Lphn2	-1.919383949	0.011715228	0.107723281
Frzb	-1.896180978	0.010925845	0.107723281
Th	-1.879714211	0.040934926	0.116939704
Upp2	-1.873942475	0.008795025	0.107600372
Dcn	-1.863080485	0.000779499	0.105745966
Sgk1	-1.861067007	0.021007515	0.109360201
Hdx	-1.857029414	0.001708938	0.105745966
Tcf7l2	-1.856506029	0.040466175	0.116683307
4922502B01Rik	-1.8471999	0.00595778	0.105745966
Gas5	-1.846158816	0.02126643	0.109523432
D4Wsu53e	-1.843239238	0.027718953	0.111732284
Cnn3	-1.834080125	0.004454321	0.105745966
Aga	-1.82793318	0.024429234	0.110161209
Hmgb1	-1.819993545	0.03966157	0.116331753
BC049635	-1.81539061	0.013824254	0.107723281
Tdrd6	-1.806916702	0.027600802	0.111732284
Acyp1	-1.806157036	0.043072694	0.117869507
Parl	-1.80278831	0.043949741	0.118614199
Tdrd3	-1.796613401	0.033004575	0.112848689
Cdkn1b	-1.794493462	0.007520488	0.107008823
Zfp455	-1.789487749	0.032329567	0.112482754
Card6	-1.786765124	0.00206798	0.105745966
Ano3	-1.772890377	0.015209411	0.107723281
Cox17	-1.765185743	0.033412781	0.113287933
Gm10507	-1.761722466	0.028696391	0.11178848
Dnajc13	-1.756877173	0.022868371	0.109894243
Ufc1	-1.754885213	0.02467576	0.110291413
Gstm6	-1.748252215	0.027838164	0.111732284
LOC100047986	-1.743033141	0.009610351	0.107723281
Gabarapl2	-1.739488732	0.041565615	0.117112093
Chrna6	-1.73527783	0.045425046	0.119390455
Resp18	-1.728870729	0.014473351	0.107723281
Chrna5	-1.724064003	0.010583339	0.107723281
Gm7827	-1.721265922	0.02038427	0.109083258
Gm8959	-1.716690546	0.011695995	0.107723281
Syt17	-1.708207619	0.030382594	0.111930776
Ufsp2	-1.707315875	0.000899751	0.105745966
2810021G02Rik	-1.706984549	0.043497794	0.118218066
Ranbp3l	-1.704600113	0.002316895	0.105745966
Ak5	-1.704107877	0.026516801	0.111072282
Armxc5	-1.701255705	0.008016321	0.107008823
Ret	-1.700214379	0.041955542	0.117112093
Trappc2l	-1.696020177	0.006509535	0.105745966
Zfp759	-1.691187556	0.002369892	0.105745966
Mettl4	-1.689613578	0.001158299	0.105745966
Eif2s3y	-1.689113961	0.004339189	0.105745966
Sumo1	-1.688251688	0.015576743	0.107723281
Npy2r	-1.681831689	0.015062172	0.107723281
1110058L19Rik	-1.679505671	0.01920112	0.107876683
Pdgfra	-1.677144119	0.01222553	0.107723281
Itih2	-1.673617683	0.011343841	0.107723281
Sfrs3	-1.672628055	0.008945402	0.107600372
Gm5512	-1.672067783	0.006677079	0.105745966
Rpa3	-1.667642448	0.047670409	0.120024917

Continued on next page

Table 6.2 – continued from previous page

Assignment	fc	pv	qv
Chordc1	-1.665182152	0.000454042	0.105745966
Ddx3x	-1.664705144	0.013079526	0.107723281
Atp5h	-1.663740006	0.000977462	0.105745966
Hspa8	-1.659467069	0.021507654	0.10956964
Efemp1	-1.659298373	0.020800948	0.109317531
Rmnd1	-1.657164324	0.016447891	0.107723281
Lphn2	-1.656440827	0.004199498	0.105745966
Hspa8	-1.646885209	0.020553272	0.109270814
Mettl5	-1.644569525	5.15E-05	0.051083022
Gm10726	-1.642037035	0.002339226	0.105745966
Psm5	-1.637343101	0.018383415	0.107723281
Cstad	-1.629911163	0.007196357	0.107008823
Arpc5	-1.627382445	0.004144678	0.105745966
Tomm22	-1.626653159	0.04662033	0.119728073
Kcnc2	-1.62426084	0.004395858	0.105745966
Psm10	-1.622996625	0.021328229	0.10956964
Gba	-1.621913261	0.025599605	0.110565417
Nrip3	-1.61672765	0.000649478	0.105745966
1810030N24Rik	-1.615846328	0.035022634	0.113799868
Gjb2	-1.615431974	0.004410946	0.105745966
2410017P09Rik	-1.611990602	0.047576823	0.119963923
Ttc39b	-1.610780598	0.045932051	0.119506979
Gm5521	-1.60743084	0.019470211	0.108210826
Adamts1	-1.607133751	0.039423927	0.116024248
1810020D17Rik	-1.605845764	0.039139568	0.115957022
Sp140	-1.605408009	0.002438355	0.105745966
Snord87	-1.604836881	0.014667822	0.107723281
Polr1d	-1.604607004	0.017318098	0.107723281
Dhrs7	-1.601621597	0.045150506	0.119126063
Rpl9	-1.596947259	0.009028466	0.107600372
Chrn3	-1.596744336	0.011044687	0.107723281
Ano3	-1.596626284	0.002484819	0.105745966
Mrp150	-1.596552506	0.011287585	0.107723281
D630004N19Rik	-1.595505225	0.0121444	0.107723281
Hdac3		0.004199016	0.105745966
Rpl5	-1.592190912	0.007986224	0.107008823
D430042O09Rik	-1.590617189	0.039335141	0.116024248
Sept4	-1.587360708	0.007660099	0.107008823
Agxt2l1	-1.585242261	0.014482225	0.107723281
Gtpbp8	-1.577634858	0.00610951	0.105745966
2610017I09Rik	-1.577208437	0.022324734	0.10956964
Gabra5	-1.575977204	0.017252598	0.107723281
Gstm1	-1.573303134	0.001694706	0.105745966
Lphn2	-1.573299499	0.001358544	0.105745966
Gm8304	-1.572914226	0.000231863	0.101410316
Rps12	-1.572521781	1.78E-05	0.025735818
Fgfr3	-1.572114904	0.023355478	0.110058377
Parl	-1.570640859	0.006944363	0.106431423
Lmo3	-1.567921503	0.002091215	0.105745966
Arpc3	-1.567736757	0.028249369	0.111732284
Gm5778	-1.566896623	0.022209946	0.10956964
4930455F23Rik	-1.563107138	0.009395818	0.107723281
Txn14b	-1.562930183	0.037845173	0.11559365
Beckd1b	-1.561767829	0.007945643	0.107008823
Gm447	-1.560180918	0.040030257	0.116437995
Gm12176	-1.559153893	0.043559463	0.118285272
Gnpnat1	-1.558170745	0.015155721	0.107723281
Ctbs	-1.556303393	0.010220326	0.107723281
Rnpep	-1.555954637	0.016161944	0.107723281
Hba-a2	-1.554919616	0.038424211	0.115781817
Atp11b	-1.5539535	0.001252108	0.105745966
Camta1	-1.552234652	0.017024474	0.107723281
Hist2h2be	-1.551556966	0.030689347	0.111930776
Klhl32	-1.550915409	0.035360611	0.114141972
D16H22S680E	-1.547836766	0.013802924	0.107723281
Rpl9	-1.547786699	0.011246319	0.107723281
Nkiras1	-1.54777597	0.02829242	0.111732284
B230380D07Rik	-1.547736634	0.019609717	0.10830935
Lepr	-1.547650811	0.023290941	0.110058377
Hist1h2bc	-1.547475605	0.027972056	0.111732284
Atp5h	-1.54715385	0.000460279	0.105745966
Ndufaf2	-1.54661774	0.018397514	0.107723281
Psm5	-1.545074782	0.02139651	0.10956964
Hba-a1	-1.545071212	0.036604766	0.114852466
Cpne2	-1.543540496	0.034294926	0.113722583
BC057170	-1.542560065	0.013751163	0.107723281
Dennd4a	-1.542314164	0.03968435	0.116339767
Rbbp8	-1.541124413	0.00696665	0.106431423

Continued on next page

Table 6.2 – continued from previous page

Assignment	fc	pv	qv
Fmn1	-1.540636667	0.02809123	0.111732284
Eef1b2	-1.539853748	0.034471601	0.113740124
Josd1	-1.538630345	0.047207309	0.119852203
Ndufa9	-1.538584131	0.036587997	0.114852466
Aqp11	-1.537972812	0.000888799	0.105745966
LOC433762	-1.536928446	0.002508739	0.105745966
LOC433762	-1.536928446	0.002508739	0.105745966
Nov	-1.535785431	0.006190693	0.105745966
Mcts1	-1.535558349	0.003462	0.105745966
Dennd4a	-1.534965965	0.007340758	0.107008823
Rnf160	-1.53411149	0.009000027	0.107600372
Arhgef6	-1.533353144	0.006350713	0.105745966
Gm3258	-1.533261034	0.024351585	0.110161209
Fech	-1.531561536	0.015369054	0.107723281
Slc38a2	-1.531016679	0.001777778	0.105745966
Eif3e	-1.530376544	0.003841968	0.105745966
Tmem68	-1.530058344	0.011458463	0.107723281
Tfam	-1.52977909	0.014987079	0.107723281
March11	-1.529369138	0.024346116	0.110161209
Gm5113	-1.529213668	0.004848662	0.105745966
Ctla2a	-1.526925846	0.041629591	0.117112093
Nudt11	-1.526322686	0.012813399	0.107723281
1700019N12Rik	-1.524733038	0.002666831	0.105745966
Rbm3	-1.524338526	0.002400175	0.105745966
Nfib	-1.522022831	0.025682835	0.110565417
Llph	-1.52070467	0.044438795	0.118749173
Zfp595	-1.519756301	0.022119974	0.10956964
Tarsl2	-1.519696608	0.021504193	0.10956964
Id2	-1.518433086	0.029227683	0.11178848
Fbxo2	-1.517759637	0.008420158	0.107008823
5830433M19Rik	-1.516732501	0.021631357	0.10956964
Exosc1	-1.516546779	0.036559224	0.114852466
Ppp2r5c	-1.516403124	0.022015579	0.10956964
Tmem19	-1.5160528	0.021336181	0.10956964
Six6os1	-1.51546444	0.012259311	0.107723281
Snca	-1.514277908	0.034200692	0.113722583
Tprkb	-1.51378117	0.003835751	0.105745966
Sf4	-1.513200684	0.041596492	0.117112093
2210012G02Rik	-1.513053849	0.030136803	0.111919493
Mcf2	-1.51130691	0.014388809	0.107723281
6720456B07Rik	-1.510259715	0.034086418	0.113722583
Cfh	-1.510092231	0.005958455	0.105745966
4933407No1Rik	-1.509729413	0.016716185	0.107723281
Plk2	-1.509286474	0.007120453	0.106791948
Dennd4a	-1.509126072	0.003010194	0.105745966
Trappc2	-1.508651939	0.024886374	0.110291413
Styx	-1.506095584	0.002901863	0.105745966
Nrn1	-1.505431085	0.004819841	0.105745966
Atp5h	-1.505125027	0.008302634	0.107008823
Ublcp1	-1.505069387	0.036027498	0.114754442
Bccip	-1.502689219	0.016251217	0.107723281
Rbm3	-1.501981108	0.00244685	0.105745966
Prdx1	-1.501099907	0.020859811	0.109349143
Ephx4	-1.50032668	0.004548999	0.105745966
Dnahc3	1.50016723	0.036831604	0.114929658
Cpb1	1.500226156	0.016737207	0.107723281
Ssty2	1.500454946	0.01011183	0.107723281
Nt5dc1	1.501436368	0.018676895	0.107723281
D19Erttd652e	1.501804132	0.041969526	0.117112093
H1fnt	1.502362891	0.004715492	0.105745966
Gm9961	1.502442731	0.027302579	0.111732284
Gm6219	1.502553819	0.007119362	0.106791948
Igsf1	1.502779492	0.010904827	0.107723281
1110018H23Rik	1.503366401	0.022627987	0.10956964
Anxa10	1.503769383	0.02715305	0.111732284
Gm9891	1.504255884	0.038643638	0.115781817
Tgm4	1.504499194	0.016539445	0.107723281
Acss3	1.504568718	0.02755261	0.111732284
Olf157	1.504944204	0.005740396	0.105745966
Tlx2	1.50651322	0.039012757	0.115781817
Gm7112	1.506875265	0.021615993	0.10956964
Gper	1.508240679	0.002312487	0.105745966
Vmn2r22	1.508753028	0.008314445	0.107008823
Gm10883	1.508951741	0.026642406	0.111072282
Gnpda1	1.509317859	0.035025006	0.113799868
Lck	1.510346953	0.025058454	0.110291413
Gvin1	1.510483055	0.037375221	0.115180202
LOC100041256	1.510856527	0.018154611	0.107723281

Continued on next page

Table 6.2 – continued from previous page

Assignment	fc	pv	qv
Scd4	1.510929836	0.000260222	0.101410316
LOC382133	1.511638673	0.004771573	0.105745966
Gm8780	1.511701542	0.023846022	0.110058377
Tnfsf15	1.511974002	0.040741112	0.116858776
Fsd2	1.512267477	0.049386388	0.120564663
Wfdc15b	1.513141249	0.011827764	0.107723281
Plazg2d	1.513392989	0.019476121	0.108210826
Sycp1	1.51412747	0.008983301	0.107600372
Olfr129	1.515082828	0.008194267	0.107008823
Aldh3b2	1.516157889	0.010035598	0.107723281
Olfr156	1.51652926	0.012222092	0.107723281
Iqcf1	1.516662415	0.034733848	0.113740124
Gm6280	1.517577296	0.008084406	0.107008823
Fam181a	1.518029682	0.013977435	0.107723281
Txlnb	1.519233195	0.021743322	0.10956964
Gsc	1.519872181	0.016979061	0.107723281
Casp1	1.521273975	0.015807825	0.107723281
Capn10	1.524465323	0.015176888	0.107723281
Try4	1.525525892	0.020950188	0.109360201
Clca6	1.525783218	0.009220906	0.107600372
Bace2	1.525973597	0.042447478	0.117395681
Gm9405	1.526396745	0.00701645	0.106630285
Ssty2	1.527801027	0.00668459	0.105745966
Neb	1.527843388	0.00117393	0.105745966
Gm7455	1.528171719	0.008054475	0.107008823
Olfr875	1.528397709	0.034141174	0.113722583
Tnfrsf17	1.528574286	0.03041327	0.111930776
Col10a1	1.529217201	0.031673294	0.112100718
Gm9198	1.529471616	0.021076947	0.1095063
Gm10863	1.529959362	0.008695036	0.107600372
LOC635992	1.53043312	0.040195503	0.116563227
BC028471	1.530998992	0.010155286	0.107723281
Phldb3	1.531193559	0.018349155	0.107723281
Myo18b	1.531409381	0.029182837	0.11178848
Mrgpra6	1.532276512	0.04921693	0.120446832
Trpd52l3	1.533225609	0.007353349	0.107008823
Il28b	1.533572813	0.04819322	0.120254373
Cd96	1.533664942	0.01476872	0.107723281
Serpine3	1.533909464	0.008654149	0.107600372
Eya4	1.53466454	0.004249565	0.105745966
1700025H01Rik	1.535466106	0.044631074	0.118853184
Mia1	1.536016095	0.035992784	0.114754442
Il2orb	1.53627519	0.035961668	0.114754442
Asb10	1.537034982	0.010671635	0.107723281
Gm2524	1.538420615	0.007346535	0.107008823
V1ri9	1.538449051	0.003781961	0.105745966
Ssty2	1.53974346	0.007896418	0.107008823
Vmn2r9	1.542043361	0.009675699	0.107723281
Prt3	1.542228642	0.009293127	0.107723281
Olfr1034	1.543722389	0.027238765	0.111732284
Ptger2	1.545078352	4.99E-05	0.051083022
Fam183b	1.545717494	0.025976152	0.110694341
Ssty2	1.546006802	0.012650682	0.107723281
LOC100134980	1.547725905	0.002384134	0.105745966
Gm10008	1.547854647	0.005245391	0.105745966
Gm4814	1.548816972	0.028922704	0.11178848
1700007L08Rik	1.549028119	0.012227636	0.107723281
Trim8	1.549973267	0.012401341	0.107723281
Ooep	1.550252626	0.013686233	0.107723281
Dmkn	1.550542783	0.028195496	0.111732284
Ssty2	1.550961993	0.006116264	0.105745966
Gm10751	1.551008579	0.044212592	0.118683725
Olfr350	1.552848051	0.031172925	0.111930776
Dub2a	1.552909046	0.010372972	0.107723281
Defb3	1.553888874	0.005774571	0.105745966
Hormad1	1.554815433	0.006273066	0.105745966
Zfp42	1.55628901	0.006131402	0.105745966
Gm10787	1.556447233	0.006364826	0.105745966
Oit3	1.557458081	0.047096735	0.119837811
A730076H11Rik	1.558365165	0.047236835	0.119852203
Olfr113	1.559031416	0.017323599	0.107723281
Gm10421	1.559161098	0.000534002	0.105745966
Prrg4	1.561471964	0.003614507	0.105745966
Gm414	1.565854323	0.00492997	0.105745966
Acrv1	1.567512195	0.045219369	0.119147006
Dao	1.56791788	0.003992695	0.105745966
Ithn1	1.568530229	0.003557167	0.105745966
Cyp2w1	1.571512049	0.046244957	0.119506979

Continued on next page

Table 6.2 – continued from previous page

Assignment	fc	pv	qv
Fgl1	1.572122169	0.0084568	0.107111315
Lrrc25	1.57302689	0.008288377	0.107008823
Lce1b	1.573379473	0.023872966	0.110058377
1700066B19Rik	1.574885198	0.028852974	0.11178848
Gm16432	1.575642242	0.008976243	0.107600372
Gal	1.575813355	0.005823011	0.105745966
Olfr1165	1.576042748	0.0219427	0.10956964
Hsn2	1.57665827	0.000877596	0.105745966
Duxbl	1.577798896	0.030748514	0.111930776
Duxbl	1.577798896	0.030748514	0.111930776
Gm10755	1.578936699	0.01878801	0.107723281
Krtap4-7	1.579505908	0.00640548	0.105745966
Olfr1410	1.579900096	0.044601259	0.118853184
LOC100046350	1.580049767	0.002956233	0.105745966
Snhg7	1.581715359	0.035756495	0.114628526
Ces1	1.581737287	0.017489869	0.107723281
Tex19.2	1.581901752	0.009247774	0.107693259
4930539E08Rik	1.582888901	0.000634382	0.105745966
Olfr983	1.583748588	0.033070248	0.112932239
Spef2	1.585854047	0.010807988	0.107723281
Cyp8b1	1.58817879	0.028230097	0.111732284
Ceacam19	1.59209159	0.004352944	0.105745966
Gm9949	1.594852866	0.008157327	0.107008823
Phldb3	1.597312584	0.013206027	0.107723281
Tmem86b	1.597655844	0.013972651	0.107723281
Olfr149	1.597906877	0.011513302	0.107723281
Mybl2	1.598253958	0.024121558	0.110084646
LOC100040031	1.598257651	0.020556124	0.109270814
LOC100041207	1.600145765	0.046417443	0.119506979
LOC100041207	1.600145765	0.046417443	0.119506979
LOC674930	1.60248035	0.03091859	0.111930776
Fam83c	1.605964497	0.017140047	0.107723281
Ccl28	1.606090662	0.040676563	0.11680661
6430601O08Rik	1.608712665	0.015753118	0.107723281
Ppef1	1.611033693	0.011613052	0.107723281
A930012O16Rik	1.611942185	0.027626529	0.111732284
Olfr481	1.614950561	0.00759182	0.107008823
Dnahc3	1.615405847	0.013357696	0.107723281
Defb26	1.617362799	0.002965037	0.105745966
Olfr448	1.619591526	0.004400433	0.105745966
Lce3c	1.620332622	0.002225063	0.105745966
Slc7a13	1.620568496	0.007980409	0.107008823
Megf6	1.622258059	0.003015354	0.105745966
2610528A11Rik	1.624561095	0.033008578	0.112848689
2310034G01Rik	1.627265888	0.001232438	0.105745966
Duxbl	1.628119582	0.007985305	0.107008823
Il2orb	1.628789312	0.025021131	0.110291413
Gm8994	1.632360833	0.033946059	0.113699285
Krtap5-3	1.633341732	0.04781024	0.12020897
Bglap1	1.639341779	0.006207674	0.105745966
LOC380994	1.643562896	0.000882866	0.105745966
Tex22	1.64789768	0.008335281	0.107008823
Dynlrb2	1.661776853	0.010216646	0.107723281
H2-M10.2	1.664839769	0.003971442	0.105745966
Ccr7	1.665717024	0.002467486	0.105745966
LOC100040329	1.665870976	0.00844197	0.107008823
Hpse	1.671086794	0.00303465	0.105745966
Megf6	1.672809701	0.005319785	0.105745966
Gm6795	1.672991366	0.006377413	0.105745966
Gabre	1.673432083	0.001889628	0.105745966
E330013P04Rik	1.678384586	0.027657487	0.111732284
Gm1968	1.6861739	0.015634537	0.107723281
Enkur	1.696890338	0.016821788	0.107723281
A130066N16Rik	1.701487635	0.034111594	0.113722583
Gm6219	1.718095225	0.017938156	0.107723281
Gm6648	1.720152731	0.005798953	0.105745966
Bhmt	1.728966601	0.032687015	0.112593722
LOC100039614	1.744475497	0.02324076	0.110058377
Olfr26	1.753284358	0.018990394	0.107723281
Gm10748	1.770221635	0.004823396	0.105745966
Pppde1	1.771158512	0.046895142	0.119728073
Olfr495	1.780550474	0.045857091	0.119506979
Cpa6	1.799916525	0.008284509	0.107008823
Hsd11b1	1.804184234	0.041100764	0.117072249
Bclp2	1.804184234	0.02714435	0.111732284
Olfr328	1.807843759	0.015964933	0.107723281
Gm10534	1.820952555	0.014456206	0.107723281
Klkb11	1.852735156	0.016132265	0.107723281

Continued on next page

Table 6.2 – continued from previous page

Assignment	fc	pv	qv
Gm5841	1.879101939	0.042109656	0.117171004
Ccl12	1.907720741	0.032423673	0.112503534
Spef2	1.969400687	0.002857891	0.105745966
Tnnt2	1.991460227	0.000830242	0.105745966
A730020M07Rik	2.011906602	0.001976607	0.105745966
Spef2	2.035570704	0.007990949	0.107008823
Spef2	2.074111329	0.04059774	0.116749128
Ccl17	2.318518653	0.019034701	0.107723281
Olfr161	2.354123487	0.009348122	0.107723281
Dbh	2.39085505	0.008901351	0.107600372
Tdgf1	2.774036301	0.000560319	0.105745966

Table 6.3: Transcripts hypermethylated in *Fto*-deficient mice

Transcript Symbol	Transcript Name	Location
0610037L13Rik		CDS
1110012J17Rik		5'UTR
1110014N23Rik	protein fat-free homolog	CDS
1110032F04Rik	hypothetical protein LOC68725 precursor	CDS
1110034B05Rik		5'UTR
1110051M20Rik	hypothetical protein LOC228356	CDS
1300018J18Rik		3'UTR
1700001K19Rik	hypothetical protein LOC66323	3'UTR
1700001O22Rik		CDS
1700017B05Rik	hypothetical protein LOC74211	3'UTR
1700020L24Rik	hypothetical protein LOC66330	CDS
1700030J22Rik	hypothetical protein LOC69528	3'UTR
1700037H04Rik	hypothetical protein LOC67326	3'UTR
1700106N22Rik	hypothetical protein LOC73582	5'UTR
1810011H11Rik	hypothetical protein LOC69069	3'UTR
1810037I17Rik	hypothetical protein LOC67704	CDS
1810043G02Rik	hypothetical protein LOC67884	CDS
2010109K11Rik	hypothetical protein LOC72123	CDS
2210018M11Rik	protein EMSY	3'UTR
2310021P13Rik	hypothetical protein LOC268721	5'UTR
2310022B05Rik	hypothetical protein LOC69551	CDS
2310022B05Rik	hypothetical protein LOC69551	3'UTR
2310061I04Rik	hypothetical protein LOC69662	3'UTR
2410001C21Rik	hypothetical protein LOC66404	5'UTR
2610002L17Rik	transmembrane protein 103	CDS
2610002M06Rik	charged multivesicular body protein 1b-2	5'UTR
2610015P09Rik		CDS
2700078E11Rik	hypothetical protein LOC78832 isoform 3	CDS
4632415K11Rik	hypothetical protein LOC74347	CDS
4930420K17Rik	hypothetical protein LOC652925	5'UTR
4930452B06Rik	hypothetical protein LOC74430	CDS
4930539E08Rik	hypothetical protein LOC207819	3'UTR
4932411E22Rik	hypothetical protein LOC214604	CDS
4932412H11Rik	hypothetical protein LOC242838	5'UTR
4933413G19Rik	hypothetical protein LOC71149	3'UTR
5330417C22Rik	hypothetical protein LOC229722	CDS
5430411K18Rik		3'UTR
6330545A04Rik	miro domain-containing protein C1orf89 homolog	CDS
6430548M08Rik	hypothetical protein LOC234797 isoform c	5'UTR
9130011E15Rik	hypothetical protein LOC71617	CDS
9430016H08Rik	hypothetical protein LOC68115 precursor	5'UTR
9430038I01Rik	hypothetical protein LOC77252	3'UTR
9930111J21Rik1	interferon-inducible GTPase family member	3'UTR
A830018L16Rik	hypothetical protein LOC320492 isoform 4	5'UTR
A830093I24Rik	hypothetical protein LOC207921	5'UTR
Aamp	angio-associated migratory cell protein isoform	3'UTR
Aamp	angio-associated migratory cell protein isoform	5'UTR
Aars	alanyl-tRNA synthetase, cytoplasmic	CDS
Abcb8	ATP-binding cassette sub-family B member 8,	CDS
Abhd2	abhydrolase domain-containing protein 2	3'UTR
Ablim2	actin-binding LIM protein 2 isoform 6	3'UTR
Abr	active breakpoint cluster region-related protein	5'UTR
Abtb2	ankyrin repeat and BTB/POZ domain-containing	5'UTR
Acads	short-chain specific acyl-CoA dehydrogenase,	CDS
Acadv1	very long-chain specific acyl-CoA dehydrogenase,	CDS
Acap3	arf-GAP with coiled-coil, ANK repeat and PH	5'UTR
Acbd6	acyl-CoA-binding domain-containing protein 6	5'UTR
Accn4	amiloride-sensitive cation channel 4	5'UTR
Acot2	acyl-coenzyme A thioesterase 2, mitochondrial	CDS
Acrbp	acrosin-binding protein isoform 2	CDS
Actb	actin, cytoplasmic 1	5'UTR
Actn4	alpha-actinin-4	5'UTR
Actr2	actin-related protein 2	5'UTR
Actr3	actin-related protein 3	5'UTR
Actr3b	actin-related protein 3B	5'UTR
Actr8	actin-related protein 8	5'UTR
Adam23	disintegrin and metalloproteinase	5'UTR
Adamts11	ADAMTS-like protein 1	CDS
Adcyap1r1	pituitary adenylate cyclase-activating	CDS
Add1	alpha-adducin isoform 2	CDS
Add1	alpha-adducin isoform 2	3'UTR
Add2	beta-adducin	3'UTR
Adra1a	alpha-1A adrenergic receptor	CDS
Adra1a	alpha-1A adrenergic receptor	5'UTR
Adra2a	alpha-2A adrenergic receptor	CDS
Adra2b	alpha-2B adrenergic receptor	CDS

Continued on next page

Table 6.3 – continued from previous page

Transcript Symbol	Transcript Name	Methylation site
Adrb3	beta-3 adrenergic receptor	CDS
Aebp2	zinc finger protein AEBP2 isoform 1	CDS
Aff1	AF4/FMR2 family member 1 isoform 1	3'UTR
Aff3	AF4/FMR2 family member 3	3'UTR
Agap2	arf-GAP with GTPase, ANK repeat and PH	5'UTR
Agbl5	cytosolic carboxypeptidase-like protein 5	CDS
Agpat9	glycerol-3-phosphate acyltransferase 3	5'UTR
Ahctf1	protein ELYS	5'UTR
Ahr	aryl hydrocarbon receptor	CDS
AI593442	hypothetical protein LOC330941 isoform 2	5'UTR
Ak3	GTP:AMP phosphotransferase, mitochondrial	CDS
Ak5	adenylate kinase isoenzyme 5	3'UTR
Akap12	A-kinase anchor protein 12	3'UTR
Akap13	A kinase (PRKA) anchor protein 13	3'UTR
Akna	AT-hook-containing transcription factor	CDS
Akt2	RAC-beta serine/threonine-protein kinase	3'UTR
Aldh16a1	aldehyde dehydrogenase family 16 member A1	CDS
Aldh7a1	alpha-aminoadipic semialdehyde dehydrogenase	3'UTR
Alg2	alpha-1,3-mannosyltransferase ALG2	CDS
Alk	ALK tyrosine kinase receptor precursor	CDS
Alkbh3	alpha-ketoglutarate-dependent dioxygenase alkb	CDS
Alkbh5	probable alpha-ketoglutarate-dependent	5'UTR
Amigo1	amphoterin-induced protein 1 isoform 1	5'UTR
Ampd2	AMP deaminase 2	3'UTR
Angptl2	angiopoietin-related protein 2 precursor	5'UTR
Ank	progressive ankylosis protein	5'UTR
Ank2	ankyrin-2 isoform 3	CDS
Ankrd13b	ankyrin repeat domain-containing protein 13B	3'UTR
Ankrd13d	ankyrin repeat domain-containing protein 13D	5'UTR
Ankrd56	ankyrin repeat domain-containing protein 56	5'UTR
Anks1	ankyrin repeat and SAM domain-containing protein	CDS
Ano6	anoctamin-6	5'UTR
Anp32e	acidic leucine-rich nuclear phosphoprotein 32	3'UTR
Aoc2	retina-specific copper amine oxidase precursor	3'UTR
Ap1b1	AP-1 complex subunit beta-1	5'UTR
Apba1	amyloid beta (A4) precursor protein binding,	5'UTR
Apc	adenomatous polyposis coli protein	5'UTR
Apitd1	centromere protein 5	CDS
Aplp1	amyloid-like protein 1	5'UTR
App	amyloid beta A4 protein	5'UTR
Arap1	arf-GAP with Rho-GAP domain, ANK repeat and PH	3'UTR
Arcn1	coatamer subunit delta	5'UTR
Arf3	ADP-ribosylation factor 3	5'UTR
Arfgap2	ADP-ribosylation factor GTPase-activating	3'UTR
Arhgap26	rho GTPase-activating protein 26	CDS
Arhgap33	rho GTPase-activating protein 33	CDS
Arhgap44		3'UTR
Arhgef11	rho guanine nucleotide exchange factor 11	CDS
Arhgef17	rho guanine nucleotide exchange factor 17	5'UTR
Arhgef18	rho guanine nucleotide exchange factor 18	CDS
Arhgef2	rho guanine nucleotide exchange factor 2	CDS
Arhgef33	rho guanine nucleotide exchange factor 33	CDS
Arhgef37	rho guanine nucleotide exchange factor 37	3'UTR
Arid1a	AT-rich interactive domain-containing protein	3'UTR
Arl6ip6	ADP-ribosylation factor-like protein	5'UTR
Arm7	armadillo repeat-containing protein 7	CDS
Arpc1a	actin-related protein 2/3 complex subunit 1A	5'UTR
Arsk	arylsulfatase K	3'UTR
Arvcf	armadillo repeat protein deleted in	CDS
Arx	homeobox protein ARX	CDS
Arx	homeobox protein ARX	3'UTR
Asb3	ankyrin repeat and SOCS box protein 3	5'UTR
Ascc2	activating signal cointegrator 1 complex subunit	3'UTR
Ascl1	achaete-scute homolog 1	5'UTR
Atf5		CDS
Atg2b	autophagy-related protein 2 homolog B	3'UTR
Atg3	ubiquitin-like-conjugating enzyme ATG3	5'UTR
Atg9a	autophagy-related protein 9A	3'UTR
Atg9b	autophagy-related protein 9B	3'UTR
Atn1	atrophin-1	CDS
Atoh8	protein atonal homolog 8	CDS
Atp10b	probable phospholipid-transporting ATPase VB	CDS
Atp13a2	probable cation-transporting ATPase 13A2 isoform	CDS
Atp1a3	sodium/potassium-transporting ATPase subunit	3'UTR
Atp1a3	sodium/potassium-transporting ATPase subunit	5'UTR
Atp2a2		5'UTR
Atp5d	ATP synthase subunit delta, mitochondrial	CDS
Atp5d	ATP synthase subunit delta, mitochondrial	5'UTR

Continued on next page

Table 6.3 – continued from previous page

Transcript Symbol	Transcript Name	Methylation site
Atp5sl	ATP synthase subunit s-like protein	CDS
Atp6voa1	V-type proton ATPase 116 kDa subunit a isoform	3'UTR
Atp6voc	V-type proton ATPase 16 kDa proteolipid subunit	5'UTR
Atp6v1g2	V-type proton ATPase subunit G 2	CDS
Atpaf2	ATP synthase mitochondrial F1 complex assembly	3'UTR
Atxn10	ataxin-10	5'UTR
Atxn7l1	ataxin-7-like protein 1 isoform 1	CDS
Atxn7l1	ataxin-7-like protein 1 isoform 1	3'UTR
AU040320	dyslexia susceptibility 2-like isoform 2	3'UTR
Avl9	late secretory pathway protein AVL9 homolog	5'UTR
B230208H17Rik	putative GTP-binding protein Parf	3'UTR
B230208H17Rik	putative GTP-binding protein Parf	5'UTR
B3gat1	galactosylgalactosylxylosylprotein	CDS
B3gat2	galactosylgalactosylxylosylprotein	5'UTR
B3gnt8	UDP-GlcNAc:betaGal	CDS
Bach2	transcription regulator protein BACH2	CDS
Bag3	BAG family molecular chaperone regulator 3	3'UTR
Baiap2l2	brain-specific angiogenesis inhibitor	3'UTR
Baiap3	BAI1-associated protein 3	CDS
Barhl2	barH-like 2 homeobox protein	3'UTR
Bazza	bromodomain adjacent to zinc finger domain	3'UTR
BC005764		5'UTR
BC006779	PPAR gamma-DNA-binding domain interacting	CDS
BC013712	protein THEMIS2	CDS
BC021891	mitogen-activated protein kinase kinase kinase	CDS
BC068157	hypothetical protein LOC73072	CDS
Bcl10	B-cell lymphoma/leukemia 10	CDS
Bcl6	B-cell lymphoma 6 protein homolog	CDS
Bcor	BCL-6 corepressor isoform d	5'UTR
Bhlha9	class A basic helix-loop-helix protein 9	CDS
Bhlhe22	class E basic helix-loop-helix protein 22	CDS
Bhlhe40	class E basic helix-loop-helix protein 40	5'UTR
Bmf	bcl-2-modifying factor	CDS
Bmp1		5'UTR
Bmp6	bone morphogenetic protein 6 precursor	5'UTR
Bmp7	bone morphogenetic protein 7 precursor	3'UTR
Brd4	bromodomain-containing protein 4 isoform 1	CDS
Brms1	breast cancer metastasis-suppressor 1 homolog	5'UTR
Brsk1	BR serine/threonine-protein kinase 1 isoform 2	CDS
Btdb11	ankyrin repeat and BTB/POZ domain-containing	5'UTR
Btrc	F-box/WD repeat-containing protein 1A isoform b	CDS
C130074G19Rik	hypothetical protein LOC226777	CDS
C1qtnf1	complement C1q tumor necrosis factor-related	CDS
C1qtnf1	complement C1q tumor necrosis factor-related	3'UTR
C1qtnf4	complement C1q tumor necrosis factor-related	5'UTR
C230096C10Rik	hypothetical protein LOC230866 isoform 2	CDS
C2cd2l	C2 domain-containing protein 2-like	CDS
C2cd2l	C2 domain-containing protein 2-like	3'UTR
C2cd2l	C2 domain-containing protein 2-like	5'UTR
C2cd3	C2 domain-containing protein 3	CDS
C2cd4d	C2 calcium-dependent domain-containing protein	CDS
C330005M16Rik	iron/zinc purple acid phosphatase-like protein	3'UTR
C330019G07Rik	hypothetical protein LOC215476	3'UTR
C630004H02Rik	hypothetical protein LOC217310	3'UTR
C77080	hypothetical protein LOC97130	CDS
C77080	hypothetical protein LOC97130	3'UTR
Cachd1	VWFA and cache domain-containing protein 1	CDS
Cacna1a	voltage-dependent P/Q-type calcium channel	CDS
Cacna1c	voltage-dependent L-type calcium channel subunit	3'UTR
Cacna1d	voltage-dependent L-type calcium channel subunit	3'UTR
Cacnb1	voltage-dependent L-type calcium channel subunit	5'UTR
Cacng4	voltage-dependent calcium channel gamma-4	CDS
Cadps	calcium-dependent secretion activator 1 isoform	5'UTR
Caly	neuron-specific vesicular protein calycon	3'UTR
Camta2	calmodulin-binding transcription activator 2	CDS
Camta2	calmodulin-binding transcription activator 2	3'UTR
Cand2	cullin-associated NEDD8-dissociated protein 2	CDS
Capn5	calpain-5	3'UTR
Caprin2	caprin-2	5'UTR
Capzb	F-actin-capping protein subunit beta isoform a	3'UTR
Card10	caspase recruitment domain-containing protein	CDS
Card6	caspase recruitment domain family, member 6	CDS
Casp9	caspase-9	CDS
Cass4	cas scaffolding protein family member 4 isoform	CDS
Cas21	zinc finger protein castor homolog 1 isoform 1	CDS
Cbfa2t3	protein CBFA2T3 isoform 2	CDS
Cbfa2t3	protein CBFA2T3 isoform 2	3'UTR
Cblb	E3 ubiquitin-protein ligase CBL-B	3'UTR

Continued on next page

Table 6.3 – continued from previous page

Transcript Symbol	Transcript Name	Methylation site
Cebe1	collagen and calcium-binding EGF	CDS
Ccbp2	chemokine-binding protein 2	3'UTR
Ccdc102a	coiled-coil domain-containing protein 102A	CDS
Ccdc120	coiled-coil domain containing 120	CDS
Ccdc142	coiled-coil domain-containing protein 142	CDS
Ccdc48	coiled-coil domain-containing protein 48	CDS
Ccdc88a	girdin	5'UTR
Ccdc88b	coiled-coil domain-containing protein 88B	CDS
Cdc96	coiled-coil domain-containing protein 96	3'UTR
Ceng1	cyclin-G1	5'UTR
Cen11	cyclin-L1	5'UTR
Cd248	endosialin precursor	CDS
Cd248	endosialin precursor	3'UTR
Cd33	myeloid cell surface antigen CD33 isoform 1	CDS
Cd40		3'UTR
Cd93	complement component C1q receptor	CDS
Cd93	complement component C1q receptor	3'UTR
Cdan1	codanin-1	CDS
Cdc25b	M-phase inducer phosphatase 2 isoform b	CDS
Cdc42bpb	serine/threonine-protein kinase MRCK beta	5'UTR
Cdc42se1	CDC42 small effector protein 1 isoform 2	CDS
Cdh13	cadherin-13 precursor	CDS
Cdh2	cadherin-2 precursor	5'UTR
Cdh22	cadherin-22 precursor	5'UTR
Cdh24	cadherin-24 precursor	CDS
Cdh5	cadherin-5 precursor	CDS
Cdh5	cadherin-5 precursor	3'UTR
Cdhr1	cadherin-related family member 1 precursor	CDS
Cdk12	cell division protein kinase 12 isoform 2	5'UTR
Cdk18	cell division protein kinase 18	3'UTR
Cdk13	cyclin-dependent kinase-like 3 isoform 6	5'UTR
Cdkn1a	cyclin-dependent kinase inhibitor 1	CDS
Cds2	phosphatidate cytidyltransferase 2	CDS
Celf3	CUGBP Elav-like family member 3	3'UTR
Celsr1	cadherin EGF LAG seven-pass G-type receptor 1	CDS
Celsr1	cadherin EGF LAG seven-pass G-type receptor 1	3'UTR
Celsr3	cadherin EGF LAG seven-pass G-type receptor 3	3'UTR
Cenpm	centromere protein M isoform 2	3'UTR
Cep350	centrosome-associated protein 350	5'UTR
Cfr	cystic fibrosis transmembrane conductance	3'UTR
Chad1	chondroadherin-like	CDS
Chd4	chromodomain-helicase-DNA-binding protein 4	5'UTR
Chga	chromogranin-A precursor	3'UTR
Chmp2b	charged multivesicular body protein 2b	5'UTR
Chrm3	muscarinic acetylcholine receptor M3	5'UTR
Chrna3	neuronal acetylcholine receptor subunit alpha-3	CDS
Chrn2	neuronal acetylcholine receptor subunit beta-2	5'UTR
Chst1	carbohydrate sulfotransferase 1	5'UTR
Chst14	carbohydrate sulfotransferase 14	CDS
Chst3	carbohydrate sulfotransferase 3	CDS
Chst5	carbohydrate sulfotransferase 5	CDS
Cit	citron Rho-interacting kinase	CDS
Cited4	cbp/p300-interacting transactivator 4	CDS
Cln1	chloride channel protein 1	CDS
Cln4-2	H(+)/Cl(-) exchange transporter 4	5'UTR
Cln7	H(+)/Cl(-) exchange transporter 7	3'UTR
Cldn11	claudin-11	CDS
Cldn26		5'UTR
Cldn3	claudin-3	CDS
Clec16a	protein CLEC16A	5'UTR
Clip3	CAP-Gly domain-containing linker protein 3	5'UTR
Clk3	dual specificity protein kinase CLK3	CDS
Clmn	calmin isoform b	CDS
Clnk	cytokine-dependent hematopoietic cell linker	3'UTR
Cltb	clathrin light chain B	5'UTR
Cmpk2	UMP-CMP kinase 2, mitochondrial precursor	CDS
Cmtm3	CKLF-like MARVEL transmembrane domain-containing	CDS
Cmya5	cardiomyopathy-associated protein 5	CDS
Cnga3	cyclic nucleotide-gated cation channel alpha-3	CDS
Cnksr3	connector enhancer of kinase suppressor of ras	CDS
Cnnm1	metal transporter CNNM1	3'UTR
Cnr1	cannabinoid receptor 1	5'UTR
Cntn2	contactin-2 precursor	5'UTR
Cntnap1	contactin-associated protein 1 precursor	CDS
Cntnap5c	contactin-associated protein like 5-3 precursor	CDS
Cobra1	negative elongation factor B	3'UTR
Cobra1	negative elongation factor B	5'UTR
Cog7	conserved oligomeric Golgi complex subunit 7	3'UTR

Continued on next page

Table 6.3 – continued from previous page

Transcript Symbol	Transcript Name	Methylation site
Col27a1	collagen alpha-1(XXVII) chain precursor	CDS
Col5a1	collagen alpha-1(V) chain precursor	3'UTR
Col6a2	collagen alpha-2(VI) chain precursor	CDS
Commd8	COMM domain-containing protein 8	CDS
Cops6	COP9 signalosome complex subunit 6	3'UTR
Cops7a	COP9 signalosome complex subunit 7a isoform 1	CDS
Cops7a	COP9 signalosome complex subunit 7a isoform 1	3'UTR
Cops7a	COP9 signalosome complex subunit 7a isoform 1	5'UTR
Coro1b	coronin-1B	5'UTR
Coro2b	coronin-2B	CDS
Cox8a	cytochrome c oxidase subunit 8A, mitochondrial	CDS
Cpne5	copine-5	3'UTR
Cpne6	copine-6 isoform a	5'UTR
Cpne7	copine-7	CDS
Cpne8	copine-8 isoform 1	3'UTR
Cpox	coproporphyrinogen-III oxidase, mitochondrial	CDS
Cpsf4	cleavage and polyadenylation specificity factor	5'UTR
Cpxm1	probable carboxypeptidase X1 precursor	3'UTR
Crebl2	cAMP-responsive element-binding protein-like 2	5'UTR
Creg1	protein CREG1	CDS
Crim1	cysteine-rich motor neuron 1 protein precursor	5'UTR
Crtc1	CREB-regulated transcription coactivator 1	3'UTR
Crtc2	CREB-regulated transcription coactivator 2	CDS
Cry2	cryptochrome-2	CDS
Cryab	alpha-crystallin B chain	CDS
Crybg3	beta/gamma crystallin domain-containing protein	3'UTR
Csd2	cold shock domain-containing protein C2	3'UTR
Csf1r	macrophage colony-stimulating factor 1 receptor	3'UTR
Csf2ra	granulocyte-macrophage colony-stimulating factor	3'UTR
Csnk1d	casein kinase I isoform delta isoform 1	5'UTR
Cspg4	chondroitin sulfate proteoglycan 4 precursor	3'UTR
Ctdspl	CTD small phosphatase-like protein	CDS
Ctnnb1	catenin beta-1	5'UTR
Ctnd2	catenin delta-2	CDS
Ctps2	CTP synthase 2 isoform a	5'UTR
Cttnbp2nl	CTTNBP2 N-terminal-like protein	CDS
Cuedc1	CUE domain-containing protein 1 isoform 2	5'UTR
Cyfp1	cytoplasmic FMR1-interacting protein 1 isoform	5'UTR
Cyfp2	cytoplasmic FMR1-interacting protein 2	CDS
Cyp2d22	cytochrome P450, family 2, subfamily d,	CDS
Cyp2d22	cytochrome P450, family 2, subfamily d,	5'UTR
Cyp2s1	cytochrome P450 2S1	CDS
Cyp2s1	cytochrome P450 2S1	3'UTR
Cyp4f16	cytochrome P450, family 4, subfamily f,	3'UTR
D16Ert472e	protein EURL homolog	5'UTR
D430042O09Rik	hypothetical protein LOC233865	CDS
D630003M21Rik	hypothetical protein LOC228846 isoform 2	CDS
D630045J12Rik	hypothetical protein LOC330286	CDS
D630045J12Rik	hypothetical protein LOC330286	3'UTR
Daam2	disheveled-associated activator of morphogenesis	5'UTR
Dab2	disabled homolog 2 isoform b	CDS
Dag1	dystroglycan precursor	5'UTR
Dap	death-associated protein 1	3'UTR
Darc	Duffy antigen/chemokine receptor	CDS
Dbn1	drebrin isoform 2	CDS
Dcaf12l1	DDB1- and CUL4-associated factor 12-like protein	5'UTR
Dcaf12l2	DDB1- and CUL4-associated factor 12-like protein	CDS
Debl2	discoilin, CUB and LCCL domain-containing	3'UTR
Dcl1	serine/threonine-protein kinase DCLK1 isoform 3	CDS
Dctn1	dynactin subunit 1	CDS
Ddx17	probable ATP-dependent RNA helicase DDX17	5'UTR
Ddx39b		5'UTR
Ddx54	ATP-dependent RNA helicase DDX54	CDS
Dennd1a	DENN domain-containing protein 1A	CDS
Dennd1a	DENN domain-containing protein 1A	3'UTR
Dennd3	DENN domain-containing protein 3	CDS
Dennd3	DENN domain-containing protein 3	3'UTR
Dgke	diacylglycerol kinase epsilon	5'UTR
Dhcr24	24-dehydrocholesterol reductase precursor	CDS
Dhx38	pre-mRNA-splicing factor ATP-dependent RNA	3'UTR
Diap1	protein diaphanous homolog 1	3'UTR
Dimt1	probable dimethyladenosine transferase	CDS
Dio2	type II iodothyronine deiodinase	5'UTR
Dio3	type III iodothyronine deiodinase	3'UTR
Dip2c	disco-interacting protein 2 homolog C	5'UTR
Dis3l	DIS3-like exonuclease 1 isoform 2	5'UTR
Disp2	protein dispatched homolog 2	CDS
Disp2	protein dispatched homolog 2	5'UTR

Continued on next page

Table 6.3 – continued from previous page

Transcript Symbol	Transcript Name	Methylation site
Dlgap1	disks large-associated protein 1 isoform 4	3'UTR
Dlx2	homeobox protein DLX-2	3'UTR
Dmp1	dentin matrix acidic phosphoprotein 1 precursor	3'UTR
Dnahc9	dynein heavy chain 9, axonemal	CDS
Dnajb5	dnaJ homolog subfamily B member 5	CDS
Dnm1	dynammin-1	CDS
Dnm1	dynammin-1	3'UTR
Dock9	dedicator of cytokinesis protein 9 isoform 4	CDS
Dopey2	protein dopey-2 isoform 2	3'UTR
Dopey2	protein dopey-2 isoform 2	5'UTR
Dot1	histone-lysine N-methyltransferase, H3 lysine-79	3'UTR
Dpp6	dipeptidyl aminopeptidase-like protein 6 isoform	5'UTR
Dpp9	dipeptidyl peptidase 9	3'UTR
Dpysl2	dihydropyrimidinase-related protein 2	5'UTR
Dpysl5	dihydropyrimidinase-related protein 5	5'UTR
Drd3	D(3) dopamine receptor	CDS
Dscam1	Down syndrome cell adhesion molecule-like	CDS
Dscam1	Down syndrome cell adhesion molecule-like	3'UTR
Dse	dermatan-sulfate epimerase precursor	5'UTR
Dtx3	protein deltex-3	CDS
Dtx3l	E3 ubiquitin-protein ligase DTX3L	CDS
Dtx4	protein deltex-4	5'UTR
Dus1	tRNA-dihydrouridine synthase 1-like	CDS
Dusp4	dual specificity protein phosphatase 4	CDS
Dvl3	segment polarity protein dishevelled homolog	CDS
Dzip1	zinc finger protein DZIP1	3'UTR
E130308A19Rik	hypothetical protein LOC230259 isoform 2	3'UTR
E130309D14Rik	hypothetical protein LOC432582	CDS
Ebf2	transcription factor COE2	3'UTR
Ece1	endothelin-converting enzyme 1	CDS
Ece1	endothelin-converting enzyme 1	3'UTR
Ece2	endothelin-converting enzyme 2 isoform e	5'UTR
Edf1	endothelial differentiation-related factor 1	5'UTR
Edil3	EGF-like repeat and discoidin I-like	5'UTR
Efh1	EF-hand domain-containing protein D1	CDS
Efnb1	ephrin-B1 precursor	3'UTR
Egr3	early growth response protein 3	3'UTR
Egr4	early growth response protein 4	CDS
Egr4	early growth response protein 4	3'UTR
Ehd4	EH domain-containing protein 4	CDS
Eif1ad	probable RNA-binding protein EIF1AD	5'UTR
Eif4g3	eukaryotic translation initiation factor 4 gamma	5'UTR
Elac2	zinc phosphodiesterase ELAC protein 2	CDS
Elfn2	leucine-rich repeat and fibronectin type-III	5'UTR
Elk3	ETS domain-containing protein Elk-3 isoform a	CDS
Elmo1	engulfment and cell motility protein 1 isoform	5'UTR
Elov14	elongation of very long chain fatty acids	5'UTR
Emilin2	EMILIN-2 precursor	CDS
En1	homeobox protein engrailed-1	CDS
Enho	adropin precursor	5'UTR
Eno2	gamma-enolase	5'UTR
Entpd3	ectonucleoside triphosphate diphosphohydrolase	3'UTR
Entpd5	ectonucleoside triphosphate diphosphohydrolase 5	3'UTR
Entpd6	ectonucleoside triphosphate diphosphohydrolase	3'UTR
Epas1	endothelial PAS domain-containing protein 1	CDS
Epb4.t11	band 4.1-like protein 1 isoform b	5'UTR
Epha8	ephrin type-A receptor 8 precursor	3'UTR
Ephb1	ephrin type-B receptor 1 isoform 2	5'UTR
Ephb3	ephrin type-B receptor 3 precursor	CDS
Ephb3	ephrin type-B receptor 3 precursor	5'UTR
Epsi511	epidermal growth factor receptor substrate	CDS
Eps8	epidermal growth factor receptor kinase	CDS
ErbB2	receptor tyrosine-protein kinase erbB-2	3'UTR
Ercc1	DNA excision repair protein ERCC-1 isoform b	3'UTR
Espn	espin isoform 2	CDS
Esrra	steroid hormone receptor ERR1	CDS
Esrrb	steroid hormone receptor ERR2 isoform 2	CDS
Etfdh	electron transfer flavoprotein-ubiquinone	5'UTR
Etl4	sickle tail protein isoform e	CDS
Etnk2	ethanolamine kinase 2	CDS
Ets1	protein C-ets-1 isoform 2	3'UTR
Ets1	protein C-ets-1 isoform 2	5'UTR
Etv6	transcription factor ETV6	CDS
Evpl	envoplakin	CDS
Exoc1	exocyst complex component 1	CDS
Exoc6b	SEC15-like 2	5'UTR
F2r	proteinase-activated receptor 1 precursor	CDS
Faim	fas apoptotic inhibitory molecule 1 Faim-L	CDS

Continued on next page

Table 6.3 – continued from previous page

Transcript Symbol	Transcript Name	Methylation site
Faim2	fas apoptotic inhibitory molecule 2 isoform 1	CDS
Faim2	fas apoptotic inhibitory molecule 2 isoform 1	3'UTR
Faim2	fas apoptotic inhibitory molecule 2 isoform 1	5'UTR
Fam100a	hypothetical protein LOC207740	CDS
Fam100b	hypothetical protein LOC319370	CDS
Fam102a	family with sequence similarity 102, member A	5'UTR
Fam120c	constitutive coactivator of PPAR-gamma-like	5'UTR
Fam135a	hypothetical protein LOC68187	5'UTR
Fam159b	membrane protein FAM159B	5'UTR
Fam160a1	hypothetical protein LOC229488	CDS
Fam160b2	family with sequence similarity 160, member B2	CDS
Fam163b	hypothetical protein LOC109349	CDS
Fam163b	hypothetical protein LOC109349	3'UTR
Fam164c	family with sequence similarity 164, member C	3'UTR
Fam167a	hypothetical protein LOC219148	CDS
Fam167b	hypothetical protein LOC230766	CDS
Fam174b	membrane protein FAM174B precursor	CDS
Fam178a	hypothetical protein LOC226151	5'UTR
Fam179b	hypothetical protein LOC328108	5'UTR
Fam184b	hypothetical protein LOC58227	CDS
Fam184b	hypothetical protein LOC58227	3'UTR
Fam184b	hypothetical protein LOC58227	5'UTR
Fam189a2	hypothetical protein LOC381217	CDS
Fam189b	hypothetical protein LOC68521	5'UTR
Fam190a	hypothetical protein LOC232035	5'UTR
Fam196a	hypothetical protein LOC627214	3'UTR
Fam199x	hypothetical protein LOC245622	5'UTR
Fam203a		CDS
Fam65a	hypothetical protein LOC75687	CDS
Fam78a	hypothetical protein LOC241303	3'UTR
Fam78a	hypothetical protein LOC241303	5'UTR
Fam82a2	regulator of microtubule dynamics protein 3	CDS
Fam89a	family with sequence similarity 89, member A	CDS
Fam89b		CDS
Fancl	E3 ubiquitin-protein ligase FANCL	CDS
Farp1	FERMRhoGEF (Arhgef) and pleckstrin domain	CDS
Fat1	FAT tumor suppressor homolog 1	3'UTR
Fat2	protocadherin Fat 2	CDS
Fbrs	fibrosin-1	CDS
Fbrsl1	fibrosin-like 1 isoform 1	CDS
Fbx112	F-box/LRR-repeat protein 12 isoform a	CDS
Fbx117	F-box/LRR-repeat protein 17	5'UTR
Fbx16	F-box/LRR-repeat protein 6	CDS
Fbx17	F-box/LRR-repeat protein 7	CDS
Fbx18	F-box/LRR-repeat protein 8	5'UTR
Fbxo10	F-box only protein 10	3'UTR
Fbxo42	F-box only protein 42	3'UTR
Fbxw7	F-box/WD repeat-containing protein 7 isoform 2	5'UTR
Fchs2d	FCH and double SH3 domains protein 2 isoform 2	5'UTR
Fcrlb	Fc receptor-like B	CDS
Fdxr	NADPH:adrenodoxin oxidoreductase, mitochondrial	CDS
Fen1	flap endonuclease 1	5'UTR
Fgd5	FYVE, RhoGEF and PH domain-containing protein 5	CDS
Fgd5	FYVE, RhoGEF and PH domain-containing protein 5	3'UTR
Fgf1	heparin-binding growth factor 1 precursor	CDS
Fgfr3	fibroblast growth factor 13	5'UTR
Fgfbp3	fibroblast growth factor-binding protein 3	CDS
Flad1	FAD synthase	CDS
Flt1	vascular endothelial growth factor receptor 1	5'UTR
Fmod	fibromodulin precursor	CDS
Fn3k	fructosamine-3-kinase isoform b	3'UTR
Fnbp1	formin-binding protein 1 isoform e	5'UTR
Fndc1	fibronectin type III domain-containing protein	3'UTR
Fndc3b	fibronectin type III domain-containing protein	CDS
Fos	proto-oncogene c-Fos	5'UTR
Fosl2	fos-related antigen 2	CDS
Foxa1	hepatocyte nuclear factor 3-alpha	CDS
Foxc1	forkhead box protein C1	CDS
Foxd1	forkhead box protein D1	3'UTR
Foxk1	forkhead box protein K1	CDS
Foxp4	forkhead box protein P4 isoform 2	CDS
Foxp4	forkhead box protein P4 isoform 2	3'UTR
Foxq1	forkhead box protein Q1	CDS
Fras1	extracellular matrix protein FRAS1 precursor	5'UTR
Frem2	FRAS1-related extracellular matrix protein 2	CDS
Frem2	FRAS1-related extracellular matrix protein 2	3'UTR
Frmf4a	FERM domain-containing protein 4A isoform 1	CDS
Frmf8	FERM domain-containing protein 8	CDS

Continued on next page

Table 6.3 – continued from previous page

Transcript Symbol	Transcript Name	Methylation site
Fscn1	fascin	3'UTR
Fto	alpha-ketoglutarate-dependent dioxygenase FTO	3'UTR
Fut4	alpha-(1,3)-fucosyltransferase	CDS
Fyc01	FYVE and coiled-coil domain-containing protein	CDS
Fyn	tyrosine-protein kinase Fyn isoform a	CDS
Fyn	tyrosine-protein kinase Fyn isoform a	5'UTR
Fzd1	frizzled-1 precursor	5'UTR
Fzd10	frizzled-10 precursor	3'UTR
G3bp2	ras GTPase-activating protein-binding protein 2	5'UTR
G6pdx	glucose-6-phosphate 1-dehydrogenase X	3'UTR
Gaa	lysosomal alpha-glucosidase precursor	3'UTR
Gaa	lysosomal alpha-glucosidase precursor	5'UTR
Gab1	GRB2-associated-binding protein 1	5'UTR
Gabbr2	gamma-aminobutyric acid type B receptor subunit	CDS
Gabra2	gamma-aminobutyric acid receptor subunit alpha-2	5'UTR
Gad1	glutamate decarboxylase 1	5'UTR
Gadd45g	growth arrest and DNA damage-inducible protein	CDS
Gal3st3	galactose-3-O-sulfotransferase 3	CDS
Gal3st3	galactose-3-O-sulfotransferase 3	5'UTR
Galnt14	polypeptide N-acetylgalactosaminyltransferase	5'UTR
Galnt2	polypeptide	CDS
Gapvd1	GTPase-activating protein and VPS9	5'UTR
Gas1	growth arrest-specific protein 1	5'UTR
Gas7	growth arrest-specific protein 7 isoform b	3'UTR
Gata2	endothelial transcription factor GATA-2	CDS
Gatsl2	GATS-like protein 2	3'UTR
Gbp7		3'UTR
Gbx2	homeobox protein GBX-2	CDS
Gcap14	granule cell antiserum positive 14 isoform 2	5'UTR
Gck	glucokinase	CDS
Gdap11	ganglioside-induced differentiation-associated	CDS
Gdf7	growth/differentiation factor 7	CDS
Gga3	ADP-ribosylation factor-binding protein GGA3	3'UTR
Gimap1	GTPase IMAP family member 1	CDS
Git1	ARF GTPase-activating protein GIT1	CDS
Gli2	GLI-Kruppel family member GLI2	3'UTR
Gli3	zinc finger protein GLI3	CDS
Gli3	zinc finger protein GLI3	5'UTR
Glt8d1	glycosyltransferase 8 domain-containing protein	5'UTR
Glud1	glutamate dehydrogenase 1, mitochondrial	5'UTR
Gm13476	hypothetical protein LOC433424 isoform 1	CDS
Gm347	hypothetical protein LOC241289	3'UTR
Gm4951	hypothetical protein LOC240327	CDS
Gm4980		CDS
Gm5151	hypothetical protein LOC381582	5'UTR
Gm52	envelope glycoprotein syncytin-A	CDS
Gm6320	hypothetical protein LOC622408	CDS
Gm6537		3'UTR
Gm7694		CDS
Gm98	myelin gene regulatory factor	CDS
Gm98	myelin gene regulatory factor	3'UTR
Gmip	GEM-interacting protein	CDS
Gnai1	guanine nucleotide binding protein, alpha	5'UTR
Gnao1	guanine nucleotide-binding protein G(o) subunit	CDS
Gnao1	guanine nucleotide-binding protein G(o) subunit	5'UTR
Gnas		5'UTR
Gnb5	guanine nucleotide-binding protein subunit	5'UTR
Got1	aspartate aminotransferase, cytoplasmic	5'UTR
Got2	aspartate aminotransferase, mitochondrial	5'UTR
Gpatch2	G patch domain-containing protein 2	3'UTR
Gpr133	probable G-protein coupled receptor 133	3'UTR
Gpr179	probable G-protein coupled receptor 179	CDS
Gpr25	probable G-protein coupled receptor 25	CDS
Gpr4	G-protein coupled receptor 4	CDS
Gpr83	probable G-protein coupled receptor 83	5'UTR
Gprc5c	G-protein coupled receptor family C group 5	CDS
Gprc5c	G-protein coupled receptor family C group 5	3'UTR
Gramd1b	GRAM domain-containing protein 1B	5'UTR
Grem1	gremlin-1 precursor	CDS
Grid2ip	delphinin isoform 1	3'UTR
Grik1	glutamate receptor, ionotropic kainate 1 isoform	5'UTR
Grik4	glutamate receptor, ionotropic kainate 4	CDS
Grin1	glutamate [NMDA] receptor subunit zeta-1 isoform	3'UTR
Grin1	glutamate [NMDA] receptor subunit zeta-1 isoform	5'UTR
Grin2d	glutamate [NMDA] receptor subunit epsilon-4	CDS
Grin2d	glutamate [NMDA] receptor subunit epsilon-4	3'UTR
Grk6	G protein-coupled receptor kinase 6 isoform b	3'UTR
Grm2	metabotropic glutamate receptor 2 precursor	CDS

Continued on next page

Table 6.3 – continued from previous page

Transcript Symbol	Transcript Name	Methylation site
Gse1	genetic suppressor element 1 isoform 2	CDS
Gse1	genetic suppressor element 1 isoform 2	5'UTR
Gstm1	glutathione S-transferase Mu 1	3'UTR
Gstt3	glutathione S-transferase, theta 3	3'UTR
Gtf2h2	general transcription factor IIH subunit 2	5'UTR
Gtf3c1	general transcription factor 3C polypeptide 1	CDS
Gtf3c1	general transcription factor 3C polypeptide 1	3'UTR
Gtf3c4	general transcription factor 3C polypeptide 4	5'UTR
Gucy1a2	guanylate cyclase 1, soluble, alpha 2	5'UTR
Gucy2e	guanylyl cyclase GC-E precursor	CDS
Gys1	glycogen [starch] synthase, muscle	CDS
H13	minor histocompatibility antigen H13 isoform 4	CDS
H2afy	core histone macro-H2A.1 isoform 1	3'UTR
H47	selenoprotein S	5'UTR
Hapl3	hyaluronan and proteoglycan link protein 3	CDS
Hcn3	potassium/sodium hyperpolarization-activated	CDS
Hcn3	potassium/sodium hyperpolarization-activated	5'UTR
Hcn4	potassium/sodium hyperpolarization-activated	CDS
Hdac7	histone deacetylase 7	3'UTR
Heatr5a	HEAT repeat-containing protein 5A	3'UTR
Hepacam	hepatocyte cell adhesion molecule precursor	3'UTR
Hes5	transcription factor HES-5	5'UTR
Hes6	transcription cofactor HES-6	CDS
Hexdc	hexosaminidase D isoform 1	CDS
Heyl	hairy/enhancer-of-split related with YRPW	3'UTR
Hgs	hepatocyte growth factor-regulated tyrosine	3'UTR
Hic1	hypermethylated in cancer 1 protein isoform 1	3'UTR
Hivep3	transcription factor HIVEP3	CDS
Hk1	hexokinase-1 isoform HK1	5'UTR
Hk2	hexokinase-2	3'UTR
Hnrnpd	heterogeneous nuclear ribonucleoprotein Do	5'UTR
Hnrnpu	heterogeneous nuclear ribonucleoprotein U	CDS
Hnrpdl	heterogeneous nuclear ribonucleoprotein D-like	5'UTR
Hnrpll	heterogeneous nuclear ribonucleoprotein L-like	5'UTR
Hook3	protein Hook homolog 3	5'UTR
Hpca	neuron-specific calcium-binding protein	5'UTR
Hpcal1	hippocalcin-like protein 1	CDS
Hps4	Hermansky-Pudlak syndrome 4 protein homolog	3'UTR
Hr	protein hairless	CDS
Hs2st1	heparan sulfate 2-O-sulfotransferase 1	5'UTR
Hs3st3a1	heparan sulfate glucosamine 3-O-sulfotransferase	5'UTR
Hsf1	heat shock factor protein 1	3'UTR
Hspa4	heat shock 70 kDa protein 4	5'UTR
Htr6	5-hydroxytryptamine receptor 6	CDS
Htt	huntingtin	CDS
Htt	huntingtin	3'UTR
Icam2	intercellular adhesion molecule 2 precursor	3'UTR
Icam4	intercellular adhesion molecule 4 precursor	CDS
Ick	serine/threonine-protein kinase ICK	CDS
Id4	DNA-binding protein inhibitor ID-4	5'UTR
Idh2	isocitrate dehydrogenase [NADP], mitochondrial	CDS
Idh3b	isocitrate dehydrogenase 3, beta subunit	5'UTR
Iffo2	intermediate filament family orphan 2	CDS
Iffo2	intermediate filament family orphan 2	3'UTR
Ifrd2	interferon-related developmental regulator 2	CDS
Igdec4	immunoglobulin superfamily DCC subclass member 4	CDS
Igf1r	insulin-like growth factor 1 receptor	5'UTR
Igf2r	cation-independent mannose-6-phosphate receptor	CDS
Igfbp4	insulin-like growth factor-binding protein 4	CDS
Igsf9b	immunoglobulin superfamily, member 9B isoform 1	5'UTR
Ikbkb	inhibitor of nuclear factor kappa-B kinase	CDS
Ikbkb	inhibitor of nuclear factor kappa-B kinase	3'UTR
Il12rb1	interleukin-12 receptor subunit beta-1	CDS
Il17rc	interleukin-17 receptor C precursor	CDS
Il6ra	interleukin-6 receptor subunit alpha precursor	3'UTR
Il6st	interleukin-6 receptor subunit beta precursor	5'UTR
Ildr1	immunoglobulin-like domain-containing receptor	CDS
Ildr2	Lisch-like	CDS
Impad1	inositol monophosphatase 3	5'UTR
Ina	alpha-internexin	3'UTR
Inha	inhibin alpha chain precursor	CDS
Inhbb	inhibin beta B chain precursor	5'UTR
Ino80d	INO80 complex subunit D isoform 1	3'UTR
Inpp1	inositol polyphosphate 1-phosphatase	5'UTR
Inpp4a	type I inositol-3,4-bisphosphate 4-phosphatase	5'UTR
Inpp5e	72 kDa inositol polyphosphate 5-phosphatase	3'UTR
Inpp5j	phosphatidylinositol 4,5-bisphosphate	CDS
Iqcd	IQ domain-containing protein D	CDS

Continued on next page

Table 6.3 – continued from previous page

Transcript Symbol	Transcript Name	Methylation site
Iqsec1	IQ motif and SEC7 domain-containing protein 1	5'UTR
Irf8	interferon regulatory factor 8	3'UTR
Irs4	insulin receptor substrate 4	CDS
Irx1	iroquois-class homeodomain protein IRX-1	CDS
Irx5	iroquois-class homeodomain protein IRX-5	CDS
Ism1	isthmin-1 precursor	5'UTR
Isoc2b	isochorismatase domain-containing protein 2B,	CDS
Isoc2b	isochorismatase domain-containing protein 2B,	3'UTR
Isy1	pre-mRNA-splicing factor ISY1 homolog	3'UTR
Itfg1	T-cell immunomodulatory protein precursor	5'UTR
Itfg3	protein ITFG3	3'UTR
Itga3	integrin alpha-3	5'UTR
Itga4	integrin alpha-4	3'UTR
Itgav	integrin alpha-V precursor	5'UTR
Its1	intersectin-1 isoform 2	3'UTR
Jam2	junctional adhesion molecule B precursor	5'UTR
Jmjd6	bifunctional arginine demethylase and	5'UTR
Jph4	junctophilin-4 isoform a	5'UTR
Kat2a	histone acetyltransferase KAT2A isoform b	CDS
Kcna6	potassium voltage-gated channel subfamily A	5'UTR
Kcnab1	voltage-gated potassium channel subunit beta-1	5'UTR
Kcnc1	potassium voltage-gated channel subfamily C	5'UTR
Kcnf1	potassium voltage-gated channel subfamily F	5'UTR
Kcng1	potassium voltage-gated channel subfamily G	CDS
Kcng4	potassium voltage-gated channel subfamily G	CDS
Kcnh4	potassium voltage-gated channel, subfamily H	3'UTR
Kcnj6	G protein-activated inward rectifier potassium	5'UTR
Kenk5	potassium channel subfamily K member 5	CDS
Kenk9	potassium channel subfamily K member 9	CDS
Kcnma1	calcium-activated potassium channel subunit	CDS
Kcnt1	potassium channel subfamily T member 1 isoform	CDS
Kctd13	BTB/POZ domain-containing adapter for	CDS
Kdelc1	KDEL motif-containing protein 1 precursor	CDS
Kdelr2	ER lumen protein retaining receptor 2	3'UTR
Kdm5c	lysine-specific demethylase 5C	3'UTR
Khsrp	far upstream element-binding protein 2	5'UTR
Kif1a	kinesin-like protein KIF1A isoform a	CDS
Kif26b	kinesin-like protein KIF26B	CDS
Kif7	kinesin family member 7	CDS
Kifap3	kinesin-associated protein 3	5'UTR
Klf12	Krueppel-like factor 12	3'UTR
Klf7	Krueppel-like factor 7	5'UTR
Klhdc2	kelch domain-containing protein 2	5'UTR
Klhdc8a	kelch domain-containing protein 8A	5'UTR
Klh6	kelch-like protein 6	CDS
Kndc1	protein very KIND	5'UTR
Kpnb1	importin subunit beta-1	5'UTR
Kri1	protein KRI1 homolog	CDS
Krt12	keratin, type I cytoskeletal 12	5'UTR
Krt20	keratin, type I cytoskeletal 20	CDS
Krt80	keratin, type II cytoskeletal 80	3'UTR
Ksr1	kinase suppressor of Ras 1	3'UTR
Ksr2	kinase suppressor of Ras 2 isoform 1	5'UTR
Ky	kyphoscoliosis peptidase	CDS
L1cam	neural cell adhesion molecule L1	CDS
Lancl3	lanC-like protein 3	5'UTR
Lasp1	LIM and SH3 domain protein 1	3'UTR
Lasp1	LIM and SH3 domain protein 1	5'UTR
Lass1	LAG1 longevity assurance homolog 1	CDS
Lass6	LAG1 longevity assurance homolog 6	5'UTR
Lbh	protein LBH	5'UTR
Ldhd	probable D-lactate dehydrogenase, mitochondrial	CDS
Ldoc1	protein LDOC1L	5'UTR
Leng8	leukocyte receptor cluster member 8 homolog	CDS
Lgals3bp	galectin-3-binding protein precursor	CDS
Lgmn	legumain precursor	CDS
Lhfp14	lipoma HMGIC fusion partner-like 4 protein	5'UTR
Lhfp15	tetraspan membrane protein of hair cell	5'UTR
Lhx1	LIM/homeobox protein Lhx1	5'UTR
Lhx5	LIM/homeobox protein Lhx5	3'UTR
Lipe	hormone-sensitive lipase isoform 2	CDS
Lipg	endothelial lipase precursor	3'UTR
Lmln	leishmanolysin-like peptidase	3'UTR
Lmna	prelamin-A/C isoform C2	5'UTR
Lmo4	LIM domain transcription factor LMO4	5'UTR
Lmtk2	serine/threonine-protein kinase LMTK2 precursor	3'UTR
Lpcat4	lysophospholipid acyltransferase LPCAT4	3'UTR
Lpin2	phosphatidate phosphatase LPIN2 isoform 1	CDS

Continued on next page

Table 6.3 – continued from previous page

Transcript Symbol	Transcript Name	Methylation site
Lrfn1	leucine-rich repeat and fibronectin type III	3'UTR
Lrfn5	leucine-rich repeat and fibronectin type-III	5'UTR
Lrp3	low density lipoprotein receptor-related protein	3'UTR
Lrp4	low-density lipoprotein receptor-related protein	CDS
Lrp5	low-density lipoprotein receptor-related protein	CDS
Lrrc14	leucine-rich repeat-containing protein 14	5'UTR
Lrrc25	leucine-rich repeat-containing protein 25	CDS
Lrrc26	leucine-rich repeat-containing protein 26	CDS
Lrrc32	leucine rich repeat containing 32	CDS
Lrrc38	leucine-rich repeat-containing protein 38	CDS
Lrrc68	leucine-rich repeat-containing protein 68	5'UTR
Lrrc8b	leucine-rich repeat-containing protein 8B	3'UTR
Lrrfip1	leucine-rich repeat flightless-interacting	CDS
Lrsam1	E3 ubiquitin-protein ligase LRSAM1	CDS
Lxn	latexin	5'UTR
Ly6g6f	lymphocyte antigen 6 complex, locus G6F	3'UTR
Ly6h	lymphocyte antigen 6H isoform b	5'UTR
Lyst	lysosomal-trafficking regulator	3'UTR
Mab21l2	protein mab-21-like 2	CDS
Madd	MAP kinase-activating death domain protein	CDS
Madd	MAP kinase-activating death domain protein	3'UTR
Maf	transcription factor Maf	5'UTR
Maged1	melanoma-associated antigen D1	CDS
Mageh1	melanoma-associated antigen H1	5'UTR
Man1b1	mannosidase, alpha, class 1B, member 1	CDS
Man1c1	mannosidase, alpha, class 1C, member 1	CDS
Man1c1	mannosidase, alpha, class 1C, member 1	3'UTR
Map3k6	mitogen-activated protein kinase kinase kinase	5'UTR
Map3k9	mitogen-activated protein kinase kinase kinase 9	3'UTR
Map6d1	MAP6 domain-containing protein 1	CDS
Mapk8ip2	C-Jun-amino-terminal kinase-interacting protein	5'UTR
Mapk8ip3	C-Jun-amino-terminal kinase-interacting protein	3'UTR
Mapkbp1	mitogen-activated protein kinase-binding protein	CDS
Mapre2	microtubule-associated protein RP/EB family	5'UTR
March4	E3 ubiquitin-protein ligase MARCH4 precursor	CDS
Marcks1	MARCKS-related protein	3'UTR
Mark2	serine/threonine-protein kinase MARK2 isoform 4	5'UTR
Mavs	mitochondrial antiviral-signaling protein	CDS
Mboat7	lysophospholipid acyltransferase 7	CDS
Mboat7	lysophospholipid acyltransferase 7	5'UTR
Mc3r	melanocortin receptor 3	3'UTR
Mcc	mutated in colorectal cancers isoform 1	3'UTR
Mchr1	melanin-concentrating hormone receptor 1	5'UTR
Mcm6	DNA replication licensing factor MCM6	CDS
Mdga1	MAM domain-containing	5'UTR
Med23	mediator of RNA polymerase II transcription	3'UTR
Med26	mediator of RNA polymerase II transcription	3'UTR
Mef2d	myocyte-specific enhancer factor 2D	CDS
Megf9	multiple epidermal growth factor-like domains	5'UTR
Mepece	7SK snRNA methylphosphate capping enzyme	5'UTR
Mettl14	methyltransferase-like protein 14	3'UTR
Mettl3	N6-adenosine-methyltransferase 70 kDa subunit	CDS
Mfap3l	microfibrillar-associated protein 3-like	5'UTR
Mfge8	lactadherin isoform 2	3'UTR
Mfsd6	major facilitator superfamily domain-containing	5'UTR
Mgat4b	alpha-1,3-mannosyl-glycoprotein	3'UTR
Mgat5b	alpha-1,6-mannosylglycoprotein	CDS
Mgrn1	E3 ubiquitin-protein ligase MGRN1	3'UTR
Mib2	E3 ubiquitin-protein ligase MIB2	3'UTR
Mib2	E3 ubiquitin-protein ligase MIB2	5'UTR
Mical2	protein MICAL-2 isoform B	CDS
Mid1	midline-1	CDS
Mid1	midline-1	3'UTR
Midn	midnolin	CDS
Midn	midnolin	5'UTR
Mif4gd	MIF4G domain-containing protein	5'UTR
Minpp1	multiple inositol polyphosphate phosphatase 1	5'UTR
Mlf2	myeloid leukemia factor 2	3'UTR
Mlf2	myeloid leukemia factor 2	5'UTR
Mlxip	MLX-interacting protein isoform 1	CDS
Mmp14	matrix metalloproteinase-14	3'UTR
Mmp15	matrix metalloproteinase-15 precursor	CDS
Mmp28	matrix metalloproteinase-28 isoform 2	3'UTR
Mmrn2	multimerin-2 precursor	3'UTR
Mn1	probable tumor suppressor protein MN1	3'UTR
Mnt	max-binding protein MNT	CDS
Mobkl2b	mps one binder kinase activator-like 2B	3'UTR
Mospd4	motile sperm domain containing 4	CDS

Continued on next page

Table 6.3 – continued from previous page

Transcript Symbol	Transcript Name	Methylation site
Mprlp	myosin phosphatase Rho-interacting protein	3'UTR
Mrgprf	mas-related G-protein coupled receptor member F	3'UTR
Mrpl4	39S ribosomal protein L4, mitochondrial	3'UTR
Mrpl46	39S ribosomal protein L46, mitochondrial	3'UTR
Mrps11	28S ribosomal protein S11, mitochondrial	3'UTR
Mrv11	protein MRV11 isoform a	CDS
Msl1	male-specific lethal 1 homolog	5'UTR
Mtap1a	microtubule-associated protein 1A isoform 2	5'UTR
Mtap1b	microtubule-associated protein 1B	5'UTR
Mtap2	microtubule-associated protein 2 isoform 2	CDS
Mtap7d1	MAP7 domain-containing protein 1 isoform 2	CDS
Mtdh	protein LYRIC	5'UTR
Mtfp1		5'UTR
Mtmr11	myotubularin-related protein 11	3'UTR
Mto1	protein MTO1 homolog, mitochondrial precursor	5'UTR
Mtus2	microtubule-associated tumor suppressor	3'UTR
Mycl1	protein L-Myc-1	5'UTR
Myh14	myosin-14	CDS
Myh7b	myosin-7B	CDS
Myh9	myosin-9 isoform 1	3'UTR
Myo16	myosin-XVI	CDS
Myo1d	myosin-Id	3'UTR
Myo1d	myosin-Id	5'UTR
Myo5b	myosin-Vb	CDS
Myst2	histone acetyltransferase MYST2 isoform 3	5'UTR
N28178	hypothetical protein LOC230085	CDS
Naf1	H/ACA ribonucleoprotein complex non-core subunit	5'UTR
Nagpa		CDS
Nat6	N-acetyltransferase 6	5'UTR
Nav2	neuron navigator 2 isoform 1	5'UTR
Ncam1	neural cell adhesion molecule 1 isoform 3	CDS
Ncdn	neurochondrin	3'UTR
Ncdn	neurochondrin	5'UTR
Nckap5	Nck-associated protein 5 isoform 2	CDS
Nckap5	Nck-associated protein 5 isoform 2	3'UTR
Nckap5l	nck-associated protein 5-like	CDS
Nckap5l	nck-associated protein 5-like	3'UTR
Ncor2	nuclear receptor corepressor 2	CDS
Ndel1	nuclear distribution protein nudeE-like 1	3'UTR
Ndfip2	NEED4 family-interacting protein 2	CDS
Ndrp1	protein NDRG1	5'UTR
Ndrp3	protein NDRG3 isoform 1	3'UTR
Ndufb10	NADH dehydrogenase [ubiquinone] 1 beta	5'UTR
Ndufv1	NADH dehydrogenase [ubiquinone] flavoprotein 1,	CDS
Neb1	nebulin	5'UTR
Nefl	neurofilament light polypeptide	5'UTR
Nefm	neurofilament medium polypeptide	5'UTR
Nek11	serine/threonine-protein kinase Nek11	3'UTR
Neo1	neogenin isoform 2	5'UTR
Nf1	neurofibromin	CDS
Nfam1	NFAT activation molecule 1	3'UTR
Nfat5	nuclear factor of activated T-cells 5 isoform a	CDS
Nfat5	nuclear factor of activated T-cells 5 isoform a	5'UTR
Nfatc2	nuclear factor of activated T-cells, cytoplasmic	3'UTR
Nfkbib	NF-kappa-B inhibitor beta	3'UTR
Ngef	ephexin-1 isoform 1	3'UTR
Nhlrc1	E3 ubiquitin-protein ligase NHLRC1	5'UTR
Nhsl2	NHS-like protein 2	CDS
Nid2	nidogen-2 precursor	CDS
Nipal3	NIPA-like protein 3	CDS
Nkain2	sodium/potassium-transporting ATPase subunit	5'UTR
Nkd1	protein naked cuticle homolog 1 isoform 2	CDS
Nkpd1	NTPase KAP family P-loop domain-containing	CDS
Nktr	NK-tumor recognition protein	3'UTR
Nkx2-1	homeobox protein Nkx-2.1	CDS
Nkx2-1	homeobox protein Nkx-2.1	3'UTR
Nkx2-2	homeobox protein Nkx-2.2 isoform 1	CDS
Nkx2-9	homeobox protein Nkx-2.8	CDS
Nkx2-9	homeobox protein Nkx-2.8	3'UTR
Nlrp1	NLR family member X1 precursor	3'UTR
Nnat	neuronatin isoform beta	5'UTR
Nod1	nucleotide-binding oligomerization	3'UTR
Nog	noggin precursor	5'UTR
Nosip	nitric oxide synthase-interacting protein	3'UTR
Notch1	neurogenic locus notch homolog protein 1	CDS
Notch2	neurogenic locus notch homolog protein 2	CDS
Npas1	neuronal PAS domain-containing protein 1	CDS
Npas4	neuronal PAS domain-containing protein 4	5'UTR

Continued on next page

Table 6.3 – continued from previous page

Transcript Symbol	Transcript Name	Methylation site
Npc1	Niemann-Pick C1 protein	CDS
Npc2	epididymal secretory protein E1 precursor	CDS
Nploc4	nuclear protein localization protein 4 homolog	5'UTR
Npr1	atrial natriuretic peptide receptor 1 precursor	CDS
Npr3	atrial natriuretic peptide receptor 3 isoform b	CDS
Nptx1	neuronal pentraxin-1 precursor	CDS
Nptx1	neuronal pentraxin-1 precursor	3'UTR
Nptx1	neuronal pentraxin-1 precursor	5'UTR
Nptx2	neuronal pentraxin-2 precursor	3'UTR
Nptxr	neuronal pentraxin receptor	CDS
Npy2r	neuropeptide Y receptor type 2	5'UTR
Nr1d1	nuclear receptor subfamily 1 group D member 1	CDS
Nr1h2	oxysterols receptor LXR-beta	CDS
Nr4a1	nuclear receptor subfamily 4 group A member 1	5'UTR
Nrgn	neurogranin	CDS
Nrip1	nuclear receptor-interacting protein 1	5'UTR
Nsun4	putative methyltransferase NSUN4	CDS
Nsun7	putative methyltransferase NSUN7	CDS
Ntn3	netrin-3 precursor	3'UTR
Ntn3	netrin-3 precursor	5'UTR
Ntsr1	neurotensin receptor type 1	CDS
Ntsr1	neurotensin receptor type 1	3'UTR
Nuak2	NUAK family SNF1-like kinase 2 isoform B	CDS
Nudcd2	nudC domain-containing protein 2	CDS
Nudt10	diphosphoinositol polyphosphate phosphohydrolase	5'UTR
Nup210	nuclear pore membrane glycoprotein 210	3'UTR
Nup214	nuclear pore complex protein Nup214	CDS
Nup62-il4i1	Nup62-Il4i1 protein	5'UTR
Nyx	nyctalopin precursor	CDS
Oaf	out at first protein homolog precursor	5'UTR
Omp	olfactory marker protein	CDS
ORF19	WAS protein family homolog 1	CDS
ORF61	membralin	CDS
Oscar	osteoclast-associated immunoglobulin-like	CDS
Oscar	osteoclast-associated immunoglobulin-like	3'UTR
Ostm1	osteopetrosis-associated transmembrane protein 1	CDS
Otud5	OTU domain-containing protein 5	CDS
Otud5	OTU domain-containing protein 5	5'UTR
Ovgp1	oviduct-specific glycoprotein precursor	CDS
Oxa1l	mitochondrial inner membrane protein OXA1L	CDS
Pacsin1	protein kinase C and casein kinase substrate in	5'UTR
Pafah1b2	platelet-activating factor acetylhydrolase IB	5'UTR
Palb2	partner and localizer of BRCA2	CDS
Papd7	DNA polymerase sigma isoform 2	5'UTR
Paqr9	progesterin and adipoQ receptor family member 9	CDS
Parm1	prostate androgen-regulated mucin-like protein 1	CDS
Parp10	poly (ADP-ribose) polymerase family, member 10	CDS
Parp10	poly (ADP-ribose) polymerase family, member 10	3'UTR
Pbx3	pre-B-cell leukemia transcription factor 3	CDS
Pcbp1	poly(rC)-binding protein 1	5'UTR
Pcdh19	protocadherin-19 isoform a	5'UTR
Pcdh8	protocadherin 8 isoform 2 precursor	5'UTR
Pcdha2	protocadherin alpha 2	3'UTR
Pcdhga8	protocadherin gamma subfamily A, 8	5'UTR
Pcdhgb5	protocadherin gamma-B5	CDS
Pcgf2	polycomb group RING finger protein 2	CDS
Pcgf6	polycomb group RING finger protein 6	CDS
Pcid2	PCI domain-containing protein 2	3'UTR
Pcif1	phosphorylated CTD-interacting factor 1	CDS
Pelo	protein piccolo isoform 2	5'UTR
Pcsk1n	proSAAS	CDS
Pcsk1n	proSAAS	3'UTR
Pcsk7	proprotein convertase subtilisin/kexin type 7	5'UTR
Pdcd11	protein RRP5 homolog	3'UTR
Pdcd2	programmed cell death protein 2	5'UTR
Pde1b	calcium/calmodulin-dependent 3',5'-cyclic	5'UTR
Pde4a	cAMP-specific 3',5'-cyclic phosphodiesterase 4A	3'UTR
Pde4c	cAMP-specific 3',5'-cyclic phosphodiesterase 4C	3'UTR
Pdgfb	platelet-derived growth factor subunit B	5'UTR
Pdpk1	3-phosphoinositide-dependent protein kinase 1	5'UTR
Pdxk	pyridoxal kinase	5'UTR
Peg3	paternally expressed 3	5'UTR
Per2	period circadian protein homolog 2	CDS
Per3	period circadian protein homolog 3	CDS
Pex14	peroxisomal membrane protein PEX14	3'UTR
Pfk1	6-phosphofructokinase, liver type	3'UTR
Pgm2	phosphoglucomutase-1	5'UTR
Pgm2l1	glucose 1,6-bisphosphate synthase	5'UTR

Continued on next page

Table 6.3 – continued from previous page

Transcript Symbol	Transcript Name	Methylation site
Pgrmc1	membrane-associated progesterone receptor	5'UTR
Phb2	prohibitin-2	5'UTR
Phf12	PHD finger protein 12	5'UTR
Phf2	PHD finger protein 2	CDS
Phf2	PHD finger protein 2	3'UTR
Phkb	phosphorylase b kinase regulatory subunit beta	5'UTR
Phlpp1	PH domain leucine-rich repeat-containing protein	5'UTR
Pi4kb	phosphatidylinositol 4-kinase beta	5'UTR
Pias3	E3 SUMO-protein ligase PIAS3 isoform 3	CDS
Picalm	phosphatidylinositol-binding clathrin assembly	5'UTR
Pigb	GPI mannosyltransferase 3	CDS
Pigo	GPI ethanolamine phosphate transferase 3	CDS
Pigv	GPI mannosyltransferase 2 isoform 3	5'UTR
Pigz	GPI mannosyltransferase 4	CDS
Pih1d1	PIH1 domain-containing protein 1	5'UTR
Pik3c2b	phosphoinositide-3-kinase, class 2 beta	3'UTR
Pik3cg	phosphatidylinositol-4,5-bisphosphate 3-kinase	CDS
Pik3r5	phosphoinositide 3-kinase regulatory subunit 5	CDS
Pip4k2c	phosphatidylinositol-5-phosphate 4-kinase type-2	CDS
Pkmyt1	membrane-associated tyrosine- and	CDS
Plagl2	zinc finger protein PLAGL2	CDS
Plagl2	zinc finger protein PLAGL2	3'UTR
Plbd2	putative phospholipase B-like 2	3'UTR
Plcb1	1-phosphatidylinositol-4,5-bisphosphate	5'UTR
Plcb3	1-phosphatidylinositol-4,5-bisphosphate	CDS
Pld3	phospholipase D3	3'UTR
Pld4	phospholipase D4	CDS
Plekha7	pleckstrin homology domain-containing family A	3'UTR
Plekhj1	pleckstrin homology domain-containing family J	5'UTR
Plekhm1	pleckstrin homology domain-containing family M	3'UTR
Plekhm2	pleckstrin homology domain-containing family M	3'UTR
Plod3	procollagen-lysine,2-oxoglutarate 5-dioxygenase	5'UTR
Plxdc1	plexin domain-containing protein 1 isoform 1	CDS
Plxna4	plexin-A4 precursor	5'UTR
Plxnb2	plexin B2	CDS
Plxnb3	plexin-B3	CDS
Plxnc1	plexin-C1 precursor	CDS
Plxnd1	plexin D1	CDS
Plxnd1	plexin D1	3'UTR
Pm2od2		5'UTR
Pnkd	probable hydrolase PNKD isoform 1	3'UTR
Pnma1	paraneoplastic antigen Ma1 homolog	5'UTR
Podxl2	podocalyxin-like protein 2	3'UTR
Pogk	pogo transposable element with KRAB domain	5'UTR
Polr1a	DNA-directed RNA polymerase I subunit RPA1	3'UTR
Polr2f	DNA-directed RNA polymerases I, II, and III	CDS
Polr3d	DNA-directed RNA polymerase III subunit RPC4	CDS
Pom121	nuclear envelope pore membrane protein POM 121	CDS
Pom121	nuclear envelope pore membrane protein POM 121	3'UTR
Pou2f1	POU domain, class 2, transcription factor 1	CDS
Pou2f2	POU domain, class 2, transcription factor 2	3'UTR
Pou6f1	POU domain, class 6, transcription factor 1	5'UTR
Ppap2b	lipid phosphate phosphohydrolase 3	3'UTR
Ppapdc3	probable lipid phosphate phosphatase PPAPDC3	CDS
Ppard	peroxisome proliferator-activated receptor	CDS
Ppard	peroxisome proliferator-activated receptor	3'UTR
Ppfia4	liprin-alpha-4	5'UTR
Ppil2	peptidyl-prolyl cis-trans isomerase-like 2	CDS
Ppm1l	protein phosphatase 1L	CDS
Ppm1l	protein phosphatase 1L	5'UTR
Ppp1r10	serine/threonine-protein phosphatase 1	CDS
Ppp1r15b	protein phosphatase 1 regulatory subunit 15B	5'UTR
Ppp1r1a	protein phosphatase 1 regulatory subunit 1A	5'UTR
Ppp5c	serine/threonine-protein phosphatase 5	CDS
Prdm8	PR domain zinc finger protein 8	CDS
Prelp	prolargin precursor	CDS
Prelp	prolargin precursor	3'UTR
Prickle2	prickle-like protein 2 isoform b	5'UTR
Prkar2b	cAMP-dependent protein kinase type II-beta	3'UTR
Prkca	protein kinase C alpha type	5'UTR
Prmt5	protein arginine N-methyltransferase 5	CDS
Prox1	prospero homeobox protein 1	3'UTR
Prpf8	pre-mRNA-processing-splicing factor 8	5'UTR
Prps2	ribose-phosphate pyrophosphokinase 2	5'UTR
Prr12	proline rich 12	3'UTR
Prr22		CDS
Prr3	proline-rich protein 3 isoform b	3'UTR
Prrt2	proline-rich transmembrane protein 2	5'UTR

Continued on next page

Table 6.3 – continued from previous page

Transcript Symbol	Transcript Name	Methylation site
Prrt4	proline-rich transmembrane protein 4	CDS
Prrx1	paired mesoderm homeobox protein 1 isoform b	CDS
Psap	sulfated glycoprotein 1 isoform D preproprotein	5'UTR
Psd	PH and SEC7 domain-containing protein 1	CDS
Psd2	PH and SEC7 domain-containing protein 2	5'UTR
Psen1	presenilin-1	CDS
Pskh1	serine/threonine-protein kinase H1	3'UTR
Psmf1	proteasome inhibitor PI31 subunit	3'UTR
Pth2r	parathyroid hormone 2 receptor precursor	CDS
Ptk7	tyrosine-protein kinase-like 7 precursor	3'UTR
Ptms	parathyrosin	5'UTR
Ptp4a3	protein tyrosine phosphatase type IVA 3 isoform	CDS
Ptplb	3-hydroxyacyl-CoA dehydratase 2	CDS
Ptpmt1	protein-tyrosine phosphatase mitochondrial 1	5'UTR
Ptpn21	tyrosine-protein phosphatase non-receptor type	3'UTR
Ptpn23	tyrosine-protein phosphatase non-receptor type	CDS
Ptpn5	tyrosine-protein phosphatase non-receptor type	CDS
Ptpnm	receptor-type tyrosine-protein phosphatase mu	5'UTR
Ptpro	protein tyrosine phosphatase, receptor type, O	CDS
Ptpro	protein tyrosine phosphatase, receptor type, O	5'UTR
Ptprs	receptor-type tyrosine-protein phosphatase S	3'UTR
Ptprz1	receptor-type tyrosine-protein phosphatase zeta	5'UTR
Ptrf	polymerase I and transcript release factor	3'UTR
Pum1	pumilio homolog 1 isoform 2	3'UTR
Pvrl2	poliovirus receptor-related protein 2 isoform 2	CDS
Pvrl2	poliovirus receptor-related protein 2 isoform 2	5'UTR
Pxdn	peroxidasin homolog precursor	CDS
Pxn	paxillin isoform alpha	3'UTR
Pycard	apoptosis-associated speck-like protein	CDS
Pygb	glycogen phosphorylase, brain form	5'UTR
Pygo1	pygopus homolog 1	5'UTR
Pygo2	pygopus homolog 2	CDS
Qprt	nicotinate-nucleotide pyrophosphorylase	CDS
R3hdm2	R3H domain-containing protein 2 isoform 2	3'UTR
Rab10	ras-related protein Rab-10	CDS
Rab11b	ras-related protein Rab-11B	5'UTR
Rab11fip1	rab11 family-interacting protein 1 isoform 1	CDS
Rab11fip1	rab11 family-interacting protein 1 isoform 1	3'UTR
Rab14	ras-related protein Rab-14	5'UTR
Rab3a	ras-related protein Rab-3A	5'UTR
Rab3il1	guanine nucleotide exchange factor for Rab-3A	5'UTR
Rad23b	UV excision repair protein RAD23 homolog B	5'UTR
Rad50	DNA repair protein RAD50	3'UTR
Rad51l3	DNA repair protein RAD51 homolog 4	CDS
Radil	ras-associating and dilute domain-containing	CDS
Rai1	retinoic acid-induced protein 1	3'UTR
Ramp3	receptor activity-modifying protein 3 precursor	3'UTR
Rap1gap2	rap1 GTPase-activating protein 2	3'UTR
Rapgef1l	rap guanine nucleotide exchange factor-like 1	3'UTR
Rapgef1l	rap guanine nucleotide exchange factor-like 1	5'UTR
Rara	retinoic acid receptor alpha isoform 1	CDS
Rara	retinoic acid receptor alpha isoform 1	5'UTR
Rarg	retinoic acid receptor gamma isoform 2	3'UTR
Rasa3	ras GTPase-activating protein 3	3'UTR
Rasa1l	rasGAP-activating-like protein 1	CDS
Rasgrf1	ras-specific guanine nucleotide-releasing factor	5'UTR
Ras10b	ras-like protein family member 10B precursor	CDS
Ras11b	ras-like protein family member 11B	5'UTR
Ras12	ras-like protein family member 12 isoform 1	3'UTR
Rassf5	ras association domain-containing protein 5	3'UTR
Raver1	ribonucleoprotein PTB-binding 1	3'UTR
Rbfox1	fox-1 homolog A isoform alpha	5'UTR
Rbfox3		CDS
Rbm20	probable RNA-binding protein 20	CDS
Rbm20	probable RNA-binding protein 20	3'UTR
Rbm24	RNA-binding protein 24	5'UTR
Rbm42	RNA-binding protein 42	CDS
Rbm45	RNA-binding protein 45	5'UTR
Rbp1	retinol-binding protein 1	CDS
Rcc1	regulator of chromosome condensation isoform 2	3'UTR
Rcn2	reticulocalbin-2 precursor	5'UTR
Reep6	receptor expression-enhancing protein 6	3'UTR
Rela	transcription factor p65	3'UTR
Rere	arginine-glutamic acid dipeptide repeats	3'UTR
Rfx7	regulatory factor X domain containing 2	5'UTR
Rgag4		5'UTR
Rgl2	ral guanine nucleotide dissociation	5'UTR
Rgma	repulsive guidance molecule A precursor	3'UTR

Continued on next page

Table 6.3 – continued from previous page

Transcript Symbol	Transcript Name	Methylation site
Rimklb	ribosomal protein S6 modification-like protein	5'UTR
Rims4	regulating synaptic membrane exocytosis protein	CDS
Rin1	ras and Rab interactor 1	CDS
Ring1	E3 ubiquitin-protein ligase RING1	5'UTR
Rnaseh1	ribonuclease H1	3'UTR
Rnaseh2a	ribonuclease H2 subunit A	CDS
Rnase1	2-5A-dependent ribonuclease	3'UTR
Rnf103	E3 ubiquitin-protein ligase RNF103	5'UTR
Rnf152	RING finger protein 152	5'UTR
Rnf165	ring finger protein 165	3'UTR
Rnf214	RING finger protein 214	5'UTR
Rnf220	E3 ubiquitin-protein ligase Rnf220	3'UTR
Rnf39	ring finger protein 39	CDS
Rnf43	RING finger protein 43 precursor	CDS
Rnpc3	RNA-binding protein 40	5'UTR
Rnps1	RNA-binding protein with serine-rich domain 1	5'UTR
Rom01	reactive oxygen species modulator 1	CDS
Rpgrip1	X-linked retinitis pigmentosa GTPase	3'UTR
Rpn2	dolichyl-diphosphooligosaccharide-protein	5'UTR
Rprd1a	regulation of nuclear pre-mRNA domain-containing	5'UTR
Rps6ka1	ribosomal protein S6 kinase alpha-1	CDS
Rreb1		3'UTR
Rsad2	radical S-adenosyl methionine domain-containing	3'UTR
Rtn4rl2	reticulon-4 receptor-like 2 precursor	CDS
Runx2	runt-related transcription factor 2 isoform type	5'UTR
Rxrb	retinoic acid receptor RXR-beta	5'UTR
Ryr1	ryanodine receptor 1, skeletal muscle	CDS
S1pr2	sphingosine 1-phosphate receptor 2	CDS
S1pr4	sphingosine 1-phosphate receptor 4	CDS
Safb	scaffold attachment factor B	CDS
Sall3	sal-like protein 3	CDS
Samd14	sterile alpha motif domain-containing protein 14	5'UTR
Samd4b	protein Smaug homolog 2	CDS
Samd4b	protein Smaug homolog 2	3'UTR
Samhd1	SAM domain and HD domain-containing protein 1	CDS
Samhd1	SAM domain and HD domain-containing protein 1	3'UTR
Sarm1	sterile alpha and TIR motif-containing protein 1	CDS
Sart1	U4/U6.U5 tri-snRNP-associated protein 1	CDS
Sash3	SAM and SH3 domain-containing protein 3	3'UTR
Satb2	DNA-binding protein SATB2	3'UTR
Sbn02	protein strawberry notch homolog 2	CDS
Scarb1	scavenger receptor class B member 1	CDS
Scarf1	scavenger receptor class F, member 1	CDS
Scarf2	scavenger receptor class F member 2 precursor	CDS
Scd2	acyl-CoA desaturase 2	CDS
Scg3	secretogranin-3 isoform 2 precursor	5'UTR
Scn3b	sodium channel subunit beta-3 precursor	5'UTR
Scn5a	sodium channel protein type 5 subunit alpha	3'UTR
Scrt2	transcriptional repressor scratch 2	CDS
Sdc4	syndecan-4 precursor	CDS
Sdf2	stromal cell-derived factor 2	5'UTR
Sdhk	succinate dehydrogenase [ubiquinone]	CDS
Sdk2	protein sidekick-2 precursor	CDS
Sdr39u1	epimerase family protein SDR39U1	3'UTR
Sec1	galactoside 2-alpha-L-fucosyltransferase 3	CDS
Sec24b	protein transport protein Sec24B	CDS
Sec31a	protein transport protein Sec31A	3'UTR
Sec61a1	protein transport protein Sec61 subunit alpha	5'UTR
Sel1l	protein sel-1 homolog 1 isoform b	5'UTR
Sema6a	semaphorin-6A precursor	3'UTR
Sema6a	semaphorin-6A precursor	5'UTR
Sema6c	semaphorin-6C precursor	CDS
Sema6c	semaphorin-6C precursor	3'UTR
Sema6d	semaphorin-6D isoform 4	5'UTR
Sept5	septin-5	CDS
Sept6	septin-6 isoform 3	5'UTR
Sept9	septin-9 isoform a	CDS
Serhl	serine hydrolase-like protein	CDS
Serpinh1	serpin H1 precursor	CDS
Serpini1	neuroserpin precursor	5'UTR
Sesn3	sestrin-3	CDS
Sestd1	SEC14 domain and spectrin repeat-containing	CDS
Setd1a	SET domain containing 1A	CDS
Setd4	SET domain-containing protein 4	CDS
Sez6l	seizure 6-like protein	CDS
Sez6l	seizure 6-like protein	5'UTR
Sf1	splicing factor 1 isoform 2	CDS
Sfi1	protein SFI1 homolog	CDS

Continued on next page

Table 6.3 – continued from previous page

Transcript Symbol	Transcript Name	Methylation site
Sfmbt1	scm-like with four MBT domains protein 1	5'UTR
Sfn	14-3-3 protein sigma	5'UTR
Sfpi1	transcription factor PU.1	3'UTR
Sfrp2	secreted frizzled-related protein 2 precursor	CDS
Sfswap	splicing factor, arginine/serine-rich 8	CDS
Sgpl1	sphingosine-1-phosphate lyase 1	5'UTR
Sgsh	N-sulfoglucosamine sulfohydrolase	3'UTR
Sgsm1	small G protein signaling modulator 1 isoform a	CDS
Sh3bp1	SH3 domain-binding protein 1	5'UTR
Sh3bp5	SH3 domain-binding protein 5	5'UTR
Sh3rf2	putative E3 ubiquitin-protein ligase SH3RF2	CDS
Sh3rf3	SH3 domain-containing RING finger protein 3	3'UTR
Shank2	SH3 and multiple ankyrin repeat domains protein	3'UTR
Shank3	SH3 and multiple ankyrin repeat domains protein	3'UTR
Shb	SH2 domain-containing adapter protein B	CDS
Shb	SH2 domain-containing adapter protein B	5'UTR
Shh	sonic hedgehog protein precursor	CDS
Shisa6	protein shisa-6 homolog precursor	3'UTR
Shisa7	protein shisa-7 precursor	CDS
Shmt1	serine hydroxymethyltransferase, cytosolic	3'UTR
Shpk	sedoheptulokinase	CDS
Shroom3	protein Shroom3 isoform 2	CDS
Shroom4	protein Shroom4	CDS
Siah3	seven in absentia homolog 3	CDS
Sidt2	SID1 transmembrane family member 2 precursor	3'UTR
Sipa11	signal-induced proliferation-associated 1-like	3'UTR
Sipa12	signal-induced proliferation-associated 1-like	3'UTR
Sipa13	signal-induced proliferation-associated 1-like	3'UTR
Slain1	SLAIN motif-containing protein 1	CDS
Slamf9	SLAM family member 9 precursor	CDS
Slamf9	SLAM family member 9 precursor	3'UTR
Slc10a4	sodium/bile acid cotransporter 4	5'UTR
Slc12a7	solute carrier family 12 member 7	3'UTR
Slc12a8	solute carrier family 12 member 8 isoform 2	CDS
Slc13a5	solute carrier family 13 member 5	3'UTR
Slc15a3	solute carrier family 15 member 3	CDS
Slc16a1	monocarboxylate transporter 1	5'UTR
Slc16a13	monocarboxylate transporter 13	CDS
Slc16a6	monocarboxylate transporter 7 isoform b	3'UTR
Slc17a7	vesicular glutamate transporter 1	3'UTR
Slc18a3	vesicular acetylcholine transporter	CDS
Slc1a1	excitatory amino acid transporter 3	5'UTR
Slc1a2	excitatory amino acid transporter 2 isoform 3	CDS
Slc1a2	excitatory amino acid transporter 2 isoform 3	5'UTR
Slc1a4	neutral amino acid transporter A	CDS
Slc22a15	solute carrier family 22 member 15	5'UTR
Slc22a17	solute carrier family 22 member 17	5'UTR
Slc22a23	solute carrier family 22 member 23	5'UTR
Slc22a4	solute carrier family 22 member 4	CDS
Slc24a4	sodium/potassium/calcium exchanger 4 precursor	5'UTR
Slc25a30	kidney mitochondrial carrier protein 1	3'UTR
Slc25a42	solute carrier family 25 member 42	3'UTR
Slc26a4	pendrin	5'UTR
Slc27a1	long-chain fatty acid transport protein 1	5'UTR
Slc27a4	long-chain fatty acid transport protein 4	CDS
Slc29a2	equilibrative nucleoside transporter 2	3'UTR
Slc29a3	equilibrative nucleoside transporter 3	CDS
Slc2a5	solute carrier family 2, facilitated glucose	5'UTR
Slc30a3	zinc transporter 3	3'UTR
Slc35c1	GDP-fucose transporter 1 isoform 1	CDS
Slc35c1	GDP-fucose transporter 1 isoform 1	5'UTR
Slc36a1	proton-coupled amino acid transporter 1	5'UTR
Slc39a6	zinc transporter ZIP6 precursor	5'UTR
Slc43a2	large neutral amino acids transporter small	CDS
Slc43a2	large neutral amino acids transporter small	5'UTR
Slc6a1	sodium- and chloride-dependent GABA transporter	CDS
Slc6a1	sodium- and chloride-dependent GABA transporter	3'UTR
Slc6a11	sodium- and chloride-dependent GABA transporter	CDS
Slc6a11	sodium- and chloride-dependent GABA transporter	3'UTR
Slc6a12	sodium- and chloride-dependent betaine	3'UTR
Slc6a17	orphan sodium- and chloride-dependent	5'UTR
Slc6a20a	sodium- and chloride-dependent transporter	3'UTR
Slc6a5	sodium- and chloride-dependent glycine	CDS
Slc7a1	high affinity cationic amino acid transporter 1	CDS
Slc7a10	asc-type amino acid transporter 1	5'UTR
Slc8a3	solute carrier family 8 (sodium/calcium	5'UTR
Slc9a1	sodium/hydrogen exchanger 1	CDS
Slc9a1	sodium/hydrogen exchanger 1	3'UTR

Continued on next page

Table 6.3 – continued from previous page

Transcript Symbol	Transcript Name	Methylation site
Slc9a1	sodium/hydrogen exchanger 1	5'UTR
Slc9a5	sodium/hydrogen exchanger 5	CDS
Slc9a5	sodium/hydrogen exchanger 5	3'UTR
Slc9a7	sodium/hydrogen exchanger 7	5'UTR
Slc9a8	sodium/hydrogen exchanger 8 isoform b	3'UTR
Slco5a1	solute carrier organic anion transporter family,	5'UTR
Slit3	slit homolog 3 protein precursor	3'UTR
Slitrk3	SLIT and NTRK-like protein 3 precursor	5'UTR
Smad6	mothers against decapentaplegic homolog 6	CDS
Smarcb1	SWI/SNF-related matrix-associated	3'UTR
Smarcc1	SWI/SNF complex subunit SMARCC1	3'UTR
Smc5	structural maintenance of chromosomes protein 5	CDS
SmeK1	serine/threonine-protein phosphatase 4	5'UTR
Smo	smoothened homolog precursor	CDS
Smurf2	E3 ubiquitin-protein ligase SMURF2	5'UTR
Smyd3	SET and MYND domain-containing protein 3	5'UTR
Sncb	beta-synuclein	5'UTR
Snrnp70	U1 small nuclear ribonucleoprotein 70 kDa	5'UTR
Sntb1	beta-1-syntrophin	CDS
Snx19	sorting nexin-19	5'UTR
Snx29	sorting nexin-29	CDS
Snx3	sorting nexin-3	CDS
Sod3	extracellular superoxide dismutase [Cu-Zn]	CDS
Sorbs1	sorbin and SH3 domain-containing protein 1	5'UTR
Sos1	son of sevenless homolog 1	5'UTR
Sostdc1	sclerostin domain-containing protein 1	3'UTR
Sox10	transcription factor SOX-10	5'UTR
Sox13	transcription factor SOX-13	CDS
Sox18	transcription factor SOX-18	CDS
Sox21	transcription factor SOX-21	CDS
Sox3	transcription factor SOX-3	CDS
Sox7	transcription factor SOX-7	CDS
Sp2	transcription factor Sp2 isoform 2	CDS
Sp8	transcription factor Sp8	CDS
Spcs3	signal peptidase complex subunit 3	5'UTR
Specc1		3'UTR
Spice1		CDS
Spint1	kunitz-type protease inhibitor 1 precursor	CDS
Spock2	testican-2 precursor	5'UTR
Spon1	spondin-1 precursor	3'UTR
Spon1	spondin-1 precursor	5'UTR
Spred2	sprouty-related, EVH1 domain-containing protein	3'UTR
Spred3	sprouty-related, EVH1 domain-containing protein	CDS
Spty2d1	protein SPT2 homolog	3'UTR
Srcin1	SRC kinase signaling inhibitor 1	CDS
Srebf2	sterol regulatory element-binding protein 2	CDS
Srgap1	SLIT-ROBO Rho GTPase-activating protein 1	CDS
Srgap2	SLIT-ROBO Rho GTPase-activating protein 2	CDS
Srrm3	serine/arginine repetitive matrix protein 3	3'UTR
Sst	somatostatin precursor	5'UTR
St13	hsc70-interacting protein	5'UTR
St8sia2	alpha-2,8-sialyltransferase 8B	CDS
St8sia2	alpha-2,8-sialyltransferase 8B	3'UTR
St8sia3	sia-alpha-2,3-Gal-beta-1,4-GlcNAc-R:alpha	5'UTR
St8sia5	alpha-2,8-sialyltransferase 8E isoform middle	CDS
St8sia5	alpha-2,8-sialyltransferase 8E isoform middle	5'UTR
Stat5b	signal transducer and activator of transcription	3'UTR
Stat6	signal transducer and transcription activator 6	3'UTR
Stk40	serine/threonine-protein kinase 40 isoform a	3'UTR
Strn	striatin	CDS
Stt3b	dolichyl-diphosphooligosaccharide-protein	5'UTR
Stub1	STIP1 homology and U box-containing protein 1	5'UTR
Stx1a	syntaxin-1A	3'UTR
Stx1b	syntaxin-1B	3'UTR
Stx3	syntaxin-3 isoform A	5'UTR
Stxbp1	syntaxin-binding protein 1 isoform b	3'UTR
Stxbp1	syntaxin-binding protein 1 isoform b	5'UTR
Sufu	suppressor of fused homolog isoform 2	3'UTR
Supt6h	transcription elongation factor SPT6	CDS
Surf4	surfeit locus protein 4	5'UTR
Susd2	sushi domain-containing protein 2 isoform 2	3'UTR
Susd3	sushi domain-containing protein 3	CDS
Susd3	sushi domain-containing protein 3	3'UTR
Sv2a	synaptic vesicle glycoprotein 2A	5'UTR
Sv2c	synaptic vesicle glycoprotein 2C	3'UTR
Sv2c	synaptic vesicle glycoprotein 2C	5'UTR
Swap70	switch-associated protein 70	CDS
Sympk	sympleskin	CDS

Continued on next page

Table 6.3 – continued from previous page

Transcript Symbol	Transcript Name	Methylation site
Syn1	synapsin-1 isoform b	CDS
Syn1	synapsin-1 isoform b	3'UTR
Syn1	synapsin-1 isoform b	5'UTR
Syn2	synapsin-2 isoform IIa	CDS
Syn2	synapsin-2 isoform IIa	5'UTR
Syng3	synaptogyrin-3	5'UTR
Synn	synemin isoform H	3'UTR
Syp	synaptophysin	CDS
Syt12	synaptotagmin-12	5'UTR
Syt3	synaptotagmin-3	CDS
Syv1	E3 ubiquitin-protein ligase synoviolin	3'UTR
Tacr1	substance-P receptor	5'UTR
Taok1	serine/threonine-protein kinase TAO1	5'UTR
Tap1	antigen peptide transporter 1 isoform 2	CDS
Tapbp	tapasin isoform 1	CDS
Tapbp	tapasin isoform 1	5'UTR
Tarbp1	TAR (HIV-1) RNA binding protein 1	CDS
Tas1r3	taste receptor type 1 member 3 precursor	CDS
Tatdn2	TatD DNase domain containing 2	5'UTR
Tbc1d10c	carabin	CDS
Tbc1d2	TBC1 domain family, member 2	3'UTR
Tbc1d22b	TBC1 domain family member 22B	CDS
Tbc1d22b	TBC1 domain family member 22B	3'UTR
Tbc1d30	TBC1 domain family member 30	5'UTR
Tbc1d5	TBC1 domain family member 5	3'UTR
Tbc1d8	TBC1 domain family member 8	3'UTR
Tbc1d9	TBC1 domain family member 9 isoform 1	5'UTR
Tbrg4	protein TBRG4	CDS
Tbx2	T-box transcription factor TBX2	CDS
Tbx3	T-box transcription factor TBX3 isoform 1	CDS
Tbx3	T-box transcription factor TBX3 isoform 1	3'UTR
Tbxa2r	thromboxane A2 receptor	3'UTR
Tcap	telethonin	3'UTR
Tcea1	transcription elongation factor A protein 1	5'UTR
Tcf12	transcription factor 12	5'UTR
Tcf25	transcription factor 25 isoform c	5'UTR
Tcf3	transcription factor E2-alpha isoform 7	CDS
Tcf7l2	transcription factor 7-like 2 isoform 7	CDS
Tcf3	transcription factor E3 isoform a	CDS
Tcf3	transcription factor E3 isoform a	5'UTR
Tchh	trichohyalin	CDS
Tcte1	T-complex-associated testis-expressed protein 1	CDS
Tead1	transcriptional enhancer factor TEF-1 isoform 2	3'UTR
Tecpr1	tectonin beta-propeller repeat-containing	CDS
Tekt4	tektin-4	CDS
Tekt5	tektin-5	CDS
Tesk1	dual specificity testis-specific protein kinase	5'UTR
Tgfb1	transforming growth factor beta-1 precursor	5'UTR
Tgfb3	transforming growth factor beta receptor type 3	CDS
Tgfb3	transforming growth factor beta receptor type 3	3'UTR
Thpo	thrombopoietin precursor	CDS
Thra	thyroid hormone receptor alpha	3'UTR
Thrsp	thyroid hormone-inducible hepatic protein	CDS
Thrsp	thyroid hormone-inducible hepatic protein	3'UTR
Thsd4	thrombospondin type-1 domain-containing protein	CDS
Thsd4	thrombospondin type-1 domain-containing protein	3'UTR
Timm17a	mitochondrial import inner membrane translocase	CDS
Timm50	mitochondrial import inner membrane translocase	CDS
Timp2	metalloproteinase inhibitor 2 precursor	5'UTR
Timp3	metalloproteinase inhibitor 3 precursor	3'UTR
Tinag11	tubulointerstitial nephritis antigen-like	CDS
Tle3	transducin-like enhancer protein 3 isoform 2	5'UTR
Tln1	talin-1	5'UTR
Tmem102	transmembrane protein 102	CDS
Tmem104	transmembrane protein 104	CDS
Tmem104	transmembrane protein 104	3'UTR
Tmem108	transmembrane protein 108 precursor	CDS
Tmem126b	transmembrane protein 126B	3'UTR
Tmem127	transmembrane protein 127	5'UTR
Tmem128	transmembrane protein 128	CDS
Tmem130	transmembrane protein 130 precursor	CDS
Tmem131	transmembrane protein 131	CDS
Tmem132d	transmembrane protein 132D precursor	5'UTR
Tmem132e	transmembrane protein 132E precursor	5'UTR
Tmem145	transmembrane protein 145	3'UTR
Tmem194	transmembrane protein 194A isoform 1	3'UTR
Tmem200c		5'UTR
Tmem201	transmembrane protein 201 isoform b	CDS

Continued on next page

Table 6.3 – continued from previous page

Transcript Symbol	Transcript Name	Methylation site
Tmem25	transmembrane protein 25 precursor	3'UTR
Tmem38b	trimeric intracellular cation channel type B	CDS
Tmem59l	transmembrane protein 59-like precursor	CDS
Tmem63b	transmembrane protein 63B	CDS
Tmem63b	transmembrane protein 63B	3'UTR
Tmem80		5'UTR
Tmtc2	transmembrane and TPR repeat-containing protein	5'UTR
Tnc	tenascin	CDS
Tnfrsf1a	tumor necrosis factor receptor superfamily	3'UTR
Tnik	traf2 and NCK-interacting protein kinase isoform	5'UTR
Trip1	TNFAIP3-interacting protein 1	3'UTR
Tnp02	transportin-2	3'UTR
Tnrc6c	trinucleotide repeat-containing gene 6C protein	5'UTR
Tnxb	tenascin-X	CDS
Tom1l2	TOM1-like protein 2 isoform b	CDS
Tomm6	mitochondrial import receptor subunit TOM6	CDS
Tor1aip1	torsin-1A-interacting protein 1 isoform 2	5'UTR
Tox2	TOX high mobility group box family member 2	3'UTR
Tpcn2	two pore calcium channel protein 2	3'UTR
Tpra1	transmembrane protein adipocyte-associated 1	5'UTR
Traf3ip2	adapter protein CIKS	CDS
Trappc5	trafficking protein particle complex subunit 5	5'UTR
Trappc9	trafficking protein particle complex subunit 9	3'UTR
Trerf1	transcriptional-regulating factor 1 isoform 1	5'UTR
Trib1	tribbles homolog 1	5'UTR
Tril		5'UTR
Trim17	E3 ubiquitin-protein ligase TRIM17	CDS
Trim25	E3 ubiquitin/ISG15 ligase TRIM25	CDS
Trim26	tripartite motif-containing protein 26 isoform	5'UTR
Trim41	E3 ubiquitin-protein ligase TRIM41	5'UTR
Trim62	tripartite motif-containing protein 62	CDS
Trim66	tripartite motif-containing protein 66 isoform	3'UTR
Trim67	tripartite motif-containing protein 67	CDS
Trim68	E3 ubiquitin-protein ligase TRIM68	CDS
Trim7	tripartite motif-containing protein 7	3'UTR
Trim9	E3 ubiquitin-protein ligase TRIM9 isoform c	CDS
Trim9	E3 ubiquitin-protein ligase TRIM9 isoform c	3'UTR
Trnp1	TMF-regulated nuclear protein 1	CDS
Trp53bp2	apoptosis-stimulating of p53 protein 2	5'UTR
Trp53i11	tumor protein p53-inducible protein 11	3'UTR
Trp73	tumor protein p73 isoform c	CDS
Trp73	tumor protein p73 isoform c	3'UTR
Trrap	transformation/transcription domain-associated	3'UTR
Tsc22d4	TSC22 domain family protein 4	CDS
Tsku	tsukushin precursor	CDS
Tsn	translin	CDS
Tspan17	tetraspanin-17	3'UTR
Ttc28	tetratricopeptide repeat protein 28	3'UTR
Ttc7b	tetratricopeptide repeat domain 7B	CDS
Ttl1	probable tubulin polyglutamylase TTL1	CDS
Ttl4	tubulin polyglutamylase TTL4	3'UTR
Ttyh1	protein tweety homolog 1 isoform 2	CDS
Ttyh2	protein tweety homolog 2	CDS
Tubb4	tubulin beta-4 chain	3'UTR
Tubb4	tubulin beta-4 chain	5'UTR
Tubg2	tubulin gamma-2 chain	CDS
Tubgcp4	gamma-tubulin complex component 4	5'UTR
Tulp4	tubby-related protein 4 isoform b	3'UTR
Txndc5	thioredoxin domain-containing protein 5	CDS
Txnrd1	thioredoxin reductase 1, cytoplasmic isoform 2	5'UTR
Tysnd1	peroxisomal leader peptide-processing protease	CDS
U2af2	splicing factor U2AF 65 kDa subunit	3'UTR
Uap1l1	UDP-N-acetylhexosamine pyrophosphorylase-like	CDS
Ubc	polyubiquitin-C	CDS
Ube2m	NEDD8-conjugating enzyme Ubc12 isoform 2	5'UTR
Ube2q2	ubiquitin-conjugating enzyme E2 Q2	CDS
Ube2ql1	ubiquitin-conjugating enzyme E2Q-like protein 1	5'UTR
Ubqln4	ubiquilin-4	CDS
Ubr2	E3 ubiquitin-protein ligase UBR2 isoform 1	5'UTR
Ubxn4	UBX domain-containing protein 4	5'UTR
Unc5a	netrin receptor UNC5A precursor	CDS
Unc5a	netrin receptor UNC5A precursor	3'UTR
Unc5b	netrin receptor UNC5B precursor	3'UTR
Unc5b	netrin receptor UNC5B precursor	5'UTR
Unc5c	netrin receptor UNC5C precursor	5'UTR
Unc5d	netrin receptor UNC5D precursor	5'UTR
Uncx	homeobox protein unc-4 homolog	CDS
Uncx	homeobox protein unc-4 homolog	3'UTR

Continued on next page

Table 6.3 – continued from previous page

Transcript Symbol	Transcript Name	Methylation site
Ung	uracil-DNA glycosylase isoform a	3'UTR
Upf1	regulator of nonsense transcripts 1 isoform a	CDS
Upf1	regulator of nonsense transcripts 1 isoform a	5'UTR
Urod	uroporphyrinogen decarboxylase	CDS
Usf2	upstream stimulatory factor 2	3'UTR
Usp19	ubiquitin carboxyl-terminal hydrolase 19 isoform	5'UTR
Usp2	ubiquitin carboxyl-terminal hydrolase 2 isoform	5'UTR
Usp22	ubiquitin carboxyl-terminal hydrolase 22	3'UTR
Usp30	ubiquitin carboxyl-terminal hydrolase 30	CDS
Usp33	ubiquitin carboxyl-terminal hydrolase 33 isoform	5'UTR
Usp43	ubiquitin carboxyl-terminal hydrolase 43	CDS
Ust	uronyl 2-sulfotransferase	CDS
Vac14	protein VAC14 homolog	CDS
Vat1	synaptic vesicle membrane protein VAT-1 homolog	CDS
Vgf	VGF nerve growth factor inducible	5'UTR
Vim	vimentin	CDS
Vps26b	vacuolar protein sorting-associated protein 26B	3'UTR
Vps37a	vacuolar protein sorting-associated protein 37A	5'UTR
Vps37d	vacuolar protein sorting-associated protein 37D	CDS
Vps37d	vacuolar protein sorting-associated protein 37D	3'UTR
Vps53	vacuolar protein sorting-associated protein 53	3'UTR
Vps8	vacuolar protein sorting-associated protein 8	3'UTR
Vsx2	visual system homeobox 2	CDS
Vtn	vitronectin precursor	CDS
Vwf	von Willebrand factor precursor	CDS
Wasf2	wiskott-Aldrich syndrome protein family member	3'UTR
Wasf3	wiskott-Aldrich syndrome protein family member	3'UTR
Wbscr27	Williams-Beuren syndrome chromosomal region 27	5'UTR
Wdfy4	WD repeat and FYVE domain containing 4	CDS
Wdr33	WD repeat domain 33 isoform 2	5'UTR
Wdr45l	WD repeat domain phosphoinositide-interacting	CDS
Wdr6	WD repeat-containing protein 6	3'UTR
Wdr82	WD repeat-containing protein 82	5'UTR
Wdtc1	WD and tetratricopeptide repeats protein 1	3'UTR
Wfikkn2	WAP, kazal, immunoglobulin, kunitz and NTR	CDS
Wfs1	wolframin	CDS
Whrn	whirlin isoform 5	3'UTR
Whrn	whirlin isoform 5	5'UTR
Wipf2	WAS/WASL-interacting protein family member 2	3'UTR
Wnk1	serine/threonine-protein kinase WNK1	5'UTR
Wnt1	proto-oncogene Wnt-1 precursor	5'UTR
Wnt7b	protein Wnt-7b isoform 1	CDS
X99384	paladin	CDS
Xpnpep1	xaa-Pro aminopeptidase 1	CDS
Xpo6	exportin-6	5'UTR
Xpot	exportin-T	CDS
Xylb	xylulose kinase	3'UTR
Ybey		CDS
Yipf2	protein YIPF2	3'UTR
Yipf2	protein YIPF2	5'UTR
Yipf3	protein YIPF3	5'UTR
Ywhag	14-3-3 protein gamma	5'UTR
Yy1	transcriptional repressor protein YY1	CDS
Zbtb26	zinc finger and BTB domain-containing protein	5'UTR
Zbtb33	transcriptional regulator Kaiso	5'UTR
Zbtb39	zinc finger and BTB domain-containing protein	CDS
Zbtb39	zinc finger and BTB domain-containing protein	3'UTR
Zbtb40	zinc finger and BTB domain-containing protein	CDS
Zbtb40	zinc finger and BTB domain-containing protein	3'UTR
Zbtb7a	zinc finger and BTB domain-containing protein	5'UTR
Zbtb7c	zinc finger and BTB domain-containing protein	3'UTR
Zc3h15	zinc finger CCCH domain-containing protein 15	CDS
Zc3h7b	zinc finger CCCH domain-containing protein 7B	CDS
Zdhhc14	probable palmitoyltransferase ZDHHC14	CDS
Zdhhc14	probable palmitoyltransferase ZDHHC14	5'UTR
Zdhhc5	probable palmitoyltransferase ZDHHC5	CDS
Zdhhc8	probable palmitoyltransferase ZDHHC8	3'UTR
Zdhhc9	palmitoyltransferase ZDHHC9	CDS
Zdhhc9	palmitoyltransferase ZDHHC9	3'UTR
Zeb2	zinc finger E-box-binding homeobox 2 isoform 2	5'UTR
Zer1	protein zer-1 homolog	3'UTR
Zfand3	AN1-type zinc finger protein 3	CDS
Zfx2	zinc finger homeobox protein 2	CDS
Zfx2	zinc finger homeobox protein 2	3'UTR
Zfp142	zinc finger protein 142	CDS
Zfp148	zinc finger protein 148	5'UTR
Zfp213	zinc finger protein 213	5'UTR
Zfp335	zinc finger protein 335	3'UTR

Continued on next page

Table 6.3 – continued from previous page

Transcript Symbol	Transcript Name	Methylation site
Zfp358	zinc finger protein 358	CDS
Zfp366	zinc finger protein 366	CDS
Zfp361	zinc finger protein 36, C3H1 type-like 1	CDS
Zfp3612	zinc finger protein 36, C3H1 type-like 2	CDS
Zfp385a	zinc finger protein 385A	CDS
Zfp385a	zinc finger protein 385A	5'UTR
Zfp395	zinc finger protein 395	CDS
Zfp395	zinc finger protein 395	3'UTR
Zfp414	zinc finger protein 414	CDS
Zfp414	zinc finger protein 414	5'UTR
Zfp423	zinc finger protein 423	CDS
Zfp428	zinc finger protein 428	5'UTR
Zfp592	zinc finger protein 592	3'UTR
Zfp598	zinc finger protein 598	3'UTR
Zfp628	zinc finger protein 628	CDS
Zfp652	zinc finger protein 652	5'UTR
Zfp655	zinc finger protein 655 isoform a	5'UTR
Zfp689	zinc finger protein 689	5'UTR
Zfp747	zinc finger protein 747	5'UTR
Zfp831	zinc finger protein 831	3'UTR
Zic2	zinc finger protein ZIC 2	CDS
Zic4	zinc finger protein ZIC 4	CDS
Zmiz1	zinc finger MIZ domain-containing protein 1	3'UTR
Znhit1	zinc finger HIT domain-containing protein 1	5'UTR
Znrf1	E3 ubiquitin-protein ligase ZNRF1 isoform c	CDS
Zscan2	zinc finger and SCAN domain-containing protein	3'UTR
Zswim1	zinc finger SWIM domain-containing protein 1	CDS
Zswim1	zinc finger SWIM domain-containing protein 1	3'UTR
Zswim5	zinc finger SWIM domain-containing protein 5	5'UTR
Zzef1	zinc finger ZZ-type and EF-hand	CDS

Danksagung

Ich möchte mich bedanken bei

- PROF. DR. JENS C. BRÜNING
für Betreuung, Unterstützung und ansteckende Begeisterung,
- PD DR. ALEKSANDRA TRIFUNOVIC & PROF. DR. PETER KLOPPENBURG
für die Bereitschaft Mitglieder meines "thesis committee" zu sein,
- SIMON HEß, LINDA VERHAGEN, SABINE JORDAN UND BENGT F. BELGARDT
für die Hilfe, Mitarbeit und Anleitung im Rahmen des Projektes,
- KATE MEYER, SAMIE JAFFREY, YOGESH SALETORE, OLIVIER ELEMENTO, MARCELO DIETRICH, TAMAS HORVATH, THOMAS FRANZ UND PETER KLOPPENBURG
für die Kollaboration im Rahmen des Projektes,
- SIMON HEß, LINDA VERHAGEN, TIM KLÖCKENER UND SARAH TURPIN
für die Bereitschaft zum Korrekturlesen,
- TIM KLÖCKENER, JESSE DENSON, JULIA GOLDAU UND DIANA KUTYNIOK
für jegliche Hilfe und Ablenkung im Labor,
- LINDA VERHAGEN UND JAN-WILHELM KORNFELD
für Hilfe, Anleitung und lunch dates,
- BRIGITTE HAMPEL
für exzellente technischen Unterstützung,
- HELLA BRÖNNEKE & JENS ALBER
für großartige Verhaltensversuche und Phenotyping Expertise,
- KERSTIN MAROHL, DEM TEAM DES RAUM 5, DER GO UND DES MPI
für die hervorragende Versorgung der Versuchstiere,
- THEODOROS ZOGRAFOU
für mentale Unterstützung und gute Diskussion,
- sowie der restlichen AG BRÜNING/AG WUNDERLICH UND ANGEHÖRIGEN DER CECAD GRADUATE SCHOOL UND DES MPI FÜR NEUROLOGISCHE FORSCHUNG
für Hilfsbereitschaft, dumme Sprüche und "socialising".

Last but not least bei meinen Eltern, Simon & Kathi sowie meiner Freundin Eri für die Unterstützung und Rücksichtnahme.

Erklärung

Die vorliegende Arbeit wurde in der Zeit von November 2009 bis November 2013 am Institut für Genetik, Arbeitsgruppe Modern Mouse Genetics and Metabolism, Universität zu Köln und im Max Planck Institut für Neurologische Forschung Köln, Forschungsgruppe Neuronal Control of Metabolism unter Anleitung von Herrn Prof. Dr. Jens C. Brüning angefertigt.

Ich versichere, dass ich die von mir vorgelegte Dissertation selbständig angefertigt, die benutzten Quellen und Hilfsmittel vollständig angegeben und die Stellen der Arbeit - einschließlich Tabellen, Karten und Abbildungen -, die anderen Werken im Wortlaut oder dem Sinn nach entnommen sind, in jedem Einzelfall als Entlehnung kenntlich gemacht habe; dass diese Dissertation noch keiner anderen Fakultät oder Universität zur Prüfung vorgelegen hat; dass sie - abgesehen von unten angegebenen Teilpublikationen - noch nicht veröffentlicht worden ist sowie, dass ich eine solche Veröffentlichung vor Abschluss des Promotionsverfahrens nicht vornehmen werde. Die Bestimmungen dieser Promotionsordnung sind mir bekannt.

Köln, März 2014

(Martin Heß)

Teilpublikation

Martin E Hess*, SIMON HESS*, KATE D MEYER, LINDA A W VERHAGEN, LINDA KOCH, HELLA S BRÖNNEKE, MARCELO O DIETRICH, SABINE D JORDAN, YOGESH SALETORE, OLIVIER ELEMENTO, BENGT F BELGARDT, THOMAS FRANZ, TAMAS L HORVATH, ULRICH RÜTHER, SAMIE R JAFFREY, PETER KLOPPENBURG & JENS C BRÜNING. 2013. The fat mass and obesity associated gene (*Fto*) regulates activity of the dopaminergic midbrain circuitry. *Nature Neuroscience*, **16**(8), 1042-1048. * equally contributing first author

Curriculum vitae

MARTIN HEß, M.Sc.

PERSÖNLICHE ANGABEN

Voller Name	Martin Erwin Heß
Geburtsort	Adenau
Geburtstag	06. April 1983
Adresse	Antwerpener Str. 24, 50672 Köln
E-mail	martin.hess@nf.mpg.de
Nationalität	deutsch

AUSBILDUNG

10/2008–01/2014	Fast Track Masters/Doctoral Programme des Fachbereichs Biologie, Abschluss Master of Science (11/2010), <i>Universität zu Köln</i>
10/2005–08/2008	Bachelor of Science , Studium der Biologie, <i>Universität zu Köln</i>
10/2004–09/2005	Studium der Regionalwissenschaft Japan, <i>Rheinische Friedrich-Wilhelms-Universität Bonn</i>
10/2003–09/2004	Studium der Japanologie, <i>Universität zu Köln</i>
05/2002–02/2003	Zivildienst, <i>Westefel-Werke gGmbH, Gerolstein</i>
08/1993–03/2002	Abitur , St. Matthias Gymnasium, Gerolstein

MASTER ARBEIT

Titel	Generation of new genetic tools for the investigation of the fat mass and obesity associated protein (<i>Fto</i>)
Betreuer	Prof. Dr. Jens C. Brüning

BACHELOR ARBEIT

Titel	The role of octopamine and DUM neurons in the modulation of motor activity in the stick insect <i>Carausius morosus</i>
Betreuer	PD Dr. Joachim Schmidt

INTERNSHIPS

06/2008–07/2008 | Ear Institute, University College London, Dr. Jörg Albert

PUBLIKATIONEN

- 2014 | **Martin E Hess** & JENS C BRÜNING. 2014. The fat mass and obesity associated gene (*Fto*): Obesity and beyond?
Biochimica et Biophysica Acta: Molecular Basis of Disease, - in press -.
- Martin E Hess** & JENS C BRÜNING. 2014. Obesity: The need to eat - overruling the homeostatic control of feeding.
Nature Reviews Endocrinology, **10**, 5-6.
- 2013 | EFTHIMIA KARRA, OWEN G O'DALY, AGHARUL I CHOUDHURY, AHMED YOUSSEIF, STEVEN MILLERSHIP, MARIANNE T NEARY, WILLIAM R SCOTT, KEVAL CHANDARANA, SEAN MANNING, **Martin E Hess**, HIROSHI IWAKURA, TAKASHI AKAMIZU, QUEENSTA MILLET, CIGDEM GELEGEN, MEGAN E DREW, SOFIA RAHMAN, JULIAN J EMMANUEL, STEVEN C R WILLIAMS, ULRICH U RÜTHER, JENS C BRÜNING, DOMINIC J WITHERS, FERNANDO O ZELAYA, AND RACHEL L BATTERHAM. 2013. A link between FTO, ghrelin, and impaired brain food-cue responsiveness.
Journal of Clinical Investigation, **123**(8), 3539-3551.
- Martin E Hess***, SIMON HESS*, KATE D MEYER, LINDA A W VERHAGEN, LINDA KOCH, HELLA S BRÖNNEKE, MARCELO O DIETRICH, SABINE D JORDAN, YOGESH SALETORE, OLIVIER ELEMENTO, BENGT F BELGARDT, THOMAS FRANZ, TAMAS L HORVATH, ULRICH RÜTHER, SAMIE R JAFFREY, PETER KLOPPENBURG & JENS C BRÜNING. 2013. The fat mass and obesity associated gene (*Fto*) regulates activity of the dopaminergic midbrain circuitry.
Nature Neuroscience, **16**(8), 1042-1048. * equally contributing first author

KONFERENZ TEILNAHMEN

- 03/2013 Keystone Symposium:
Neuronal Control of Appetite, Metabolism and Weight,
Banff, Kanada
Poster: The Obesity-Associated *Fto* Gene Regulates the Activity of the Dopaminergic Midbrain Circuitry
- 09/2012 EMBO-Symposium: Diabetes and Obesity,
Heidelberg, Deutschland
Poster: The Obesity-Associated *Fto* Gene Regulates the Activity of the Dopaminergic Midbrain Circuitry
- 01/2012 Keystone Symposium:
Genetic and Molecular Basis of Obesity and Body Weight Regulation,
Santa Fe, NM, USA

Köln, März 2014